UCLA

UCLA Previously Published Works

Title

THE METAL ABUNDANCES ACROSS COSMIC TIME (　　　　) SURVEY. I. OPTICAL SPECTROSCOPY IN THE SUBARU DEEP FIELD

Authors

Ly, Chun
Malhotra, Sangeeta
Malkan, Matthew A
et al.

Peer reviewed

THE METAL ABUNDANCE ACROSS COSMIC TIME ($\mathcal{MACT}$) SURVEY I: OPTICAL SPECTROSCOPY IN THE SUBARU DEEP FIELD

Chun Ly,[1] Sangeeta Malhotra,[2] Matthew A. Malkan,[3] Jane R. Rigby,[1] Nobunari Kashikawa,[4,5] Mithi A. de los Reyes,[6] and James E. Rhoads[2]

Submitted to the Astrophysical Journal Supplements on February 1, 2016

ABSTRACT

Deep rest-frame optical spectroscopy is key for characterizing and understanding the physical conditions and properties of the ionized gas in galaxies. Here, we present a new spectroscopic survey called "Metal Abundances across Cosmic Time" or $\mathcal{MACT}$, which will obtain rest-frame optical spectra for ∼3,000 emission-line galaxies. This paper focuses on the optical spectroscopy that has been conducted with MMT/Hectospec and Keck/DEIMOS for ≈1,900 $z = 0.1$–1 emission-line galaxies selected from our narrowband and intermediate-band imaging in the Subaru Deep Field. In addition, we present a sample of 164 galaxies for which we have measured the weak [O III] λ4363 line (66 with at least 3σ detections and 98 with significant upper limits). This nebular emission line determines the gas-phase metallicity by measuring the electron temperature of the ionized gas. This paper presents the optical spectra, emission-line measurements, interstellar properties (e.g., metallicity, gas density), and stellar properties (e.g., star formation rates, stellar mass). Paper II of the $\mathcal{MACT}$ survey (Ly et al.) presents first results on the stellar mass–gas metallicity relation at $z \lesssim 1$ using the sample with [O III] λ4363 measurements.

Subject headings: galaxies: abundances — galaxies: distances and redshifts — galaxies: evolution — galaxies: ISM — galaxies: photometry — galaxies: star formation

1. INTRODUCTION

The ionized gas of the interstellar medium (ISM) is a key component in galaxies that is directly affected by (1) photo-ionizing radiation from young massive stars, (2) heating from lower mass stars, (3) accretion of pristine and enriched gas on ∼10–100 kpc scales and from nearby interacting galaxies, and (4) gas outflows from the stellar winds of supernova. To diagnose and understand the physical conditions of the ISM, deep spectroscopy is necessary, preferably in the rest-frame optical (3000Å–7000Å) where hydrogen Balmer recombination lines and collisionally-excited ionic metal lines are available to characterize the interstellar gas.

For example, the Baldwin–Phillips–Terlevich ("BPT") diagnostic diagrams (Baldwin et al. 1981; Veilleux & Osterbrock 1987) of [O III]λ5007/Hβ as a function of [N II]λ6583/Hα, [S II]λ6716,6731/Hα, or [O I]λ6300/Hα are fundamental for classifying galaxies and understanding whether massive young stars, shocks, or active galactic nuclei (AGNs) power the photo-ionization of the gas.

The hydrogen Balmer lines directly trace high-mass star formation, as they are recombination lines that arise from the ionizing radiation produced by short-lived ($\lesssim$10 Myr) OB stars (e.g., Kennicutt 1998a; Ly et al. 2011b; Lee et al. 2012). Also, the intrinsic flux ratios

Electronic address: astro.chun@gmail.com
[1] Observational Cosmology Laboratory, NASA Goddard Space Flight Center, 8800 Greenbelt Road, Greenbelt, MD 20771, USA;
[2] School of Earth and Space Exploration, Arizona State University, Tempe, AZ 85287, USA
[3] Department of Physics and Astronomy, UCLA, Los Angeles, CA, USA
[4] Optical and Infrared Astronomy Division, National Astronomical Observatory, Mitaka, Tokyo, Japan
[5] Department of Astronomy, School of Science, Graduate University for Advanced Studies, Mitaka, Tokyo, Japan
[6] Department of Physics, North Carolina State University, Raleigh, NC

of the Balmer lines (e.g., Hα/Hβ, known as the Balmer decrement)—governed by atomic recombination transition rates—determine the interstellar reddening from dust.

Finally, the gas-phase heavy-element abundance ("metallicity") of the ISM is primarily set by enrichment from star formation, but diluted by the accretion of new pristine gas, and loss within winds that drive gas out of the galaxies (e.g., Dalcanton 2007; Davé et al. 2011; Lilly et al. 2013). For this reason, the gas metallicity, when combined with stellar mass and SFR determinations, is a fundamental observable that allows for an understanding of how galaxies process gas.

The Sloan Digitial Sky Survey (SDSS; York et al. 2000) is the largest optical spectroscopic study of local ($z \lesssim 0.2$) galaxies that has (1) classified galaxies and AGNs (Kauffmann et al. 2003); (2) determined SFRs and interstellar dust reddening (Brinchmann et al. 2004); and (3) examined the dependence of the gas metallicity on stellar properties, such as the stellar mass–metallicity ($M_\star$–Z) relation (Tremonti et al. 2004).

At $z \gtrsim 0.2$, optical spectroscopic surveys such as zCOSMOS (Lilly et al. 2009), DEEP2 (Newman et al. 2013), and AGES (Kochanek et al. 2012), have struggled to determine the physical properties of the interstellar gas in *individual* galaxies over a wide range in redshift and stellar mass. These limitations are driven mainly by the design of the surveys to determine spectroscopic redshifts often with only one or two emission or absorption lines.

For example, Cresci et al. (2012) used the zCOSMOS catalog of ∼10,000 bright ($I_{AB} < 22.5$) galaxies to measure metallicity in only 3% of the zCOSMOS sample (334 galaxies) at $z \lesssim 0.75$. The low success of obtaining metallicity is due to a combination of the relatively short integration (one hour) and low spectral resolution

($\lambda/\Delta\lambda \sim 600$). For the DEEP2 survey, 9% of the DEEP2 sample have metallicity measurements due to a combination of a limited spectral coverage (6000Å–9000Å) and a pre-selection using broadband colors for galaxies at $z \gtrsim 0.7$ (4140 galaxies; Ly et al. 2015). While DEEP2 has measured the $M_\star$–Z relation over 1.5 dex in stellar mass (Zahid et al. 2011), the limiting spectral coverage and selection function reduce the metallicity sample to galaxies in a small redshift range of $z \approx 0.75$–0.82.

Another limitation of these surveys is the lack of galaxies below $M_\star \sim 10^9 M_\odot$. For example, AGES targeted $\sim$3,000 galaxies at $0.05 \lesssim z \lesssim 0.75$. However, they were limited to galaxies brighter than $I_{AB} \approx 20.5$, and thus were unable to study the $M_\star$–Z relation below $M_\star \approx 10^{10}$ $M_\odot$ ($\approx 10^{11} M_\odot$) at $z \gtrsim 0.35$ ($z \gtrsim 0.55$) (Moustakas et al. 2011). While the magnitude-limited selections of zCOSMOS and DEEP2 ($R_{AB} \lesssim 24$) are fainter than AGES, they limit $z \sim 0.7$ galaxies to $M_\star \approx 2 \times 10^9 M_\odot$.

To address the lack of deep rest-frame optical spectroscopy for thousands of galaxies at $z \lesssim 1$, specifically those with lower stellar masses ($M_\star \lesssim 10^9 M_\odot$), we have conducted a spectroscopic survey called "Metal Abundances across Cosmic Time" or $\mathcal{MACT}$ that targets $\approx$1,900 $z \lesssim 1$ star-forming galaxies. This survey has obtained between 2 and 12 hours of on-source integration for each galaxy with optical spectrographs on Keck and MMT. The primary goal of the survey is to obtain reliable measurements of the gas-phase metallicity and other physical properties of the interstellar medium (ISM) in galaxies, such as the SFR, gas density, ionization parameter, dust content, and the source of photoionizing radiation (star formation and/or AGN). The galaxy sample of $\mathcal{MACT}$ encompasses more than 3 dex in stellar mass, including galaxies with stellar masses as low as $M_\star \sim 3 \times 10^6 M_\odot$ and $3 \times 10^7 M_\odot$ at $z \sim 0.1$ and $z \sim 1$, respectively. To effectively select low-mass galaxies over a wide range in redshift, $\mathcal{MACT}$ targeted galaxies in the Subaru Deep Field (SDF; Kashikawa et al. 2004) that have excess flux in narrowband and/or intermediate-band filters, which is now understood to be produced by nebular emission lines from star formation or AGN (e.g., Ly et al. 2007, 2011b, and references therein).

Another advantage of $\mathcal{MACT}$ from previous spectroscopic surveys is that it is the first to use the electron temperature (T_e) method to measure the evolution of the $M_\star$–Z relation over $\approx$8 billion years. This approach uses the flux/luminosity of the weak [O III] λ4363 nebular emission line, which is governed by the ability for the gas to cool from a higher oxygen abundance, O/H (Aller 1984). Previous studies have been limited to the use of strong nebular emission lines for metallicity estimations. Such "strong-line" calibrations have received concerns on their validity for higher redshift due to growing support that the physical conditions of the ISM in $z \gtrsim 1$ galaxies are different from local galaxies (e.g., Cowie et al. 2016).

This paper (Paper I) describes the optical spectroscopy conducted for the $\mathcal{MACT}$ survey, and discusses the sample of 66 galaxies with detections of [O III] λ4363 at $z = 0.05$–0.95 (average of $z = 0.53 \pm 0.25$; median of 0.48) and robust [O III] λ4363 upper limits for 98 galaxies at $z = 0.04$–0.96 (average of $z = 0.52 \pm 0.23$; median of 0.48). We refer readers to Ly et al. (2016) (hereafter Paper II), which focuses on first scientific results that

pertain to the evolution of the $M_\star$–Z relation using the T_e method. The outline of Paper I is as follows. In Section 2 we describe the imaging survey of the SDF, the selection of over 9,000 emission-line galaxies, and the follow-up optical spectroscopy with Keck and MMT. In Section 3 we discuss detections and measurements of nebular emission lines, which yield a spectroscopic sample with [O III] λ4363 detections and reliable non-detections. Section 4 describes how we determine the: (1) dust attenuation, (2) electron temperature and gas-phase (O/H) metallicity, (3) dust-corrected SFR, (4) stellar properties from spectral energy distribution (SED) fitting, and (5) gas density for the samples of [O III] λ4363 detections and non-detections. We summarize the $\mathcal{MACT}$ survey and our [O III] λ4363-detected and [O III] λ4363-non-detected samples in Section 5

Throughout this paper, we adopt a flat cosmology with $\Omega_\Lambda = 0.7$, $\Omega_M = 0.3$, and $H_0 = 70$ km s^{-1} Mpc^{-1}. Magnitudes are reported on the AB system (Oke 1974). For reference, we adopt $12 + \log(\text{O/H})_\odot = 8.69$ (Allende Prieto et al. 2001) as solar metallicity, $Z_\odot$. Unless otherwise indicated, we report 68% confidence measurement uncertainties, and "[O III]" alone refers to the 5007Å emission line.

2. THE SUBARU DEEP FIELD

The SDF has the most sensitive optical imaging in several narrowband and intermediate-band filters in the sky, and is further complemented with ultra-deep multi-band imaging between 1500Å and 4.5μm. A summary of the ancillary imaging is available in Ly et al. (2011a) and later in Section 4.4. The emission-line galaxies in this paper are selected from imaging in five narrowband filters (NB704, NB711, NB816, NB921, NB973), and two intermediate-band filters (IA598 and IA679). A summary of the filter properties is in Table 1 and Ly14.

These SDF data were acquired with Suprime-Cam (Miyazaki et al. 2002), the optical imager mounted at the prime focus of the Subaru telescope, between 2001 March and 2007 May. The acquisition and reduction of these data have been discussed extensively in Kashikawa et al. (2004), Kashikawa et al. (2006), Ly et al. (2007) (hereafter Ly07), as well as in Ly et al. (2012b) for the narrowband data, and in Nagao et al. (2008) for the intermediate-band data. In brief, data were obtained mostly under photometric conditions with average seeing of $0''.9$–$1''.0$ for all five narrowband and two intermediate-band filters. These data were reduced following standard reduction procedures using SDFRED (Yagi et al. 2002; Ouchi et al. 2004), a software package designed especially for Suprime-Cam data.

The most prominent emission lines entering these filters are Hα, [O III], Hβ, and [O II], at well-defined redshift windows between $z = 0.01$ and $z = 1.62$. This results in probing 64% of the redshift space and 67% of the comoving volume from $z = 0$ out to $z \leq 1.03$. Compared to the previous narrowband-selected metallicity study at $z = 0.24$–0.85 (Hu et al. 2009), our survey probes 4.7 (3.8) times more redshift (volume) space, and is deeper by $\approx$1.5 mag in the narrowband imaging.

2.1. Selection of Emission-line Galaxies

To select narrowband and intermediate-band excess emitters due to the presence of nebular emission line(s),

TABLE 1
Summary of Filters, Emission-line Samples, and Spectroscopic Samples for the Subaru Deep Field

Filter	λ_c (Å)	FWHM (Å)	$m_{\lim}(3\sigma)$ (mag)	Area (arcmin^2)	N	$N_{\rm total}$	$N_{\rm target}$			$N_{\rm specz}$		
							MMT	Keck	Total	MMT	Keck	Total
(1)	(2)	(3)	(4)	(5)	(6)	(7)	(8)	(9)	(10)	(11)	(12)	(13)
IA598	6007	303	26.79	870.4	118097	641	48	28	71	45	12	52
IA679	6780	340	27.39	870.4	139585	790	110	124	193	101	105	165
NB704	7046	100	26.71	870.4	123123	1695	279	226	423	253	191	362
NB711	7111	72	26.07	870.4	97632	1480	131	188	276	115	160	232
NB816	8150	120	26.90	870.4	133273	1602	221	209	381	166	152	270
NB921	9196	132	26.71	870.4	119541	2361	277	530	710	237	458	598
NB973	9755	200	25.69	788.7	84786	1243	87	171	222	79	110	153
Total	...	...	...	...	...	9264	845	1313	1911	708	1031	1493

Note. — (1): Name of narrowband or intermediate-band filter. (2): Central wavelength of filter, λ_c. (3): Full width at half maximum of filter. (4): 3σ limiting imaging depth, $m_{\lim}(3\sigma)$. (5): Surveyed area. (6): Number of sources detected in each image mosaic, N. (7) Number of narrowband or intermediate-band excess emitters, $N_{\rm total}$. (8)–(10): Number of galaxies with targeted MMT and/or Keck spectra, $N_{\rm target}$. (11)–(13): Number of galaxies with robust spectroscopic redshift, $N_{\rm specz}$. As discussed in Section 2.1, some excess emitters are selected by more than one filter. Thus the total number of galaxies for each column (last row) is less than the sum.

we use the standard color excess selection, where photometry in these filters is compared against magnitudes for adjacent broad-band filters that sample the continuum. Since the technique has been extensively used, we briefly summarize it below, and refer readers to Fujita et al. (2003), Ly et al. (2011b), and Lee et al. (2012). Table 1 provides an overview of the SDF emission-line survey, and we illustrate the selection of NB704 and NB711 excess emitters in Figure 1, NB816 excess emitters in Figure 2, NB921 and NB973 excess emitters in Figure 3, and IA598 and IA679 excess emitters in Figure 4.

The measured continuum adjacent to the line is determined by the two broad-band filters closest to the narrow bandpass. For NB921 and NB973, we start with the z'-band. Since the central wavelengths of these filters are longer than that of the z' filter, we correct for the differences using the $i'-z'$ color (Ly et al. 2012a,b). The remaining filters use a flux-weighted combination of either the V- and $R_{\rm C}$-band (IA598), the $R_{\rm C}$- and i'-band (NB704, NB711, and IA679), or the i'- and z'-band (NB816):

$$f_{\rm cont} = \epsilon f_{\rm blue} + (1 - \epsilon) f_{\rm red}, \qquad (1)$$

where $f_{\rm blue}$ and $f_{\rm red}$ are the flux density in erg s^{-1} cm^{-2} Hz^{-1} for the bluer and redder broad-band filters, respectively (e.g., i' and z' for NB816), and $\epsilon = 0.45$ (IA598), 0.5 (NB704, NB711), 0.75 (IA679), and 0.6 (NB816).

Photometric measurements for broad-band data are obtained by running SExtractor (version 2.5.0; Bertin & Arnouts 1996) in "dual-image" mode, where the respective narrowband or intermediate-band image is used as the "detection" image. This works well because all broad-band, intermediate-band, and narrowband mosaicked images have very similar seeing, so that excess colors are determined within the same physical scale on the galaxies. For the extraction of fluxes and selection of sources, we use a $2''$ diameter circular aperture. The 3σ sensitivities for the V, $R_{\rm C}$, i', and z' images are between 26.27 and 27.53 mag, which are generally ≈ 1 mag deeper than the narrowband and intermediate-band imaging.

We also masked out regions affected by poor coverage and contamination by bright foreground stars. The unmasked regions cover 870.4 arcmin^2 for all filters with the exception of NB973, which covers 788.7 arcmin^2. The latter is smaller due to higher systematic noise in one of the ten CCDs, which we mask to avoid significant spuri-

ous detections. In total, we detect between $\approx 85{,}000$ and $\approx 140{,}000$ sources in the unmasked regions of the narrowband or intermediate-band mosaics (see Table 1). We select narrowband and intermediate-band excess emitters with a minimum Cont–NB or Cont–IA color of 0.15 mag for IA598, IA679, NB704, NB711, and NB816, 0.20 mag for NB921, and 0.25 mag for NB973. These minimum color excesses are shown in Figures 1–4 as dashed horizontal lines. In addition, we require that the Cont–NB or Cont–IA color exceeds

$$-2.5 \log \left(1 - \frac{\sqrt{f_{\nu,3\sigma\rm NB/IA}^2 + f_{\nu,3\sigma\rm Cont}^2}}{f_{\nu,\rm NB/IA}} \right), \quad (2)$$

where $f_{\nu,3\sigma\rm Cont}$ and $f_{\nu,3\sigma\rm NB/IA}$ are the 3σ flux density limits for the continuum band(s) and the narrowband or intermediate-band, respectively, and $f_{\nu,\rm NB/IA}$ is the flux density for a given narrowband or intermediate-band magnitude. This selection yielded between ≈ 640 and ≈ 2360 excess emitters in each narrowband or intermediate-band filter.

Some of our sources are independently selected by more than one filter. This is due to some fortuitous redshift overlap of our narrowband/intermediate-band filters such that different emission lines (e.g., Hα and [O III]) are detectable at the same redshift. Accounting for duplicate galaxies, the complete SDF emission-line galaxy sample consists of 9264 galaxies mostly at $z = 0.01$ to $z = 1.62$ with some at higher redshift due to Lyα emission. We note that the sample presented in this paper supersedes our earlier multi-narrowband study (Ly07), Specifically, our previous study computed the continuum for narrowband/intermediate excess selection using magnitudes instead of flux densities (see Equation 1). Also, a fifth narrowband filter (NB973) was later included (Ly et al. 2012a,b).

2.2. Optical Spectroscopy

The primary results of this paper are based on optical spectroscopy conducted with Keck's Deep Imaging Multi-Object Spectrograph (DEIMOS; Faber et al. 2003) and MMT's Hectospec (Fabricant et al. 2005). These spectrographs are complementary in sensitivity, spectral coverage, and multi-plexing capabilities. Specifically,
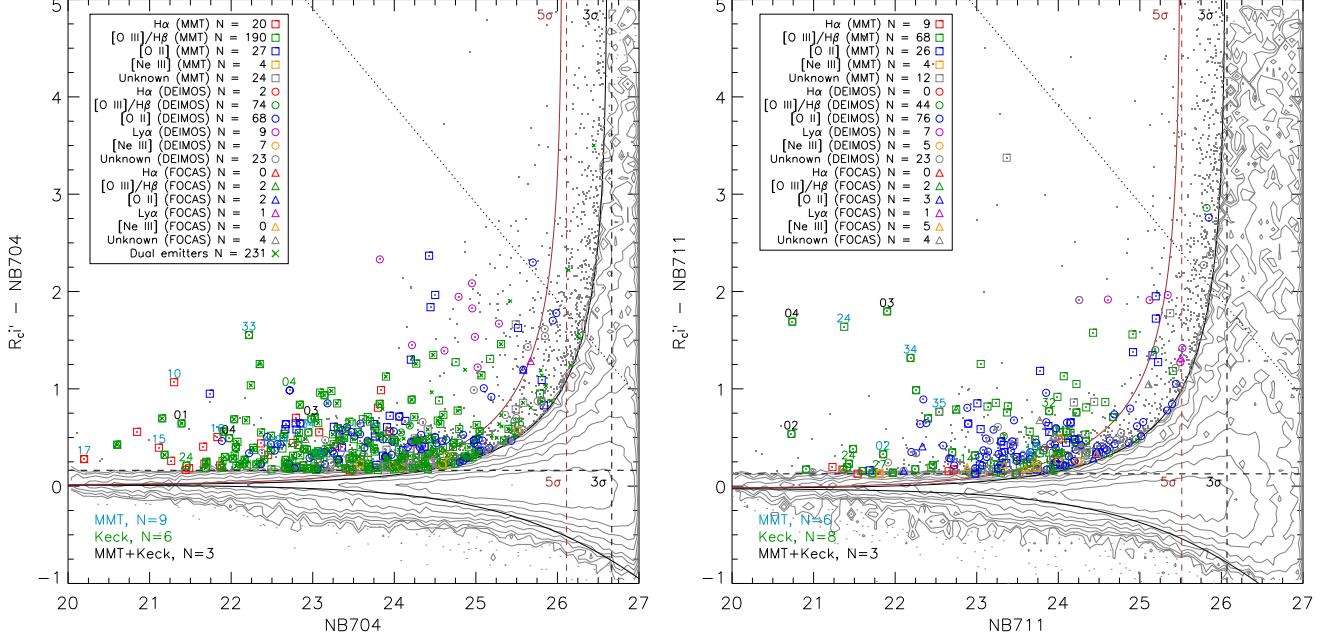
FIG. 1.— Narrowband excess plots for NB704 (left) and NB711 (right) excess emitters. Solid curves show detections that are significant at 5.0σ (brown) and 3.0σ (black). Contours of source densities are shown following logarithmic intervals. Spectroscopically targeted sources are overlaid with symbols representing different instruments: Keck/DEIMOS (circles), MMT/Hectospec (squares), and Subaru/FOCAS (triangles). Hα, [O III], [O II], Lyα, and unidentified sources are distinguished by red, green, blue, purple, and grey colors, respectively. Sources above the diagonal line are undetected in the R_C and i'-band at 3σ. Vertical lines refer to 3σ (black) and 5σ (brown) NB704 or NB711 magnitude limits. Galaxies in the [O III] $\lambda4363$-detected sample are labelled with their two-digit identification number in blue (MMT), green (Keck), and black (MMT+Keck).
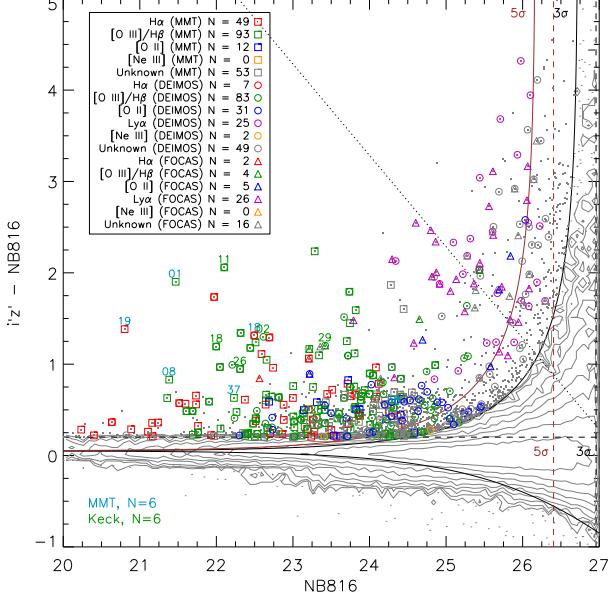
FIG. 2.— Same as Figure 1 but for NB816 excess emitters.

DEIMOS has greater sensitivity than Hectospec (especially above 8000 Å); however it can only target ≈100 galaxies within a $5'\times17'$ slitmask field-of-view, and lacks spectral coverage below ≈6000 Å. Hectospec, with optical fibers, can target up to ≈270 galaxies over a much larger 1° diameter field-of-view, and has spectral coverage extending down to ≈3700 Å. To maximize the scientific productivity of observing time on both spectrographs, we use Hectospec to primarily target our lower redshift sample ($z \lesssim 0.5$) and DEIMOS for the higher redshift sample ($z \gtrsim 0.6$). We include some overlap at

$z \sim 0.4$–0.65 to improve the spectral coverage (i.e., observe redder emission lines, e.g., Hα) and for consistency checks on emission-line measurements (see Section 2.3 for further discussion). In total, we obtain 3243 optical spectra for 1911 narrowband/intermediate-band excess emitters (roughly 20% of our narrowband/intermediate-band excess samples), and successfully detect emission lines to determine redshift for 1493 galaxies or 78% of the targeted sample. A summary of the spectroscopically confirmed excess emitters is provided in Table 1.

As illustrated in Figures 1–4, our optical spectroscopy spans six magnitudes in luminosity and three magnitudes in narrowband or intermediate-band excess flux. Observations prior to 2014 targeted emission-line galaxies in a more uniform manner, while more recent observations utilized available information (narrowband/intermediate-band excess flux, previous spectra) to target galaxies where a high success rate of obtaining gas metallicities would be achieved. Specifically, there was a moderate bias toward galaxies with stronger nebular emission lines.

2.2.1. MMT/Hectospec Observing Program

The MMT observations were conducted on 2008-03-13, 2008-04-10/11, 2008-04-14, 2014-02-27/28, 2014-03-25, and 2014-03-28/31, and correspond to an equivalent of three full nights. The sky was either clear or had thin cirrus clouds, with seeing of $0''.7$–$1''.4$. We utilized the 270 mm^{-1} grating blazed at 5200Å, to yield spectral coverage of 3650–9200Å with a spectral resolution of ≈5 Å, at a dispersion of 1.2Å pixel^{-1}. Because of the queue observing mode for Hectospec, observations consisted of 60 to 120 minutes of on-source integration (each night), with 20–25 minutes for each individual exposure. A total of 1820 spectra that targeted
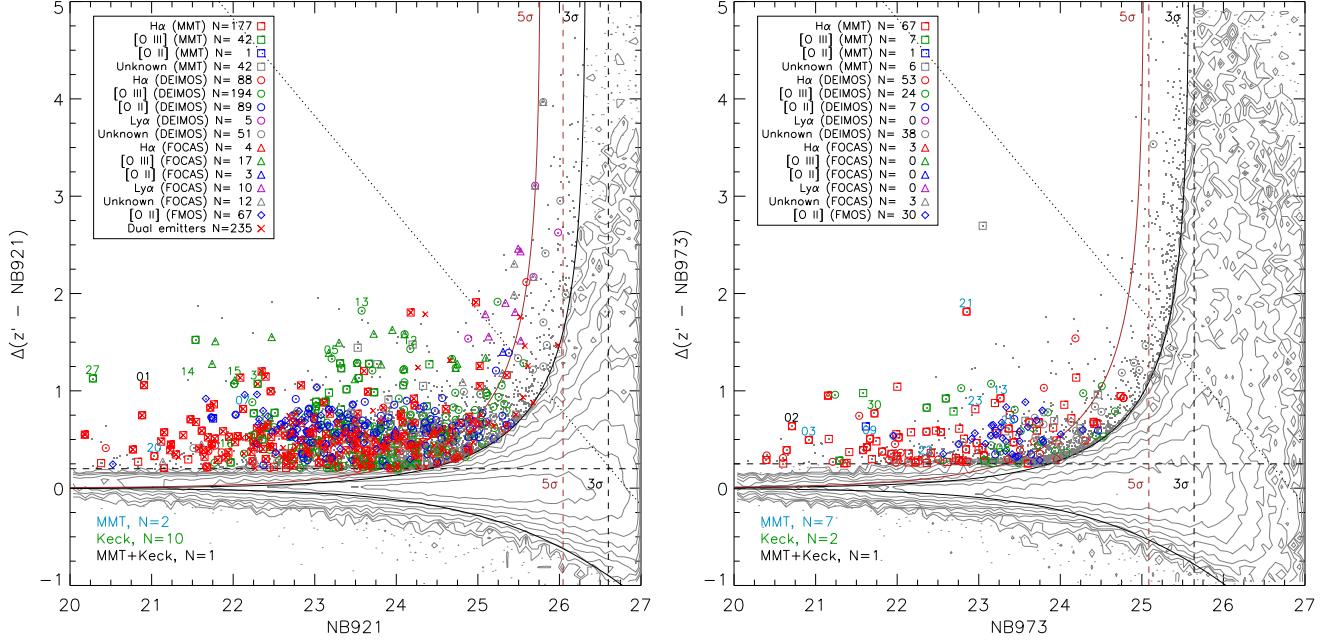
FIG. 3.— Same as Figures 1–2 but for NB921 (left) and NB973 (right) excess emitters. [O II] emitters that are spectroscopically confirmed with Subaru/FMOS (Hayashi et al. 2015) are shown as blue diamonds.
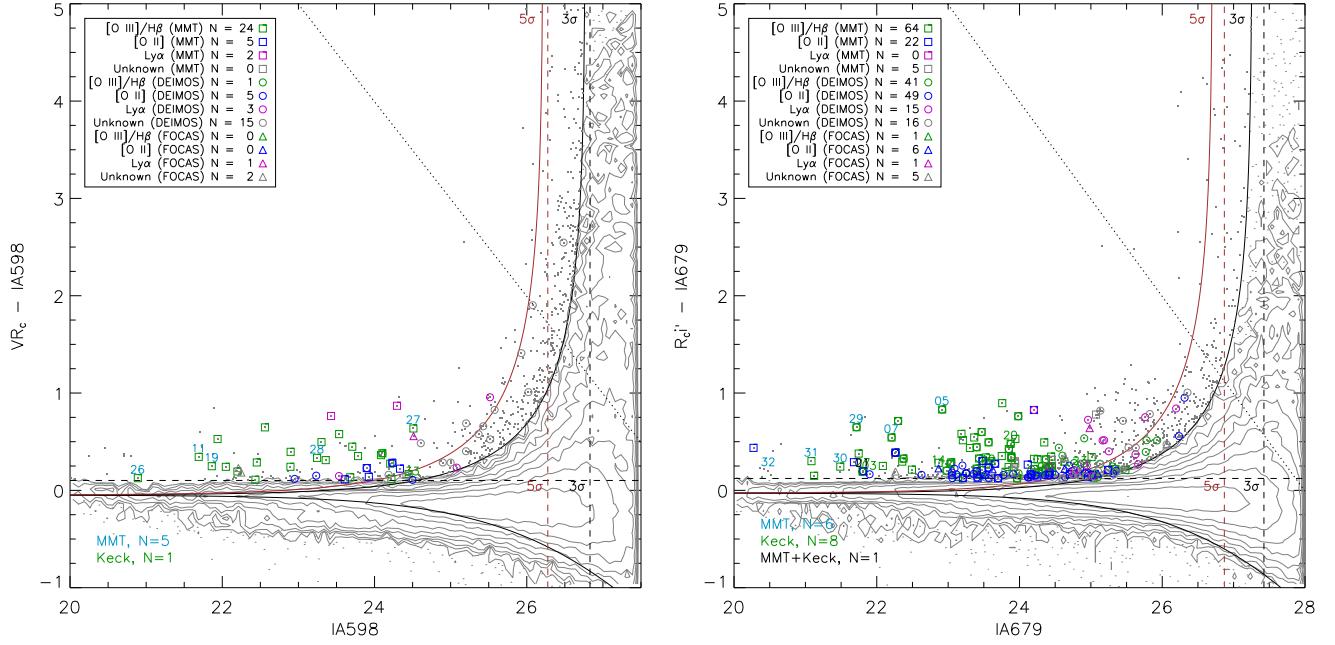
FIG. 4.— Same as Figures 1–3 but for IA598 (left) and IA679 (right) excess emitters.

845 narrowband/intermediate-band excess emitters were obtained. These MMT spectra provided redshifts for 708 galaxies (84% successful confirmation); the majority of the unsuccessful spectra targeted fainter galaxies. These observations were reduced using External SPECROAD,[7] an IRAF-based reduction pipeline developed by the Smithsonian Astrophysical Observatory, but with improvements by Juan Cabanela (Humphreys et al. 2011). Since spectra for any given source were obtained over multiple nights, we stacked the data, with weighting inversely proportional to the variance (σ^2) in the spec-

trum. In general, the root mean square noise in the spectrum improves as the square root of the integration time, t_{int}. The integration times vary between 80 and 725 minutes with an average (median) of 228 (220) minutes. The distribution of on-source integration times is illustrated in Figure 5.

2.2.2. Keck/DEIMOS Observing

The Keck observations were conducted on 2004-04-23/24, 2008-05-01/02, 2009-04-25/28, 2014-05-02, and 2015-03-17/19/26. The majority of the observations were obtained in 2014–2015. The 2004 spectroscopic observations have been discussed in Kashikawa et al. (2006) and

[7] http://astronomy.mnstate.edu/cabanela/research/ESPECROAD.
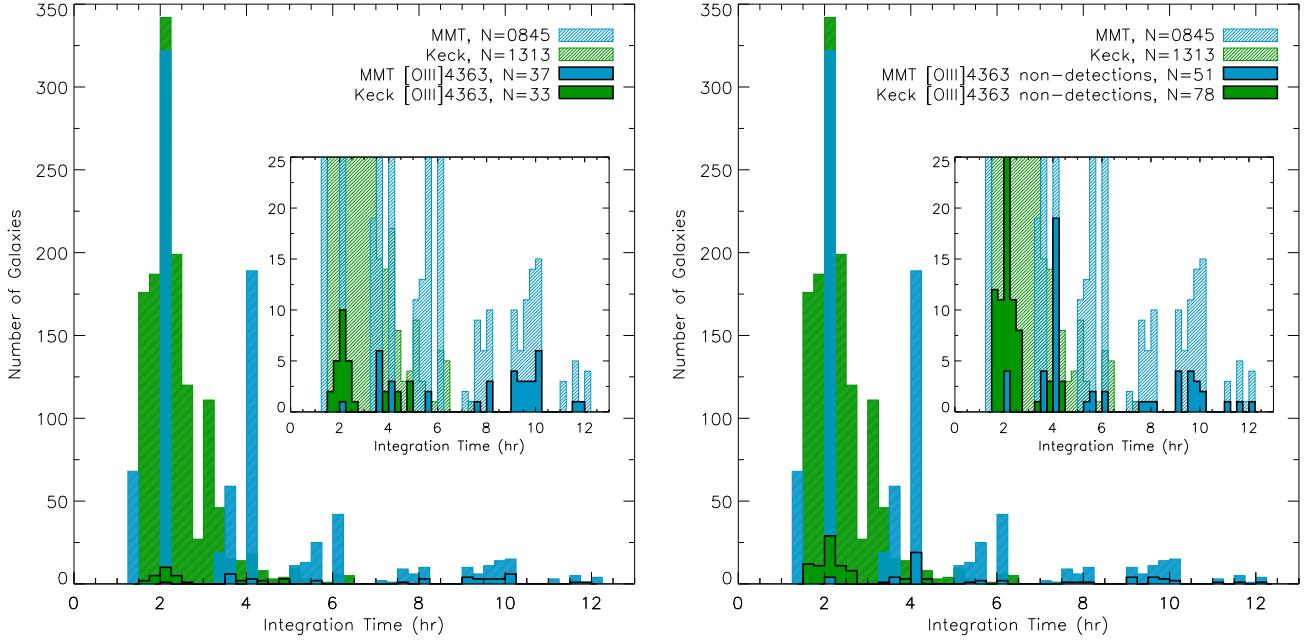
FIG. 5.— On-source integration time for MMT (blue shades) and Keck (green shades) spectroscopy. The full samples are shown by the line-filled distributions. The solid-filled distributions with black outlines show the [O III] $\lambda 4363$-detected and [O III] $\lambda 4363$-non-detected samples in the left and right panels, respectively.

Ly07, and the 2008–2009 data have been discussed in Kashikawa et al. (2011). In brief, we constructed 22 slit-masks with $1''$ slit widths, and used the 830 line mm^{-1} grating and GG495 order-cut filter. This configuration yielded a spectral resolution of $R \sim 3600$ at 8500Å, at a dispersion of 0.47Å $pixel^{-1}$. A total of 1423 spectra that targeted 1313 narrowband/intermediate-band excess emitters were obtained. These Keck spectra provided redshifts for 1031 galaxies (79% successful confirmation). The data were reduced using the Keck DEIMOS spec2d pipeline (Cooper et al. 2012),[8] with improvements made by Peter Capak.[9] A subset of our galaxy sample was observed twice on different dates with Keck. We stacked those data, following the same approach as described for MMT data. The on-source integration times, which vary between 91.0 and 447.8 minutes with an average (median) of 142 (120) minutes, are illustrated in Figure 5.

2.3. Accurate Flux Calibration of MMT and Keck Spectra

To obtain [O III] $\lambda 4363$-based metallicities, which use emission-line diagnostics from rest-frame ≈ 3700Å to ≈ 5010Å, proper flux calibration of our spectra is important. Since the spectroscopic data are obtained from two different instruments, MMT/Hectospec and Keck/DEIMOS, using different observational configurations (fibers versus slits) and in various observational conditions (seeing: $0''.5$–$1''.5$), we use the approach developed by Ly14 to flux calibrate and unify the spectroscopic data. The approach is as follows.

First, spectro-photometric standard stars are observed. These observations are generally obtained on the same night; however, in some cases, these calibration data are taken a few days apart.[10] For DEIMOS, the sensitivity is

not identical for all eight CCDs (four detectors for blue side, four for the red side). To address this issue, we dithered the telescope so that the same standard star is available in all detectors.

Reducing the calibration data in identical or similar ways to our science spectra, we determine the sensitivity function(s) using standard IRAF processing techniques (i.e., the *onedspec* package). We then apply these sensitivity functions to our data to yield "first-pass" flux-calibrated spectroscopic products.

Second, we examine the reliability of our flux calibration for each slit mask or fiber configuration by comparing them to broad-band photometric data. Here we only consider the brightest galaxies such that the continuum is well-detected. For the MMT and DEIMOS data, we restrict the calibration sample to $R_{\rm C} \leq 22.0$ mag and $i' \leq 23.0$ or 23.5 mag, respectively. This typically has ≈ 10–20 galaxies per set-up. To avoid the effects of OH skylines, we generate smoothed spectra where a boxcar median is used. From there we convolved our smoothed spectra against the filter responses and determine fluxes. These fluxes are compared against the photometric data to examine slit/fiber losses and if any wavelength-dependent corrections are needed. In most cases, specifically MMT/Hectospec observations, the comparison against photometric data only show a systematic offset due to fiber losses. For Keck/DEIMOS, we found that the photometric–spectroscopic comparison required an additional first-order wavelength-dependent correction.

Next, we compare the emission-line fluxes of the MMT and Keck spectra when galaxies are observed with both telescopes. In this analysis, we compare Keck measurements of several emission lines against those from MMT. We chose MMT as the reference because (1) Hectospec has an atmospheric dispersion compensator to correct

---

[8] http://deep.ps.uci.edu/spec2d/primer.html.
[9] http://www.astro.caltech.edu/~capak/software/deimos.html.
[10] For MMT, the Hectospec team provides all observers dur-

ing a semester with reduced spectra for a few spectrophotometric standards to use.

for wavelength-dependent fiber losses; (2) the spectral coverage is consistently the same unlike Keck slit spectroscopy, which depends on the position on the slitmask; and (3) independent analyses from the Hectospec instrument team have demonstrated that the MMT flux calibration is accurate and precise (Fabricant et al. 2008). For the MMT–Keck analyses, we perform them on each slitmask to ensure that the observing conditions did not affect measurements. To account for differences between MMT and Keck, we apply corrections on an individual source basis by determining the median offset based on several emission-line measurements. We illustrate the comparison before and after the median-based correction is applied for one Keck/DEIMOS slitmask in Figure 6. Table 2 summarizes the MMT–Keck comparison and the improvements with the median-based correction applied on an individual basis. We find that the steps taken to flux calibrate the spectra yield consistent fluxes between MMT and Keck, and the dispersion is further reduced when the median-based corrections are applied.

Finally, to ensure that the flux calibration is reliable, we use our measurements of nebular emission lines from narrowband imaging data to compare against the spectroscopic measurements. The narrowband excess fluxes are derived from a combination of narrowband and broadband fluxes:

$$F_{\text{Line}} = \Delta \text{NB} \frac{f_{\text{NB}} - f_{\text{BB}}}{1 - \epsilon(\Delta \text{NB}/\Delta \text{BB})}, \qquad (3)$$

where f_{NB} and f_{BB} are the flux densities for the narrowband and broadband filters, respectively, in units of erg s^{-1} cm^{-2} Hz^{-1}, and ΔNB and ΔBB are the FWHM of the filters. We use the spectroscopic redshift to correct the narrowband flux for when the emission line(s) falls in the filter's wing. This comparison is illustrated in Figure 7 for the MMT spectra and Figure 8 for Keck. For brevity, we present the comparison against MMT spectroscopic measurements for NB704 and NB816 excess emitters, and NB816 ad NB921 excess emitters for Keck measurements. Table 3 provides the accuracy and precision of the flux calibration based on comparison with narrowband excess fluxes. Typically, the accuracy is no more than ±0.05 dex with precision of ≲0.2 dex. These flux calibration comparisons against narrowband excess fluxes are conducted on individual spectra, as well as, stacked spectra. Overall, our flux calibration analyses suggest that we have conducted reliable flux calibration across the full spectral coverage for both MMT and Keck.

3. SAMPLE SELECTION FOR Paper II

3.1. *The [O III]λ4363-detected Sample*

To extract fluxes of emission lines in these spectra, we fit each emission line with a Gaussian profile[11] using the IDL routine MPFIT (Markwardt 2009). The expected location of emission lines was based on *a priori* redshift determined by either the [O III] or Hα (for lower redshift) lines. A local spectral median, $\langle f \rangle$, is computed within a 200Å-wide band, excluding regions affected by OH skylines and nebular emission lines. In addition, the standard deviation $\sigma(f)$ is measured locally. To determine the significance of emission lines, we integrate the

spectrum between $l_{\text{C}} - 2.5\sigma_{\text{G}}$ and $l_{\text{C}} + 2.5\sigma_{\text{G}}$, where l_{C} is the central wavelength and σ_{G} is the Gaussian width:

$$\text{Flux} \equiv \sum_{-2.5\sigma_{\text{G}}}^{+2.5\sigma_{\text{G}}} [f(\lambda - l_{\text{C}}) - \langle f \rangle] \times l'. \qquad (4)$$

Here, l' is the spectral dispersion (1.21Å pixel^{-1} for MMT and ≈0.47Å pixel^{-1} for Keck). We then compute the signal-to-noise (S/N) of the line by dividing the integrated flux by:

$$\text{Noise} \equiv \sigma(f) \times l' \times \sqrt{N_{\text{pixel}}}, \qquad (5)$$

where $N_{\text{pixel}} = 5\sigma_G/l'$.

Adopting a minimum significance threshold of 3σ, we identify 67 and 119 [O III] λ4363 detections with MMT and Keck, respectively. We visually inspected each [O III] λ4363 detection. For MMT, we find that OH sky-lines contaminated [O III] λ4363 in 14 cases and Hβ in one other galaxy. For two galaxies, we lack spectral coverage of [O III], and for another 13 galaxies, the [O III] λ4363 detections are marginal or are likely affected by cosmic rays. Cosmic rays are easily identified when narrow peaks (less than a spectral resolution element) are seen. We classify detections as marginal when a visual comparison of the strength of the [O III] λ4363 line against the local root mean square in the spectra indicated that such detections may be misjudged as being above S/N = 3. This results in a final MMT sample of 37 [O III] λ4363 detections. This sample includes 12 of the 14 MMT detections from our previous study (Ly14), with two galaxies (MMT06 and MMT12) not meeting the [O III] λ4363 S/N = 3 cut.[12] For Keck, OH sky-lines contaminated [O III] λ4363 in 55 cases and [O II] measurements in 1 other case, while 20 galaxies lack full spectral coverage (missing [O II], Hβ, and/or [O III] λλ4959,5007),[13] and 10 spectra were affected by cosmic rays on [O III] λ4363 or exhibited active galactic nucleus (AGN) properties (e.g., broad emission lines). This reduced the [O III] λ4363 Keck sample to 33 galaxies. This includes all six Keck detections from our previous study (Ly14). A subset of the MMT and Keck [O III] λ4363 detections are shown in Figure 9. The full spectra are provided in Figures 10–16 for MMT and Figures 17–22 for Keck. Four of our [O III] λ4363-detected galaxies have both MMT and Keck spectra, providing independent confirmations. Thus, our final sample of [O III] λ4363 detections consists of 66 galaxies. We refer to the overlapping cases, from MMT and Keck, as the merged sample with IDs of MK01 to MK04. The MMT and Keck spectra for these galaxies are shown in Figure 23. A summary of our [O III] λ4363-detected sample is provided in Tables 4 and 5, and we provide the emission-line fluxes for strong and weak emission lines in Tables 6 and 7.

Emission-line luminosities and rest-frame equivalent widths (EW$_0$) are illustrated in Figure 24. The emission-line luminosities are primarily determined from spectroscopy, with the exception of a subset of galaxies where Hα measurements are unavailable (indicated with red squares in Figure 24), so we use either the NB921 or

---

[11] Since the [O II] λλ3726,3728 doublet is resolved with Keck, we fit both emission lines with a double Gaussian profile.

[12] MMT12 is in the [O III] λ4363-non-detected sample (see Section 3.2).

[13] There are four galaxies (Keck02, 04, 14, 29) that we include in our sample for various reasons. discussed in Ly14 and Table 6.
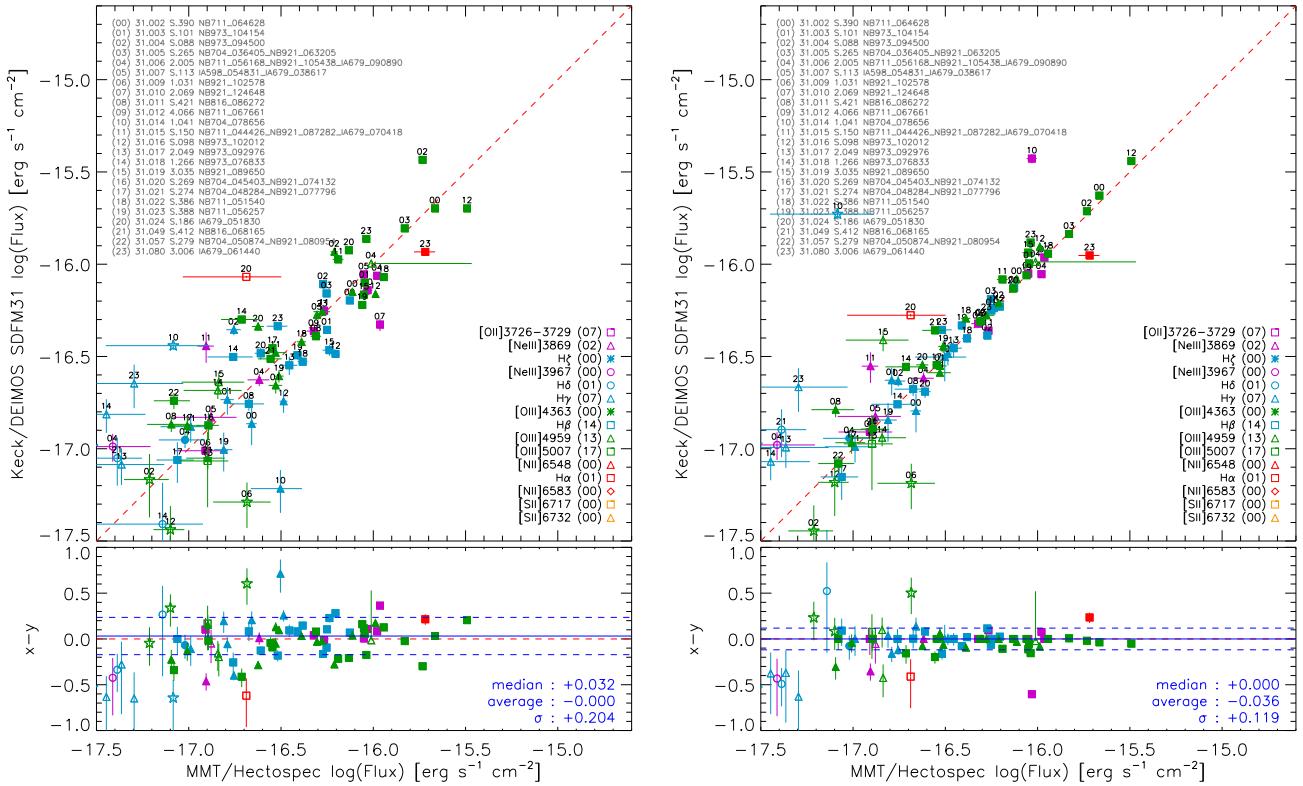
FIG. 6.— Illustration of the reliable emission-line fluxes obtained from Keck (y-axes) and MMT (x-axes). Here we compare measurements for one DEIMOS slitmask (SDFM31), which has 24 galaxies observed with both telescopes. Different color and symbols indicate nebular emission lines (see legend in the lower-right corner). Each data point is indicated with a two-digit number to specify the galaxy (see upper-left legend). The median, average, and dispersion are determined when emission lines are detected above S/N=3 by both MMT and Keck (filled points); unfilled data points are those with low S/N. The red dashed lines show one-to-one correspondence. The left panel illustrates the comparison in flux after applying (1) the sensitivity function of the instrument, and (2) slit-loss correction based on photometric data (see Section 2.3). The right panel illustrates the improvement, ≈2 lower in dispersion, after a median-based correction is applied for each individual galaxy. The bottom panels illustrate the difference with the median and 1-σ dispersion indicated by the blue solid and blue dashed lines, respectively. The results of the MMT–Keck comparisons are provided for all DEIMOS slitmasks in Table 2.

NB973 excess measurements. The line luminosity is $L = 4\pi d_L^2 F_{\rm Line}$, where d_L is the luminosity distance, and $F_{\rm Line}$ is the emission-line flux. The EWs are determined from the ratio of the measured emission-line flux and the continuum. Since the continuum is not always well-measured from spectra, we measure it from the broad-band SEDs, with corrections for emission-line contamination (see Section 4.4). In Figure 24, we compare our [O III] λ4363-detected sample against local galaxies from SDSS (grey points). Since Paper II will also incorporate metal-poor galaxies with [O III] λ4363-based metallicities from the DEEP2 Survey (Ly et al. 2015), we also overlay these DEEP2 galaxies as blue squares. Compared to local galaxies, the [O III] λ4363-detected sample consists of galaxies with higher emission-line EWs and luminosities. While this bias exists, it can be seen that the [O III] λ4363-detected sample spans 1.5 dex in EWs. Additionally, the [O III] λ4363-detected sample probes lower luminosities than Ly et al. (2015). The wide range in EW and luminosity is due to the deep spectroscopy of $\mathcal{MACT}$.

3.2. The [O III] λ4363-non-detected Sample

An advantage of our study is the significant number of deep optical spectra (see Figure 5). They supplement our primary sample of [O III] λ4363 detections, by providing reliable *upper limits* on T_e. The construction of a sample of reliable non-detections reduces the selec-

tion bias of targeting more strongly star-forming and/or metal-poor galaxies in our primary sample, which we discuss in Section 4.1 of Paper II. We construct our reliable [O III] λ4363-non-detected samples as follows:

First, we estimate the sensitivity for each spectrum based on the rms in the continuum near [O III]λ5007. The sensitivity varies by a factor of 2–3 between the deepest and shallowest observations (see Figure 5). Due to the inhomogeneity in the observations, we have chosen to adopt a [O III]λ5007 line flux limit that, to first order, corresponds to a minimum S/N of 100. By adopting a flux limit, rather than a S/N limit, it is more straightforward to model the selection function. Adopting a flux limit also include galaxies with very high [O III]λ5007 fluxes, but have shallow spectra. This results in a less biased selection than a S/N cut.

The flux limit is determined by considering the distribution of $100 \times \sigma([{\rm O\,III}]\lambda5007)$ in several redshift bins. To minimize selection bias, we adopt a less restrictive [O III]λ5007 flux limit that encompasses 85% of galaxies in each redshift bin. These flux limits for MMT and Keck are provided in Table 8.

These selections initially give us 67 galaxies from MMT and 132 from Keck. We then visually inspected the spectra for these galaxies and excluded those where [O III] λ4363 is compromised by nearby night skylines or telluric bands. This reduced the sample to 51 MMT and 78 Keck galaxies, 8 of which are in both [O III] λ4363-non-

TABLE 2
Comparison between MMT and Keck Spectroscopic Emission-line Fluxes

Mask Name	N	Before Median-based Correction			After Median-based Correction		
		Median (dex)	Average (dex)	σ (dex)	Median (dex)	Average (dex)	σ (dex)
(1)	(2)	(3)	(4)	(5)	(6)	(7)	(8)
SDFM01	1	+0.011	+0.016	0.041	0.000	+0.006	0.041
SDFM02	2	+0.044	+0.049	0.159	0.000	−0.034	0.081
SDFM04	0	...	...	...	...	...	...
SDFM06	1	−0.037	−0.095	0.097	0.000	−0.059	0.097
SDFM07	3	−0.009	+0.139	0.265	0.000	+0.018	0.110
SDFM10	1	+0.029	+0.036	0.025	0.000	+0.007	0.025
SDFM11	8	+0.077	+0.062	0.222	0.000	−0.001	0.187
SDFM22	1	+0.012	+0.012	...	0.000	0.000	...
SDFM24	2	+0.218	+0.253	0.415	0.000	+0.068	0.317
SDFM25	2	−0.074	−0.125	0.084	0.000	−0.025	0.090
SDFM27	1	−0.050	−0.099	0.146	0.000	−0.049	0.146
SDFM28	0	...	...	...	...	...	...
SDFM30	9	−0.010	+0.059	0.311	0.000	−0.041	0.164
SDFM31	24	+0.032	0.000	0.204	0.000	−0.036	0.119
SDFM32	14	−0.001	+0.017	0.248	0.000	−0.044	0.141
SDFM33	26	+0.052	+0.110	0.232	0.000	−0.008	0.108
SDFM34	26	−0.038	−0.004	0.137	0.000	−0.038	0.122
SDFM35	25	+0.005	+0.014	0.164	0.000	−0.030	0.111
SDFM36	30	+0.042	+0.072	0.213	0.000	−0.025	0.133
SDFM37	22	+0.046	+0.078	0.210	0.000	+0.001	0.165
SDFM38	22	+0.108	+0.140	0.221	0.000	−0.039	0.142
SDFM39	23	−0.030	+0.042	0.252	0.000	−0.047	0.164
Stacked	23	...	...	...	−0.003	−0.028	0.194

NOTE. — (1): Keck/DEIMOS mask name. (2): Number of galaxies with both MMT and Keck spectra. (3)–(5): Median, average, and dispersion for the difference between MMT and Keck spectroscopic fluxes *before* a median-based correction is applied on individual galaxies. (6)–(8): Median, average, and dispersion for the difference between MMT and Keck spectroscopic fluxes *after* a median-based correction is applied on individual galaxies. The median-based correction is discussed in Section 2.3. Differences in fluxes are provided in units of dex. An illustration of this MMT–Keck comparison is provided in Figure 6.
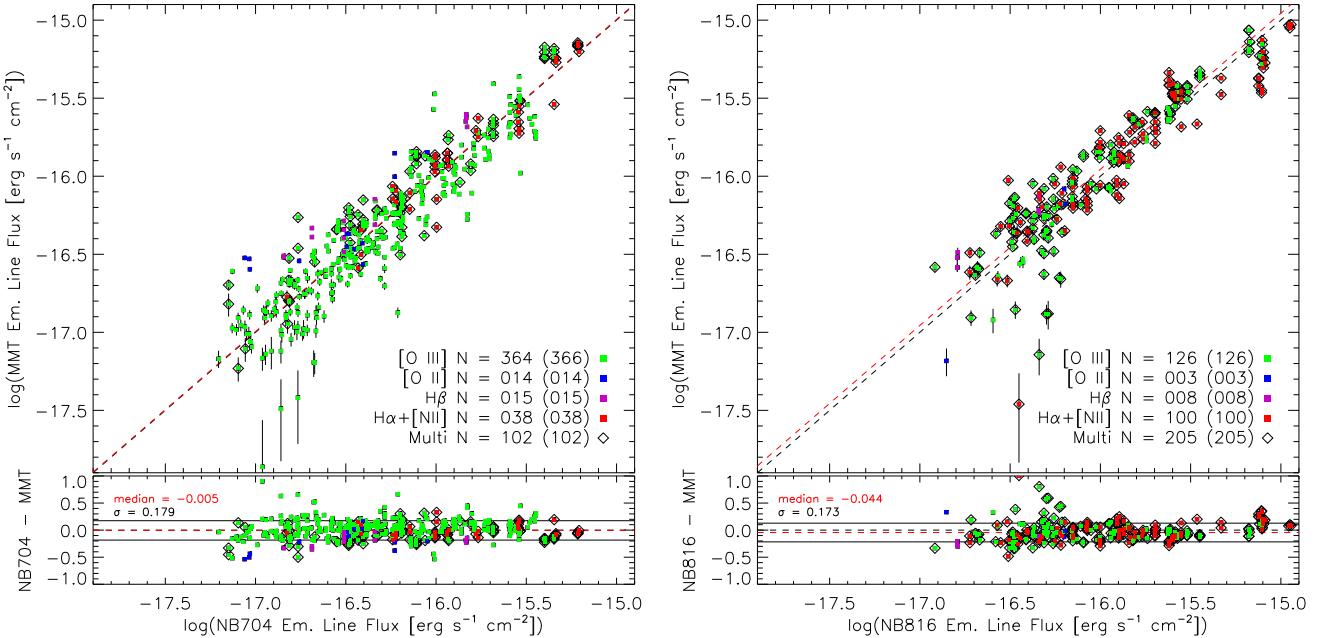
Fig. 7.— Comparisons between MMT/Hectospec emission-line flux measurements (y-axes) against NB704 (left) and NB816 (right) excess fluxes. The narrowband excess fluxes are derived from Equation 3. The top panels show the comparison while the bottom panels show the difference (narrowband excess flux – MMT fluxes) on the y-axes. Green, blue, purple, and red squares indicate [O III]λλ4959,5007, [O II], Hβ, Hα+[N II] excess emitters, respectively. Black diamonds indicate measurements with more than one emission line in the narrowband filter (e.g., the [O III] doublet, Hα and [N II]). The black dashed lines in the top and bottom panels show the median difference between narrowband excess fluxes and MMT emission-line fluxes, while the black solid lines in the bottom panels show the 1σ dispersion. These comparisons illustrate a good agreement between photometric and spectroscopic measurements (red dashed lines indicate one-to-one correspondence), and demonstrate that the flux calibration is performed at a reliable level over 3 dex in emission-line flux. The results of the narrowband–spectroscopy comparison are provided in Table 3.
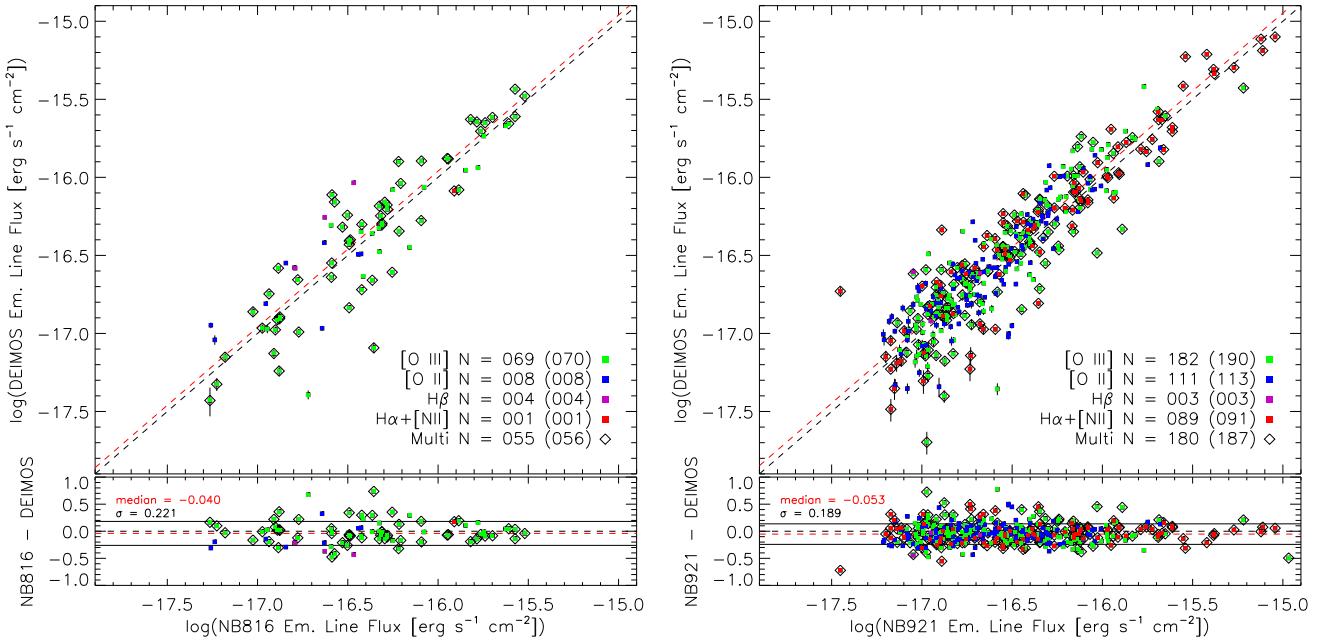
FIG. 8.— Same as Figure 7 but for Keck/DEIMOS measurements and comparisons are illustrated against NB816 (left) and NB921 (right) excess fluxes. The results of the narrowband–spectroscopy comparison are provided in Table 3.
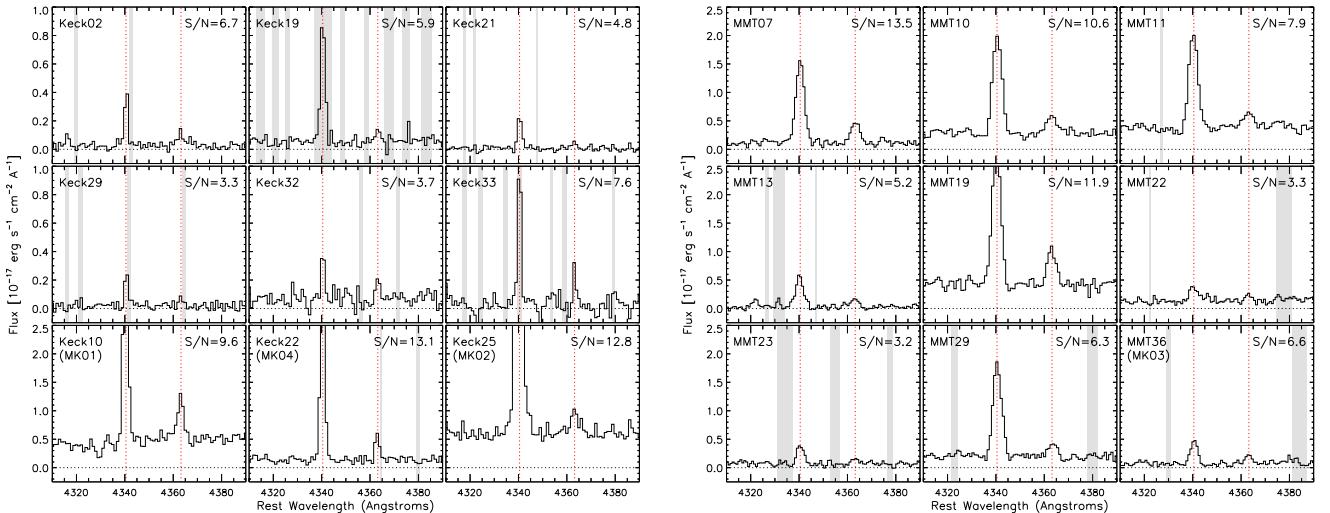
FIG. 9.— Detections of [O III] λ4363 in 18 galaxies, 9 with Keck (left) and 9 with MMT (right). These examples illustrate the full range of S/N (indicated in the upper right) present in our [O III] λ4363-detected sample. The rest-frame spectra are shown in black, with vertical red dashed lines indicating the locations of Hγλ4340 and [O III] λ4363. The wavelengths contaminated OH sky-lines are indicated by light grey vertical bands. The galaxy identifying names are provided in the upper left.
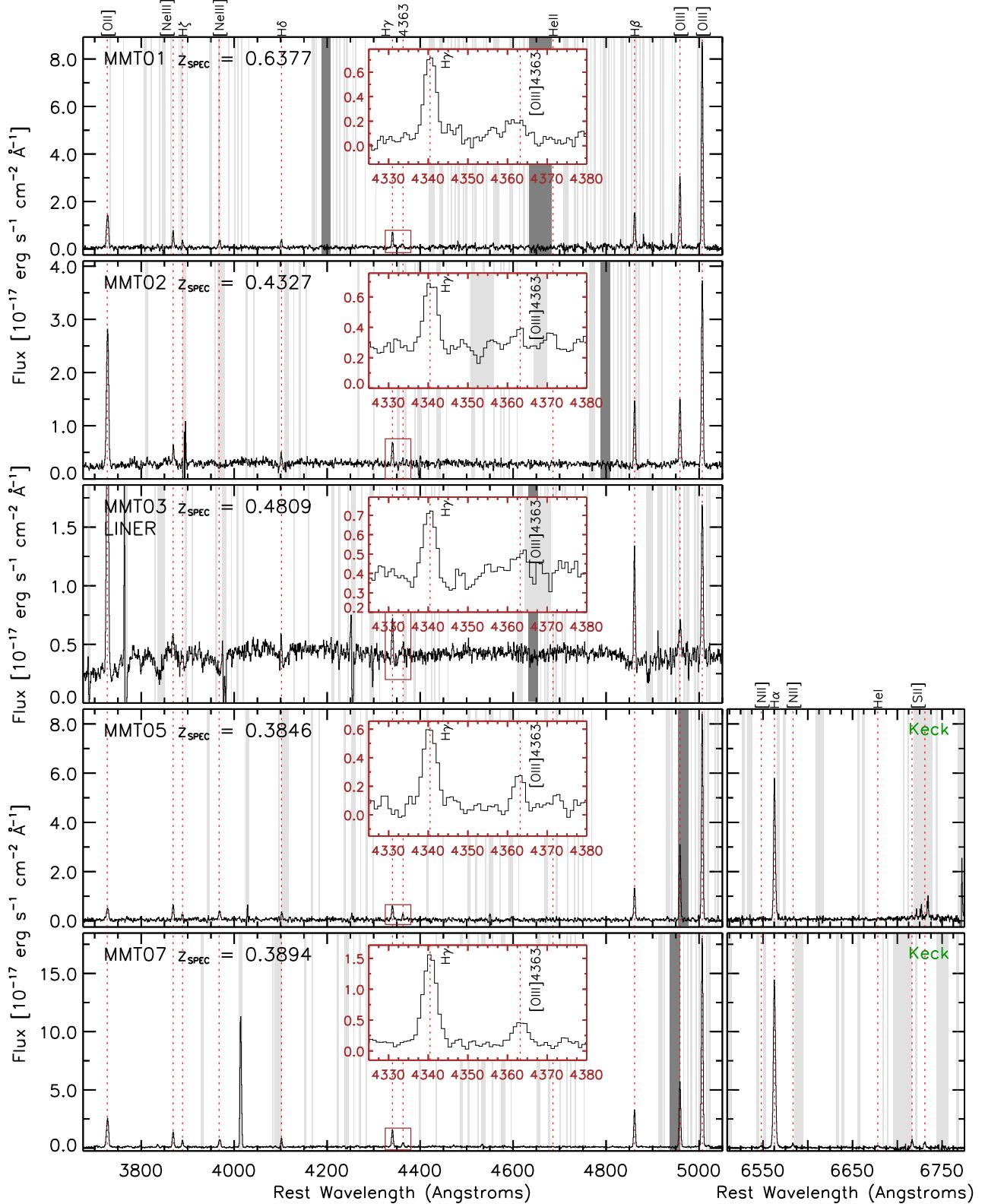
FIG. 10.— MMT spectra for a subset of [O III] λ4363-detected galaxies from the SDF. The blue-end of the spectra, spanning [O II] λ3727 to Hβ+[O III] λ5007, are shown on the left. Where available, we also illustrate (on the right) the red-end of the spectra that span Hα+[N II] λλ6548,6583 and [S II] λλ6717,6731. The insets provide a closer view on Hγ and [O III] λ4363 (rectangular region outlined in brown). For the right panels, Keck spectra are shown where available or if the Keck measurements are more reliable than MMT. The vertical light gray bands indicate spectral regions contaminated by night-sky lines while the darker grey bands indicate the telluric A- and B-bands. Nebular emission lines are indicated by the vertical dashed red lines.

12   Ly et al.
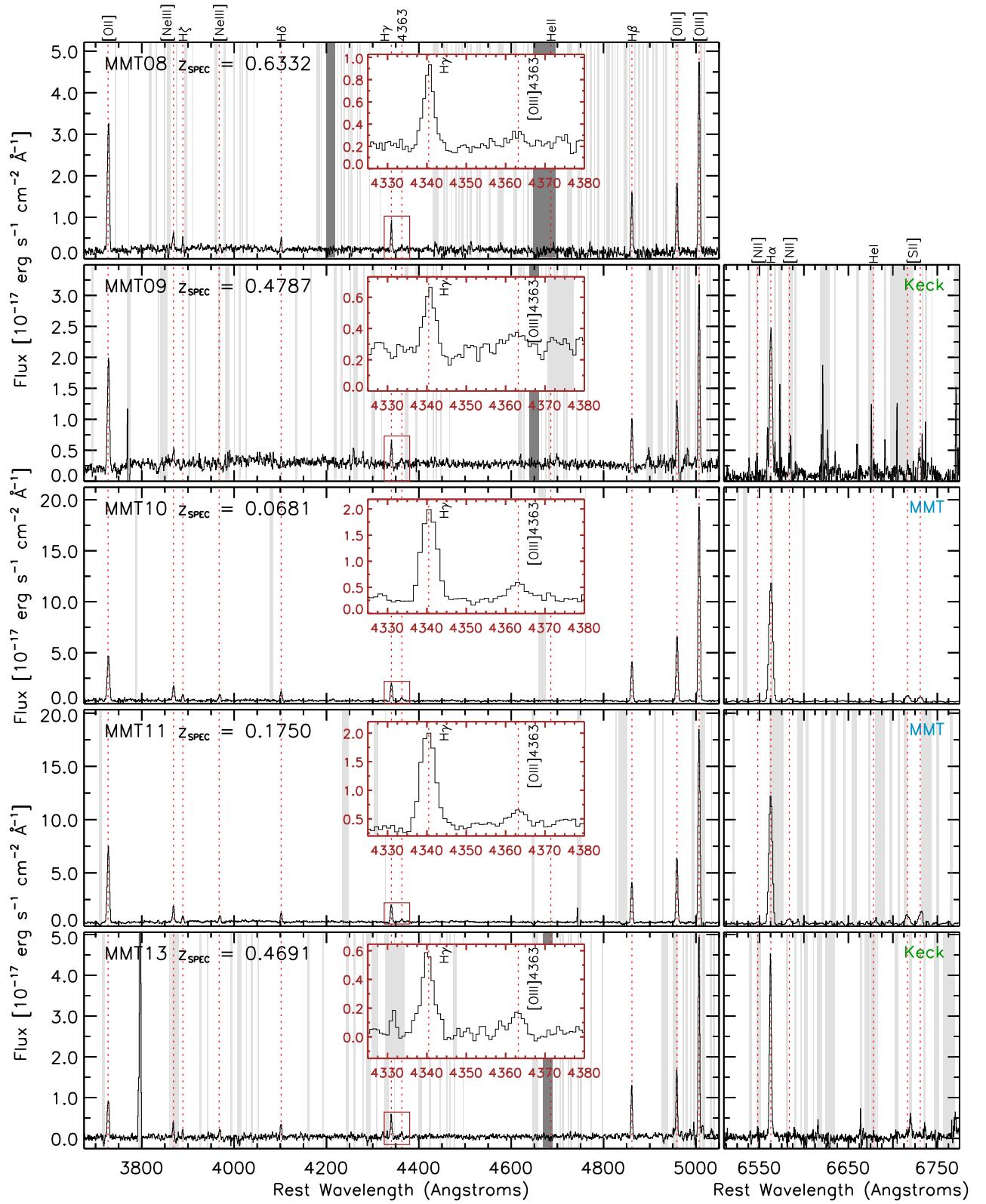
Fig. 11.— Same as Figure 10.
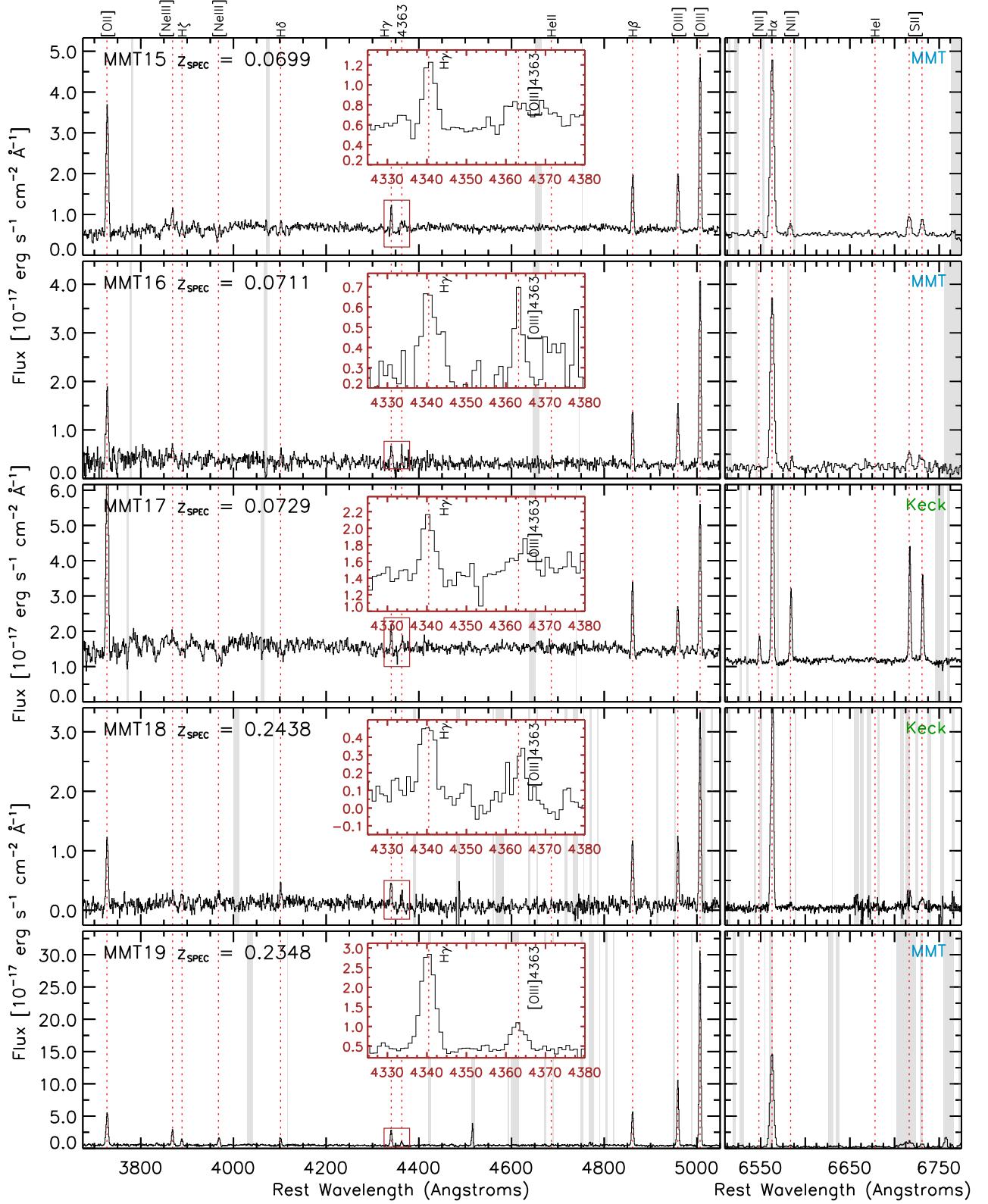
FIG. 12.— Same as Figures 10–11.
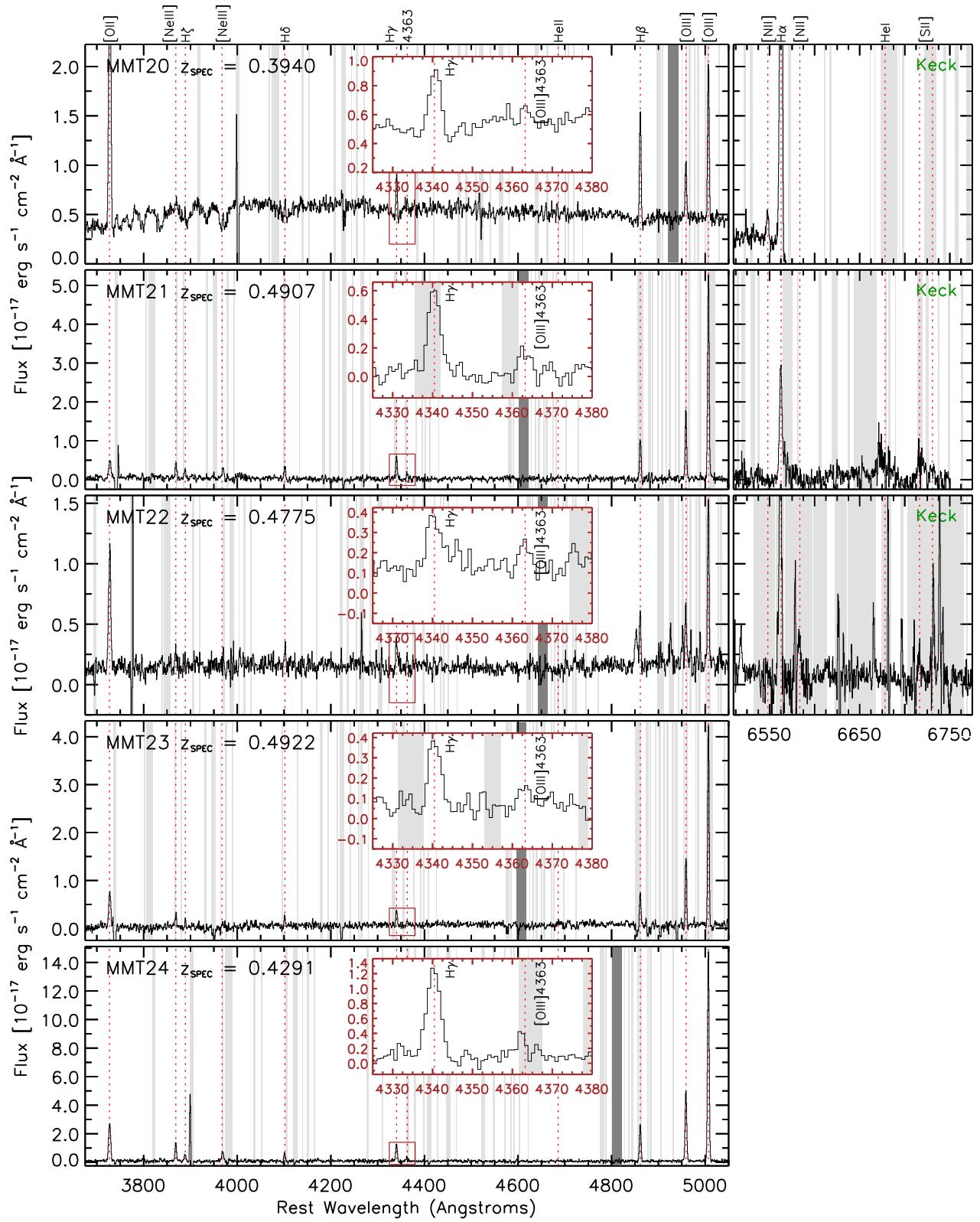
Fig. 13.— Same as Figures 10–12.
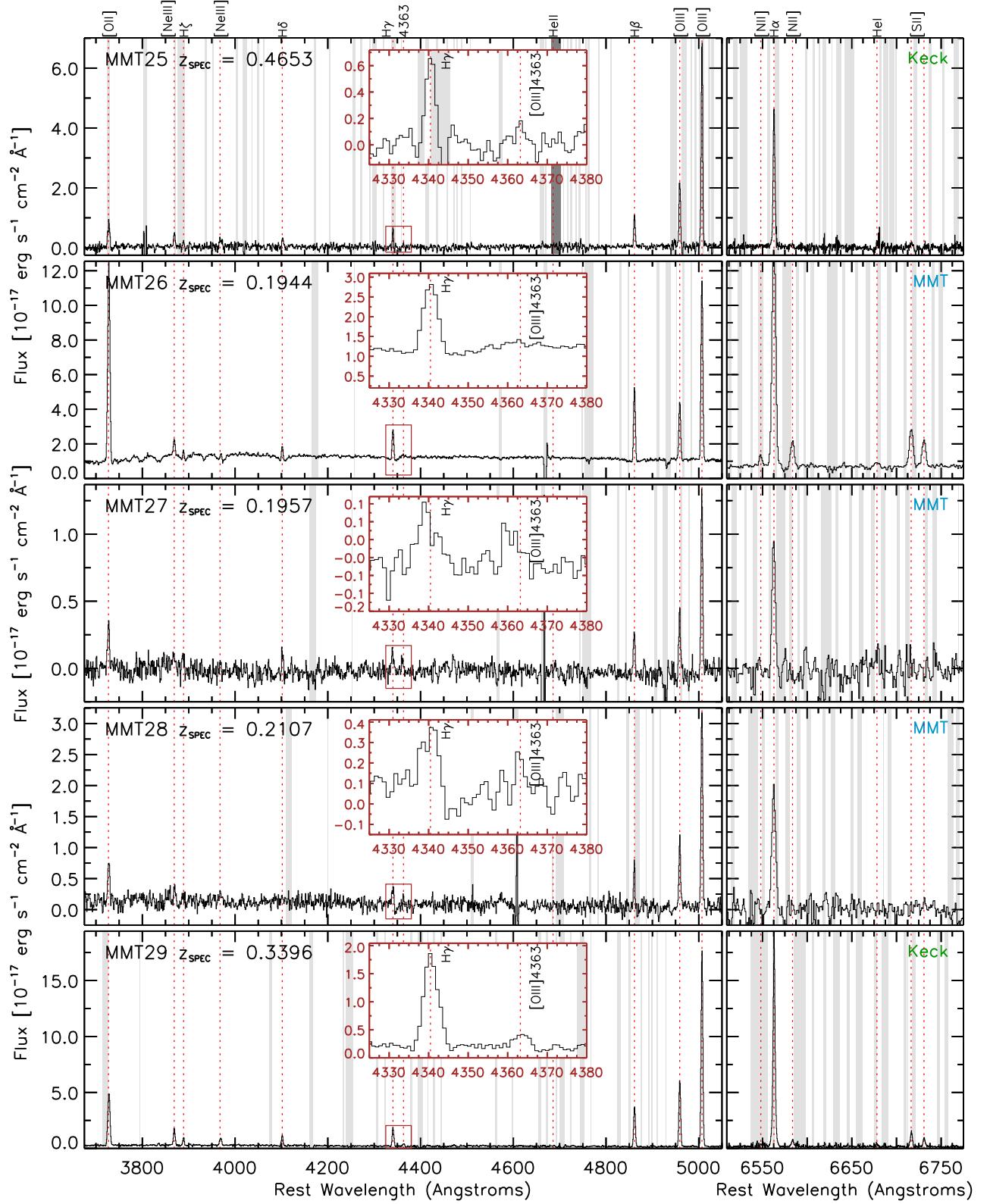
FIG. 14.— Same as Figures 10–13.
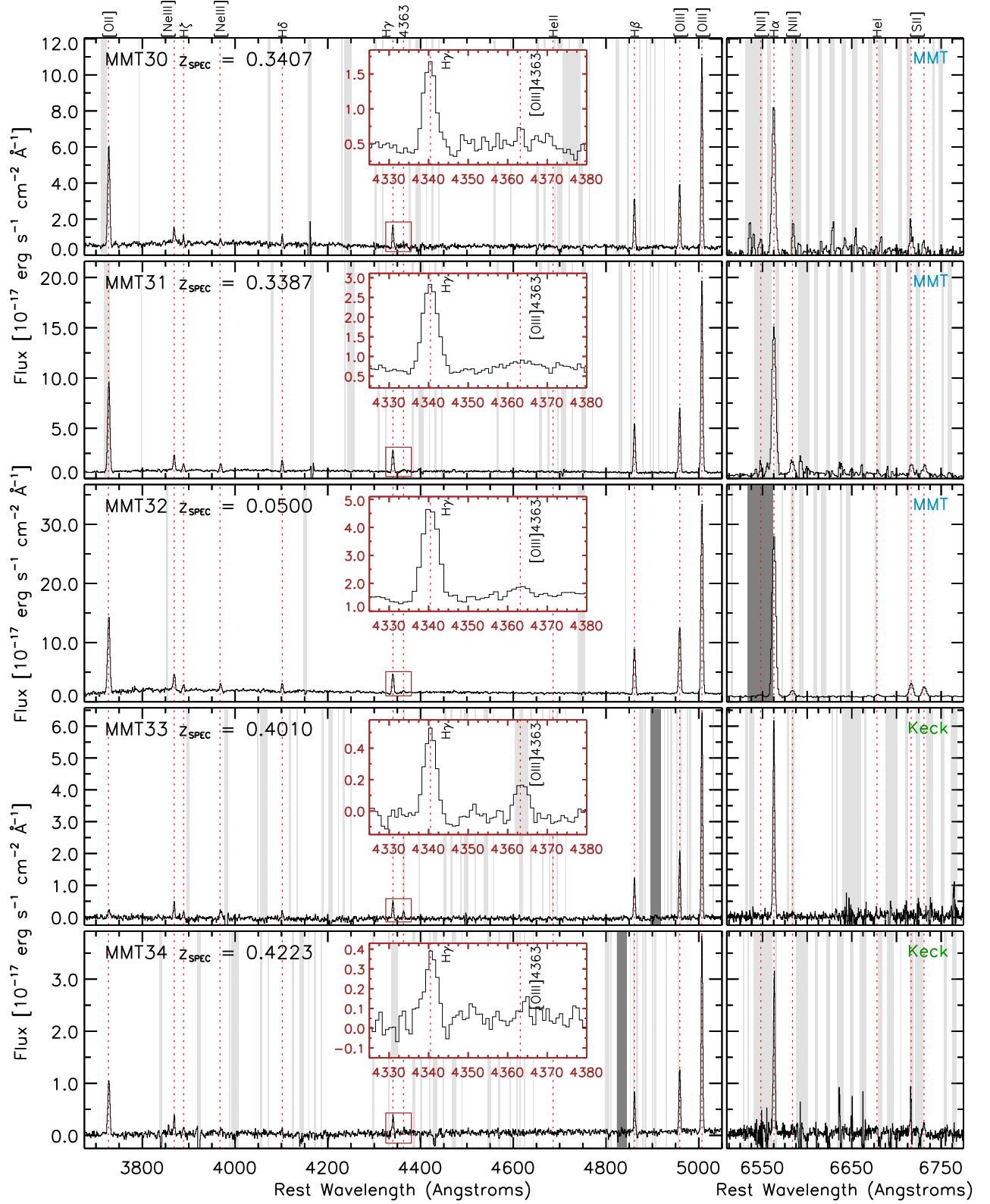
FIG. 15.— Same as Figures 10–14.
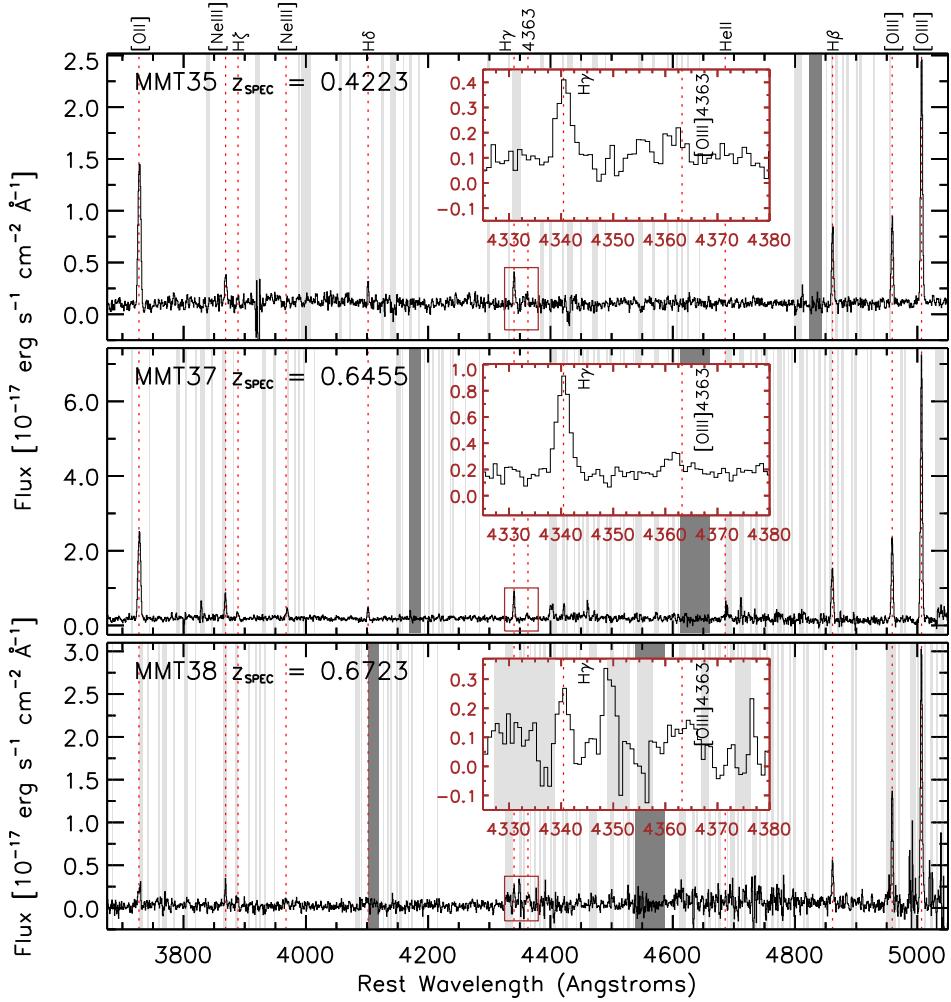
Fig. 16.— Same as Figures 10–15.

TABLE 3
Comparison between Spectroscopic and
Narrowband Excess Fluxes

Filter		Individual			Stacked	
	N	Median	σ	N	Median	σ
		(dex)	(dex)		(dex)	(dex)
(1)	(2)	(3)	(4)	(5)	(6)	(7)
MMT/Hectospec Spectroscopy						
NB704	433	−0.005	0.179	158	0.000	0.176
NB816	237	−0.044	0.173	88	−0.044	0.144
NB921	90	+0.036	0.282	25	+0.061	0.139
Keck/DEIMOS Spectroscopy						
NB704	147	−0.078	0.204	...	...	...
NB816	82	−0.040	0.221	...	...	...
NB921	385	−0.053	0.189	...	...	...
NB973	73	+0.041	0.244	...	...	...

Note. — (1): Filter name. (2)–(7): Number of galaxies (N) with detections of nebular emission lines that are responsible for the narrowband excess, and median and dispersion difference between spectroscopic fluxes and narrowband excess fluxes. Comparisons are made against individual spectra (Cols. 2–4), as well as, stacked spectra (Cols. 5–7).

detected samples. We refer to these 8 galaxies as MK05 to MK12. We illustrate the [O III] $\lambda4363$-non-detected samples in Figure 25. Compared to galaxies with [O III] $\lambda4363$ detections, these plots show that our non-detection limits extend to lower [O III] $\lambda4363$/[O III]$\lambda5007$

flux ratio, and hence lower T_e (higher metallicity). A summary of our [O III] $\lambda4363$-non-detected sample is provided in Tables 9 and 10.

The above [O III] flux limits are adopted to define the [O III] $\lambda4363$-non-detected samples. For analyses involving the $M_\star$–Z relation and its dependence on SFR, which are presented in Paper II, we adopt stricter flux limits[14] to avoid galaxies with weaker emission lines. These stricter flux limits and the sample sizes are provided in Table 8 in parentheses. The [O III] $\lambda4363$-non-detected samples with the stricter flux limits consist of 40 galaxies from MMT and 63 from Keck, with 5 galaxies in both [O III] $\lambda4363$-non-detected samples. For clarity, we indicate those that are excluded with the stricter flux limit in Tables 9 and 10.

4. DERIVED PROPERTIES

4.1. *Dust Attenuation Correction from Balmer Decrements*

To correct the emission-line fluxes for dust attenuation, we use Balmer decrement measurements (Hα/Hβ and Hγ/Hβ) obtained from a combination of our spectroscopy and narrowband imaging. Since the lines in our [O III] $\lambda4363$-detected emission-line galaxies tend to

---

[14] Encompass 75% of the distribution in $100 \times \sigma$([O III]$\lambda5007$).
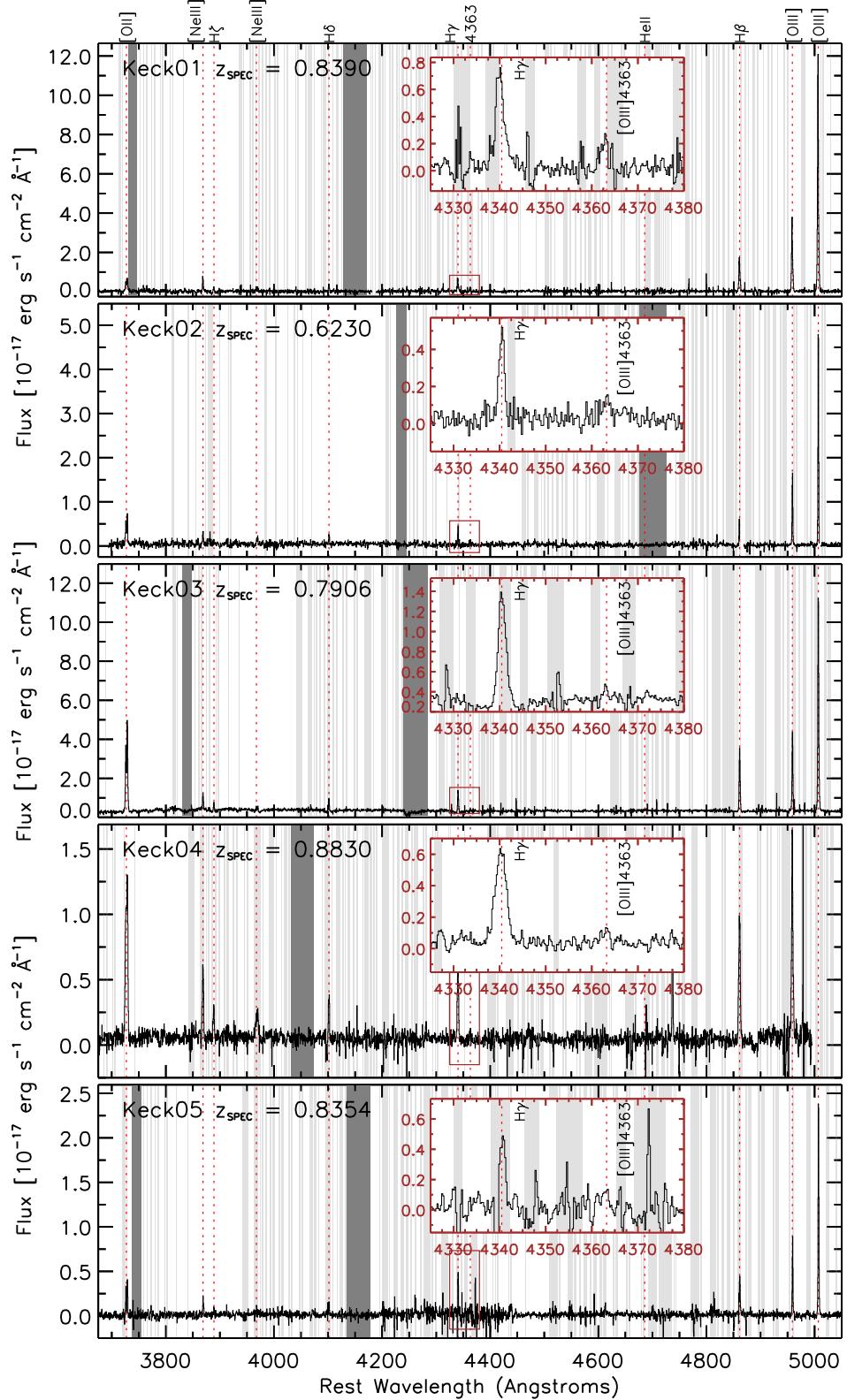
FIG. 17.— Keck spectra for a subset of [O III] λ4363-detected galaxies from the SDF. The blue-end of the spectra, spanning [O II] λ3727 to Hβ+[O III] λ5007, are shown on the left. Where available, we also illustrate (on the right) the red-end of the spectra that span Hα+[N II] λλ6548,6583 and [S II] λλ6717,6731. The insets provide a closer view on Hγ and [O III] λ4363 (rectangular region outlined in brown). For the left panels, we also overlay the MMT spectra (where available) in light blue when the Keck spectra lacks the bluest spectral coverage. The vertical light gray bands indicate spectral regions contaminated by night-sky lines while the darker grey bands indicate the telluric A- and B-bands. Nebular emission lines are indicated by the vertical dashed red lines.
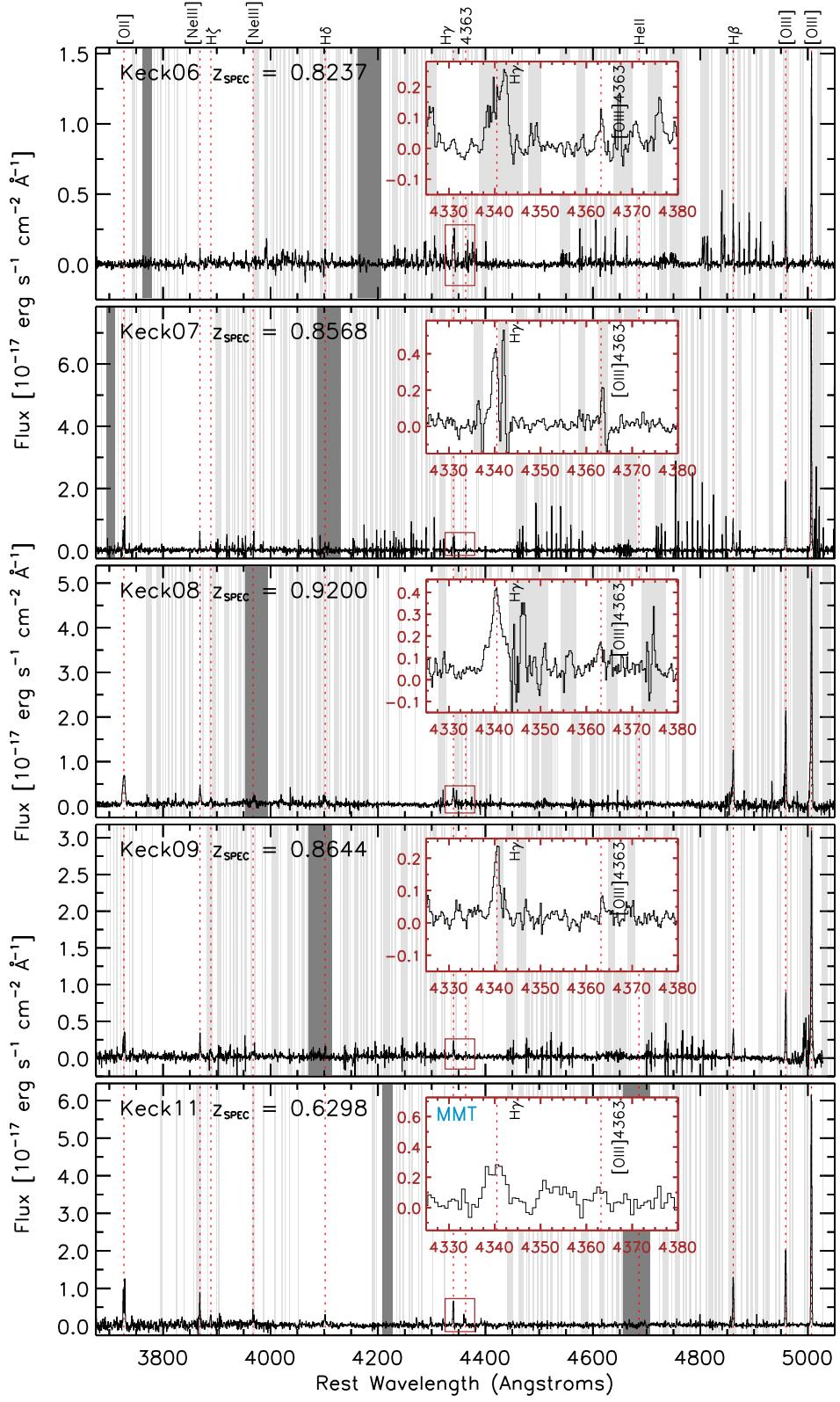
Fig. 18.— Same as Figure 17. The MMT spectrum is illustrated for the inset of Keck11 since [O III] λ4363 is contaminated by a cosmic ray in the Keck spectrum.
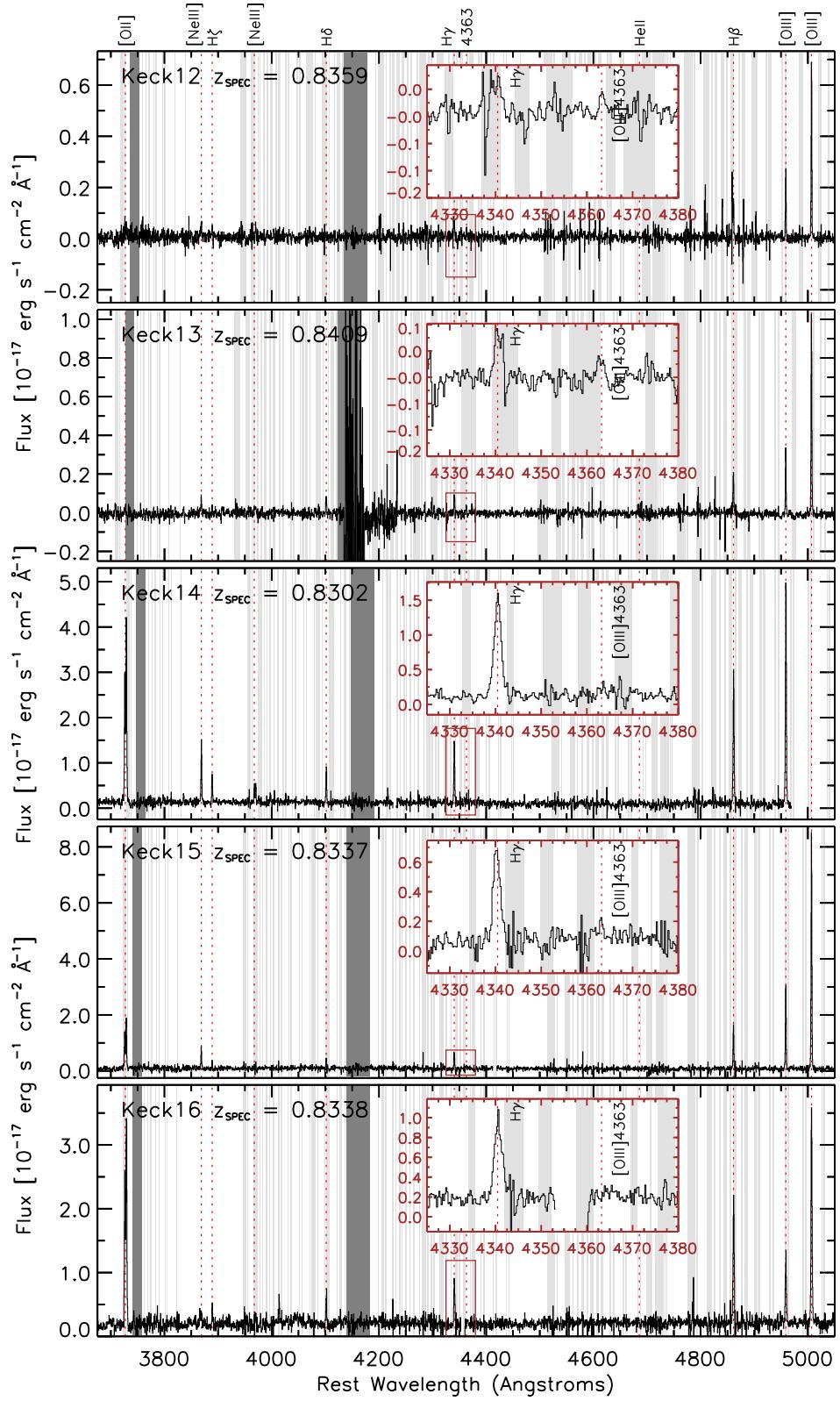
FIG. 19.— Same as Figures 17–18.
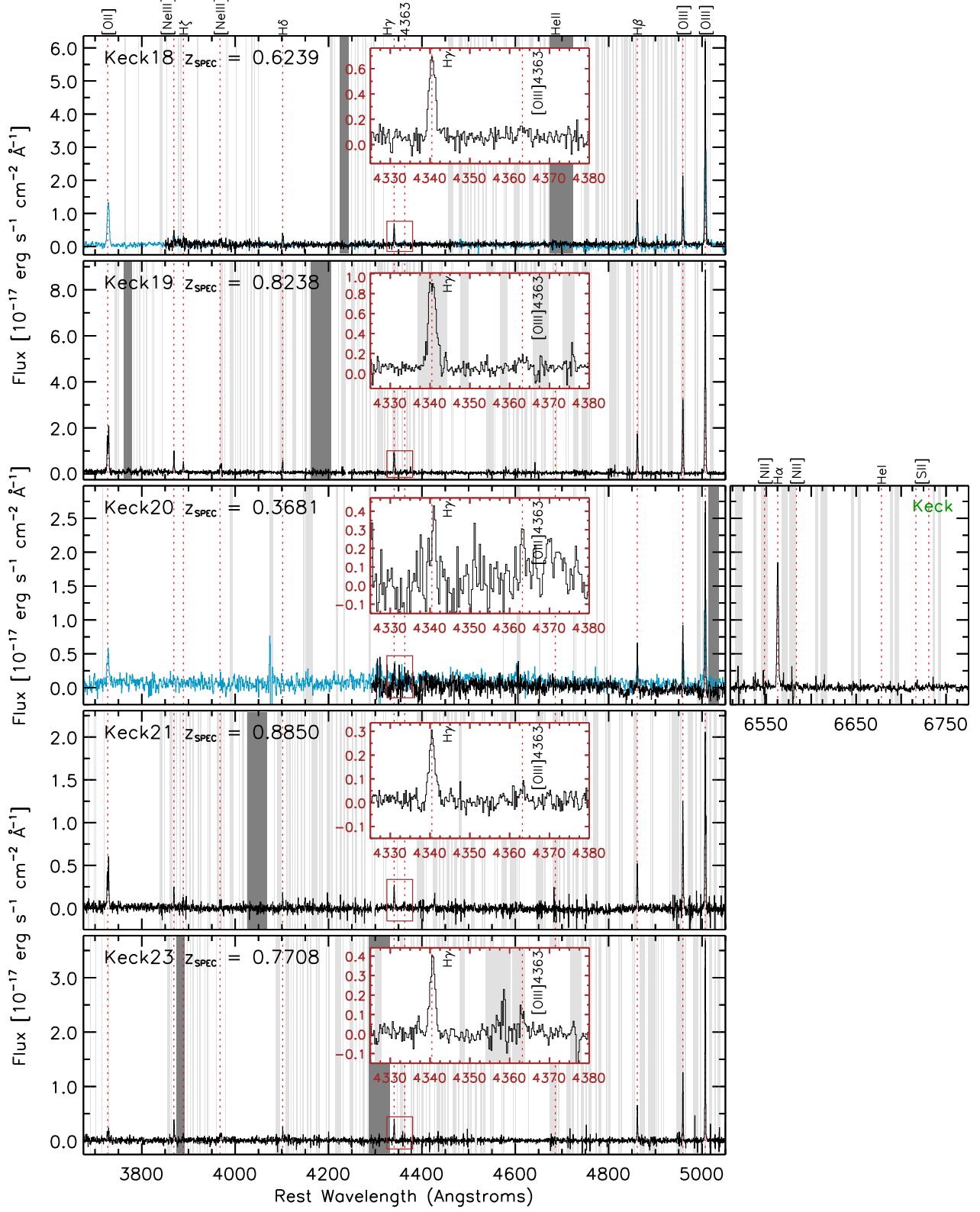
FIG. 20.— Same as Figures 17–19.
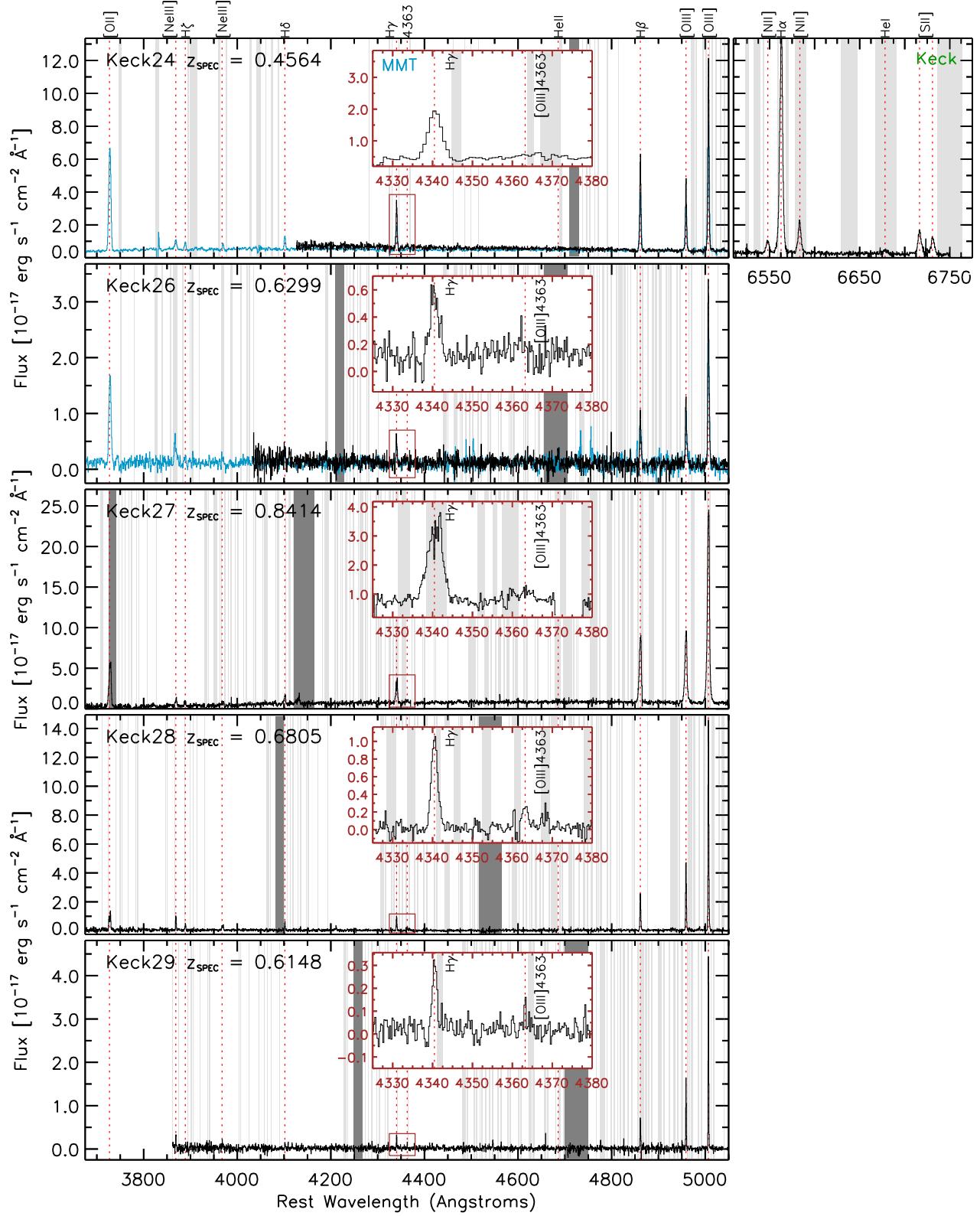
FIG. 21.— Same as Figures 17–20.
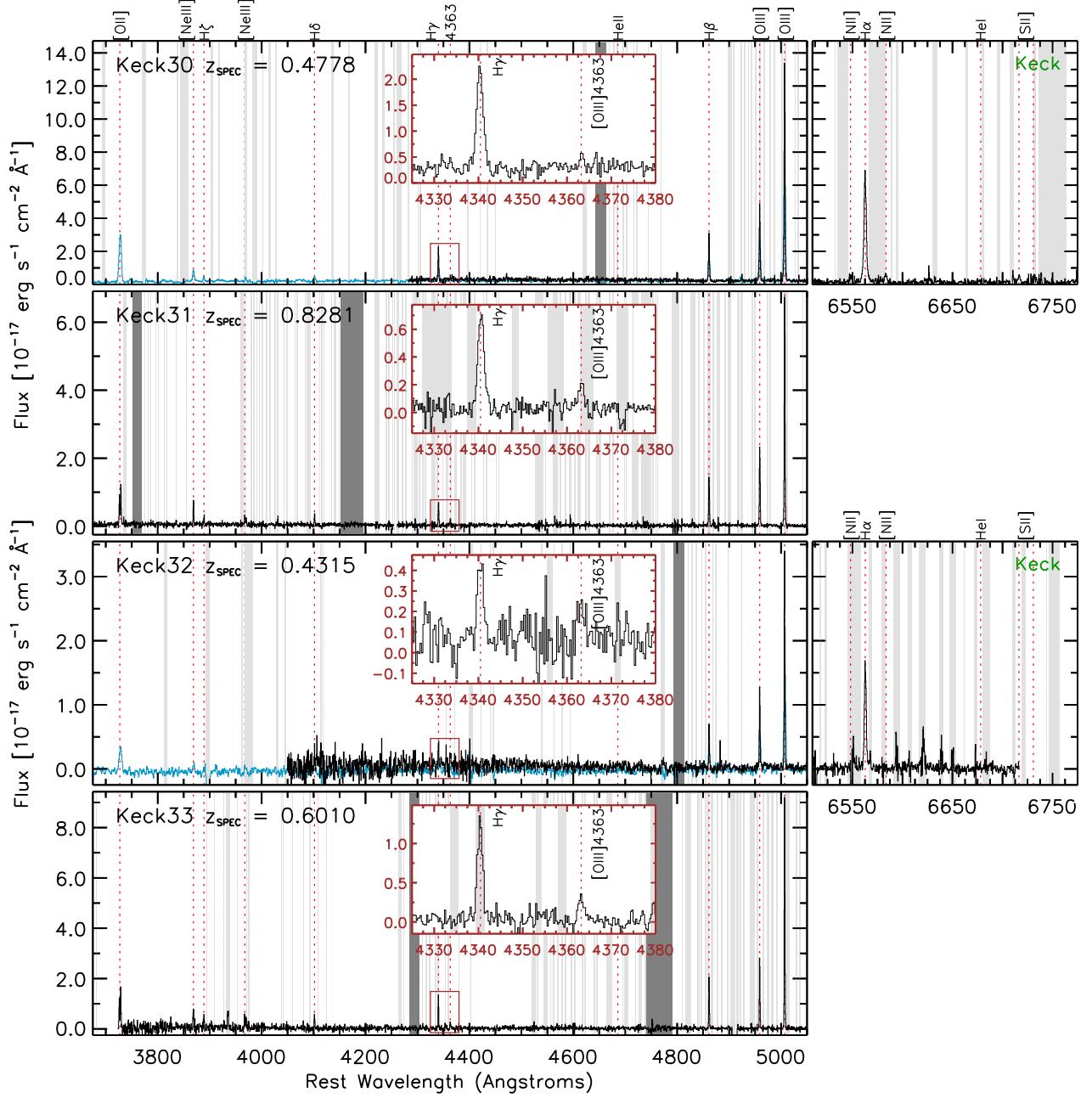
FIG. 22.— Same as Figures 17–21.
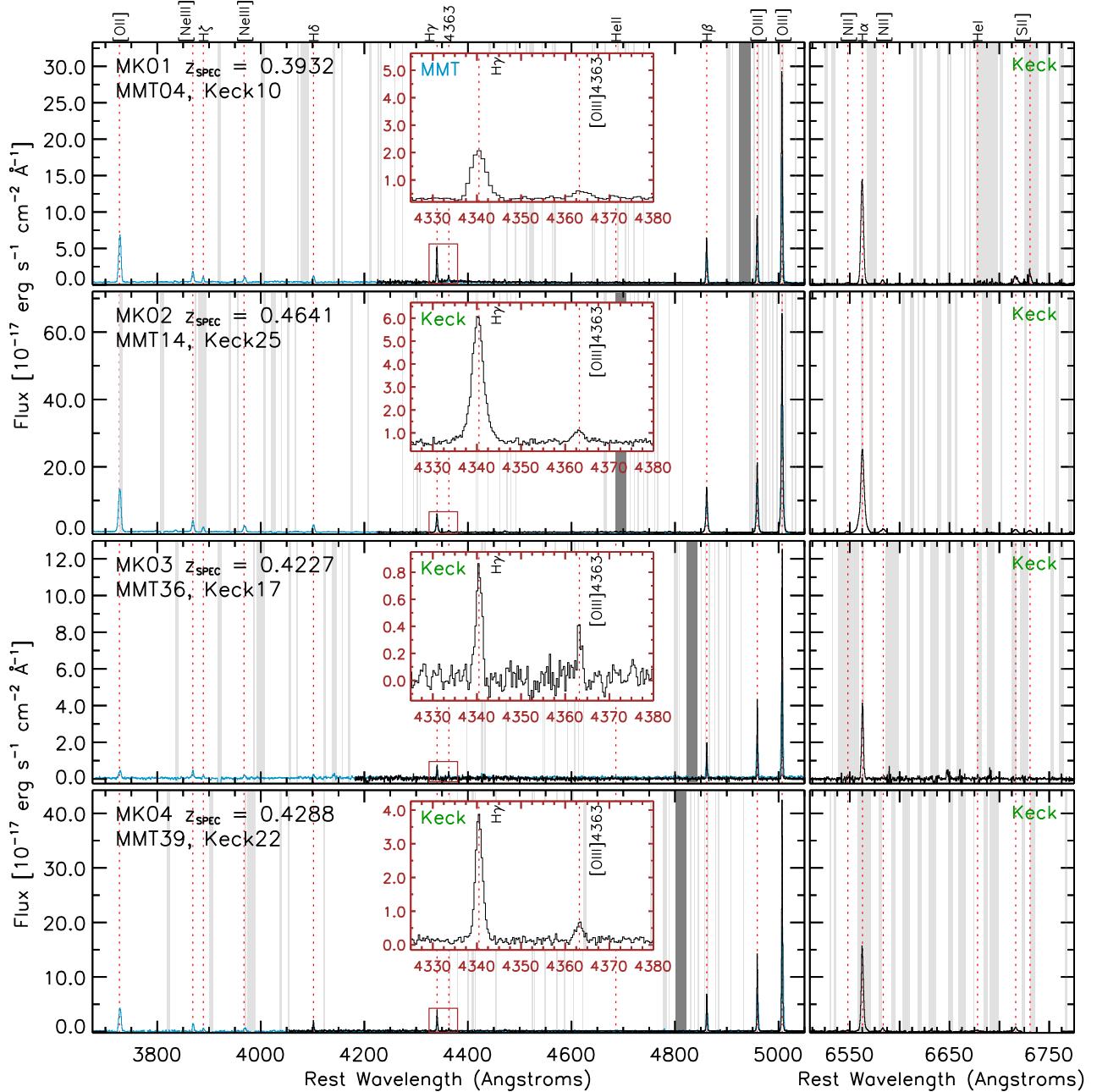
FIG. 23.— Same as Figures 10–22 but for galaxies where [O III] λ4363 is detected in both MMT and Keck spectra. The Keck spectra are illustrated in black (except for the inset panel for MK01), while MMT spectra are shown in light blue.

have high EWs, 42, 59, and 66 galaxies have Hδ, Hγ, and Hβ detected at $\gtrsim 10\sigma$, respectively. In addition, Hα measurements are available for 33 galaxies (i.e., half of the sample). For MMT23, the Hα flux is available from NB973 excess measurement. We note that for MMT03, the NB921 flux is not reliable for Balmer decrement determinations; MMT03 may suffer from significant [N II] contamination in the NB921 filter as a LINER candidate.

A significant problem encountered when using Balmer decrements to determine dust attenuation is correcting for the underlying stellar absorption. For a subset of our [O III] λ4363-detected sample, the spectra have sufficient signal-to-noise ratio in the continuum to fit and remove the stellar absorption, or use IRAF's splot command to re-measure the continuum from the absorption

trough. For the remaining galaxies, the S/N of our spectra are insufficient to model the stellar absorption. To correct these galaxies, we adopt $EW_{abs}(H\delta) = 2$Å and $EW_{abs}(H\gamma) = 1$Å. These values correspond to thresholds where the amount of stellar absorption is difficult to measure from visual examination. We assume the stellar absorption under Hβ and Hα is negligible. This is reasonable, since the measured rest-frame emission-line EWs are very large (Hβ: median of 54Å, average of 82Å; see Figure 24). The stellar absorption corrections are provided in Table 11, and the Balmer decrements are illustrated in Figure 26.

Under the assumption that the hydrogen nebular emission originates from a optically thick region and undergoes Case B recombination, the intrinsic Balmer flux
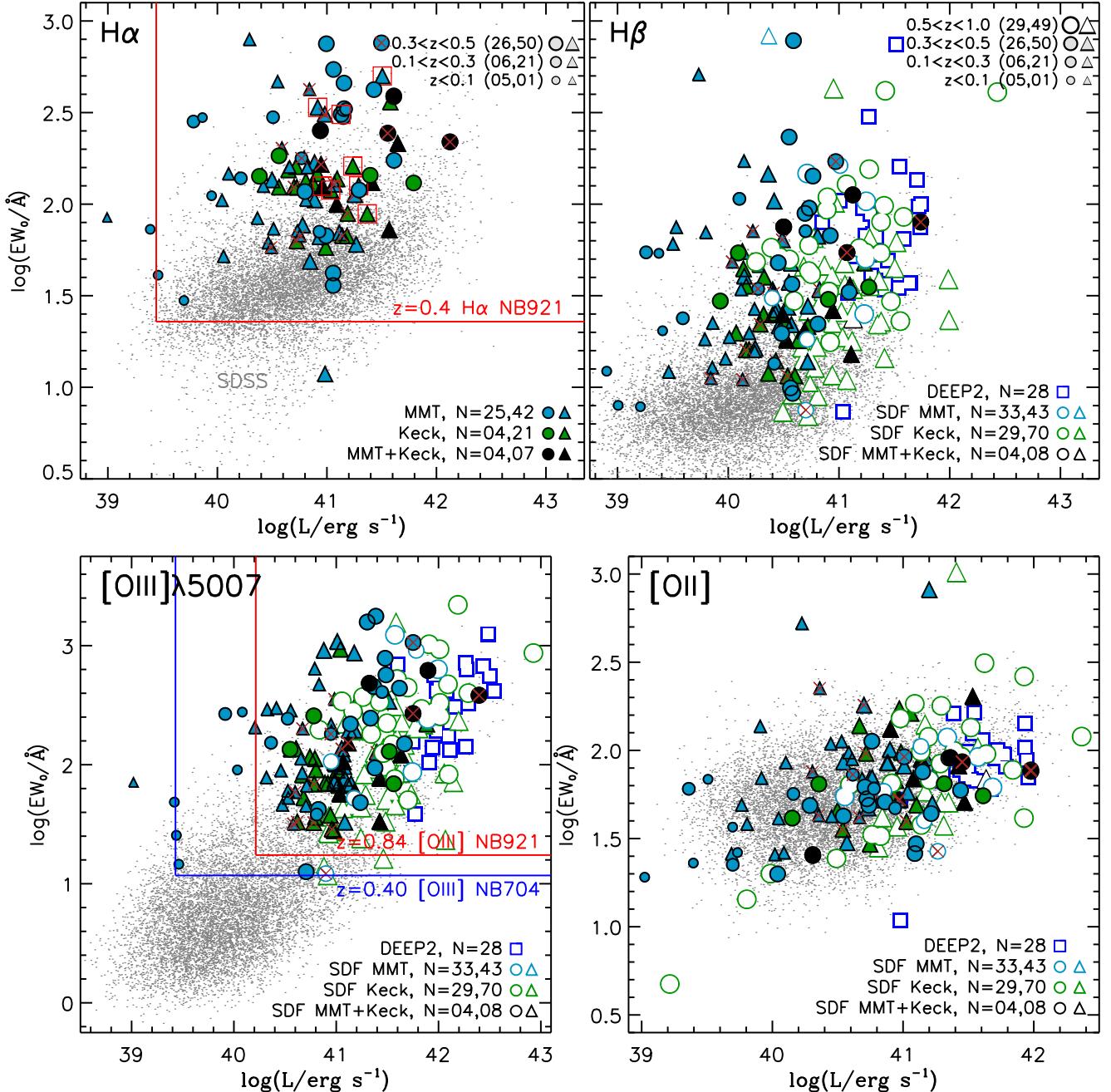
FIG. 24.— Emission-line luminosities and rest-frame EWs for our [O III] λ4363-detected (circles) and [O III] λ4363-non-detected (triangles) samples from MMT (light blue), Keck (green), and both (black). The triangles show galaxies that have a lower limit on metallicity. Filled points are galaxies with Hα measurements. Red squares in top left panel identify those with Hα fluxes from NB921 or NB973 excess fluxes. All fluxes are observed, before correction for dust attenuation. The size of the data points indicates the redshift of the galaxies. Gray points illustrate the SDSS DR7 sample with at least 5σ detections in all four emission lines. In addition, we overlay the $z \sim 0.8$ Ly et al. (2015) DEEP2 [O III] λ4363-detected sample as dark blue squares. Compared to local galaxies, the [O III] λ4363-detected and [O III] λ4363-non-detected samples consist of galaxies with higher emission-line EWs and luminosities. While this bias toward stronger nebular emission exists, it can be seen that the samples span 1.5 dex in EWs. Also, the [O III] λ4363-detected and [O III] λ4363-non-detected samples probe lower luminosities than Ly et al. (2015). The wide range in EW and luminosity is due to deep spectroscopy. For comparison, we show the EW and luminosity limits of our NB921 imaging (solid red lines) for $z = 0.4$ Hα (top left) and $z = 0.84$ [O III] (bottom left) and NB704 imaging (solid blue lines) for $z = 0.4$ [O III]. AGNs and LINERs are indicated by red crosses.
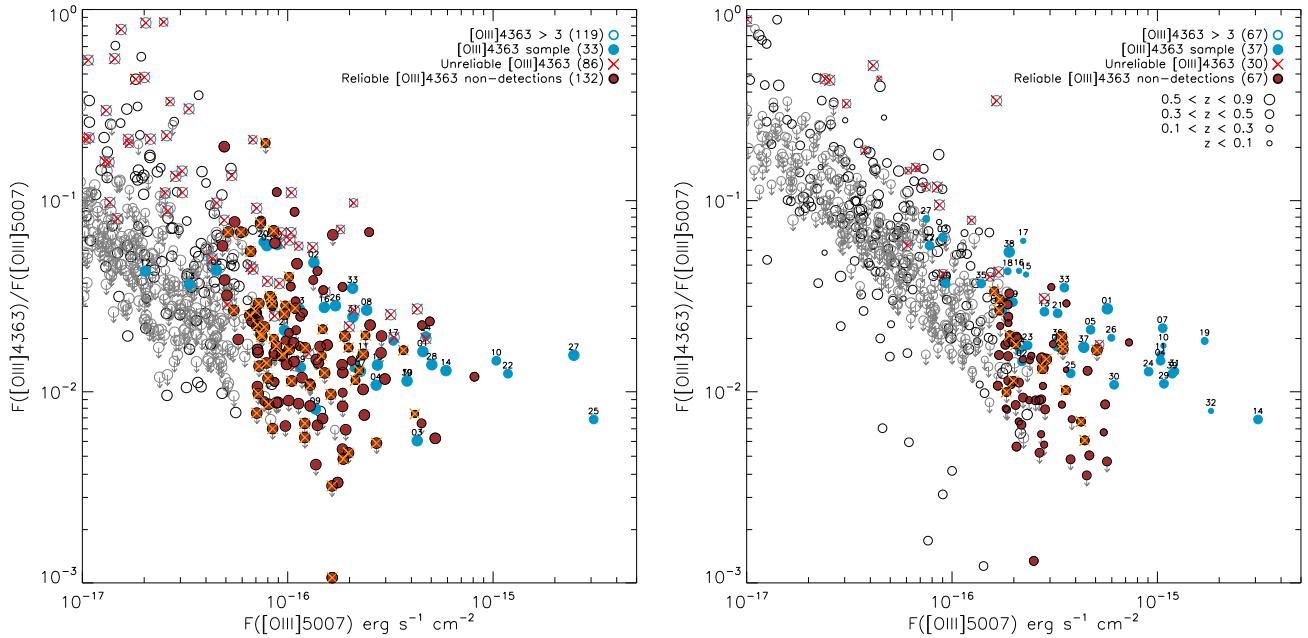
FIG. 25.— Comparison of the [O III] $\lambda 4363$/[O III] $\lambda 5007$ flux ratio against [O III] $\lambda 5007$ line flux for Keck (left) and MMT (right) spectra. The samples with [O III] $\lambda 4363$ detections at $\geq 3\sigma$ (i.e., the [O III] $\lambda 4363$-detected sample) are illustrated in filled blue circles. Those excluded by visual examination of the spectra are indicated by red crosses on unfilled blue circles. The [O III] $\lambda 4363$-non-detected samples are shown by the brown circles with yellow crosses indicating those excluded by visual examination of spectra. Arrows indicate [O III] $\lambda 4363$ 1σ limits, and symbol sizes indicate redshift. This figure illustrates that by including reliable [O III] $\lambda 4363$ non-detections, high-EW galaxies that are more metal-rich than the [O III] $\lambda 4363$-detected galaxies are incorporated in our study.

ratios are: $(\mathrm{H}\alpha/\mathrm{H}\beta)_0 = 2.86$, $(\mathrm{H}\gamma/\mathrm{H}\beta)_0 = 0.468$, and $(\mathrm{H}\delta/\mathrm{H}\beta)_0 = 0.259$ for $T_e = 10^4$ K (Osterbrock & Ferland 2006). If dust attenuates these measurements, then the observed ratios are:

$$\frac{(\mathrm{H}n/\mathrm{H}\beta)_{\mathrm{obs}}}{(\mathrm{H}n/\mathrm{H}\beta)_0} = 10^{-0.4E(B-V)[k(\mathrm{H}n)-k(\mathrm{H}\beta)]}, \qquad (6)$$

where $E(B-V)$ is the *nebular* color excess, and $k(\lambda) \equiv A(\lambda)/E(B-V)$ is the reddening curve at λ. The latter is dependent on the dust reddening formalism. We illustrate in Figure 26 the observed Balmer decrements under Calzetti et al. (2000) dust reddening with $k(\mathrm{H}\alpha) = 3.33$, $k(\mathrm{H}\beta) = 4.60$, $k(\mathrm{H}\gamma) = 5.12$, and $k(\mathrm{H}\delta) = 5.39$.

Although the scatter in individual galaxies is substantial, the extinctions inferred from different pairs of Balmer lines (e.g., $\mathrm{H}\alpha/\mathrm{H}\beta$ vs. $\mathrm{H}\gamma/\mathrm{H}\beta$) are generally consistent with each other. Specifically, the median (average) difference in E(B-V) is –0.02 mag (–0.12 mag) with a dispersion of 0.25 mag. The average and median $E(B-V)$ for our [O III] $\lambda4363$-detected sample are 0.13 and 0.06 mag, respectively.

For the [O III] $\lambda4363$-non-detected sample, the galaxies have lower emission-line EWs and thus lower S/N on the Balmer lines for reliable individual measurements. We instead stacked the MMT and Keck spectra and fitted the Balmer line profiles with a double Gaussian (emission and stellar absorption). The stacking was performed in bins of $\mathrm{H}\beta$ emission-line luminosity, the highest signal-to-noise hydrogen recombination line available for all galaxies. Three (four) bins of 17 (19–20) spectra are used for the MMT (Keck) samples. Where available, we use Keck measurements since those are more sensitive. The average (median) reddening for the [O III] $\lambda4363$-non-detected sample is $E(B-V) = 0.13$ (0.11). We provide the Balmer decrements from spectral stacking in Table 12.

4.2. T_e and Metallicity Determinations

To determine the gas-phase metallicity for our galaxies, we first estimate $T_e([\mathrm{O\,III}])$ using the auroral-to-nebular [O III] flux ratio, $\mathcal{R}$:

$$\mathcal{R} \equiv \frac{F(\lambda4363)}{F(\lambda5007) + F(\lambda4959)}, \qquad (7)$$

$$T_e = a\left(-\log(\mathcal{R}) - b\right)^{-c}, \text{ where} \qquad (8)$$

$a = 13205$, $b = 0.92506$, and $c = 0.98062$ (Nicholls et al. 2014). These coefficients utilized the latest collision strength data for O^{++} (Palay et al. 2012). In general, revised estimates with the above relation yield T_e estimates that are lower than Izotov et al. (2006b) by 5% (Nicholls et al. 2013). We correct the nebular-to-auroral [O III] flux ratio for dust attenuation (see Section 4.1), which increases our estimated T_e.

We also correct $\mathcal{R}$ for Eddington (1913) bias, which can boost the [O III] $\lambda4363$ line flux for galaxies near the adopted S/N = 3 limit. Since there is a direct relation between $\mathcal{R}$ and T_e, this bias can result in higher T_e. We perform this correction empirically, by comparing the measured $\mathcal{R}$ values of previous observations of the Ly14 sample of 20 [O III] $\lambda4363$-detected galaxies. These comparisons are illustrated in Figure 27. It can be seen that the [O III] $\lambda4363$/[O III] $\lambda5007$ line ratio is elevated when the observations are shallow. Using the measured

[O III] $\lambda4363$ S/N, we apply the following corrections to $\log\left(\mathcal{R}^{-1}\right)$ for MMT measurements:

$$3.718 - 1.042x \text{ dex}, \quad (3.00 \le x < 3.4), \qquad (9)$$
$$0.329 - 0.045x \text{ dex}, \quad (3.40 \le x \le 7.28), \qquad (10)$$
$$0.0 \text{ dex}, \quad (7.28 < x), \qquad (11)$$

where $x = \mathrm{S/N}([\mathrm{O\,III}]\,\lambda4363)$. For Keck measurements, the corrections are:

$$0.258 - 0.040x \text{ dex}, \quad (3.00 \le x \le 6.41), \qquad (12)$$
$$0.0 \text{ dex}, \quad (6.41 < x). \qquad (13)$$

Our [O III] $\lambda4363$ measurements have a large dynamic range: the strongest [O III] $\lambda4363$ line is as much as 0.065 of the [O III] flux (MMT03 and Keck05), while the weakest is 0.007 (Keck03 and MK02). We find that the average and median $\lambda4363/\lambda5007$ flux ratio for our sample are 0.023 and 0.018, respectively. The derived electron temperatures for our galaxy sample spans 1×10^4 K to 3.4×10^4 K. T_e measurements for all 66 objects are tabulated in Table 13.

For the [O III] $\lambda4363$-non-detected sample, the lack of a detection yields an upper limit on T_e. We find from visual examination that spectra with [O III] $\lambda4363$ detections at a level of S/N = 2–3 are marginal, while those below S/N = 2 are weaker or undetected. For this reason, we determine upper limit $\mathcal{R}$ values by adopting [O III] $\lambda4363$ fluxes that correspond to S/N = 2.5 for those with $2 \le \mathrm{S/N} < 3$, 1.5 for $1 \le \mathrm{S/N} < 2$, and 1.0 for S/N < 1. For the [O III] $\lambda4363$-non-detected sample, we do not apply the Eddington (1913) bias correction because the lack of a detection suggests that the bias is weak. The derived upper limits on T_e span 0.8×10^4 to 3×10^4 K, and are provided in Table 14.

Throughout this paper, we generate multiple realizations of the emission-line fluxes to construct probability distribution functions (PDFs) for all observed and derived measurements. This is critical, as the distributions are non-Gaussian in the domain of low S/N ratio ($\lesssim5$; Ly14), and it allows us to propagate our measurement uncertainties, including $E(B-V)$.

To determine the ionic abundances of oxygen, we use two emission-line flux ratios, [O II] $\lambda\lambda3726,3729/\mathrm{H}\beta$ and [O III] $\lambda\lambda4959,5007/\mathrm{H}\beta$ (Izotov et al. 2006b):

$$12 + \log\left(\frac{\mathrm{O}^+}{\mathrm{H}^+}\right) = \log\left(\frac{[\mathrm{O\,II}]}{\mathrm{H}\beta}\right) + 5.961 + \frac{1.676}{t_2} \qquad (14)$$
$$-0.4\log t_2 - 0.034 t_2 + \log\left(1 + 1.35x\right)$$

$$12 + \log\left(\frac{\mathrm{O}^{++}}{\mathrm{H}^+}\right) = \log\left(\frac{[\mathrm{O\,III}]}{\mathrm{H}\beta}\right) + 6.200 + \frac{1.251}{t_3} \qquad (15)$$
$$-0.55\log t_3 - 0.014 t_3.$$

Here, $t_2 \equiv T_e([\mathrm{O\,II}])/10^4$ K and $t_3 \equiv T_e([\mathrm{O\,III}])/10^4 K$. For our metallicity estimation, we adopt a standard two-zone temperature model with $t_2 = 0.7 t_3 + 0.17$ for $t_3 < 2.0$ and $t_2 = 1.57$ for $t_3 \ge 2.0$ (Andrews & Martini 2013, hereafter AM13). In computing $\mathrm{O}^+/\mathrm{H}^+$, we also correct the [O II]/Hβ ratio for dust attenuation.

Since the most abundant ions of oxygen in H II regions are O^+ and O^{++}, the oxygen abundances are given by: $\mathrm{O/H} = (\mathrm{O}^+ + \mathrm{O}^{++})/\mathrm{H}^+$. For 13 of our Keck galaxies (1 in the [O III] $\lambda4363$-detected sample, 12 in the [O III] $\lambda4363$-non-detected sample), our spectra do not include the [O II] $\lambda\lambda3726,3729$ doublet emission line as they
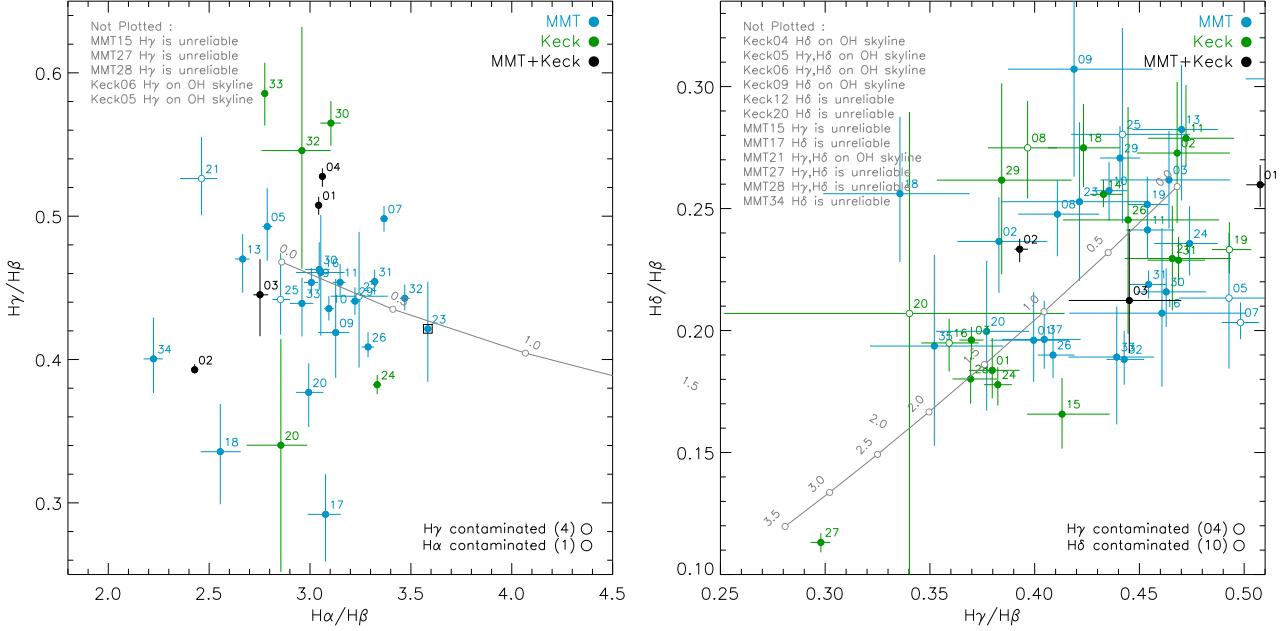
FIG. 26.— Reddening estimation by using Balmer emission-line ratios from the MMT (light blue), Keck (green) and merged (black) [O III] λ4363-detected samples. The left panel shows those galaxies at low enough redshifts to have observed Hα fluxes (Hα measurement from NB973 imaging is indicated by the black square). The Hα/Hβ ratio is plotted against the second most reliable reddening indicator, Hγ/Hβ. The right panel instead compares Hγ/Hβ with Hδ/Hβ ratio. The error bars show Balmer decrements for individually labelled galaxies. The curves show the expected values assuming an intrinsic Case B recombination ratio and a reddening law of Calzetti et al. (2000). Tick marks indicate increments of 0.5 mag in A(Hα). Galaxies without reliable Balmer decrement measurements due to contamination from OH night skylines are denoted with open circles (see Table 11 for further details).

are at lower redshifts. For these Keck galaxies (#29, 43, 47, 53, 54, 58, 59, 73, 80, 91, 92, 93, 110), we estimate the [O II] fluxes by assuming that they obey the approximate inverse correlation between [O II]/Hβ and [O III]/Hβ, shown in Figure 28, for the other SDF galaxies. The uncertainties on the assumed [O II] fluxes are based on the observed scatter in this correlation.

Table 13 provides observed and de-reddened flux ratios, estimates of T_e([O III]), log(O$^+$/H$^+$), log(O^{++}/H$^+$), and $12 + \log(\text{O/H})$ for our [O III] λ4363-detected sample. Likewise, Table 14 provides these measurements for the [O III] λ4363-non-detected sample. The distribution in $12 + \log(\text{O/H})$ for the [O III] λ4363-detected sample and lower limit on $12 + \log(\text{O/H})$ for the [O III] λ4363-non-detected sample are illustrated in Figure 29. The average and median metallicities for our [O III] λ4363-detected sample are $12 + \log(\text{O/H}) = 7.97 \pm 0.34$ and 8.03, respectively. For the [O III] λ4363-non-detected sample, the average and median lower limits on metallicity are $12 + \log(\text{O/H}) = 8.16 \pm 0.36$ and 8.17, respectively.

4.3. Dust-corrected Star Formation Rates

We determine dust-corrected SFRs using the hydrogen recombination lines, which are sensitive to the most recent star formation, $\lesssim 10$ Myr. Assuming a Chabrier (2003) (hereafter Chabrier) initial mass function (IMF) with minimum and maximum masses of 0.1 and 100 $M_\odot$, and solar metallicity (Kennicutt 1998a), the SFR can be determined from the dust-corrected Hα luminosity as:

$$\text{SFR}(M_\odot \text{ yr}^{-1}) = 4.4 \times 10^{-42} L(\text{erg s}^{-1}). \qquad (16)$$

This relation is calibrated at solar metallicity, and overestimates the SFR at lower metallicities due to the greater increase in escape of ionizing photons from more metal-poor (less blanketed) O star atmospheres. To account for

the metallicity dependence, we use predictions of the Hα luminosity from Starburst99 spectral synthesis models (Leitherer et al. 1999). Here, we adopt the Padova stellar tracks (Bressan et al. 1993; Fagotto et al. 1994a,b), a constant star-formation history, a Kroupa (2001) IMF[15], and metallicities of 0.02, 0.20, 0.40, 1.0, and $2.5Z_\odot$. Since we are adopting Chabrier IMF, we apply an offset of ≈ 0.1 dex to the Hα luminosities. The best-fit to the metallicity-dependent $L(\text{H}\alpha)$–SFR relation is:

$$\log\left[\frac{\text{SFR}}{L(\text{H}\alpha)}\right] = -41.34 + 0.39y + 0.127y^2, \qquad (17)$$

where $y = \log(\text{O/H}) + 3.31$.[16] For galaxies without Hα measurements, SFRs can be determined from de-reddened Hβ, by assuming the intrinsic Case B ratio, $(\text{H}\alpha/\text{H}\beta)_0 = 2.86$.

Our SFR estimates are illustrated in Figure 30 and summarized in Table 15 for the [O III] λ4363-detected sample and Table 16 for the [O III] λ4363-non-detected sample. Our [O III] λ4363-detected galaxies have dust-corrected $\log(\text{SFR}/M_\odot \text{ yr}^{-1}) = -2.1$ to 3.0 with an average (median) of -0.16 ± 0.85 (-0.19). The average and median for the [O III] λ4363-non-detected sample are -0.16 ± 0.85 and -0.193, respectively.

4.4. Spectral Energy Distributions and Stellar Masses

One significant advantage of studying low-mass galaxies in the SDF is the ultra-deep imaging in twenty-four bands from the UV to the IR, which allows us to characterize their stellar properties. The SDF has been imaged with: (1) GALEX (Martin et al. 2005) in both the FUV

---

[15] Starburst99 does not allow for a Chabrier IMF.
[16] $y = 0$ corresponds to solar oxygen abundances.
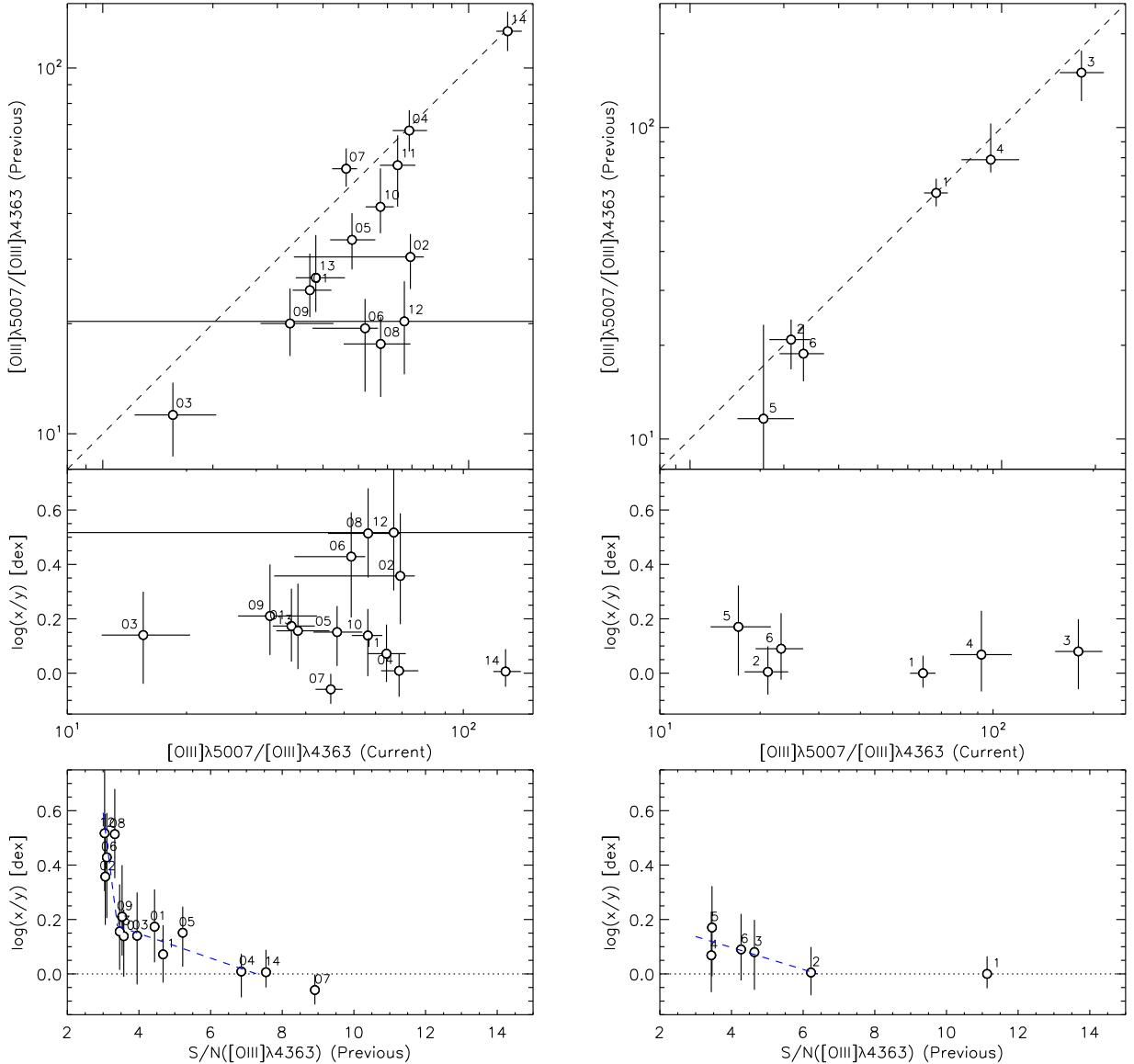
FIG. 27.— Comparisons between previous measurements (Ly14) and measurements from this paper of [O III]$\lambda5007$/[O III] $\lambda4363$ (top panels) for MMT (left) and Keck (right) sources. The previous measurements underestimated the [O III]$\lambda5007$/[O III] $\lambda4363$ ratio (i.e., overestimated T_e) due to Eddington (1913) bias by 0.3 and 0.1 dex for MMT and Keck, respectively. The middle panels illustrate this difference as a function of the current [O III]$\lambda5007$/[O III] $\lambda4363$ measurements. The bottom panels illustrate this difference as a function of S/N([O III] $\lambda4363$), and show the necessary statistical corrections to apply to [O III]$\lambda5007$/[O III] $\lambda4363$ flux ratio, based on the measured S/N. The blue dashed lines are the least-squares fits, and are provided in Equations 9–13.

and *NUV* bands;[17] (2) KPNO's Mayall telescope using MOSAIC in *U*; (3) Subaru telescope with Suprime-Cam in 14 bands ($BVR_Ci'z'z_bz_r$, and the five narrowband and two intermediate-band filters as mentioned previously); (4) KPNO's Mayall telescope using NEWFIRM (Probst et al. 2008) in *H*; (5) UKIRT using WFCAM in *J* and *K*; and (6) *Spitzer* in the four IRAC bands (3.6μm, 4.5μm, 5.8μm, and 8.0μm).

Most of these imaging data have been discussed in Ly et al. (2011a), except for the WFCAM *J*-band data and most of the NEWFIRM *H*-band data. The more recent NEWFIRM imaging data were acquired on 2012-03-06/07 and 2013-03-27/30 with photometric observing conditions at KPNO, clear skies, and 0.″9 seeing. These conditions were significantly better than in 2008

where the seeing was 1.″3 with transparency varying by as much as $\approx$2 magnitudes. The improved observing conditions yielded a mosaicked image that is $\approx$1.8 mag deeper than our previous *H*-band observations (Ly et al. 2011a). These NEWFIRM data were reduced following the steps outlined in Ly et al. (2011b) with the IRAF *nfextern* package. The WFCAM data were obtained on 2005-04-14/15, 2010-03-15/20 and 2010-04-22/23 with photometric observing conditions and $\approx$1″ seeing. These *J*-band observations are $\approx$1.6 mag deeper than previous NEWFIRM *J*-band observations obtained in poor observing conditions (Ly et al. 2011a). The reduction of the WFCAM *J*-band data follows the procedure outlined in Hayashi et al. (2009).

We obtained source catalogs for all narrowband/intermediate-band excess emitters by running SExtractor in "dual-image" mode for all optical

---

[17] Details on the *GALEX* imaging are available in Ly et al. (2009) and Ly et al. (2011a).
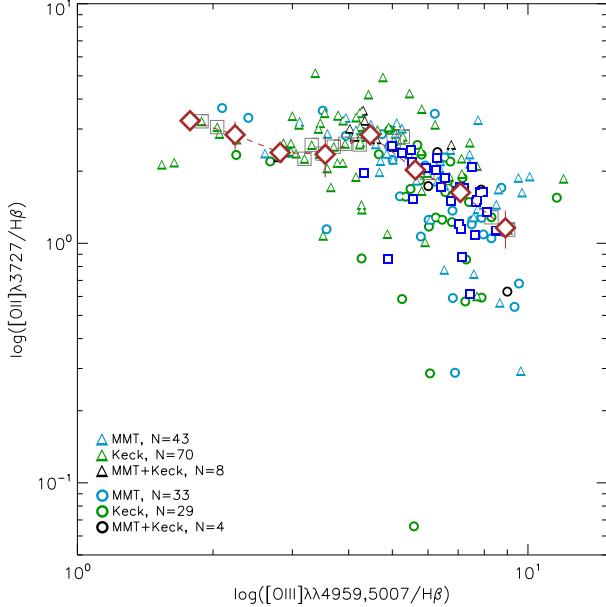
FIG. 28.— [O II] $\lambda3727$/Hβ as a function of [O III] $\lambda4959,5007$/Hβ for galaxies with [O III] $\lambda4363$ detections (circles) and reliable [O III] $\lambda4363$ non-detections (triangles). The MMT, Keck, and MMT+Keck samples are shown in light blue, green, and black, respectively. In addition, we overlay [O III] $\lambda4363$-detected galaxies from DEEP2 as blue squares (Ly et al. 2015). Median [O II]/Hβ values are shown for each [O III]/Hβ bin as brown diamonds with uncertainties determined from bootstrapping. The dashed brown line shows a linear interpolation between the median values. We use these median emission-line ratios to estimate the [O II] fluxes for 13 galaxies without [O II] spectral measurements (grey squares).

and near-infrared data (i.e., imaging that spans U to K). For *GALEX* measurements, since almost all our galaxies are virtually point sources,[18] we obtain more accurate photometry in the *FUV* and *NUV* bands by PSF-fitting with IRAF/DAOPHOT (vers. 2.16; Stetson 1987). Our examination of the residuals for each source suggests that the PSF-fitting is extremely successful[19], and that none of these galaxies is affected by contamination from nearby sources. Among the Keck sample, 32 (21) galaxies are detected in the *NUV* (*FUV*). Because the MMT [O III] $\lambda4363$ galaxies are brighter, nearly all of them are detected in the *NUV* (36 of 37) and *FUV* bands (35 of 37), allowing for robust UV SFR determinations.[20] The photometric fluxes are provided in Table 17.

Since our galaxies have very high emission-line EWs, we correct the broad-band photometry for the contribution from nebular emission lines using emission-line measurements from our spectroscopy and narrowband imaging. We generate a spectrum for each galaxy with zero continuum and emission lines located at the redshifted wavelengths for [O II], [Ne III], Hβ, [O III], Hα, higher order Balmer lines, and other weaker emission lines. These spectra are then convolved with the filter bandpasses to determine excess fluxes, which are then are removed from the broad-band photometry. For 33 galaxies, spectroscopy provided Hα measurements. For MMT23, we use the NB973 excess as an estimate of the

Hα flux. However, for our higher redshift galaxies, Hα is redshifted into the near-IR or unavailable from optical spectroscopy. To correct Hα in these 33 galaxies, we use Hβ fluxes and assume that Hα is three times stronger. Of course, higher dust reddening will yield stronger Hα corrections. We adopt a minimum correction of $A($H$\alpha)$ = 0.14 mag.

In addition, we correct the photometry for nebular continuum emission from free-free, free-bound, and two-photon emission. To estimate the nebular contributions toward the total light, we generate spectral synthesis models from Starburst99. Our models assume a constant SFR, a Kroupa (2001) IMF[21], Geneva stellar evolutionary models, and $Z/Z_{\odot} = 0.2$, 0.4, and 1.0 (depending on the gas-phase metallicity; see Equations 18–20). The nebular continuum emission is then scaled by the dust-corrected Hα or Hβ luminosity and reddened for dust attenuation by assuming a Calzetti et al. (2000) formalism with $E(B-V)$ estimates from Balmer decrements (see Section 4.1). These corrections are illustrated in Figure 31 for four of our [O III] $\lambda4363$-detected galaxies. The black circles show the original broad-band photometry, while the blue circles show the corrected continuum fluxes after the removal of nebular continua and emission lines. We also overlay the spectrum of the nebular emission. Finally, both the original and corrected SEDs were fit with stellar population synthesis models (Bruzual & Charlot 2003) by the Fitting and Assessment of Synthetic Templates (FAST; Kriek et al. 2009) code. We use exponentially-declining star formation histories (i.e., τ models) similar to previous fitting by Ly et al. (2011a) and many other groups. We have chosen this star-formation history (SFH) because: (1) broad-band data are generally unable to distinguish between more complicated SFHs (e.g., a constant SFR with a recent burst, which may be more representative of our galaxies); (2) the inclusion of a recent burst in star formation does not significantly alter stellar mass estimates, since the mass-to-light ratio is set by the rest-frame optical-to-infrared light from the older stellar population; and (3) as we will later show, these fits that assume an exponentially declining SFH are consistent with the data, with nearly unity χ^2_ν values.

In these models, we adopt Calzetti et al. (2000) reddening (A_V is free parameter which ranged from 0 and 3 mag), inter-galactic medium attenuation following Madau (1995), τ values between 10^7 and 10^{10} yr, and a Chabrier IMF. The only differences from our previous [O III] $\lambda4363$ study (Ly14) is that we use stellar atmosphere models with abundances consistent with the gas-phase metallicity:

$$Z_\star = 0.004, \ (12 + \log(\mathrm{O/H}) \leq 8.17), \qquad (18)$$

$$Z_\star = 0.008, \ (8.17 < 12 + \log(\mathrm{O/H}) \leq 8.39), \quad (19)$$

$$Z_\star = 0.02 \equiv Z_\odot, \ (8.39 < 12 + \log(\mathrm{O/H})). \qquad (20)$$

The latter assumption differs for our previous study (Ly14), where $Z_\star = 0.004$ was used for all galaxies.

Our SED-fitting results are illustrated in Figure 32 and summarized in Table 15 for the [O III] $\lambda4363$-detected sample and Table 16 for the [O III] $\lambda4363$-non-detected sample. We find that these galaxies are typically low-mass systems (median of $1.3 \times 10^8 \ M_\odot$, average of

---

[18] MMT17 is resolved as an edge-on disk at $z \approx 0.08$, so we use Kron aperture photometry.

[19] The root-mean-square in the residual image is consistent with Poisson noise from the background.

[20] MMT05 is adjacent to a bright source, preventing accurate measurements in the UV images.

[21] This is similar to a Chabrier IMF.
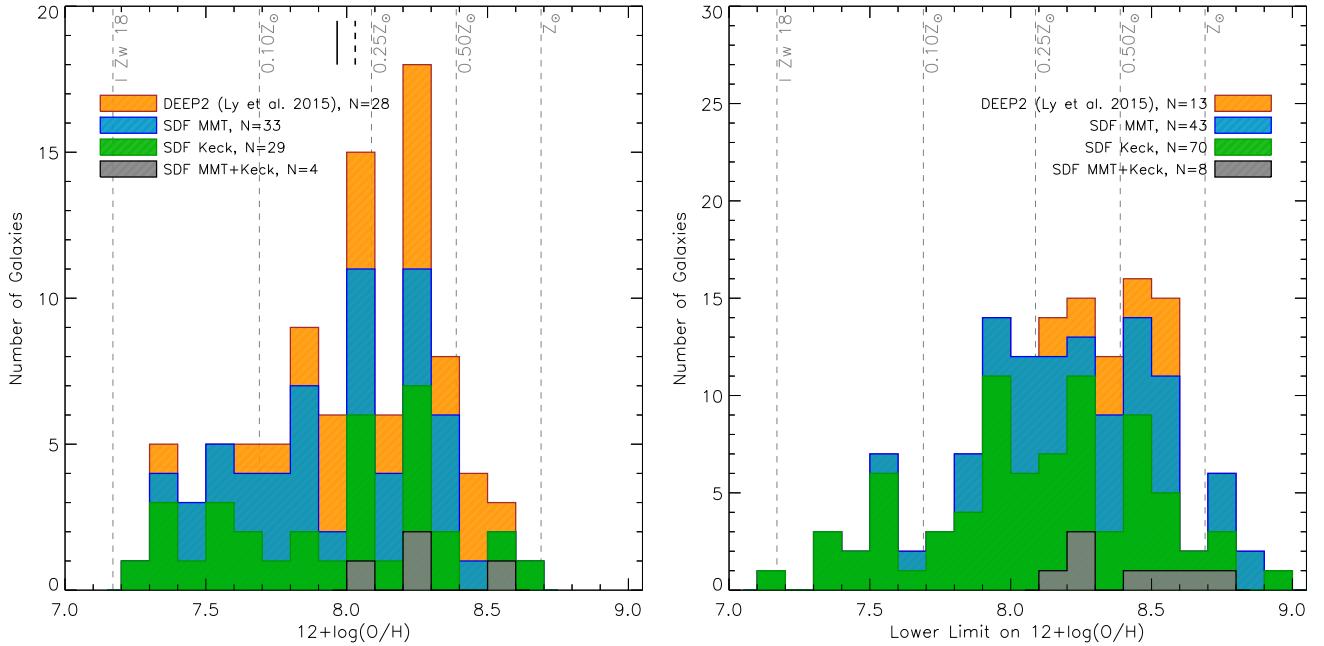
FIG. 29.— Distribution in $12 + \log(\mathrm{O/H})$ for the [O III] $\lambda4363$-detected sample (left) and lower limit on $12 + \log(\mathrm{O/H})$ for the [O III] $\lambda4363$-non-detected (right) sample. Our SDF samples are shown in light blue (MMT), green (Keck), and grey (MMT+Keck). The average (median) metallicity for the SDF samples is shown by the solid (dashed) black lines. Also overlaid in orange is the Ly et al. (2015) DEEP2 sample. Vertical dashed lines indicate abundances relative to solar. For comparison, the gas metallicity measurement for I Zw 18 (Izotov et al. 2006a) is shown.
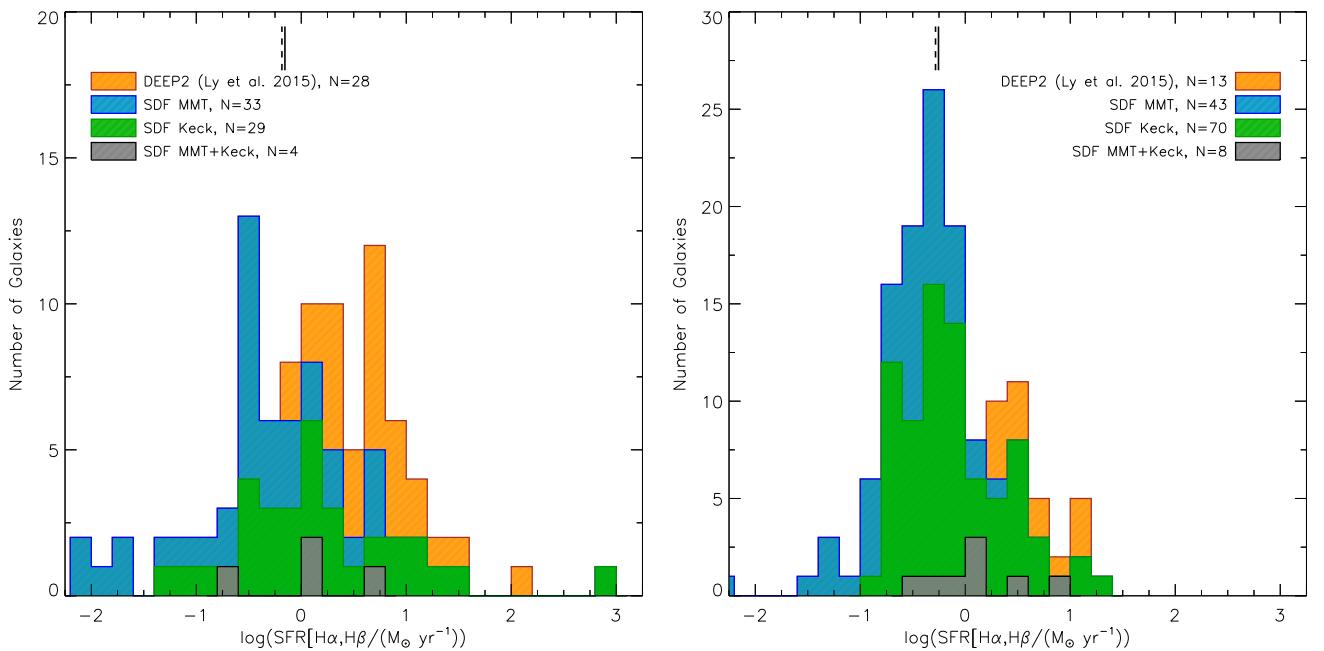
FIG. 30.— Distribution in star formation rate (SFR) for [O III] $\lambda4363$-detected (left) and [O III] $\lambda4363$-non-detected (right) sample determined from dust-corrected Hα or Hβ luminosities (see Section 4.3). Our SDF samples are shown in light blue (MMT), green (Keck), and grey (MMT+Keck). The average (median) SFR for the SDF samples is shown by the solid (dashed) black lines. Also overlaid in orange is the Ly et al. (2015) DEEP2 sample.
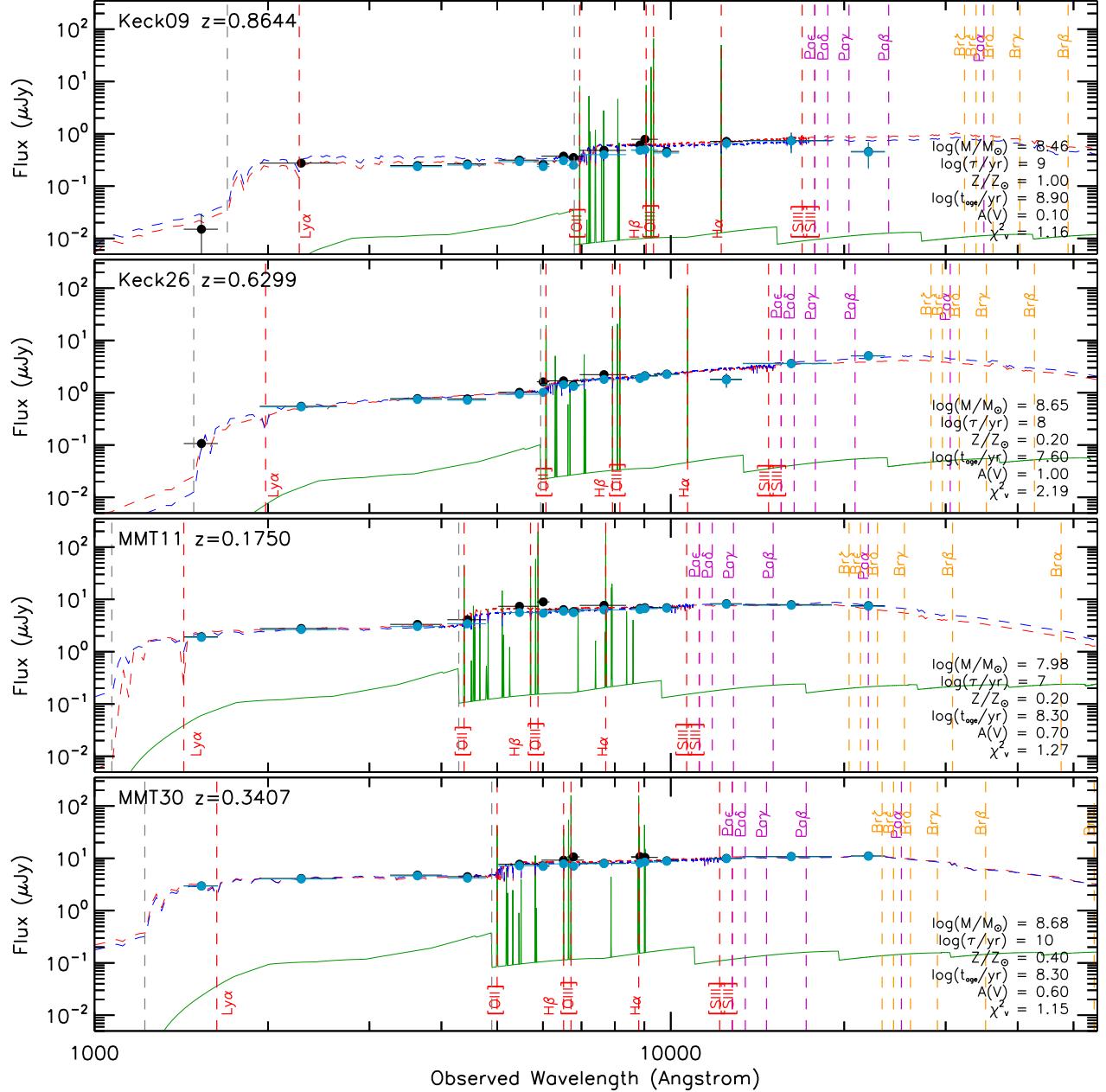
Fig. 31.— Spectral energy distributions (SEDs) and the best-fitting stellar population results from modeling the SED in four galaxies: Keck09, Keck26, MMT11, and MMT30. The observed fluxes are shown by the black circles while the light blue circles illustrate the corrections for nebular continuum and line emission. Errorbars along the x-axis demonstrate the FWHM of the filters while those along the y-axis are 1σ. The SEDs for the nebular emission are illustrated by the green solid lines. The best χ^2 fits to the original and nebular emission corrected SEDs are shown by the red and blue dashed lines, respectively. The SED fitting results after nebular emission corrections are reported on the right. Grey vertical lines indicate the locations of the Balmer and Lyman continuum breaks, while red, purple, and orange vertical lines show the location of various redshifted nebular emission lines. When correcting for nebular emission, the χ^2 values are reduced by a factor of 2.7–4.3 in these four cases.

$1.5 \times 10^8 \ M_\odot$), with a stellar mass distribution that extends from 4.3×10^6 to $3.9 \times 10^9 \ M_\odot$. The estimated light-weighted stellar ages of $t_{\rm age}/ = 10^7$–$10^{9.9}$ yr (average of $10^{8.0}$ yr) suggest that these galaxies formed most of their stars only recently, which explains why they were detected by our emission-line flux sample.

We combine our dust-corrected SFRs (Section 4.3) and stellar mass determinations to locate our galaxies on the $M_\star$–SFR relation in Figure 2 of Paper II. We emphasize that the inverse of the sSFR is consistent with the stellar ages derived from SED fitting, which are provided in Table 15. That is, these galaxies could have formed most of their stars by maintaining the measured SFRs over their lifetimes.

4.5. *ISM Gas Densities*

The gas or electron density (n_e) is critical for understanding the multi-phased ISM, specifically characterizing the neutral, ionized, and molecular gas components of the ISM. In addition, the strength of nebular emission lines, such as hydrogen emission lines (e.g., Hα, Hβ) emitted from the recombination of ionized hydrogen gas and collisionally-excited forbidden transition emission lines (e.g., [O III], [O II]), is proportional to n_e^2.

To estimate the electron density of the ISM, we use the flux ratios of the [S II] $\lambda\lambda6716,6731$ and [O II] $\lambda\lambda3726,3729$ doublets. These ratios are illustrated in Figure 33 and the inferred densities are tabulated in Table 13. To compute electron densities, we use an IDL-based routine that is based on the IRAF TEMDEN package, but with improvements with new atomic data (Berg et al. 2015; Croxall et al. 2015).[22] For consistency, we account for the n_e dependence on T_e for each individual galaxy (see curves of different colors and line styles in Figure 33). The average (median) n_es derived from [S II] measurements are 462 (214) cm^{-3} for the [O III] $\lambda4363$-detected sample and 614 (443) cm^{-3} for the [O III] $\lambda4363$-non-detected sample. Likewise, the [O II] measurements yield averages (medians) of 190 (93) cm^{-3} for the [O III] $\lambda4363$-detected sample and 257 (169) cm^{-3} for the [O III] $\lambda4363$-non-detected sample.[23] While these gas densities are higher than the integrated measurements from SDSS ($\sim$10 cm^{-3}; Hayashi et al. 2015), they are consistent with the typical densities (10^2–10^4 cm^{-3}) of individual H II regions. The high gas densities suggest that the filling factor of ionized gas is large, encompassing most of the galaxies in our sample. We note that we are unable to compare directly the electron densities derived from [S II] and [O II] line ratios since [S II] measurements are only available for lower redshift galaxies and the resolved [O II] measurements are from Keck, which are only available at higher redshift.

5. CONCLUSIONS

This paper (Paper I) describes the large spectroscopic survey, called "Metal Abundances across Cosmic Time" ($\mathcal{MACT}$), that we have conducted. Using the MMT/Hectospec and Keck/DEIMOS spectrographs, we

have obtained optical spectra for $\approx$1,900 star-forming galaxies. These galaxies are pre-selected from narrowband or intermediate-band imaging in the Subaru Deep Field, which detects redshifted nebular emission lines at redshifts between 0.07 and 1.61. The focus of $\mathcal{MACT}$ is to obtain robust measurements of the gas metallicity and other properties (e.g., gas density, ionization parameter) of the interstellar gas from deep rest-frame optical spectroscopy.

$\mathcal{MACT}$ is unique from previous spectroscopic surveys because our spectroscopy has obtained measurements of the weak [O III] $\lambda4363$ nebular emission for a large number of galaxies. The strength of the [O III] $\lambda4363$ line is set by the electron temperature for the ionized gas. Since the gas temperature is regulated by the metal content—collisionally-excited metal emission lines enable the gas to cool—an inverse relationship exists between gas-phase oxygen abundance and [O III] $\lambda4363$ line strength. Specifically, $\mathcal{MACT}$ has measured the [O III] $\lambda4363$ line in 164 galaxies (66 galaxies have detections at S/N $\geq$ 3, referred to as the [O III] $\lambda4363$-detected sample, and 98 galaxies have reliable lower limits on metallicity, referred to as the [O III] $\lambda4363$-non-detected sample). Combined with multi-wavelength imaging data that spans rest-frame UV to near-infrared, we describe how we determine dust attenuation, metallicity, SFR and stellar mass for these galaxies in the [O III] $\lambda4363$-detected and [O III] $\lambda4363$-non-detected samples. Paper II of the $\mathcal{MACT}$ survey utilizes the [O III] $\lambda4363$-based metallicities to study, for the first time, the evolution of the stellar mass–gas metallicity relation and its secondary dependence on SFR over 8 billion years ($z \lesssim 1$) using a temperature-sensitive metallicity diagnostics.

---

[22] Developed by John Moustakas, Brian Moore, and Kevin Croxall. The code called *impro* is available here: https://github.com/moustakas/impro.

[23] Averages and medians exclude galaxies with doublet ratios beyond the low-density limit.

FIG. 32.— Distribution in stellar mass for [O III] λ4363-detected (left) and [O III] λ4363-non-detected (right) sample determined from SED modeling (see Section 4.4). Our SDF samples are shown in light blue (MMT), green (Keck), and grey (MMT+Keck). The average (median) stellar mass for the SDF samples is shown by the solid (dashed) black lines. Also overlaid in orange is the Ly et al. (2015) DEEP2 sample.
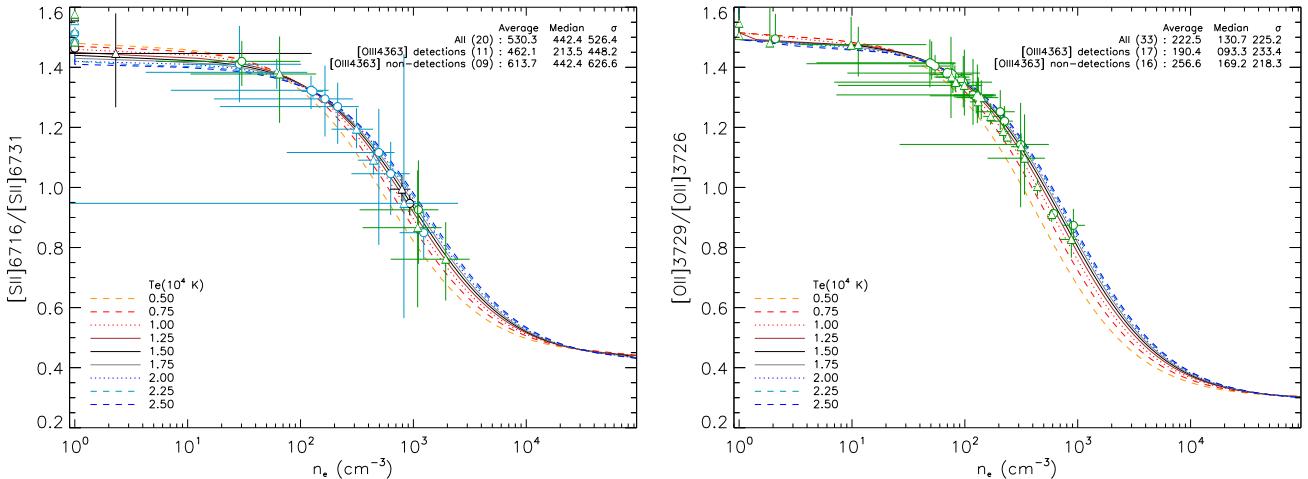
FIG. 33.— The electron densities derived from two emission line doublet ratios, [S II] λ6716/6731 (left) and [O II] λ3729/3726 (right). The observed doublet ratios for SDF galaxies are shown on the y-axes, along with their uncertainties and name designations. These are then translated into *inferred* electron densities on the x-axes. This transformation is illustrated as a function of electron temperature (indicated by various color and line types from 5,000 to 25,000 K). For consistency, we use the T_e derived in Section 4.2. Average and median densities are reported in the upper right of the figure. The derived electron densities are relatively high compared to integral measurements from SDSS; however, they are consistent with individual H II regions. Galaxies with doublet ratios at or beyond the low-density limit are plotted at $n_e = 1$ cm^{-3}. These electron densities are provided in Table 13.

FIRM), UKIRT (WFCAM)

<div style="text-align:center">REFERENCES</div>

Allende Prieto, C., Lambert, D. L., & Asplund, M. 2001, ApJ, 556, L63

Aller, L. H. 1984, Astrophysics and Space Science Library, (Dordrecht: Reidel)

Andrews, B. H., & Martini, P. 2013, ApJ, 765, 140 [AM13]

Baldwin, A., Phillips, M. M., & Terlevich, R. 1981, PASP, 93, 817

Berg, D. A., Skillman, E. D., Croxall, K. V., et al. 2015, ApJ, 806, 16

Bertin, E., & Arnouts, S. 1996, A&AS, 117, 393

Bressan, A., Fagotto, F., Bertelli, G., & Chiosi, C. 1993, A&AS, 100, 647

Brinchmann, J., Charlot, S., White, S. D. M., et al. 2004, MNRAS, 351, 1151

Bruzual, G., & Charlot, S. 2003, MNRAS, 344, 1000

Calzetti, D., Armus, L., Bohlin, R. C., Kinney, A. L., Koornneef, J., & Storchi-Bergmann, T. 2000, ApJ, 533, 682

Chabrier, G. 2003, PASP, 115, 763

Cooper, M. C., Newman, J. A., Davis, M., Finkbeiner, D. P., & Gerke, B. F. 2012, Astrophysics Source Code Library, 1203.003

Cowie, L. L., Barger, A. J., & Songaila, A. 2016, ApJ, 817, 57

Cresci, G., Mannucci, F., Sommariva, V., et al. 2012, MNRAS, 421, 262

Croxall, K. V., Pogge, R. W., Berg, D. A., Skillman, E. D., & Moustakas, J. 2015, ApJ, 808, 42

Dalcanton, J. J. 2007, ApJ, 658, 941

Davé, R., Finlator, K., & Oppenheimer, B. D. 2011, MNRAS, 416, 1354

de los Reyes, M. A., Ly, C., Lee, J. C., et al. 2015, AJ, 149, 79

Eddington, A. S. 1913, MNRAS, 73, 359

Faber, S. M., Phillips, A. C., Kibrick, R. I., et al. 2003, Proc. SPIE, 4841, 1657

Fabricant, D., Fata, R., Roll, J., et al. 2005, PASP, 117, 1411

Fabricant, D. G., Kurtz, M. J., Geller, M. J., et al. 2008, PASP, 120, 1222

Fagotto, F., Bressan, A., Bertelli, G., & Chiosi, C. 1994a, A&AS, 105, 29

Fagotto, F., Bressan, A., Bertelli, G., & Chiosi, C. 1994b, A&AS, 104, 365

Fujita, S. S., Ajiki, M., Shioya, Y., et al. 2003, ApJ, 586, L115

Hayashi, M., Ly, C., Shimasaku, K., et al. 2015, PASJ, 67, 80

Hayashi, M., Motohara, K., Shimasaku, K., et al. 2009, ApJ, 691, 140

Henry, A., Scarlata, C., Domínguez, A., et al. 2013b, ApJ, 776, L27

Humphreys, R. M., Beers, T. C., Cabanela, J. E., et al. 2011, AJ, 141, 131

Hu, E. M., Cowie, L. L., Kakazu, Y., & Barger, A. J. 2009, ApJ, 698, 2014

Izotov, Y. I., Papaderos, P., Guseva, N. G., Fricke, K. J., & Thuan, T. X. 2006, A&A, 454, 137

Izotov, Y. I., Stasińska, G., Meynet, G., Guseva, N. G., & Thuan, T. X. 2006a, A&A, 448, 955

Kauffmann, G., Heckman, T. M., Tremonti, C., et al. 2003, MNRAS, 346, 1055

Kashikawa, N., Shimasaku, K., Malkan, M. A., et al. 2006, ApJ, 648, 7

Kashikawa, N., Shimasaku, K., Matsuda, Y., et al. 2011, ApJ, 734, 119

Kashikawa, N., Shimasaku, K., Yasuda, N., et al. 2004, PASJ, 56, 1011

Kennicutt, R. C. 1998a, ARA&A, 36, 189

Kochanek, C. S., Eisenstein, D. J., Cool, R. J., et al. 2012, ApJS, 200, 8

Kriek, M., van Dokkum, P. G., Labbé, I., Franx, M., Illingworth, G. D., Marchesini, D., & Quadri, R. F. 2009, ApJ, 700, 221

Kroupa, P. 2001, MNRAS, 322, 231

Lee, J. C., Ly, C., Spitler, L., et al. 2012, PASP, 124, 782

Leitherer, C., Schaerer, D., Goldader, J. D., et al. 1999, ApJS, 123, 3

Lilly, S. J., Carollo, C. M., Pipino, A., Renzini, A., & Peng, Y. 2013, ApJ, 772, 119

Lilly, S. J., Le Brun, V., Maier, C., et al. 2009, ApJS, 184, 218

Ly, C., Malkan, M. A., Kashikawa, N., et al. 2007, ApJ, 657, 738

Ly, C., Malkan, M. A., Treu, T., et al. 2009, ApJ, 697, 1410

Ly, C., Malkan, M. A., Hayashi, M., et al. 2011a, ApJ, 735, 91

Ly, C., Lee, J. C., Dale, D. A., et al. 2011b, ApJ, 726, 109

Ly, C., Malkan, M. A., Kashikawa, N., et al. 2012a, ApJ, 747, L16

Ly, C., Malkan, M. A., Kashikawa, N., et al. 2012b, ApJ, 757, 63

Ly, C., Malkan, M. A., Nagao, T., et al. 2014, ApJ, 780, 122

Ly, C., Malkan, M. A., Rigby, J. R., Nagao, T. 2016, ApJ, submitted [Paper II]

Ly, C., Rigby, J., Cooper, M., & Yan, R. 2015, ApJ, 805, 45

Madau, P. 1995, ApJ, 441, 18

Markwardt, C. B. 2009, Astronomical Data Analysis Software and Systems XVIII, 411, 251

Martin, D. C., Fanson, J., Schiminovich, D., et al. 2005, ApJ, 619, L1

Miyazaki, S., Komiyama, Y., Sekiguchi, M., et al. 2002, PASJ, 54, 833

Moustakas, J., Zaritsky, D., Brown, M., et al. 2011, ApJ, submitted (arXiv:1112.3300)

Nagao, T., Sasaki, S. S., Maiolino, R., et al. 2008, ApJ, 680, 100

Newman, J. A., Cooper, M. C., Davis, M., et al. 2013, ApJS, 208, 5

Nicholls, D. C., Dopita, M. A., Sutherland, R. S., Kewley, L. J., & Palay, E. 2013, ApJS, 207, 21

Nicholls, D. C., Dopita, M. A., Sutherland, R. S., Jerjen, H., & Kewley, L. J. 2014, ApJ, 790, 75

Oke, J. B. 1974, ApJS, 27, 21

Osterbrock, D. E., & Ferland, G. J. 2006, Astrophysics of gaseous nebulae and active galactic nuclei, 2nd. ed. by D.E. Osterbrock and G.J. Ferland. Sausalito, CA: University Science Books, 2006,

Ouchi, M., Shimasaku, K., Okamura, S., et al. 2004, ApJ, 611, 660

Palay, E., Nahar, S. N., Pradhan, A. K., & Eissner, W. 2012, MNRAS, 423, L35

Probst, R. G., George, J. R., Daly, P. N., Don, K., & Ellis, M. 2008, Proc. SPIE, 7014, 70142S

Salim, S., Rich, R. M., Charlot, S., et al. 2007, ApJS, 173, 267

Stetson, P. B. 1987, PASP, 99, 191

Tremonti, C. A., Heckman, T. M., Kauffmann, G., et al. 2004, ApJ, 613, 898

Veilleux, S., & Osterbrock, D. E. 1987, ApJS, 63, 295

Whitaker, K. E., Franx, M., Leja, J., et al. 2014a, ApJ, 795, 104

Yagi, M., Kashikawa, N., Sekiguchi, M., Doi, M., Yasuda, N., Shimasaku, K., & Okamura, S. 2002, AJ, 123, 66

York, D. G., Adelman, J., Anderson, J. E., Jr., et al. 2000, AJ, 120, 1579

Zahid, H. J., Kewley, L. J., & Bresolin, F. 2011, ApJ, 730, 137

TABLE 4
Summary of MMT [O III] λ4363-detected Spectroscopic Sample

Merged ID	ID	Name	Line Sel.	R.A. (hr)	Decl. (deg)	z_{spec}	Obs. Dates (UT)	t_{int} (min.)
(1)	(2)	(3)	(4)	(5)	(6)	(7)	(8)	(9)
. . .	MMT01	NB816–140623	[O III]	13:25:16.868	+27:39:06.920	0.6377	2008 Apr 14, 2014 Feb 27, Mar 25, 29–31	580.0
. . .	MMT02	NB711–064628	[O III]	13:23:39.133	+27:32:52.705	0.4327	2008 Mar 13, 2014 Feb 27–28, Mar 29	585.0
. . .	MMT03[a]	NB973–104154	Hα	13:23:39.170	+27:31:47.336	0.4809	2008 Mar 13, 2014 Feb 28, Mar 25, 29–31	605.0
MK01	MMT04	IA679–112491_NB704–088982_NB921–126525	[O III]+Hβ,Hα	13:24:46.633	+27:34:56.981	0.3932	2008 Mar 13, Apr 11, 2014 Feb 28, Mar 29	485.0
. . .	MMT05	IA679–031637	[O III]+Hβ	13:25:03.365	+27:17:23.770	0.3846	2008 Mar 13, 2014 Feb 27, Mar 29	340.0
. . .	MMT07	IA679–062450_NB704–049936_NB921–079428	[O III]+Hβ,Hα	13:24:06.943	+27:24:01.763	0.3894	2008 Mar 13, Apr 11, 2014 Mar 25, 30–31	480.0
. . .	MMT08	NB816–081644	[O III]	13:23:42.968	+27:26:35.592	0.6332	2008 Apr 10, 2014 Feb 28, Mar 25, 29–31	565.0
. . .	MMT09	NB973–094500	Hα+[S II]	13:23:49.797	+27:28:35.316	0.4787	2008 Apr 10, 2014 Feb 27, Mar 25, 29–31	540.0
. . .	MMT10	NB704–009999	Hα	13:23:56.393	+27:13:32.981	0.0681	2008 Apr 10, 2014 Feb 28, Mar 25, 29–31	565.0
. . .	MMT11	IA598–079010	[O III]	13:24:13.641	+27:25:09.274	0.1750	2008 Apr 10, 2014 Feb 27, Mar 25, 29–31	540.0
. . .	MMT13	NB711–102472_NB973–156739	Hβ,Hα+[S II]	13:24:28.883	+27:45:51.883	0.4691	2008 Apr 11, 2014 Feb 27, Mar 25, 29–31	580.0
MK02	MMT14	NB711–077774_NB973–125003	Hβ,Hα+[S II]	13:25:22.936	+27:37:40.327	0.4642	2008 Apr 11, 2014 Feb 27, Mar 29	340.0
. . .	MMT15	NB704–045509	Hα	13:23:42.814	+27:22:56.484	0.0699	2008 Mar 13, 2014 Feb 28, Mar 25, 29–31	605.0
. . .	MMT16	NB704–092132	Hα	13:23:57.444	+27:35:40.851	0.0711	2014 Feb 27, Mar 29	220.0
. . .	MMT17	NB704–093044	Hα	13:23:41.807	+27:36:55.661	0.0729	2014 Feb 27, Mar 29	220.0
. . .	MMT18	NB816–136351	Hα	13:25:05.544	+27:38:10.025	0.2438	2014 Feb 28, Mar 29	245.0
. . .	MMT19	NB816–153816_IA598–142084	[O III]+Hβ,Hα	13:24:21.420	+27:41:47.252	0.2348	2014 Mar 25, 30–31	240.0
. . .	MMT20	NB921–052748	Hα	13:23:37.833	+27:18:04.303	0.3940	2008 Mar 13, 2014 Feb 27–28, Mar 29	585.0
. . .	MMT21	NB973–102012	Hα	13:23:49.391	+27:31:07.332	0.4907	2008 Apr 11, 2014 Feb 27, Mar 28, 29	460.0
. . .	MMT22	NB973–102051	Hα+[S II]	13:24:39.617	+27:31:06.618	0.4775	2008 Apr 10, 2014 Feb 28, Mar 25, 29–31	565.0
. . .	MMT23	NB973–109072	Hα	13:24:07.533	+27:33:06.184	0.4922	2008 Apr 14, 2014 Feb 28, Mar 25, 29–31	605.0
. . .	MMT24	NB704–078586_NB711–061791	[O III]	13:24:02.571	+27:31:54.347	0.4291	2014 Feb 27, Mar 29	220.0
. . .	MMT25	NB711–110522_NB973–155435	Hβ,Hα+[S II]	13:24:53.470	+27:45:34.916	0.4653	2014 Feb 27, Mar 29	220.0
. . .	MMT26	IA598–040541	[O III]	13:23:56.462	+27:15:31.421	0.1944	2008 Mar 13, Apr 11, 2014 Feb 27–28, Mar 29	705.0
. . .	MMT27	IA598–111780	[O III]+Hβ	13:24:26.371	+27:33:50.424	0.1957	2008 Mar 13, 2014 Feb 28, Mar 25, 29–31	605.0
. . .	MMT28	IA598–129900	[O III]+Hβ	13:25:12.598	+27:38:45.984	0.2107	2014 Feb 27, Mar 29	220.0
. . .	MMT29	IA679–012177	[O III]	13:24:39.353	+27:13:08.798	0.3396	2008 Apr 14, 2014 Feb 27–28, Mar 29	485.0
. . .	MMT30	IA679–028424	[O III]	13:24:32.791	+27:16:38.183	0.3407	2014 Feb 28, Mar 29	245.0
. . .	MMT31	IA679–042056	[O III]	13:23:40.620	+27:19:45.693	0.3387	2008 Apr 10, 2014 Feb 27, Mar 25, 29–31	540.0
. . .	MMT32	IA679–061647	Hα	13:23:55.452	+27:24:06.460	0.0500	2014 Feb 27, Mar 29	220.0
. . .	MMT33	NB704–013089	[O III]	13:25:29.366	+27:14:09.566	0.4010	2008 Apr 14, 2014 Feb 28, Mar 25, 29–31	605.0
. . .	MMT34	NB704–018048_NB711–015612	[O III]	13:25:22.152	+27:15:25.406	0.4223	2008 Mar 13, 2014 Feb 28, Mar 25, 29–31	605.0
. . .	MMT35	NB704–116614_NB711–092356	[O III]	13:24:23.558	+27:42:26.267	0.4223	2008 Mar 13, 2014 Feb 27–28, Mar 29	585.0
MK03	MMT36	NB704–118311_NB711–093368	[O III]	13:24:17.062	+27:43:01.554	0.4227	2008 Apr 11, 14, 2014 Feb 27, Mar 25, 29–31	700.0
. . .	MMT37	NB816–125394	[O III]	13:25:32.838	+27:36:05.385	0.6455	2008 Apr 10, 2014 Feb 27–28, Mar 29	545.0
. . .	MMT38	NB816–142736	Hβ	13:23:58.993	+27:39:25.885	0.6723	2008 Apr 11, 2014 Febx 27, Mar 25, 29–31	580.0
MK04	MMT39	NB704–040313_NB711–033384	[O III]	13:24:51.108	+27:21:15.581	0.4288	2014 Mar 28	120.0

Note. — (1): Abbreviated MMT+Keck merged name. (2): Abbreviated name for MMT [O III] λ4363-detected galaxy. (3): Full narrowband and/or intermediate-band excess emitter name. (4): Emission line(s) responsible for narrowband and/or intermediate-band excess. (5): Right ascension in units of hours, minutes, and seconds. (6): Declination in units of degrees, arcminutes, and arcseconds. (7): Spectroscopic redshift. (8): UT observation dates. (9): On-source integration time in units of minutes.

[a]This source is likely a LINER (see Section 2 of Paper II).

TABLE 5
Summary of Keck [O III] λ4363-detected Spectroscopic Sample

Merged ID	ID	Name	Line Sel.	R.A. (hr)	Decl. (deg)	z_{spec}	Obs. Dates (UT)	t_{int} (min.)
(1)	(2)	(3)	(4)	(5)	(6)	(7)	(8)	(9)
...	Keck01	IA679–079866_NB711–049857	[O II],[Ne III]	13:25:11.938	+27:27:31.204	0.8390	2004 Apr 23	120.0
...	Keck02	NB816–070113	[O III]	13:24:34.911	+27:24:10.195	0.6230	2004 Apr 23, 2014 May 02	117.6
...	Keck03	IA679–077341	[O II]+[Ne III]	13:23:53.540	+27:27:13.008	0.7906	2004 Apr 23, 2015 Mar 17	217.6
...	Keck04	NB704–087569	[O II]	13:23:43.510	+27:34:20.980	0.8830	2008 May 02, 2015 Mar 17	230.0
...	Keck05	NB921–078003	[O III]	13:24:43.656	+27:23:34.861	0.8354	2009 Apr 28, 2014 May 02	300.0
...	Keck06[a]	NB704–060432	[Ne III]	13:24:58.623	+27:26:40.468	0.8237	2009 Apr 28, 2014 May 02	300.0
...	Keck07	IA679–066277	[O II]	13:24:57.971	+27:24:44.603	0.8568	2009 Apr 28, 2014 May 02	120.0
...	Keck08	NB711–035903_NB973–073302	[O II],[O III]	13:24:32.827	+27:22:11.509	0.9200	2014 May 02, 2015 Mar 19	211.2
...	Keck09	NB921–163959	[O III]	13:25:15.062	+27:42:46.399	0.8644	2015 Mar 16, 19	240.0
MK01	Keck10	IA679–112491_NB704–088982_NB921–126525	[O III]+Hβ,Hα	13:24:46.633	+27:34:56.981	0.3932	2015 Mar 16, 26	268.7
...	Keck11	NB816–073513	[O III]	13:25:08.544	+27:24:49.925	0.6298	2014 May 02, 2015 Mar 26	260.0
...	Keck12	NB921–079119	[O III]	13:24:44.106	+27:23:44.329	0.8359	2004 Apr 23, 2014 May 02	237.6
...	Keck13	NB921–089119	[O III]	13:25:09.177	+27:25:59.427	0.8409	2009 Apr 27, 2014 May 02	300.0
...	Keck14	IA679–045777_NB711–030882_NB921–063503	[O II],[Ne III],[O III]	13:24:24.635	+27:20:14.875	0.8302	2014 May 02	120.0
...	Keck15	NB711–039017_NB921–077859	[Ne III],[O III]	13:24:38.672	+27:23:35.005	0.8337	2014 May 02	120.0
...	Keck16	NB921–079255	[O III]	13:24:49.980	+27:23:56.449	0.8338	2014 May 02	120.0
MK03	Keck17	NB704–118311_NB711–093368	[O III]	13:24:17.062	+27:43:01.554	0.4227	2015 Mar 17	120.0
...	Keck18	NB816–169110	[O III]	13:24:49.651	+27:44:40.685	0.6239	2015 Mar 17	120.0
...	Keck19	IA679–149913_NB704–117007_NB921–162669	[O II],[Ne III],[O III]	13:25:09.393	+27:42:32.481	0.8238	2015 Mar 17	120.0
...	Keck20	IA679–149898	[O III]+Hβ	13:24:55.459	+27:42:30.723	0.3681	2015 Mar 17	120.0
...	Keck21	NB704–124271	[O II]	13:24:17.593	+27:44:27.556	0.8850	2015 Mar 17	120.0
MK04	Keck22	NB704–040313_NB711–033384	[O III]	13:24:51.108	+27:21:15.581	0.4288	2015 Mar 19	91.2
...	Keck23	IA679–049157	[O II]+[Ne III]	13:24:33.647	+27:20:56.493	0.7708	2015 Mar 19	91.2
...	Keck24	NB704–018532_NB711–016028	Hβ	13:24:19.058	+27:15:37.422	0.4564	2015 Mar 19	120.0
MK02	Keck25	NB711–077774_NB973–125003	Hβ,Hα+[S II]	13:25:22.936	+27:37:40.327	0.4641	2015 Mar 19	120.0
...	Keck26	NB816–092852	[O III]	13:25:29.326	+27:29:00.488	0.6299	2015 Mar 19	120.0
...	Keck27	IA679–108617_NB711–067586_NB921–122085	[O II],[Ne III],[O III]	13:25:22.104	+27:33:55.245	0.8414	2015 Mar 19	120.0
...	Keck28	NB816–084418	Hβ	13:24:35.673	+27:27:05.894	0.6805	2015 Mar 26	135.0
...	Keck29	NB816–078942	[O III]	13:24:15.264	+27:25:59.997	0.6148	2015 Mar 26	135.0
...	Keck30	NB973–080087	Hα+[S II]	13:25:16.923	+27:24:28.982	0.4778	2015 Mar 26	140.0
...	Keck31	IA679–050336_NB704–040278_NB711–033474_NB921–067937	[O II],[Ne III],[O III]	13:25:15.388	+27:21:13.652	0.8281	2015 Mar 26	140.0
...	Keck32	NB711–031598	[O III]	13:25:13.092	+27:20:26.891	0.4315	2015 Mar 26	140.0
...	Keck33	IA598–123435	[O II]+[Ne III]	13:23:49.417	+27:36:52.935	0.6010	2015 Mar 26	150.0

Note. — (1): Abbreviated MMT+Keck merged name. (2): Abbreviated name for Keck [O III] λ4363-detected galaxy. (3): Full narrowband and/or intermediate-band excess emitter name. (4): Emission line(s) responsible for narrowband and/or intermediate-band excess. (5): Right ascension in units of hours, minutes, and seconds. (6): Declination in units of degrees, arcminutes, and arcseconds. (7): Spectroscopic redshift. (8): UT observation dates. (9): On-source integration time in units of minutes.

[a]This galaxy was previously targeted for its NB921 excess flux due to [O III]. It was not identified as a NB921 emitter in the re-selection because of its faintness. The NB704 excess is due to [Ne III] λ3869.

TABLE 6
STRONG NEBULAR EMISSION LINES FOR THE [O III] λ4363-DETECTED SAMPLE

ID (1)	[O II] 3727 (2)	[Ne III] 3869 (3)	[Ne III],Hε 3967,3970 (4)	Hδ 4101 (5)	Hγ 4340 (6)	[O III] 4363 (7)	Hβ 4861 (8)	[O III] 4959 (9)	[O III] 5007 (10)	Hα 6563 (11)	[S II] 6717 (12)	[S II] 6731 (13)
MK01	2.40±0.01[b]	0.41±0.01[b]	0.20±0.01[b]	0.26±0.01[b]	0.51±0.01[b]	0.07±0.01[b]	21.74±0.08[a]	1.53[a]	4.77[a]	3.04[a]	0.28±0.01[a]	0.30±0.01[a]
MK02	1.73±0.01[b]	0.34±0.01[b]	0.22[b]	0.23[b]	0.39[a]	0.03[a]	68.00±0.17[a]	1.47[a]	4.54[a]	2.43±0.01[da]	0.13[a]	0.09[a]
MK03	0.64±0.03[b]	0.50±0.03[b]	0.23±0.03[b]	0.21±0.03[b]	0.45±0.03[b]	0.12±0.02[a]	4.91±0.07[a]	2.35±0.01[a]	6.65±0.01[a]	2.75±0.02[a]	<0.05[a]	<0.05[a]
MK04	1.68±0.03[b]	0.39±0.02[b]	0.23±0.02[b]	0.27±0.01[a]	0.53±0.01[a]	0.07±0.01[a]	19.96±0.09[a]	1.95[da]	5.92[a]	3.06[a]	0.16±0.01[a]	...[c]
MMT01	1.23±0.02	0.40±0.02	0.22±0.02	0.20±0.02[d]	0.40±0.02	0.15±0.02	10.17±0.30	1.92±0.03	5.61±0.02	...[c]	...[c]	...[c]
MMT02	2.82±0.03	0.25±0.02	<0.05	0.24±0.02	0.38±0.02	0.04±0.01	7.55±0.15	1.04±0.02	2.90±0.02	...[c]	...[c]	...[c]
MMT03	3.68±0.06	0.24±0.04	<0.00	0.26±0.02	0.46±0.02	0.10±0.03	5.71±0.17	0.51±0.04	1.58±0.03	...[c]	...[c]	...[c]
MMT05	0.55±0.03	0.49±0.03	0.35±0.03	0.21±0.03	0.49±0.03	0.15±0.02	6.87±0.06[a]	2.46±0.01[a]	6.88±0.01[a]	2.79±0.01[a]	<0.02[a]	<0.03[a]
MMT07	1.09±0.01	0.44±0.01	0.27±0.01	0.20±0.01	0.50±0.01	0.13±0.01[d]	17.60±0.09[a]	1.93±0.01[a]	6.03[a]	3.37[a]	0.12±0.01[a]	0.09±0.01[a]
MMT08	2.86±0.02	0.27±0.02	<0.04	0.25±0.02	0.41±0.01	0.06±0.01	9.92±0.25	1.18±0.03	3.29±0.03	...[c]	...[c]	...[c]
MMT09	3.45±0.06	0.31±0.05	<0.08	0.31±0.04	0.42±0.04	0.14±0.04	4.21±0.09[a]	1.50±0.02[a]	4.71±0.02[a]	3.13±0.03[da]	0.13±0.04[a]	0.36±0.05[da]
MMT10	1.36±0.02	0.37±0.01	0.14±0.01	0.26±0.01	0.44±0.01	0.09±0.01	20.93±0.16	1.69±0.01	5.11±0.01	3.09±0.01	0.16±0.01	0.12±0.01
MMT11	2.22±0.01	0.36±0.01	0.12±0.01	0.24±0.01	0.45±0.01	0.07±0.01	21.74±0.19	1.57±0.01	4.76±0.01	3.15±0.01	0.24±0.02[d]	0.29±0.02
MMT13	1.07±0.08	0.26±0.02	0.17±0.03[d]	0.28±0.03	0.47±0.02	0.11±0.02	6.52±0.07[a]	1.46±0.01[a]	4.32±0.01[a]	2.67±0.02[a]	<0.04[a]	<0.04[a]
MMT15	2.45±0.05	0.34±0.05	<0.08	0.14±0.02	0.33±0.02	0.11±0.03	8.49±0.18	0.91±0.02	2.70±0.02	2.84±0.02	0.28±0.02	0.21±0.02
MMT16	1.32±0.10	0.17±0.05	<0.00	0.21±0.03	0.46±0.04	0.14±0.04	6.46±0.22	1.05±0.03	3.28±0.04	3.05±0.03	0.25±0.04	0.22±0.04
MMT17	3.36±0.07	<0.18	<0.07	<0.04	0.29±0.03	0.11±0.03	12.37±0.32	0.60±0.02	1.80±0.03	3.08±0.01[a]	0.68±0.01[a]	0.52±0.01[a]
MMT18	1.15±0.05	0.16±0.04	0.18±0.05	0.26±0.03	0.34±0.04	0.11±0.03	7.01±0.30	0.91±0.04	2.66±0.03	2.56±0.01[a]	0.18±0.01[a]	0.12±0.01[da]
MMT19	1.20±0.01	0.44±0.01	0.24±0.01	0.25±0.01	0.45±0.01	0.10±0.01	30.17±0.31	1.87±0.01	5.63±0.01	3.01±0.01	...[c]	0.08±0.01
MMT20	3.22±0.04	0.17±0.05	<0.07	0.20±0.03	0.38±0.02	0.05±0.02	6.98±0.15	0.47±0.02	1.33±0.02	2.99±0.02[da]	...[c]	...[c]
MMT21	0.60±0.07	0.38±0.03	0.28±0.03	0.30±0.02	0.53±0.03	0.13±0.03[d]	6.32±0.17[d]	1.64±0.02	5.17±0.02[d]	2.46±0.06[a]	0.74±0.20[a]	<0.42[a]
MMT22	2.39±0.06	0.21±0.04	<0.07	0.42±0.05	0.44±0.05	0.13±0.04	3.52±0.16[a]	0.74±0.04[a]	2.21±0.04[a]	3.24±0.03[a]	0.29±0.04[a]	<0.10[a]
MMT23	1.46±0.06	0.37±0.04	...[c]	0.25±0.03	0.42±0.03	0.10±0.03	4.05±0.33	1.91±0.06	5.75±0.05[d]	...[c]	...[c]	...[c]
MMT24	1.34±0.02	0.49±0.08	0.32±0.09	0.24±0.02	0.47±0.04	0.08±0.01	15.31±0.22	2.01±0.01[d]	5.92±0.02	...[c]	...[c]	...[c]
MMT25	1.03±0.05[d]	0.48±0.04	0.37±0.06	0.28±0.04	0.44±0.03	0.08±0.02	6.09±0.09[a]	2.08±0.01[a]	6.21±0.01[a]	2.85±0.02[a]	0.11±0.03[a]	<0.16[a]
MMT26	3.34±0.02	0.25±0.02	<0.04	0.19±0.01	0.41±0.01	0.05±0.01	24.07±0.23	0.79±0.01	2.48±0.01	3.29±0.01	0.57±0.01	0.38±0.01[d]
MMT27	1.27±0.12	0.49±0.15	<0.27	0.49±0.10	0.64±0.09	0.36±0.09	1.65±0.14	1.48±0.11	4.53±0.10	3.34±0.14	<0.98	<0.29
MMT28	1.28±0.11	0.38±0.10	0.45±0.11	<0.21	0.51±0.08	0.16±0.05	3.00±0.28	1.96±0.09	5.93±0.08	4.21±0.20	<0.33	...[c]
MMT29	1.69±0.01[d]	0.41±0.01	0.21±0.01	0.27±0.01	0.44±0.01	0.05±0.01	21.66±0.18	1.65±0.01	4.97±0.01	3.22[a]	0.23±0.01[da]	0.14±0.01[a]
MMT30	2.54±0.02	0.33±0.02	0.06±0.01	0.22±0.01	0.46±0.02	0.04±0.01	16.63±0.26	1.22±0.01	3.70±0.01	3.05±0.05	0.36±0.04	0.15±0.04[d]
MMT31	2.23±0.01[d]	0.30±0.01	0.12±0.01	0.22±0.01	0.45±0.01	0.05±0.01	32.20±0.19	1.24±0.01	3.76±0.01	3.32±0.02	0.23±0.02	0.22±0.02
MMT32	1.95±0.04	0.34±0.02	0.12±0.01	0.19±0.01	0.44±0.01	0.03±0.01	43.08±0.32	1.47±0.01	4.24±0.01	3.47±0.01	0.29±0.01	0.22±0.01[d]
MMT33	0.28±0.03	0.39±0.03	0.29±0.03	0.19±0.02	0.44±0.02	0.18±0.02	6.82±0.12[a]	1.72±0.02[da]	5.17±0.01[a]	2.96±0.02[a]	<0.05[a]	<0.05[a]
MMT34	1.87±0.03	0.39±0.04	0.12±0.03	<0.09	0.40±0.03	0.08±0.02	4.40±0.08[a]	1.61±0.02[a]	4.86±0.02[da]	2.22±0.02[a]	0.30±0.02[a]	0.15±0.03[a]
MMT35	2.86±0.04	0.44±0.04	<0.07	0.19±0.04	0.35±0.03	0.13±0.04	3.88±0.14	1.17±0.03	3.58±0.03[d]	...[c]	...[c]	...[c]
MMT37	2.15±0.02	0.37±0.02	0.16±0.02[d]	0.20±0.01	0.40±0.02	0.08±0.02	9.73±0.33	1.41±0.02	4.50±0.03	...[c]	...[c]	...[c]
MMT38	0.69±0.09	0.56±0.06[a]	0.27±0.06[d]	0.28±0.03[a]	0.54±0.03[a]	0.39±0.12	2.61±0.10[a]	2.28±0.03[a]	7.27±0.03[a]	...[c]	...[c]	...[c]
Keck01	0.60±0.02	0.34±0.02	0.17±0.02	0.18±0.01	0.38±0.01	0.10±0.01	7.72±0.09[d]	1.99±0.01	5.90±0.01	...[c]	...[c]	...[c]
Keck02	1.48±0.05	0.37±0.03	0.24±0.05	0.27±0.03	0.47±0.02	0.27±0.04	2.40±0.04[e]	1.80±0.02	5.60±0.02[d]	...[c]	...[c]	...[c]
Keck03	2.35±0.01	0.22±0.01	0.04±0.01	0.20±0.01	0.37±0.01	0.02[d]	12.21±0.08	1.17±0.01	3.50±0.01	...[c]	...[c]	...[c]
Keck04	1.82±0.02	0.46±0.01	0.29±0.02	0.25±0.01	0.52±0.01[d]	0.05±0.01[d]	6.19±0.10	1.40±0.02	4.35±0.02[df]	...[c]	...[c]	...[c]
Keck05	1.25±0.04	0.38±0.03	0.30±0.05	0.27±0.02	0.66±0.04[d]	0.29±0.07[d]	1.60±0.04[d]	1.49±0.02	4.96±0.02[d]	...[c]	...[c]	...[c]
Keck06	<0.09	0.19±0.03	<0.27	0.23±0.04	1.37±0.08	0.18±0.03[d]	1.10±0.02[d]	1.48±0.02	4.10±0.02	...[c]	...[c]	...[c]
Keck07	1.17±0.04	0.40±0.02	<0.07	0.23±0.02	0.52±0.02[d]	0.09±0.01	3.27±0.05	2.13±0.02[d]	6.91±0.03	...[c]	...[c]	...[c]
Keck08	1.17±0.02	0.40±0.01	0.24±0.02	0.27±0.02	0.40±0.01	0.12±0.01	5.63±0.13	1.72±0.03	4.30±0.02	...[c]	...[c]	...[c]
Keck09	1.53±0.06	0.78±0.04	0.51±0.06[d]	0.39±0.04	0.46±0.02	0.08±0.02	1.46±0.04	2.26±0.05	9.33±0.07	...[c]	...[c]	...[c]
Keck11	1.23±0.04	0.47±0.03	0.35±0.03	0.28±0.02	0.47±0.02[d]	<0.12[b]	4.62±0.05	1.73±0.01	5.05±0.01[d]	...[c]	...[c]	...[c]
Keck12	0.54±0.08	0.43±0.06	0.27±0.04	<0.00	0.50±0.06	0.16±0.03	0.53±0.03[d]	1.43±0.04	3.83±0.04	...[c]	...[c]	...[c]

Ly et al.

TABLE 6
Strong Nebular Emission Lines for the [O iii] λ4363-detected Sample

Keck13	0.26±0.06	0.42±0.04	0.22±0.05	0.42±0.04	0.44±0.03	0.17±0.03	0.72±0.02	1.42±0.03	4.64±0.03	…[c]	…[c]	…[c]
Keck14	2.20±0.01	0.36±0.01	0.22±0.01	0.26±0.01	0.43±0.01	0.07±0.01	11.59±0.10	1.64±0.01	5.09±0.01[f]	…[c]	…[c]	…[c]
Keck15	1.89±0.02	0.41±0.02[d]	0.10±0.01	0.17±0.01	0.41±0.02[d]	0.07±0.02	5.22±0.09	1.91±0.02	5.25±0.02	…[c]	…[c]	…[c]
Keck16	2.34±0.02	0.17±0.02[d]	<0.04	0.19±0.01	0.36±0.01	0.05±0.01[d]	8.83±0.13	0.54±0.01	1.71±0.01	…[c]	…[c]	…[c]
Keck18	2.36±0.04[b]	0.39±0.04[b]	0.15±0.03	0.27±0.02	0.42±0.02	0.06±0.02	4.97±0.06[d]	1.49±0.01	4.31±0.01	…[c]	…[c]	…[c]
Keck19	1.64±0.02	0.45±0.01	0.29±0.02	0.23±0.01	0.49±0.01[d]	0.06±0.01[d]	7.88±0.08[d]	1.71±0.01	4.84±0.01[d]	…[c]	…[c]	…[c]
Keck20	1.67±0.15[b]	<0.50[b]	…[c]	<0.32[b]	0.34±0.08	0.25±0.08	1.82±0.10	1.31±0.05	4.17±0.06	2.86±0.03	0.11±0.03	<0.07
Keck21	1.65±0.03	0.35±0.02	…[c]	0.23±0.02	0.47±0.02	0.09±0.02	2.15±0.05	2.17±0.03	4.49±0.04[d]	…[c]	…[c]	…[c]
Keck23	0.55±0.04	0.58±0.03	0.39±0.04	0.29±0.03	0.55±0.02	0.15±0.02	2.04±0.05	1.69±0.02[d]	5.57±0.02	…[c]	…[c]	…[c]
Keck24	2.20±0.01[b]	0.17±0.01[b]	…[c]	0.18±0.01[b]	0.38±0.01[b]	0.04±0.01[b]	24.02±0.13	0.72	1.96	3.33±0.01	0.38±0.01	0.26±0.01
Keck26	3.06±0.06[b]	0.73±0.07[b]	…[c]	0.25±0.04	0.44±0.03	0.10±0.03	4.78±0.15	1.35±0.03	3.58±0.03[d]	…[c]	…[c]	…[c]
Keck27	0.86±0.01[d][b]	0.08±0.01	0.02	0.11	0.30±0.01	0.05±0.01	78.73±0.38[d]	1.13±0.01	3.14±0.01	…[c]	…[c]	…[c]
Keck28	0.85±0.02	0.32±0.01[d]	0.22±0.01	0.18±0.01	0.37±0.01	0.08±0.01	9.23±0.08	1.84±0.01	5.46±0.01	…[c]	…[c]	…[c]
Keck29	1.34±0.21[g]	0.41±0.05	0.24±0.07	0.26±0.04	0.38±0.03	0.08±0.03	1.85±0.06	2.06±0.03	6.24±0.03	…[c]	…[c]	…[c]
Keck30	2.58±0.03[b]	0.42±0.02[b]	…[c]	0.23±0.02[b]	0.56±0.02	0.05±0.01	9.28±0.11	1.56±0.01	4.12±0.01	3.10±0.03	0.14±0.02	0.15±0.02
Keck31	1.28±0.02	0.46±0.01	0.25±0.02	0.23±0.01	0.47±0.01[d]	0.11±0.01	4.65±0.05	1.78±0.01	4.47±0.01[d]	…[c]	…[c]	…[c]
Keck32	1.84±0.10[b]	0.37±0.11[b]	…[c]	0.25±0.08	0.55±0.08	0.29±0.08	1.82±0.09	1.76±0.04	4.89±0.03	2.96±0.05	<0.13	…[c]
Keck33	1.56±0.07	0.49±0.04	0.40±0.05	0.37±0.02	0.59±0.02	0.14±0.02	5.24±0.07[d]	1.40±0.01	3.95±0.01	…[c]	…[c]	…[c]

Note. — (1): Abbreviated name for MMT/Keck [O iii] λ4363-detected galaxy. (2)–(13): Emission-line fluxes from shorter to longer wavelengths. All fluxes are observed values, prior to any correction for dust attenuation. All line fluxes, except for Hβ, are reported relative to the Hβ intensity. The Hβ observed fluxes are normalized to 10^{-17} erg s^{-1} cm^{-2}. Upper limits are provided for emission lines undetected at 3σ.

[a] Measurements are from Keck/DEIMOS.

[b] Measurements are from MMT/Hectospec.

[c] Measurements are unavailable due to limited spectral coverage.

[d] Measurements may be affected by OH night skyline contamination. This is determined if at least half of the line flux falls on a region with any OH skyline emission. This does not account for the strength of the emission line.

[e] The Hβ line fell inside a CCD gap. The reported flux here is derived from Hγ assuming zero reddening.

[f] [O iii] λ5007 are unavailable due to limited spectral coverage. We adopt a flux that is 3.1 times the 4959Å flux.

[g] [O ii] fluxes were unavailable. We adopt a relation between [O ii]/Hβ and [O iii]/Hβ (see Figure 28).

TABLE 7
WEAK NEBULAR EMISSION LINES FOR THE [O III] λ4363-DETECTED SAMPLE

ID (1)	H10 3798 (2)	H9 3835 (3)	Hζ,He I 3889 (4)	He I 4471 (5)	He I 5876 (6)	[O I] 6300 (7)	[N II] 6548 (8)	[N II] 6584 (9)	He I 6678 (10)	He I 7065 (11)	[Ar III] 7135 (12)	[O II] 7319 (13)	[O II] 7330 (14)
MK01	<0.50[b]	<0.09[b]	0.17±0.01[b]	0.04±0.00[a]	0.10±0.00[da]	0.11±0.00[da]	0.03[a]	0.10[a]	<0.06[a]	...[c]	...[c]	...[c]	...[c]
MK02	<0.01[b]	<0.11[b]	0.13±0.01[b]	0.03±0.00[a]	0.12±0.00[a]	0.06±0.00[a]	<0.01[a]	0.15±0.01[a]	<0.01[a]	...[c]	...[c]	...[c]	...[c]
MK03	<0.15[b]	<1.91[b]	0.14±0.03[b]	<0.07[b]	0.10±0.01[a]	0.04±0.01[da]	<0.04[a]	<0.08[a]	0.08±0.01[a]	...[c]	...[c]	...[c]	...[c]
MK04	...[c]	<0.27[b]	0.15±0.02[b]	0.04±0.01[a]	0.13±0.00[a]	0.02±0.00[da]	0.04[a]	0.12[a]	0.06±0.01[a]	...[c]	...[c]	...[c]	...[c]
MMT01	<0.06	<0.13	0.12±0.02	<0.07	...[c]	...[c]	...[c]	...[c]	...[c]	...[c]	...[c]	...[c]	...[c]
MMT02	<0.31	...[c]	<0.06	<0.05	0.15±0.02[da]	<0.36	...[c]	...[c]	...[c]	...[c]	...[c]	...[c]	...[c]
MMT03	<0.16	<0.09	<0.10	0.06±0.02	0.28±0.09	0.42±0.04[a]	...[c]	...[c]	...[c]	...[c]	...[c]	...[c]	...[c]
MMT05	<0.15	<0.17	0.14±0.02	<0.07	0.07±0.01[a]	<0.04[a]	0.02±0.01[da]	0.02±0.01[a]	<0.01[a]	<0.04[a]	<0.04[a]	...[c]	...[c]
MMT07	<0.27	<0.13	0.17±0.01	0.04±0.01	0.12±0.00[a]	0.04±0.00[a]	0.04[a]	0.08[a]	0.05±0.01[a]	<0.01[a]	...[c]	...[c]	...[c]
MMT08	<0.04	<0.09	0.09±0.01	<0.04	...[c]	...[c]	...[c]	...[c]	...[c]	...[c]	...[c]	...[c]	...[c]
MMT09	<0.17	<0.08	<0.18	<0.11[a]	0.13±0.02[a]	<0.08[a]	<0.07[a]	<0.08[a]	<0.07[a]	...[c]	...[c]	...[c]	...[c]
MMT10	<0.24	<0.09	0.13±0.01	0.05±0.01	0.11±0.01	0.04±0.01	<0.01	0.08±0.01	<0.05	<0.01	0.12±0.01	0.07±0.01	<0.03
MMT11	<0.01	<0.08	0.12±0.01	0.04±0.01	0.11±0.01	...[c]	<0.03	0.12±0.02	<0.06	...[c]	0.07±0.02[d]	0.08±0.02	<0.01
MMT13	5.41±0.03[d]	<0.05	0.11±0.02	0.04±0.01[a]	0.10±0.01[da]	0.03±0.01[a]	0.04±0.01[da]	<0.04[a]	<0.04[a]	...[c]	...[c]	...[c]	...[c]
MMT15	<0.42	0.36±0.06	<0.12	0.12±0.16	0.11±0.02[d]	0.09±0.02	0.06±0.02	0.13±0.01	<0.09	<0.06	<0.06	<0.09	
MMT16	<0.28	<0.12	<0.18	<0.08	0.23±0.09	0.09±0.03	<0.10	0.10±0.02	<0.09	<0.17	<0.12	<0.11	0.25±0.05
MMT17	<0.41	<0.09	<0.00	<0.08	0.12±0.02[d]	0.13±0.01[a]	0.14±0.01[a]	0.43±0.01[a]	<0.16[a]	<0.04[a]	0.06±0.01[a]	0.16±0.03[d]	0.03±0.01[a]
MMT18	<0.18	<0.07	0.17±0.05	<0.06	0.10±0.01[a]	0.02±0.01[a]	<0.06[a]	0.04±0.01[da]	<0.04[a]	0.02±0.01[a]	0.06±0.01[a]	<0.01	<0.01[a]
MMT19	<0.26	<0.14	0.23±0.01	0.04±0.01	0.11±0.01[d]	0.06±0.01	<0.03	0.04±0.01	<0.01	<0.04	<0.09	<0.04	...[c]
MMT20	<0.01	<0.06	<0.08	0.08±0.02	0.14±0.02[da]	0.15±0.05	0.15±0.02[a]	0.44±0.02[a]	...[c]	...[c]	...[c]	...[c]	...[c]
MMT21	<0.14	<0.10	0.20±0.03	<0.06	0.25±0.03[da]	<0.19[a]	...[c]	<0.18[a]	<0.16[a]	...[c]	...[c]	...[c]	...[c]
MMT22	<0.08	<0.23	<0.10	0.10±0.03[a]	0.17±0.02[a]	<0.15[a]	<0.08[a]	0.40±0.04[a]	<0.12[a]	...[c]	...[c]	...[c]	...[c]
MMT23	<0.14	<0.30	0.16±0.03	0.07±0.02	1.41±0.15[d]	...[c]	...[c]	...[c]	...[c]	...[c]	...[c]	...[c]	...[c]
MMT24	<0.26	<0.26	<0.25	<0.01	<0.31	...[c]	...[c]	...[c]	...[c]	...[c]	...[c]	...[c]	...[c]
MMT25	<0.07	<0.08	0.15±0.04	<0.07	0.13±0.01[a]	<0.01[a]	<0.07[a]	<0.04[a]	<0.05[a]	...[c]	...[c]	...[c]	...[c]
MMT26	<0.01	<0.09	<0.04	<0.01	0.13±0.01	0.14±0.02[d]	0.13±0.01	0.34±0.01[d]	<0.22	<0.04	...[c]	<0.26	<0.12
MMT27	<0.30	<0.28	0.34±0.10	0.37±0.09	<0.15	<0.21	<0.32	<0.26	0.71±0.18	<0.49	...[c]	<0.44	...[c]
MMT28	<0.31	...[c]	<0.30	<0.15	0.25±0.07	...[c]	<0.17	<0.78	<1.04	<0.27	0.46±0.14[d]	<0.45	<0.47
MMT29	<0.68	<0.12	0.16±0.01	0.02±0.01	0.11±0.00[da]	0.05±0.00[a]	<0.01[a]	0.12±0.01[a]	0.03±0.01[da]	...[c]	...[c]	...[c]	...[c]
MMT30	<0.41	<0.07	0.08±0.01	<0.03	0.10±0.03	<0.07	0.22±0.04	0.36±0.04[d]	<0.12	...[c]	...[c]	...[c]	...[c]
MMT31	...[c]	<0.08	0.12±0.01	0.03±0.01	0.13±0.01	0.05±0.01	0.12±0.01	0.31±0.02[d]	...[c]	...[c]	...[c]	...[c]	...[c]
MMT32	<0.34	<0.08	0.24±0.02	0.03±0.01	0.13±0.01	0.06±0.01	0.04±0.01	0.14±0.01	...[c]	0.03±0.01	0.11±0.01	<0.01	0.03±0.01
MMT33	<0.06	<0.14	0.15±0.02	<0.05	0.11±0.01[a]	...[c]	...[c]	0.10±0.03[a]	0.05±0.01[a]	...[c]	...[c]	...[c]	...[c]
MMT34	<0.01	<0.21	0.14±0.04	<0.06[a]	0.10±0.01[a]	0.34±0.11[d]	<0.05[a]	0.08±0.03[a]	0.06±0.02[a]	...[c]	...[c]	...[c]	...[c]
MMT35	<0.01	<0.01	<0.09	<0.06	<0.60	...[c]	...[c]	...[c]	...[c]	...[c]	...[c]	...[c]	...[c]
MMT37	<0.06	...[c]	0.20±0.02	0.06±0.01[d]	...[c]	...[c]	...[c]	...[c]	...[c]	...[c]	...[c]	...[c]	...[c]
MMT38	<0.11	<0.12	0.26±0.08	...[c]	<0.16[a]	...[c]	...[c]	...[c]	...[c]	...[c]	...[c]	...[c]	...[c]
Keck01	<0.04	<0.06	0.08±0.01	0.05±0.01	...[c]	...[c]	...[c]	...[c]	...[c]	...[c]	...[c]	...[c]	...[c]
Keck02	<0.09	<0.14	0.10±0.03	<0.06	...[c]	...[c]	...[c]	...[c]	...[c]	...[c]	...[c]	...[c]	...[c]
Keck03	0.10±0.01	...[c]	0.15±0.01	0.03±0.01	...[c]	...[c]	...[c]	...[c]	...[c]	...[c]	...[c]	...[c]	...[c]
Keck04	0.05±0.01	<0.05	0.17±0.01	<0.04	...[c]	...[c]	...[c]	...[c]	...[c]	...[c]	...[c]	...[c]	...[c]
Keck05	0.03±0.01[d]	<0.12	0.15±0.03[d]	<0.10	...[c]	...[c]	...[c]	...[c]	...[c]	...[c]	...[c]	...[c]	...[c]
Keck06	...[c]	<0.11	0.14±0.03	<0.04	...[c]	...[c]	...[c]	...[c]	...[c]	...[c]	...[c]	...[c]	...[c]
Keck07	0.14±0.02	<0.08	0.17±0.02[d]	...[c]	...[c]	...[c]	...[c]	...[c]	...[c]	...[c]	...[c]	...[c]	...[c]
Keck08	<0.04	<0.07	0.17±0.01	<0.03	...[c]	...[c]	...[c]	...[c]	...[c]	...[c]	...[c]	...[c]	...[c]
Keck09	<0.14	<0.13	0.30±0.06[d]	<0.08	...[c]	...[c]	...[c]	...[c]	...[c]	...[c]	...[c]	...[c]	...[c]
Keck11	0.14±0.03	0.17±0.03	0.20±0.03	...[c]	0.12±0.02	<0.12	...[c]	...[c]	...[c]	...[c]	...[c]	...[c]	...[c]
Keck12	<0.18	<0.18	0.25±0.06	0.07±0.02	...[c]	...[c]	...[c]	...[c]	...[c]	...[c]	...[c]	...[c]	...[c]
Keck13	<0.08	<0.14	0.15±0.03[d]	0.08±0.02	...[c]	...[c]	...[c]	...[c]	...[c]	...[c]	...[c]	...[c]	...[c]

TABLE 7 — *Continued*

ID (1)	H10 3798 (2)	H9 3835 (3)	Hζ,He I 3889 (4)	He I 4471 (5)	He I 5876 (6)	[O I] 6300 (7)	[N II] 6548 (8)	[N II] 6584 (9)	He I 6678 (10)	He I 7065 (11)	[Ar III] 7135 (12)	[O II] 7319 (13)	[O II] 7330 (14)
Keck14	0.05±0.01[d]	<0.08	0.18±0.01	0.04±0.00[d]	...[c]	...[c]	...[c]	...[c]	...[c]	...[c]	...[c]	...[c]	...[c]
Keck15	<0.06	<0.10	0.13±0.02[d]	<0.01	...[c]	...[c]	...[c]	...[c]	...[c]	...[c]	...[c]	...[c]	...[c]
Keck16	<0.05	<0.05	0.14±0.01	<0.01	...[c]	...[c]	...[c]	...[c]	...[c]	...[c]	...[c]	...[c]	...[c]
Keck18	...[c]	...[c]	0.16±0.02	0.05±0.01	0.15±0.02	...[c]	...[c]	...[c]	...[c]	...[c]	...[c]	...[c]	...[c]
Keck19	0.07±0.01	<0.11	0.18±0.01	0.04±0.01	...[c]	...[c]	...[c]	...[c]	...[c]	...[c]	...[c]	...[c]	...[c]
Keck20	...[c]	...[c]	<0.27[b]	<0.21[b]	<0.08[b]	0.18±0.04[d]	<0.10	0.12±0.03[d]	<0.07[b]	<0.14	...[c]	...[c]	...[c]
Keck21	<0.07	<0.08	0.12±0.02	0.05±0.02[d]	...[c]	...[c]	...[c]	...[c]	...[c]	...[c]	...[c]	...[c]	...[c]
Keck23	0.11±0.04	<0.11	0.14±0.02	...[c]	...[c]	...[c]	...[c]	...[c]	...[c]	...[c]	...[c]	...[c]	...[c]
Keck24	...[c]	...[c]	0.16±0.01[b]	0.04±0.01	0.14±0.00	0.11±0.00	0.19±0.01	0.46±0.01	<0.14	...[c]	...[c]	...[c]	...[c]
Keck26	...[c]	...[c]	0.16±0.05[b]	...[c]	<0.12	...[c]	...[c]	...[c]	...[c]	...[c]	...[c]	...[c]	...[c]
Keck27	<0.01[b]	<0.01	0.05±0.01[d]	0.02±0.00	...[c]	...[c]	...[c]	...[c]	...[c]	...[c]	...[c]	...[c]	...[c]
Keck28	0.03±0.01	<0.08	0.15±0.01	0.02±0.00	...[c]	...[c]	...[c]	...[c]	...[c]	...[c]	...[c]	...[c]	...[c]
Keck29	...[c]	...[c]	<0.19	0.07±0.02	<0.13	...[c]	...[c]	...[c]	...[c]	...[c]	...[c]	...[c]	...[c]
Keck30	...[c]	...[c]	0.15±0.02[b]	0.09±0.01	0.16±0.01	0.07±0.01	0.16±0.02[d]	0.22±0.03	<0.03	...[c]	...[c]	...[c]	...[c]
Keck31	<0.03[b]	...[c]	0.17±0.01	0.06±0.01	...[c]	...[c]	...[c]	...[c]	...[c]	...[c]	...[c]	...[c]	...[c]
Keck32	...[c]	...[c]	<0.30[b]	<0.10	0.11±0.02	0.10±0.03	<0.11	<0.12	<0.09	...[c]	...[c]	...[c]	...[c]
Keck33	<0.08	<0.20	0.25±0.03	<0.04	0.09±0.01	...[c]	...[c]	...[c]	...[c]	...[c]	...[c]	...[c]	...[c]

NOTE. — (1): Abbreviated name for MMT/Keck [O III] λ4363-detected galaxy. (2)–(14): Emission-line fluxes from shorter to longer wavelengths. All fluxes are observed values, prior to any correction for dust attenuation. All line fluxes, except for Hβ, are reported relative to the Hβ intensity. The Hβ observed fluxes are normalized to 10^{-17} erg s^{-1} cm^{-2}. Upper limits are provided for emission lines undetected at 3σ.

[a] Measurements are from Keck/DEIMOS.

[b] Measurements are from MMT/Hectospec.

[c] Measurements are unavailable due to limited spectral coverage.

[d] Measurements are affected by OH night skyline contamination. This is determined if at least half of the line flux falls on a region with any OH skyline emission. This does not account for the strength of the emission line.

Ly et al.

TABLE 8
FLUX SELECTION FOR [O III] $\lambda 4363$-NON-DETECTED SAMPLES

Redshift (1)	Flux([O III]) (2)	N_z (3)	$N_{\rm [O\,III]}$ (4)	$N_{\rm ND}$ (5)	$N_{\rm final}$ (6)
MMT/Hectospec Selection
$z \leq 0.3$	1.67×10^{-16} (1.86×10^{-16})	101	100	22	22 (21)
$0.3 < z \leq 0.5$	1.59×10^{-16} (1.91×10^{-16})	389	378	38	28 (19)
$0.5 < z \leq 1.0$	2.58×10^{-16} (3.28×10^{-16})	148	122	7	1 (0)
Keck/DEIMOS Selection
$0.10 < z \leq 0.30$	1.30×10^{-16} (1.50×10^{-16})	26	25	1	0 (0)
$0.30 < z \leq 0.50$	6.95×10^{-17} (8.11×10^{-17})	255	252	41	29 (24)
$0.50 < z \leq 0.70$	4.73×10^{-17} (5.88×10^{-17})	123	119	32	21 (16)
$0.70 < z \leq 0.88$	5.50×10^{-17} (6.61×10^{-17})	302	290	48	20 (19)
$0.88 < z \leq 0.94$	9.22×10^{-17} (1.10×10^{-16})	133	114	7	5 (2)
$0.94 < z \leq 1.00$	1.48×10^{-16} (1.72×10^{-16})	38	38	3	3 (2)

NOTE. — (1): Redshift range. (2): [O III]$\lambda 5007$ emission-line flux limit in units of erg s^{-1} cm^{-2}. The first values are the initial flux limits for sample selection. The values in parentheses are stricter flux limits that are later adopted for the $M_\star$–Z relation analysis in Paper II. (3): Number of galaxies with MMT/Keck spectra within redshift range, N_z. (4): Number of N_z galaxies with [O III] measurements, $N_{\rm [O\,III]}$. (5): Number of $N_{\rm [O\,III]}$ galaxies that meet the [O III] flux limit, $N_{\rm ND}$. (6): Number of $N_{\rm ND}$ galaxies that remains after visual examination, $N_{\rm final}$ (see Section 3.2). The values in parentheses are those with the stricter [O III] flux limits.

TABLE 9
Summary of MMT [O iii] λ4363-non-detected Spectroscopic Sample

Merged ID	ID	Name	Line Sel.	R.A. (hr)	Decl. (deg)	z_{spec}	Obs. Dates (UT)	t_{int} (min.)
(1)	(2)	(3)	(4)	(5)	(6)	(7)	(8)	(9)
MK05	MMT12[a]	NB816–112403	[O iii]	13:25:21.779	+27:33:15.694	0.6404	2008 Apr 10, 2014 Feb 27–28, Mar 29	545.0
...	MMT40	NB816–020228	Hα	13:25:00.341	+27:14:10.575	0.2294	2008 Apr 10, 2014 Feb 27, Mar 25, 29–31	540.0
...	MMT41	NB816–042325	Hα	13:24:33.171	+27:18:15.605	0.2396	2008 Mar 13, 2014 Feb 27, Mar 25, 29–31	580.0
...	MMT42	NB816–049386	Hα	13:23:58.502	+27:19:42.156	0.2485	2008 Apr 11, 2014 Feb 27, Mar 25, 29–31	580.0
...	MMT43	NB816–053897	Hα	13:23:44.341	+27:20:41.263	0.2412	2008 Apr 14, 2014 Feb 27–28, Mar 29	585.0
...	MMT44	IA598–070330_NB816–063052	[O iii]+Hβ,Hα	13:25:11.510	+27:22:46.493	0.2328	2008 Apr 10, 2014 Feb 27–28, Mar 29	545.0
...	MMT45	NB816–067584	Hα	13:23:41.276	+27:23:43.814	0.2472	2008 Apr 14, 2014 Feb 28, Mar 25, 29–31	605.0
...	MMT46	NB816–068175	Hα	13:24:39.064	+27:23:49.369	0.2474	2008 Apr 11, 2014 Feb 27–28, Mar 29	585.0
...	MMT47	NB816–074041	Hα	13:23:45.608	+27:25:05.161	0.2476	2008 Apr 11, 2014 Feb 27, Mar 25, 29–31	580.0
...	MMT48	IA598–079058_NB816–074265	[O iii]+Hβ,Hα	13:23:55.902	+27:25:10.222	0.2320	2008 Mar 13, 2014 Feb 28, Mar 29	365.0
...	MMT49	NB816–087125	Hα	13:25:21.010	+27:28:00.881	0.2468	2014 Feb 27–28, Mar 29	465.0
...	MMT50	NB816–131598	Hα	13:23:38.752	+27:37:20.078	0.2488	2014 Mar 25, 30–31	240.0
...	MMT51	IA598–143748_NB816–155612	[O iii]+Hβ,[S ii]	13:25:00.103	+27:42:13.749	0.2069	2014 Mar 25, 30–31	240.0
...	MMT52	NB921–120215	Hα	13:24:39.357	+27:33:17.424	0.4000	2008 Apr 14, 2014 Feb 27, Mar 29	340.0
MK06	MMT53	NB973–046385	Hα+[S ii]	13:24:22.789	+27:16:32.622	0.4791	2014 Feb 28, Mar 29	245.0
MK07	MMT54[a]	NB973–082280	Hα	13:25:04.585	+27:24:59.256	0.4875	2008 Mar 13, 2014 Feb 27–28, Mar 29	585.0
...	MMT55	NB973–098596	Hα+[S ii]	13:24:03.322	+27:29:59.856	0.4786	2008 Apr 10, 2014 Feb 27–28, Mar 29	545.0
...	MMT56[a]	NB704–022868_NB711–019473	Hβ	13:24:53.145	+27:16:36.192	0.4557	2014 Feb 28, Mar 29	245.0
...	MMT57[a]	NB711–103300_NB973–151966	Hβ,Hα+[S ii]	13:25:27.817	+27:44:39.181	0.4673	2014 Mar 25, 30–31	240.0
...	MMT58	IA598–092080	[O iii]+Hβ	13:24:04.197	+27:28:29.219	0.2045	2008 Mar 13, 2014 Mar 28	240.0
...	MMT59	IA598–103632	[O iii]+Hβ	13:24:55.005	+27:31:43.732	0.2248	2014 Feb 27, Mar 29	220.0
...	MMT60	IA598–129517	[O iii]	13:24:27.891	+27:38:39.351	0.1926	2014 Mar 25, 30–31	240.0
...	MMT61	IA598–131217	[O iii]+Hβ	13:24:46.102	+27:39:04.256	0.2061	2014 Feb 28, Mar 29	245.0
...	MMT62	IA598–136216	[O iii]+Hβ	13:23:50.936	+27:40:23.268	0.2056	2014 Mar 25, 30–31	240.0
...	MMT63	IA598–148236	[O iii]	13:25:09.529	+27:43:12.952	0.1747	2014 Mar 25, 30–31	240.0
...	MMT64[a]	IA679–016985	[O iii]	13:23:58.107	+27:14:06.661	0.3464	2008 Mar 13, 2014 Feb 27, Mar 28, 29	460.0
...	MMT65	IA679–070658	[O iii]+Hβ	13:25:29.561	+27:25:35.072	0.3845	2014 Feb 28, Mar 29	245.0
...	MMT66	IA679–078892	[O iii]+Hβ	13:25:33.981	+27:27:21.660	0.3590	2008 Apr 10, 2014 Feb 28, Mar 29	325.0
...	MMT67	IA679–082069	[O iii]+Hβ	13:25:02.845	+27:28:03.078	0.3695	2008 Apr 14, 2014 Mar 25, 30–31	360.0
MK08	MMT68	IA679–106896	[O iii]+Hβ	13:25:14.498	+27:33:33.361	0.3692	2014 Mar 25, 30–31	240.0
...	MMT69	IA679–130624	[O iii]+Hβ	13:23:38.976	+27:38:29.999	0.3780	2014 Feb 28, Mar 29	245.0
...	MMT70[a]	IA679–135120	[O iii]+Hβ	13:24:54.858	+27:39:25.233	0.3706	2014 Feb 27, Mar 29	220.0
...	MMT71	IA679–144904	Hα+[S ii]	13:23:40.045	+27:41:45.061	0.0354	2014 Mar 25, 30–31	240.0
...	MMT72	IA679–148882	[O iii]+Hβ	13:23:46.377	+27:42:25.903	0.3665	2014 Feb 27, Mar 29	220.0
...	MMT73	IA679–176359	[O iii]+Hβ	13:24:37.317	+27:46:24.615	0.3612	2014 Feb 28, Mar 29	245.0
MK09	MMT74	NB704–023151_NB921–045274	[O iii],Hα	13:24:08.822	+27:16:51.127	0.4079	2014 Mar 25, 30–31	240.0
...	MMT75	NB704–036595_NB921–063857	[O iii],Hα	13:23:54.924	+27:20:16.152	0.3994	2014 Mar 25, 30–31	240.0
...	MMT76	NB704–065690_NB921–098686	[O iii],Hα	13:25:16.893	+27:28:12.492	0.3927	2014 Mar 25, 30–31	240.0
MK10	MMT77	NB704–067108_NB711–052756	[O iii]	13:24:42.913	+27:28:37.685	0.4209	2008 Apr 11, 2014 Feb 27, Mar 29	340.0
...	MMT78	NB704–069067_NB921–102626	[O iii],Hα	13:25:10.052	+27:29:10.802	0.3999	2008 Apr 11, 14, 2014 Feb 27, Mar 25, 29–31	700.0
...	MMT79[a]	NB704–088011_NB921–125515	[O iii],Hα	13:23:50.530	+27:34:31.712	0.4004	2008 Apr 11, 14, 2014 Feb 28, Mar 25, 29–31	725.0
...	MMT80	NB704–102796_NB921–143736	[O iii],Hα	13:23:45.853	+27:38:41.033	0.3993	2008 Mar 13, Apr 10, 2014 Feb 27–28, Mar 29	665.0
...	MMT81	NB704–107226_NB921–150262	[O iii],Hα	13:24:18.446	+27:40:08.560	0.3945	2014 Feb 28, Mar 29	245.0
...	MMT82[a]	IA679–140466_NB704–109627_NB921–152799	[O iii]+Hβ,Hα	13:24:11.144	+27:40:32.030	0.3923	2014 Feb 28, Mar 25, 29–31	485.0
MK11	MMT83	NB704–116143_NB711–092151_NB921–161808	[O iii],Hα	13:24:14.454	+27:42:23.328	0.4068	2008 Apr 11, 2014 Feb 27, Mar 25, 29–31	580.0
MK12	MMT84[a]	NB704–121337_NB921–168358	[O iii],Hα	13:25:06.738	+27:43:46.096	0.4050	2014 Feb 27, Mar 29	220.0
...	MMT85[a]	NB711–109221	[O iii]	13:24:21.123	+27:46:03.103	0.4229	2008 Apr 14, 2014 Feb 28, Mar 25, 29–31	605.0
...	MMT86	IA598–121381	[O iii]+Hβ	13:24:14.418	+27:36:25.036	0.2063	2014 Feb 27	120.0
...	MMT87	IA679–083407	[O iii]	13:24:25.587	+27:28:22.586	0.3323	2014 Mar 28	120.0
...	MMT88[a]	IA598–120619	[O iii]+Hβ	13:24:19.380	+27:36:11.104	0.2061	2014 Mar 28	120.0
...	MMT89	IA598–129182	[O iii]+Hβ	13:25:15.813	+27:38:36.550	0.2113	2014 Mar 28	120.0

TABLE 9
Summary of MMT [O III] λ4363-non-detected Spectroscopic Sample

Note. — (1): Abbreviated MMT+Keck merged name. (2): Abbreviated name for MMT [O III] λ4363-non-detected galaxy. (3): Full narrowband and/or intermediate-band excess emitter name. (4): Emission line(s) responsible for narrowband and/or intermediate-band excess. (5): Right ascension in units of hours, minutes, and seconds. (6): Declination in units of degrees, arcminutes, and arcseconds. (7): Spectroscopic redshift. (8): UT observation dates. (9): On-source integration time in units of minutes.

[a] Excluded from [O III] λ4363-non-detected sample with stricter [O III]λ5007 flux limit for $M_\star$−Z relation analyses.

TABLE 10
Summary of Keck [O III] λ4363-non-detected Spectroscopic Sample

Merged ID	ID	Name	Line Sel.	R.A. (hr)	Decl. (deg)	z_{spec}	Obs. Dates (UT)	t_{int} (min.)
(1)	(2)	(3)	(4)	(5)	(6)	(7)	(8)	(9)
. . .	Keck034	NB973–066061	Hα	13:24:37.504	+27:20:03.909	0.4830	2015 Mar 19, 2015 Mar 26	231.2
. . .	Keck035	NB704–089683_NB921–127544	Hα	13:24:44.854	+27:34:53.163	0.3924	2015 Mar 16, 26	268.7
. . .	Keck036[a]	NB711–044949_NB973–085127	Hβ,Hα+[S II]	13:25:08.009	+27:25:43.799	0.4638	2004 Apr 23, 2014 May 02	240.0
. . .	Keck037	NB816–031351	[O III]	13:24:27.480	+27:16:08.479	0.6338	2015 Mar 19, 2015 Mar 26	260.0
. . .	Keck038	NB816–044249	[O III]	13:24:47.966	+27:18:42.144	0.6361	2015 Mar 19, 2015 Mar 26	231.2
. . .	Keck039	NB816–055523	[O III]	13:25:20.409	+27:21:08.928	0.6381	2004 Apr 23, 2015 Mar 26	260.0
. . .	Keck040[a]	NB816–062942	[O III]	13:25:22.943	+27:22:36.976	0.6350	2009 Apr 27, 2015 Mar 26	140.0
. . .	Keck041	NB921–116861	[O III]	13:25:16.212	+27:32:31.769	0.8414	2004 Apr 24	153.2
. . .	Keck042	NB921–076426	[O III]	13:24:16.187	+27:23:14.783	0.8353	2004 Apr 23	117.6
. . .	Keck043	IA679–137004	[O II]+[Ne III]	13:24:46.685	+27:39:50.536	0.7893	2009 Apr 25	209.2
. . .	Keck044	IA679–060131_NB921–077548	[O III]	13:24:39.119	+27:23:32.952	0.8335	2014 May 02	120.0
MK07	Keck045	NB973–082280	Hα	13:25:04.585	+27:24:59.256	0.4875	2014 May 02	120.0
. . .	Keck046	NB921–096499	[O III]	13:25:26.221	+27:27:41.552	0.8491	2014 May 02	120.0
. . .	Keck047[a]	NB704–053974_NB921–084866	[O III],Hα	13:25:00.026	+27:25:03.967	0.4012	2014 May 02	120.0
. . .	Keck048[a]	NB921–066641	[O III]	13:24:31.652	+27:20:51.926	0.8378	2014 May 02	120.0
. . .	Keck049	NB921–075429	[O III]	13:24:42.836	+27:22:55.646	0.8620	2014 May 02	120.0
. . .	Keck050[a]	NB816–086272	[O III]	13:23:47.670	+27:27:29.323	0.6353	2015 Mar 17	100.0
. . .	Keck051	NB711–056257	[O III]	13:23:48.468	+27:29:56.944	0.4321	2015 Mar 17	100.0
. . .	Keck052	NB704–039343_NB711–032801	[O II]	13:23:52.639	+27:20:59.452	0.8962	2015 Mar 17	100.0
. . .	Keck053	NB973–088437	Hα	13:23:50.464	+27:26:47.444	0.4956	2015 Mar 17	100.0
. . .	Keck054	NB973–065432	Hα	13:23:56.250	+27:19:48.659	0.4982	2015 Mar 17	100.0
. . .	Keck055	IA679–061440	[O III]+Hβ	13:23:45.007	+27:23:45.208	0.3719	2015 Mar 17	100.0
. . .	Keck056	NB816–126254	Hβ	13:25:03.226	+27:36:06.868	0.6782	2015 Mar 17	118.7
. . .	Keck057	NB973–097546	Hα	13:24:02.732	+27:29:33.434	0.4857	2015 Mar 17	118.7
. . .	Keck058	NB816–088339	[O III]	13:24:07.075	+27:28:01.794	0.6225	2015 Mar 17	118.7
. . .	Keck059[a]	NB711–067164	[O III]	13:24:42.418	+27:33:46.662	0.4339	2015 Mar 17	118.7
. . .	Keck060	NB816–166713	[O III]	13:24:56.334	+27:44:15.066	0.6291	2015 Mar 17	120.0
. . .	Keck061	NB816–195145	[O III]	13:25:06.324	+27:46:32.031	0.6389	2015 Mar 17	120.0
MK11	Keck062	NB704–116143_NB711–092151_NB921–161808	[O III],Hα	13:24:14.454	+27:42:23.328	0.4067	2015 Mar 17	120.0
. . .	Keck063	NB704–119701_NB921–166360	[O III],Hα	13:25:05.013	+27:43:21.926	0.4126	2015 Mar 17	120.0
MK12	Keck064	NB704–121337_NB921–168358	[O III],Hα	13:25:06.738	+27:43:46.096	0.4049	2015 Mar 17	120.0
. . .	Keck065	NB921–161262	[O III]	13:24:40.551	+27:42:11.422	0.8426	2015 Mar 17	120.0
. . .	Keck066[a]	NB704–115977_NB711–091728_NB921–161613	[O II],Hβ	13:24:53.057	+27:42:14.443	0.8960	2015 Mar 17	120.0
. . .	Keck067[a]	NB704–117591	[O II]	13:25:08.778	+27:42:45.878	0.8868	2015 Mar 17	120.0
. . .	Keck068	NB704–023238_NB711–020109	[O III]	13:25:23.167	+27:16:47.769	0.4226	2015 Mar 19	91.2
. . .	Keck069	IA679–039224_NB921–056687	[O II],[O III]	13:25:01.388	+27:18:42.720	0.8308	2015 Mar 19	91.2
. . .	Keck070	IA598–056812	[O II]+[Ne III]	13:25:08.599	+27:19:07.144	0.5784	2015 Mar 19	91.2
. . .	Keck071	IA679–046035_NB921–064036	[O II],[O III]	13:24:52.419	+27:20:16.777	0.8303	2015 Mar 19	91.2
. . .	Keck072	IA679–028106_NB921–043761	[O II],[O III]	13:25:18.695	+27:16:28.261	0.8309	2015 Mar 19	91.2
. . .	Keck073	NB711–034815	[O III]	13:24:34.801	+27:21:57.453	0.4274	2015 Mar 19	91.2
MK06	Keck074	NB973–046385	Hα+[S II]	13:24:22.789	+27:16:32.622	0.4791	2015 Mar 19	120.0
MK09	Keck075	NB704–023151_NB921–045274	[O III],Hα	13:24:08.822	+27:16:51.127	0.4079	2015 Mar 19	120.0
. . .	Keck076	NB973–027748	Hα	13:24:33.146	+27:13:25.092	0.4973	2015 Mar 19	120.0
. . .	Keck077	IA598–051177_IA679–034589_NB921–052062	[O II],[O III]	13:24:25.305	+27:17:50.666	0.8527	2015 Mar 19	120.0
. . .	Keck078	NB973–045384	Hα	13:23:58.630	+27:16:20.605	0.4905	2015 Mar 19	120.0
. . .	Keck079[a]	NB816–025223	[O III]	13:24:43.074	+27:14:57.391	0.6311	2015 Mar 19	120.0
. . .	Keck080	NB816–042601	[O III]	13:24:03.409	+27:18:17.836	0.6303	2015 Mar 19	120.0
. . .	Keck081	IA679–038002_NB921–055672	[O III]	13:24:09.763	+27:18:28.170	0.8270	2015 Mar 19	120.0
. . .	Keck082	NB816–099821	[O III]	13:25:17.303	+27:30:40.684	0.6249	2015 Mar 19	120.0
. . .	Keck083	NB816–124363	[O III]	13:25:17.358	+27:35:44.696	0.6312	2015 Mar 19	120.0
MK05	Keck084	NB816–112403	[O III]	13:25:21.779	+27:33:15.694	0.6403	2015 Mar 19	120.0
. . .	Keck085	NB704–114264_NB921–159460	[O III],Hα	13:25:20.779	+27:41:53.061	0.3968	2015 Mar 19	120.0

TABLE 10
SUMMARY OF KECK [O III] λ4363-NON-DETECTED SPECTROSCOPIC SAMPLE

...	Keck086	NB816–128513	[O III]	13:25:13.026	+27:36:52.035	0.6142	2015 Mar 19	120.0
...	Keck087	NB921–124275	[O III]	13:25:27.473	+27:34:11.525	0.8419	2015 Mar 19	120.0
MK08	Keck088	IA679–106896	[O III]+Hβ	13:25:14.498	+27:33:33.361	0.3691	2015 Mar 19	120.0
...	Keck089[a]	NB704–109832_NB921–153297	[O III],Hα	13:25:12.993	+27:40:34.495	0.3986	2015 Mar 19	120.0
...	Keck090	NB704–091490_NB921–129670	[O III],Hα	13:25:16.274	+27:35:27.784	0.3935	2015 Mar 19	120.0
...	Keck091	NB816–133656	[O III]	13:25:26.774	+27:37:36.056	0.6572	2015 Mar 19	120.0
...	Keck092[a]	NB816–138010	[O III]	13:25:25.979	+27:38:35.121	0.6274	2015 Mar 19	120.0
...	Keck093[a]	NB973–112974	Hα+[S II]	13:25:25.276	+27:34:05.235	0.4772	2015 Mar 19	120.0
...	Keck094	IA679–147997	[O II]+[Ne III]	13:25:19.973	+27:42:07.151	0.7982	2015 Mar 19	120.0
MK10	Keck095	NB704–067108_NB711–052756	[O III]	13:24:42.913	+27:28:37.685	0.4207	2015 Mar 26	135.0
...	Keck096[a]	NB973–101901	[O III]	13:24:43.356	+27:31:03.199	0.9436	2015 Mar 26	135.0
...	Keck097	NB973–081775	Hα+[S II]	13:24:29.615	+27:25:05.704	0.4781	2015 Mar 26	135.0
...	Keck098	NB973–076558	Hα	13:25:22.991	+27:23:13.279	0.4931	2015 Mar 26	140.0
...	Keck099	NB973–076891	[O III]	13:25:05.585	+27:23:21.464	0.9553	2015 Mar 26	140.0
...	Keck100	IA679–043223_NB921–061111	[O III]	13:24:44.656	+27:19:35.345	0.8309	2015 Mar 26	140.0
...	Keck101	NB704–042024	Hδ	13:25:00.989	+27:21:50.278	0.7381	2015 Mar 26	140.0
...	Keck102[a]	NB816–069804	[O III]	13:25:06.866	+27:24:19.877	0.6335	2015 Mar 26	140.0
...	Keck103	NB921–065125	[O III]	13:24:52.112	+27:20:32.838	0.8443	2015 Mar 26	140.0
...	Keck104	NB816–058365	Hβ	13:25:03.962	+27:21:34.608	0.6762	2015 Mar 26	140.0
...	Keck105	NB973–121151	[O III]	13:24:18.732	+27:36:29.410	0.9550	2015 Mar 26	150.0
...	Keck106	NB816–123872	[O III]	13:24:07.888	+27:35:35.735	0.6335	2015 Mar 26	150.0
...	Keck107	NB711–081909	[O II]	13:24:41.023	+27:39:03.143	0.9035	2015 Mar 26	150.0
...	Keck108[a]	NB711–082636	[O II]	13:24:06.292	+27:39:16.629	0.9066	2015 Mar 26	150.0
...	Keck109	NB921–136194	[O III]	13:24:12.144	+27:36:53.285	0.8615	2015 Mar 26	150.0
...	Keck110	NB973–125544	Hα	13:24:20.581	+27:37:48.718	0.4934	2015 Mar 26	150.0
...	Keck111	IA679–129250	[O II]+[Ne III]	13:23:45.267	+27:38:06.873	0.7955	2015 Mar 26	150.0

NOTE. — (1): Abbreviated MMT+Keck merged name. (2): Abbreviated name for Keck [O III] λ4363-non-detected galaxy. (3): Full narrowband and/or intermediate-band excess emitter name. (4): Emission line(s) responsible for narrowband and/or intermediate-band excess. (5): Right ascension in units of hours, minutes, and seconds. (6): Declination in units of degrees, arcminutes, and arcseconds. (7): Spectroscopic redshift. (8): UT observation dates. (9): On-source integration time in units of minutes.

[a] Excluded from [O III] λ4363-non-detected sample with stricter [O III]λ5007 flux limit for $M_\star$–Z relation analyses.

Ly et al.

TABLE 11
Balmer Decrement Measurements and Derived Dust Reddening for
[O III] λ4363-detected Sample

ID	Hα/Hβ	Hγ/Hβ	EW(Hβ) (Å)	EW(Hγ) (Å)	EW(Hδ) (Å)	Source	E(B–V) (mag)
(1)	(2)	(3)	(4)	(5)	(6)	(7)	(8)
MK01	$3.04^{+0.01}_{-0.01}$	$0.51^{+0.01}_{-0.01}$	0.0	3.3	2.1	Hα/Hβ	0.05
MK02	$2.43^{+0.01}_{-0.01}$	$0.39^{+0.00}_{-0.00}$	0.0	1.0	1.6	Hα/Hβ	0.00[a]
MK03	$2.75^{+0.04}_{-0.04}$	$0.45^{+0.03}_{-0.02}$	0.0	1.0	2.0	Hα/Hβ	0.00±0.01[a]
MK04	$3.06^{+0.02}_{-0.02}$	$0.53^{+0.01}_{-0.01}$	0.0	0.0	2.0	Hα/Hβ	0.06
MMT01	. . .	$0.40^{+0.02}_{-0.02}$	0.0	1.0	2.0	Hγ/Hβ	$0.33^{+0.09}_{-0.10}$
MMT02	. . .	$0.38^{+0.02}_{-0.02}$	2.8	2.0	3.8	Hγ/Hβ	$0.41^{+0.13}_{-0.12}$
MMT03	. . .	$0.46^{+0.03}_{-0.03}$	1.7	2.4	2.4	Hγ/Hβ	$0.02^{+0.10}_{-0.13}$
MMT05	$2.79^{+0.03}_{-0.02}$	$0.49^{+0.03}_{-0.02}$	0.0	0.0	0.0	Hα/Hβ	0.00±0.01[a]
MMT07	$3.37^{+0.02}_{-0.02}$	$0.50^{+0.01}_{-0.01}$	0.0	0.0	0.0	Hα/Hβ	$0.14^{+0.01}_{-0.00}$
MMT08	. . .	$0.41^{+0.02}_{-0.02}$	0.0	2.8	5.3	Hγ/Hβ	$0.27^{+0.09}_{-0.10}$
MMT09	$3.13^{+0.07}_{-0.09}$	$0.42^{+0.04}_{-0.03}$	0.0	. . . [b]	2.7	Hα/Hβ	0.08±0.02
MMT10	$3.09^{+0.03}_{-0.02}$	$0.44^{+0.01}_{-0.01}$	0.0	1.2	2.9	Hα/Hβ	0.07±0.01
MMT11	$3.15^{+0.03}_{-0.04}$	$0.45^{+0.01}_{-0.01}$	1.8	2.7	3.7	Hα/Hβ	0.08±0.01
MMT13	$2.67^{+0.03}_{-0.04}$	$0.47^{+0.02}_{-0.02}$	0.0	1.0	2.0	Hα/Hβ	0.00±0.01[a]
MMT15	$2.84^{+0.06}_{-0.06}$	$0.33^{+0.02}_{-0.02}$	2.0	1.0	1.7	Hα/Hβ	0.00±0.02[a]
MMT16	$3.05^{+0.12}_{-0.12}$	$0.46^{+0.04}_{-0.04}$	3.7	4.7	1.7	Hα/Hβ	0.06±0.03
MMT17	$3.08^{+0.08}_{-0.09}$	$0.29^{+0.03}_{-0.03}$	2.0	. . . [b]	0.0	Hα/Hβ	0.06±0.02
MMT18	$2.56^{+0.10}_{-0.10}$	$0.34^{+0.03}_{-0.04}$	0.0	1.0	2.0	Hα/Hβ	0.00±0.03[a]
MMT19	$3.01^{+0.03}_{-0.04}$	$0.45^{+0.01}_{-0.01}$	0.0	1.0	2.0	Hα/Hβ	0.04±0.01
MMT20	$2.99^{+0.07}_{-0.06}$	$0.38^{+0.02}_{-0.02}$	1.8	2.3	1.0	Hα/Hβ	0.04±0.02
MMT21	$2.46^{+0.08}_{-0.11}$	. . . [c]	0.0	0.0	0.0	Hα/Hβ	0.00±0.03[a]
MMT22	$3.24^{+0.14}_{-0.14}$	$0.44^{+0.04}_{-0.05}$	0.0	1.0	4.1	Hα/Hβ	0.11±0.04
MMT23	$3.58^{+0.00}_{-0.00}$	$0.42^{+0.03}_{-0.04}$	6.4	1.0	2.0	Hα/Hβ	0.19
MMT24	. . .	$0.47^{+0.01}_{-0.02}$	0.0	1.0	8.2	Hγ/Hβ	$0.00^{+0.08}_{-0.05}$[a]
MMT25	$2.85^{+0.05}_{-0.04}$	. . . [c]	0.0	1.0	2.0	Hα/Hβ	0.00±0.01[a]
MMT26	$3.29^{+0.03}_{-0.03}$	$0.41^{+0.01}_{-0.01}$	1.4	1.5	2.4	Hα/Hβ	0.12±0.01
MMT27	$3.34^{+0.31}_{-0.33}$	$0.64^{+0.07}_{-0.12}$	0.0	0.0	0.0	Hα/Hβ	0.13±0.08
MMT28	$4.21^{+0.38}_{-0.44}$	$0.51^{+0.08}_{-0.10}$	0.0	0.0	0.0	Hα/Hβ	$0.33^{+0.07}_{-0.09}$
MMT29	$3.22^{+0.03}_{-0.02}$	$0.44^{+0.01}_{-0.01}$	0.0	0.0	3.4	Hα/Hβ	0.10±0.01
MMT30	$3.05^{+0.05}_{-0.07}$	$0.46^{+0.02}_{-0.01}$	3.0	3.7	2.9	Hα/Hβ	0.05±0.02
MMT31	$3.32^{+0.02}_{-0.03}$	$0.45^{+0.01}_{-0.01}$	1.7	2.2	2.0	Hα/Hβ	0.13±0.01
MMT32	$3.47^{+0.02}_{-0.02}$	$0.44^{+0.01}_{-0.01}$	1.0	2.0	1.5	Hα/Hβ	0.16±0.01
MMT33	$2.96^{+0.06}_{-0.06}$	$0.44^{+0.02}_{-0.02}$	0.0	0.0	0.0	Hα/Hβ	$0.03^{+0.01}_{-0.02}$
MMT34	$2.22^{+0.05}_{-0.05}$	$0.40^{+0.03}_{-0.02}$	0.0	0.0	0.0	Hα/Hβ	0.00±0.02[a]
MMT35	. . .	$0.35^{+0.03}_{-0.03}$	0.0	0.0	0.0	Hγ/Hβ	$0.59^{+0.23}_{-0.19}$
MMT37	. . .	$0.40^{+0.02}_{-0.02}$	0.0	2.3	3.1	Hγ/Hβ	$0.30^{+0.11}_{-0.10}$
MMT38	. . .	$0.54^{+0.04}_{-0.03}$	0.0	1.0	2.0	Hγ/Hβ	$0.00^{+0.12}_{-0.14}$[a]
Keck01	. . .	$0.38^{+0.01}_{-0.01}$	0.0	0.0	0.0	Hγ/Hβ	$0.43^{+0.05}_{-0.06}$
Keck02	. . .	. . . [d]	0.0	0.0	0.0	. . .	0.00[e]
Keck03	. . .	$0.37^{+0.01}_{-0.01}$	0.0	2.6	1.7	Hγ/Hβ	0.49±0.03
Keck04	. . .	$0.52^{+0.01}_{-0.01}$	0.0	0.0	0.0	Hγ/Hβ	0.00±0.05[a]
Keck05	. . .	. . . [c]	0.0	0.0	0.0	. . .	0.13±0.18
Keck06	. . .	. . . [c]	0.0	0.0	0.0	. . .	0.13±0.18

TABLE 11
Balmer Decrement Measurements and Derived Dust Reddening for
[O III] λ4363-detected Sample

(1)	(2)	(3)	(4)	(5)	(6)	(7)	(8)
Keck07	...	$0.52^{+0.02}_{-0.02}$	0.0	1.0	2.0	Hγ/Hβ	$0.00^{+0.09}_{-0.08}$ a
Keck08	...	$0.40^{+0.01}_{-0.02}$	0.0	1.0	0.0	Hγ/Hβ	$0.34^{+0.08}_{-0.07}$
Keck09	...	$0.46^{+0.02}_{-0.02}$	0.0	1.0	0.0	Hγ/Hβ	$0.02^{+0.09}_{-0.11}$
Keck11	...	$0.47^{+0.02}_{-0.02}$	0.0	1.0	2.0	Hγ/Hβ	$0.00^{+0.11}_{-0.09}$ a
Keck12	...	$0.50^{+0.06}_{-0.08}$	0.0	1.0	0.0	Hγ/Hβ	$0.00^{+0.20}_{-0.26}$ a
Keck13	...	$0.44^{+0.03}_{-0.05}$	0.0	0.0	0.0	Hγ/Hβ	$0.13^{+0.19}_{-0.15}$
Keck14	...	$0.43^{+0.01}_{-0.01}$	0.0	1.0	2.0	Hγ/Hβ	$0.16^{+0.03}_{-0.05}$
Keck15	...	$0.41^{+0.02}_{-0.02}$	0.0	1.0	1.3	Hγ/Hβ	$0.26^{+0.07}_{-0.10}$
Keck16	...	$0.36^{+0.01}_{-0.01}$	0.0	1.0	0.0	Hγ/Hβ	$0.55^{+0.09}_{-0.08}$
Keck18	...	$0.42^{+0.02}_{-0.02}$	0.0	1.0	4.8	Hγ/Hβ	$0.21^{+0.09}_{-0.08}$
Keck19	...	$0.49^{+0.01}_{-0.01}$	0.0	1.0	0.0	Hγ/Hβ	$0.00^{+0.03}_{-0.05}$ a
Keck20	$2.86^{+0.13}_{-0.17}$	$0.34^{+0.07}_{-0.09}$	0.0	1.0	0.0	Hα/Hβ	$0.00^{+0.04}_{-0.05}$ a
Keck21	...	$0.47^{+0.03}_{-0.02}$	0.0	1.0	2.0	Hγ/Hβ	0.01±0.11
Keck23	...	$0.55^{+0.02}_{-0.03}$	0.0	1.0	2.0	Hγ/Hβ	$0.00^{+0.10}_{-0.09}$ a
Keck24	$3.33^{+0.02}_{-0.02}$	$0.38^{+0.01}_{-0.01}$	0.0	1.0	0.6	Hα/Hβ	0.13
Keck26	...	$0.44^{+0.04}_{-0.03}$	0.0	1.0	2.0	Hγ/Hβ	$0.11^{+0.15}_{-0.19}$
Keck27	...	$0.30^{+0.00}_{-0.00}$	0.0	1.0	2.0	Hγ/Hβ	0.93±0.03
Keck28	...	$0.37^{+0.01}_{-0.01}$	0.0	1.0	2.0	Hγ/Hβ	$0.49^{+0.05}_{-0.07}$
Keck29	...	$0.38^{+0.03}_{-0.03}$	0.0	1.0	6.5	Hγ/Hβ	$0.41^{+0.16}_{-0.19}$
Keck30	$3.10^{+0.05}_{-0.05}$	$0.56^{+0.02}_{-0.02}$	0.0	0.0	4.1	Hα/Hβ	$0.07^{+0.02}_{-0.01}$
Keck31	...	$0.47^{+0.01}_{-0.01}$	0.0	1.0	3.1	Hγ/Hβ	$0.00^{+0.07}_{-0.05}$ a
Keck32	$2.96^{+0.14}_{-0.20}$	$0.55^{+0.09}_{-0.08}$	0.0	1.0	2.0	Hα/Hβ	$0.03^{+0.05}_{-0.04}$
Keck33	...	$0.59^{+0.02}_{-0.02}$	0.0	0.0	... b	Hγ/Hβ	$0.00^{+0.08}_{-0.07}$ a

Note. — (1): Abbreviated name for MMT/Keck [O III] λ4363-detected galaxy. (2): Hα/Hβ Balmer decrement. (3): Hγ/Hβ Balmer decrement. (4): Equivalent width of stellar absorption correction for Hβ. (5): Equivalent width of stellar absorption correction for Hγ. (6): Equivalent width of stellar absorption correction for Hδ. (7): Balmer decrement used to determine nebular reddening. (8): Derived color excess for dust reddening in the nebular gas.

[a] Negative reddening was seen. We adopt $E(B–V) = 0.0$.
[b] The continuum is too weak to measure the equivalent width of stellar absorption correction.
[c] Hγ is affected by an OH sky-line.
[d] Hβ affected by a gap between the blue and red CCDs.
[e] The Hγ and Hδ fluxes suggest no reddening.

TABLE 12
Stacked Balmer Decrement Measurements for
[O III] $\lambda4363$-non-detected Sample

		MMT			Keck		
$\log(L[\mathrm{H}\beta]/\mathrm{erg\ s}^{-1})$ (1)	Redshift (2)	Hα/Hβ (3)	Hγ/Hβ (4)	Hδ/Hβ (5)	Hα/Hβ (6)	Hγ/Hβ (7)	Hδ/Hβ (8)
MMT Sample							
38.452–40.127	0.035–0.346	3.60±0.07 (12)	0.50±0.02 (15)	0.25±0.02 (14)	. . .	. . .	. . .
40.129–40.460	0.206–0.467	3.80±0.14 (10)	0.40±0.01 (17)	0.26±0.03 (14)	5.83±0.14 (02)	. . .	. . .
40.468–41.126	0.359–0.640	2.40±0.07 (05)	0.47±0.01 (16)	0.26±0.02 (14)	3.07±0.02 (10)	0.64±0.03 (07)	0.17±0.02 (02)
Keck Sample							
40.072–40.518	0.369–0.633	2.52±0.32 (06)	0.34±0.03 (15)	0.26±0.05 (15)	3.46±0.06 (13)	0.63±0.04 (18)	0.14±0.03 (06)
40.525–40.783	0.405–0.676	. . .	0.46±0.03 (13)	0.25±0.02 (13)	5.67±0.11 (05)	0.57±0.03 (19)	0.28±0.03 (14)
40.800–41.048	0.407–0.907	. . .	. . .	. . .	. . .	0.56±0.02 (20)	0.30±0.01 (19)
41.054–41.993	0.408–0.955	. . .	. . .	. . .	6.39±0.11 (03)	0.44±0.02 (19)	0.21±0.03 (16)

Note. — (1): Range in Hβ luminosity for each $\log(L[\mathrm{H}\beta])$ bin. (2): Range in redshift. (3): Hα/Hβ Balmer decrement from MMT spectra. (4): Hγ/Hβ Balmer decrement from MMT spectra. (5): Hδ/Hβ Balmer decrement from MMT spectra. (6): Hα/Hβ Balmer decrement from Keck spectra. (7): Hγ/Hβ Balmer decrement from Keck spectra. (8): Hδ/Hβ Balmer decrement from Keck spectra. Values within parentheses for Cols. 3–8 indicate the number of galaxies used to compute the Balmer decrements.

TABLE 13
EMISSION-LINE RATIOS, ELECTRON DENSITIES AND TEMPERATURES, AND
GAS-PHASE METALLICITIES FOR [O III] λ4363-DETECTED GALAXIES

ID	$\log\left(\frac{[\text{O III}]}{[\text{O III}]\,\lambda4363}\right)$		$\log\left(T_e/\text{K}\right)$		$\log\left(\frac{\text{O II}}{\text{H}\beta}\right)$		$\log\left(\frac{\text{O III}}{\text{H}\beta}\right)$	$\log\left(\frac{\text{O}^+}{\text{H}^+}\right)$		$\log\left(\frac{\text{O}^{++}}{\text{H}^+}\right)$	$12+\log\left(\frac{\text{O}}{\text{H}}\right)$		n_e
	(dex)	(dex)	(dex)	(dex)	(dex)	(dex)	(dex)	(dex)	(dex)	(dex)	(dex)	(dex)	(cm^{-3})
(1)	(2)	(3)	(4)	(5)	(6)	(7)	(8)	(9)	(10)	(11)	(12)	(13)	(14)
MK01	$1.96^{+0.04}_{-0.04}$	$1.94^{+0.04}_{-0.04}$	$4.11^{+0.01}_{-0.02}$	$4.11^{+0.02}_{-0.02}$	$+0.38^{+0.00}_{-0.00}$	$+0.41^{+0.00}_{-0.00}$	$0.80^{+0.00}_{-0.00}$	$-4.08^{+0.07}_{-0.07}$	$-4.07^{+0.08}_{-0.06}$	$-4.12^{+0.04}_{-0.05}$	$8.21^{+0.06}_{-0.06}$	$8.21^{+0.06}_{-0.06}$	927^{+153}_{-99}
MK02	$2.27^{+0.03}_{-0.03}$	$2.27^{+0.03}_{-0.03}$	$4.00^{+0.01}_{-0.01}$	$4.00^{+0.01}_{-0.01}$	$+0.24^{+0.00}_{-0.00}$	$+0.24^{+0.00}_{-0.00}$	$0.78^{+0.00}_{-0.00}$	$-3.80^{+0.05}_{-0.06}$	$-3.80^{+0.05}_{-0.06}$	$-3.77^{+0.04}_{-0.04}$	$8.51^{+0.03}_{-0.05}$	$8.51^{+0.03}_{-0.05}$	<1
MK03	$1.87^{+0.06}_{-0.07}$	$1.87^{+0.06}_{-0.07}$	$4.15^{+0.03}_{-0.03}$	$4.15^{+0.03}_{-0.03}$	$-0.20^{+0.03}_{-0.02}$	$-0.20^{+0.03}_{-0.02}$	$0.95^{+0.00}_{-0.01}$	$-4.79^{+0.08}_{-0.14}$	$-4.79^{+0.08}_{-0.14}$	$-4.05^{+0.06}_{-0.08}$	$8.02^{+0.08}_{-0.09}$	$8.02^{+0.08}_{-0.09}$	...
MK04	$2.03^{+0.03}_{-0.03}$	$2.01^{+0.03}_{-0.03}$	$4.08^{+0.01}_{-0.01}$	$4.08^{+0.01}_{-0.02}$	$+0.22^{+0.01}_{-0.01}$	$+0.26^{+0.01}_{-0.01}$	$0.90^{+0.00}_{-0.00}$	$-4.13^{+0.05}_{-0.06}$	$-4.13^{+0.05}_{-0.06}$	$-3.94^{+0.04}_{-0.03}$	$8.29^{+0.04}_{-0.05}$	$8.28^{+0.05}_{-0.05}$	...
MMT01	$1.69^{+0.05}_{-0.07}$	$1.61^{+0.06}_{-0.08}$	$4.23^{+0.03}_{-0.03}$	$4.28^{+0.03}_{-0.04}$	$+0.10^{+0.01}_{-0.02}$	$+0.25^{+0.06}_{-0.04}$	$0.88^{+0.01}_{-0.01}$	$-4.77^{+0.09}_{-0.13}$	$-4.75^{+0.10}_{-0.13}$	$-4.45^{+0.08}_{-0.08}$	$7.79^{+0.08}_{-0.09}$	$7.73^{+0.09}_{-0.09}$	...
MMT02	$1.97^{+0.15}_{-0.13}$	$1.87^{+0.11}_{-0.15}$	$4.10^{+0.05}_{-0.07}$	$4.15^{+0.05}_{-0.08}$	$+0.45^{+0.01}_{-0.01}$	$+0.67^{+0.05}_{-0.07}$	$0.60^{+0.01}_{-0.01}$	$-3.99^{+0.27}_{-0.28}$	$-3.93^{+0.21}_{-0.28}$	$-4.41^{+0.16}_{-0.17}$	$8.19^{+0.24}_{-0.20}$	$8.19^{+0.26}_{-0.21}$	...
MMT03	$1.31^{+0.09}_{-0.13}$	$1.31^{+0.09}_{-0.16}$	$4.52^{+0.09}_{-0.15}$	$4.53^{+0.12}_{-0.17}$	$+0.56^{+0.01}_{-0.01}$	$+0.57^{+0.04}_{-0.02}$	$0.32^{+0.01}_{-0.02}$	$...^{\text{a}}$	$...^{\text{a}}$	$...^{\text{a}}$	$...^{\text{a}}$	$...^{\text{a}}$	...
MMT05	$1.81^{+0.07}_{-0.06}$	$1.81^{+0.07}_{-0.06}$	$4.17^{+0.03}_{-0.03}$	$4.17^{+0.03}_{-0.03}$	$-0.27^{+0.04}_{-0.01}$	$-0.27^{+0.04}_{-0.01}$	$0.97^{+0.00}_{-0.00}$	$-4.95^{+0.11}_{-0.12}$	$-4.95^{+0.11}_{-0.12}$	$-4.11^{+0.08}_{-0.07}$	$7.95^{+0.09}_{-0.10}$	$7.95^{+0.09}_{-0.10}$	...
MMT07	$1.79^{+0.02}_{-0.03}$	$1.75^{+0.03}_{-0.03}$	$4.18^{+0.02}_{-0.02}$	$4.20^{+0.02}_{-0.01}$	$+0.04^{+0.01}_{-0.00}$	$+0.11^{+0.00}_{-0.01}$	$0.90^{+0.00}_{-0.00}$	$-4.68^{+0.05}_{-0.06}$	$-4.66^{+0.05}_{-0.06}$	$-4.25^{+0.03}_{-0.04}$	$7.92^{+0.04}_{-0.04}$	$7.89^{+0.04}_{-0.05}$	213^{+114}_{-194}
MMT08	$1.89^{+0.07}_{-0.11}$	$1.82^{+0.09}_{-0.10}$	$4.13^{+0.05}_{-0.04}$	$4.17^{+0.05}_{-0.04}$	$+0.45^{+0.02}_{-0.00}$	$+0.58^{+0.06}_{-0.04}$	$0.65^{+0.01}_{-0.01}$	$-4.10^{+0.15}_{-0.16}$	$-4.07^{+0.13}_{-0.20}$	$-4.41^{+0.10}_{-0.12}$	$8.10^{+0.12}_{-0.16}$	$8.10^{+0.14}_{-0.15}$	...
MMT09	$1.65^{+0.10}_{-0.11}$	$1.63^{+0.09}_{-0.12}$	$4.26^{+0.06}_{-0.07}$	$4.27^{+0.06}_{-0.07}$	$+0.54^{+0.01}_{-0.02}$	$+0.57^{+0.02}_{-0.01}$	$0.79^{+0.01}_{-0.01}$	$-4.40^{+0.19}_{-0.20}$	$-4.39^{+0.20}_{-0.20}$	$-4.51^{+0.15}_{-0.16}$	$7.86^{+0.17}_{-0.21}$	$7.85^{+0.17}_{-0.22}$	...
MMT10	$1.88^{+0.04}_{-0.03}$	$1.87^{+0.03}_{-0.04}$	$4.14^{+0.02}_{-0.01}$	$4.15^{+0.02}_{-0.02}$	$+0.14^{+0.01}_{-0.01}$	$+0.17^{+0.01}_{-0.01}$	$0.83^{+0.00}_{-0.00}$	$-4.44^{+0.07}_{-0.08}$	$-4.43^{+0.06}_{-0.07}$	$-4.18^{+0.05}_{-0.05}$	$8.03^{+0.05}_{-0.05}$	$8.02^{+0.04}_{-0.06}$	28^{+72}_{-19}
MMT11	$1.93^{+0.04}_{-0.06}$	$1.91^{+0.05}_{-0.06}$	$4.12^{+0.02}_{-0.02}$	$4.13^{+0.02}_{-0.02}$	$+0.36^{+0.01}_{-0.00}$	$+0.40^{+0.00}_{-0.01}$	$0.82^{+0.00}_{-0.00}$	$-4.14^{+0.08}_{-0.10}$	$-4.13^{+0.08}_{-0.10}$	$-4.14^{+0.06}_{-0.07}$	$8.17^{+0.06}_{-0.09}$	$8.16^{+0.07}_{-0.09}$	1234^{+320}_{-478}
MMT13	$1.71^{+0.07}_{-0.10}$	$1.71^{+0.07}_{-0.10}$	$4.23^{+0.05}_{-0.05}$	$4.23^{+0.05}_{-0.05}$	$+0.03^{+0.03}_{-0.03}$	$+0.03^{+0.03}_{-0.03}$	$0.76^{+0.00}_{-0.00}$	$-4.81^{+0.16}_{-0.18}$	$-4.81^{+0.16}_{-0.18}$	$-4.44^{+0.09}_{-0.11}$	$7.71^{+0.10}_{-0.14}$	$7.71^{+0.10}_{-0.14}$	...
MMT15	$1.65^{+0.09}_{-0.11}$	$1.65^{+0.09}_{-0.11}$	$4.26^{+0.05}_{-0.09}$	$4.26^{+0.04}_{-0.08}$	$+0.46^{+0.01}_{-0.01}$	$+0.47^{+0.02}_{-0.01}$	$0.63^{+0.01}_{-0.01}$	$-4.48^{+0.16}_{-0.21}$	$-4.48^{+0.17}_{-0.20}$	$-4.65^{+0.12}_{-0.13}$	$7.75^{+0.13}_{-0.19}$	$7.75^{+0.13}_{-0.19}$	164^{+126}_{-147}
MMT16	$1.65^{+0.11}_{-0.13}$	$1.64^{+0.16}_{-0.11}$	$4.26^{+0.05}_{-0.09}$	$4.27^{+0.07}_{-0.08}$	$+0.20^{+0.04}_{-0.04}$	$+0.23^{+0.04}_{-0.04}$	$0.72^{+0.02}_{-0.02}$	$-4.74^{+0.22}_{-0.24}$	$-4.73^{+0.26}_{-0.25}$	$-4.58^{+0.15}_{-0.16}$	$7.66^{+0.18}_{-0.19}$	$7.65^{+0.17}_{-0.21}$	493^{+185}_{-418}
MMT17	$1.54^{+0.09}_{-0.14}$	$1.53^{+0.11}_{-0.12}$	$4.33^{+0.05}_{-0.12}$	$4.34^{+0.07}_{-0.13}$	$+0.52^{+0.02}_{-0.01}$	$+0.55^{+0.03}_{-0.01}$	$0.38^{+0.02}_{-0.01}$	$-4.53^{+0.25}_{-0.28}$	$-4.50^{+0.30}_{-0.30}$	$-5.06^{+0.17}_{-0.17}$	$7.58^{+0.28}_{-0.27}$	$7.60^{+0.28}_{-0.23}$	128^{+29}_{-26}
MMT18	$1.62^{+0.09}_{-0.10}$	$1.62^{+0.09}_{-0.10}$	$4.27^{+0.06}_{-0.05}$	$4.27^{+0.06}_{-0.05}$	$+0.06^{+0.03}_{-0.03}$	$+0.06^{+0.03}_{-0.03}$	$0.55^{+0.02}_{-0.02}$	$-4.92^{+0.19}_{-0.18}$	$-4.92^{+0.19}_{-0.18}$	$-4.76^{+0.12}_{-0.13}$	$7.47^{+0.14}_{-0.16}$	$7.47^{+0.14}_{-0.16}$	<1
MMT19	$1.86^{+0.03}_{-0.03}$	$1.85^{+0.03}_{-0.04}$	$4.15^{+0.01}_{-0.02}$	$4.16^{+0.02}_{-0.02}$	$+0.08^{+0.01}_{-0.01}$	$+0.10^{+0.01}_{-0.01}$	$0.87^{+0.00}_{-0.00}$	$-4.53^{+0.06}_{-0.06}$	$-4.52^{+0.06}_{-0.06}$	$-4.16^{+0.04}_{-0.04}$	$8.01^{+0.05}_{-0.05}$	$8.00^{+0.05}_{-0.04}$	...
MMT20	$2.12^{+0.10}_{-0.16}$	$2.11^{+0.11}_{-0.14}$	$4.05^{+0.05}_{-0.04}$	$4.05^{+0.05}_{-0.06}$	$+0.51^{+0.01}_{-0.01}$	$+0.53^{+0.02}_{-0.01}$	$0.26^{+0.01}_{-0.01}$	$-3.73^{+0.20}_{-0.18}$	$-3.72^{+0.16}_{-0.23}$	$-4.47^{+0.12}_{-0.19}$	$8.35^{+0.20}_{-0.24}$	$8.35^{+0.17}_{-0.21}$	...
MMT21	$1.80^{+0.06}_{-0.08}$	$1.80^{+0.06}_{-0.08}$	$4.18^{+0.04}_{-0.03}$	$4.18^{+0.04}_{-0.03}$	$-0.23^{+0.05}_{-0.05}$	$-0.23^{+0.05}_{-0.05}$	$0.83^{+0.01}_{-0.01}$	$-4.92^{+0.12}_{-0.17}$	$-4.92^{+0.12}_{-0.17}$	$-4.25^{+0.07}_{-0.11}$	$7.83^{+0.08}_{-0.11}$	$7.83^{+0.08}_{-0.11}$	...
MMT22	$1.61^{+0.12}_{-0.13}$	$1.58^{+0.11}_{-0.13}$	$4.28^{+0.07}_{-0.11}$	$4.30^{+0.09}_{-0.08}$	$+0.38^{+0.02}_{-0.02}$	$+0.44^{+0.02}_{-0.03}$	$0.47^{+0.02}_{-0.02}$	$-4.63^{+0.20}_{-0.26}$	$-4.63^{+0.23}_{-0.24}$	$-4.90^{+0.15}_{-0.16}$	$7.57^{+0.21}_{-0.20}$	$7.56^{+0.17}_{-0.25}$	...
MMT23	$1.88^{+0.10}_{-0.15}$	$1.83^{+0.14}_{-0.10}$	$4.14^{+0.05}_{-0.06}$	$4.16^{+0.03}_{-0.08}$	$+0.23^{+0.03}_{-0.04}$	$+0.23^{+0.03}_{-0.04}$	$0.94^{+0.03}_{-0.03}$	$-4.35^{+0.21}_{-0.27}$	$-4.33^{+0.18}_{-0.25}$	$-4.11^{+0.18}_{-0.11}$	$8.13^{+0.13}_{-0.21}$	$8.10^{+0.17}_{-0.17}$	...
MMT24	$2.02^{+0.06}_{-0.06}$	$2.02^{+0.06}_{-0.06}$	$4.08^{+0.02}_{-0.02}$	$4.08^{+0.02}_{-0.02}$	$+0.12^{+0.01}_{-0.01}$	$+0.13^{+0.02}_{-0.01}$	$0.90^{+0.01}_{-0.01}$	$-4.24^{+0.11}_{-0.09}$	$-4.24^{+0.11}_{-0.09}$	$-3.93^{+0.06}_{-0.07}$	$8.25^{+0.09}_{-0.07}$	$8.25^{+0.08}_{-0.08}$	...
MMT25	$2.03^{+0.11}_{-0.15}$	$2.03^{+0.10}_{-0.15}$	$4.08^{+0.05}_{-0.05}$	$4.08^{+0.05}_{-0.05}$	$+0.02^{+0.02}_{-0.03}$	$+0.02^{+0.01}_{-0.03}$	$0.92^{+0.01}_{-0.01}$	$-4.34^{+0.23}_{-0.25}$	$-4.34^{+0.23}_{-0.25}$	$-3.90^{+0.12}_{-0.16}$	$8.24^{+0.15}_{-0.18}$	$8.24^{+0.15}_{-0.18}$	...
MMT26	$1.95^{+0.08}_{-0.10}$	$1.92^{+0.11}_{-0.09}$	$4.11^{+0.04}_{-0.04}$	$4.12^{+0.03}_{-0.04}$	$+0.55^{+0.00}_{-0.01}$	$+0.61^{+0.02}_{-0.00}$	$0.54^{+0.00}_{-0.00}$	$-3.91^{+0.13}_{-0.17}$	$-3.90^{+0.12}_{-0.18}$	$-4.39^{+0.07}_{-0.13}$	$8.22^{+0.11}_{-0.17}$	$8.22^{+0.11}_{-0.17}$	<1
MMT27	$1.36^{+0.11}_{-0.12}$	$1.33^{+0.10}_{-0.11}$	$4.47^{+0.07}_{-0.12}$	$4.51^{+0.08}_{-0.14}$	$+0.10^{+0.06}_{-0.05}$	$+0.18^{+0.07}_{-0.07}$	$0.78^{+0.04}_{-0.03}$	$-4.96^{+0.35}_{-0.33}$	$-4.89^{+0.39}_{-0.35}$	$-4.96^{+0.23}_{-0.15}$	$7.37^{+0.27}_{-0.26}$	$7.38^{+0.23}_{-0.29}$	...
MMT28	$2.06^{+0.11}_{-0.14}$	$1.97^{+0.10}_{-0.16}$	$4.07^{+0.05}_{-0.05}$	$4.10^{+0.05}_{-0.06}$	$+0.11^{+0.04}_{-0.06}$	$+0.29^{+0.06}_{-0.09}$	$0.90^{+0.05}_{-0.05}$	$-4.21^{+0.16}_{-0.26}$	$-4.17^{+0.17}_{-0.27}$	$-3.99^{+0.14}_{-0.16}$	$8.28^{+0.15}_{-0.18}$	$8.23^{+0.16}_{-0.20}$	...
MMT29	$2.13^{+0.06}_{-0.07}$	$2.10^{+0.05}_{-0.08}$	$4.04^{+0.02}_{-0.02}$	$4.05^{+0.02}_{-0.02}$	$+0.23^{+0.00}_{-0.00}$	$+0.28^{+0.01}_{-0.01}$	$0.82^{+0.00}_{-0.00}$	$-4.00^{+0.10}_{-0.11}$	$-3.98^{+0.09}_{-0.13}$	$-3.91^{+0.06}_{-0.09}$	$8.37^{+0.07}_{-0.10}$	$8.36^{+0.08}_{-0.10}$	<1
MMT30	$2.09^{+0.14}_{-0.15}$	$2.07^{+0.12}_{-0.17}$	$4.06^{+0.05}_{-0.05}$	$4.06^{+0.06}_{-0.07}$	$+0.40^{+0.01}_{-0.01}$	$+0.43^{+0.02}_{-0.01}$	$0.69^{+0.01}_{-0.01}$	$-3.87^{+0.23}_{-0.23}$	$-3.87^{+0.19}_{-0.27}$	$-4.07^{+0.16}_{-0.15}$	$8.34^{+0.22}_{-0.20}$	$8.34^{+0.18}_{-0.24}$	...

TABLE 13
Emission-line Ratios, Electron Densities and Temperatures, and
Gas-Phase Metallicities for [O III] λ4363-detected Galaxies

MMT31	$2.09^{+0.07}_{-0.08}$	$2.05^{+0.07}_{-0.08}$	$4.06^{+0.03}_{-0.03}$	$4.07^{+0.03}_{-0.03}$	$+0.35^{+0.00}_{-0.00}$	$+0.41^{+0.01}_{-0.01}$	$0.70^{+0.00}_{-0.00}$	$-3.93^{+0.12}_{-0.13}$	$-3.91^{+0.12}_{-0.14}$	$-4.09^{+0.08}_{-0.10}$	$8.31^{+0.09}_{-0.11}$	$8.31^{+0.10}_{-0.11}$	629^{+298}_{-347}
MMT32	$2.23^{+0.07}_{-0.10}$	$2.19^{+0.07}_{-0.10}$	$4.01^{+0.04}_{-0.03}$	$4.02^{+0.04}_{-0.03}$	$+0.30^{+0.01}_{-0.01}$	$+0.39^{+0.01}_{-0.01}$	$0.77^{+0.00}_{-0.00}$	$-3.78^{+0.12}_{-0.16}$	$-3.76^{+0.13}_{-0.18}$	$-3.86^{+0.10}_{-0.12}$	$8.50^{+0.12}_{-0.15}$	$8.49^{+0.12}_{-0.15}$	123^{+53}_{-116}
MMT33	$1.58^{+0.06}_{-0.06}$	$1.57^{+0.06}_{-0.05}$	$4.30^{+0.03}_{-0.04}$	$4.31^{+0.03}_{-0.04}$	$-0.54^{+0.04}_{-0.05}$	$-0.53^{+0.04}_{-0.05}$	$0.84^{+0.01}_{-0.01}$	$-5.61^{+0.10}_{-0.12}$	$-5.59^{+0.10}_{-0.12}$	$-4.54^{+0.07}_{-0.08}$	$7.50^{+0.08}_{-0.07}$	$7.50^{+0.10}_{-0.10}$	$\ldots$
MMT34	$1.90^{+0.07}_{-0.12}$	$1.90^{+0.07}_{-0.12}$	$4.13^{+0.04}_{-0.04}$	$4.13^{+0.04}_{-0.04}$	$+0.27^{+0.02}_{-0.01}$	$+0.27^{+0.02}_{-0.01}$	$0.81^{+0.01}_{-0.01}$	$-4.27^{+0.14}_{-0.19}$	$-4.27^{+0.14}_{-0.19}$	$-4.16^{+0.10}_{-0.15}$	$8.09^{+0.12}_{-0.15}$	$8.09^{+0.12}_{-0.15}$	$\ldots$
MMT35	$1.72^{+0.10}_{-0.14}$	$1.58^{+0.13}_{-0.15}$	$4.22^{+0.06}_{-0.07}$	$4.30^{+0.06}_{-0.12}$	$+0.46^{+0.02}_{-0.01}$	$+0.74^{+0.13}_{-0.09}$	$0.68^{+0.02}_{-0.01}$	$-4.36^{+0.24}_{-0.28}$	$-4.31^{+0.19}_{-0.27}$	$-4.70^{+0.15}_{-0.19}$	$7.87^{+0.22}_{-0.20}$	$7.84^{+0.22}_{-0.25}$	$\ldots$
MMT37	$1.98^{+0.06}_{-0.10}$	$1.91^{+0.06}_{-0.10}$	$4.10^{+0.03}_{-0.04}$	$4.13^{+0.04}_{-0.04}$	$+0.32^{+0.02}_{-0.01}$	$+0.49^{+0.06}_{-0.04}$	$0.77^{+0.02}_{-0.02}$	$-4.09^{+0.14}_{-0.16}$	$-4.05^{+0.15}_{-0.15}$	$-4.19^{+0.08}_{-0.12}$	$8.21^{+0.11}_{-0.14}$	$8.19^{+0.11}_{-0.15}$	$\ldots$
MMT38	$1.73^{+0.09}_{-0.15}$	$1.73^{+0.09}_{-0.15}$	$4.21^{+0.07}_{-0.10}$	$4.21^{+0.07}_{-0.10}$	$-0.17^{+0.06}_{-0.05}$	$-0.17^{+0.06}_{-0.05}$	$0.98^{+0.02}_{-0.02}$	$-4.97^{+0.20}_{-0.26}$	$-4.97^{+0.20}_{-0.26}$	$-4.19^{+0.12}_{-0.18}$	$7.87^{+0.11}_{-0.22}$	$7.87^{+0.11}_{-0.22}$	$\ldots$
Keck01	$1.92^{+0.04}_{-0.04}$	$1.81^{+0.05}_{-0.04}$	$4.12^{+0.02}_{-0.02}$	$4.17^{+0.02}_{-0.02}$	$-0.23^{+0.01}_{-0.01}$	$-0.02^{+0.05}_{-0.01}$	$0.90^{+0.01}_{-0.00}$	$-4.74^{+0.07}_{-0.07}$	$-4.69^{+0.07}_{-0.08}$	$-4.18^{+0.04}_{-0.05}$	$8.03^{+0.05}_{-0.05}$	$7.93^{+0.05}_{-0.05}$	96^{+77}_{-89}
Keck02	$1.45^{+0.07}_{-0.07}$	$1.45^{+0.07}_{-0.07}$	$4.40^{+0.04}_{-0.05}$	$4.40^{+0.04}_{-0.05}$	$+0.17^{+0.02}_{-0.02}$	$+0.17^{+0.02}_{-0.02}$	$0.87^{+0.01}_{-0.01}$	$-4.89^{+0.15}_{-0.14}$	$-4.89^{+0.15}_{-0.14}$	$-4.69^{+0.08}_{-0.09}$	$7.52^{+0.11}_{-0.11}$	$7.52^{+0.11}_{-0.11}$	915^{+243}_{-178}
Keck03	$2.38^{+0.07}_{-0.08}$	$2.26^{+0.06}_{-0.07}$	$3.96^{+0.02}_{-0.02}$	$4.00^{+0.02}_{-0.03}$	$+0.37^{+0.00}_{-0.00}$	$+0.62^{+0.01}_{-0.02}$	$0.67^{+0.00}_{-0.00}$	$-3.53^{+0.10}_{-0.11}$	$-3.44^{+0.09}_{-0.12}$	$-3.89^{+0.07}_{-0.07}$	$8.67^{+0.09}_{-0.09}$	$8.69^{+0.08}_{-0.11}$	69^{+8}_{-7}
Keck04	$2.09^{+0.09}_{-0.10}$	$2.09^{+0.09}_{-0.10}$	$4.06^{+0.04}_{-0.05}$	$4.06^{+0.04}_{-0.05}$	$+0.26^{+0.00}_{-0.01}$	$+0.26^{+0.00}_{-0.01}$	$0.76^{+0.01}_{-0.01}$	$-4.02^{+0.15}_{-0.18}$	$-4.02^{+0.15}_{-0.18}$	$-3.99^{+0.09}_{-0.13}$	$8.30^{+0.13}_{-0.15}$	$8.30^{+0.13}_{-0.15}$	612^{+36}_{-34}
Keck05	$1.35^{+0.10}_{-0.12}$	$1.32^{+0.08}_{-0.12}$	$4.49^{+0.09}_{-0.13}$	$4.52^{+0.11}_{-0.12}$	$+0.10^{+0.02}_{-0.02}$	$+0.10^{+0.11}_{-0.02}$	$0.81^{+0.01}_{-0.01}$	$-4.96^{+0.34}_{-0.32}$	$-4.89^{+0.33}_{-0.37}$	$-4.94^{+0.19}_{-0.18}$	$7.38^{+0.19}_{-0.26}$	$7.38^{+0.21}_{-0.29}$	205^{+70}_{-80}
Keck06	$1.50^{+0.07}_{-0.08}$	$1.46^{+0.07}_{-0.08}$	$4.36^{+0.04}_{-0.06}$	$4.38^{+0.05}_{-0.08}$	$-1.18^{+0.14}_{-0.29}$	$-1.21^{+0.22}_{-0.22}$	$0.75^{+0.01}_{-0.01}$	$-6.40^{+0.34}_{-0.21}$	$-6.33^{+0.35}_{-0.30}$	$-4.78^{+0.10}_{-0.12}$	$7.28^{+0.10}_{-0.10}$	$7.23^{+0.11}_{-0.14}$	$\ldots$
Keck07	$2.01^{+0.04}_{-0.04}$	$2.01^{+0.03}_{-0.04}$	$4.09^{+0.02}_{-0.02}$	$4.09^{+0.02}_{-0.01}$	$+0.06^{+0.02}_{-0.01}$	$+0.07^{+0.02}_{-0.02}$	$0.96^{+0.01}_{-0.01}$	$-4.32^{+0.07}_{-0.06}$	$-4.32^{+0.07}_{-0.06}$	$-3.88^{+0.04}_{-0.05}$	$8.25^{+0.06}_{-0.05}$	$8.25^{+0.05}_{-0.05}$	<1
Keck08	$1.72^{+0.05}_{-0.06}$	$1.63^{+0.05}_{-0.05}$	$4.22^{+0.02}_{-0.03}$	$4.27^{+0.03}_{-0.04}$	$+0.07^{+0.01}_{-0.02}$	$+0.23^{+0.06}_{-0.04}$	$0.78^{+0.01}_{-0.01}$	$-4.76^{+0.11}_{-0.08}$	$-4.73^{+0.11}_{-0.07}$	$-4.52^{+0.07}_{-0.07}$	$7.75^{+0.07}_{-0.07}$	$7.69^{+0.08}_{-0.07}$	224^{+41}_{-67}
Keck09	$2.18^{+0.09}_{-0.10}$	$2.18^{+0.08}_{-0.10}$	$4.02^{+0.03}_{-0.03}$	$4.02^{+0.03}_{-0.04}$	$+0.19^{+0.01}_{-0.03}$	$+0.19^{+0.04}_{-0.02}$	$1.06^{+0.01}_{-0.01}$	$-3.96^{+0.15}_{-0.15}$	$-3.96^{+0.14}_{-0.17}$	$-3.58^{+0.12}_{-0.11}$	$8.57^{+0.12}_{-0.11}$	$8.57^{+0.11}_{-0.13}$	118^{+63}_{-110}
Keck11	$1.93^{+0.13}_{-0.22}$	$1.93^{+0.13}_{-0.22}$	$4.12^{+0.09}_{-0.10}$	$4.12^{+0.08}_{-0.09}$	$+0.09^{+0.01}_{-0.01}$	$+0.09^{+0.03}_{-0.01}$	$0.83^{+0.00}_{-0.00}$	$-4.41^{+0.19}_{-0.44}$	$-4.41^{+0.21}_{-0.43}$	$-4.10^{+0.13}_{-0.29}$	$8.07^{+0.14}_{-0.29}$	$8.07^{+0.18}_{-0.25}$	129^{+59}_{-80}
Keck12	$1.53^{+0.06}_{-0.08}$	$1.53^{+0.05}_{-0.10}$	$4.33^{+0.05}_{-0.06}$	$4.33^{+0.08}_{-0.06}$	$-0.23^{+0.04}_{-0.08}$	$-0.23^{+0.06}_{-0.09}$	$0.72^{+0.02}_{-0.02}$	$-5.32^{+0.15}_{-0.17}$	$-5.32^{+0.12}_{-0.20}$	$-4.71^{+0.08}_{-0.14}$	$7.38^{+0.09}_{-0.12}$	$7.38^{+0.10}_{-0.13}$	<1
Keck13	$1.56^{+0.05}_{-0.07}$	$1.53^{+0.05}_{-0.09}$	$4.31^{+0.04}_{-0.04}$	$4.34^{+0.05}_{-0.05}$	$-0.54^{+0.04}_{-0.13}$	$-0.55^{+0.16}_{-0.08}$	$0.78^{+0.02}_{-0.02}$	$-5.64^{+0.12}_{-0.21}$	$-5.58^{+0.17}_{-0.25}$	$-4.66^{+0.07}_{-0.12}$	$7.43^{+0.07}_{-0.11}$	$7.39^{+0.09}_{-0.12}$	$\ldots$
Keck14	$2.01^{+0.07}_{-0.10}$	$1.97^{+0.08}_{-0.09}$	$4.09^{+0.03}_{-0.03}$	$4.10^{+0.03}_{-0.03}$	$+0.34^{+0.01}_{-0.00}$	$+0.41^{+0.03}_{-0.01}$	$0.83^{+0.00}_{-0.00}$	$-4.04^{+0.14}_{-0.14}$	$-4.02^{+0.14}_{-0.15}$	$-4.06^{+0.10}_{-0.09}$	$8.28^{+0.10}_{-0.13}$	$8.26^{+0.10}_{-0.14}$	69^{+12}_{-9}
Keck15	$2.00^{+0.07}_{-0.11}$	$1.93^{+0.07}_{-0.12}$	$4.09^{+0.04}_{-0.04}$	$4.12^{+0.03}_{-0.04}$	$+0.27^{+0.01}_{-0.01}$	$+0.42^{+0.03}_{-0.06}$	$0.85^{+0.01}_{-0.01}$	$-4.13^{+0.14}_{-0.16}$	$-4.09^{+0.13}_{-0.21}$	$-4.08^{+0.09}_{-0.13}$	$8.24^{+0.15}_{-0.12}$	$8.22^{+0.10}_{-0.16}$	81^{+28}_{-27}
Keck16	$1.79^{+0.12}_{-0.11}$	$1.65^{+0.11}_{-0.12}$	$4.18^{+0.06}_{-0.06}$	$4.26^{+0.07}_{-0.07}$	$+0.37^{+0.01}_{-0.01}$	$+0.63^{+0.05}_{-0.02}$	$0.35^{+0.01}_{-0.01}$	$-4.34^{+0.16}_{-0.23}$	$-4.29^{+0.21}_{-0.21}$	$-4.92^{+0.15}_{-0.17}$	$7.81^{+0.18}_{-0.19}$	$7.80^{+0.20}_{-0.20}$	93^{+19}_{-18}
Keck18	$2.00^{+0.12}_{-0.16}$	$1.95^{+0.11}_{-0.15}$	$4.09^{+0.06}_{-0.04}$	$4.11^{+0.06}_{-0.05}$	$+0.37^{+0.01}_{-0.01}$	$+0.46^{+0.06}_{-0.03}$	$0.76^{+0.00}_{-0.01}$	$-4.03^{+0.15}_{-0.27}$	$-4.00^{+0.18}_{-0.25}$	$-4.15^{+0.13}_{-0.16}$	$8.25^{+0.17}_{-0.20}$	$8.23^{+0.13}_{-0.24}$	$\ldots$
Keck19	$2.09^{+0.06}_{-0.08}$	$2.09^{+0.06}_{-0.08}$	$4.05^{+0.03}_{-0.02}$	$4.05^{+0.03}_{-0.02}$	$+0.21^{+0.01}_{-0.01}$	$+0.21^{+0.01}_{-0.01}$	$0.82^{+0.00}_{-0.00}$	$-4.05^{+0.09}_{-0.14}$	$-4.05^{+0.09}_{-0.14}$	$-3.93^{+0.07}_{-0.08}$	$8.32^{+0.09}_{-0.12}$	$8.32^{+0.09}_{-0.12}$	54^{+19}_{-22}
Keck20	$1.47^{+0.15}_{-0.14}$	$1.47^{+0.11}_{-0.18}$	$4.38^{+0.09}_{-0.15}$	$4.38^{+0.10}_{-0.14}$	$+0.23^{+0.05}_{-0.04}$	$+0.27^{+0.01}_{-0.08}$	$0.74^{+0.03}_{-0.02}$	$-4.83^{+0.32}_{-0.35}$	$-4.83^{+0.34}_{-0.33}$	$-4.78^{+0.17}_{-0.23}$	$7.50^{+0.25}_{-0.30}$	$7.50^{+0.28}_{-0.27}$	$\ldots$
Keck21	$1.91^{+0.07}_{-0.08}$	$1.91^{+0.08}_{-0.09}$	$4.13^{+0.03}_{-0.04}$	$4.13^{+0.04}_{-0.04}$	$+0.23^{+0.00}_{-0.03}$	$+0.22^{+0.04}_{-0.02}$	$0.82^{+0.01}_{-0.01}$	$-4.30^{+0.12}_{-0.15}$	$-4.30^{+0.14}_{-0.13}$	$-4.13^{+0.11}_{-0.10}$	$8.10^{+0.10}_{-0.12}$	$8.09^{+0.12}_{-0.13}$	50^{+32}_{-46}
Keck23	$1.68^{+0.06}_{-0.06}$	$1.68^{+0.06}_{-0.06}$	$4.24^{+0.04}_{-0.04}$	$4.24^{+0.04}_{-0.04}$	$-0.24^{+0.02}_{-0.05}$	$-0.24^{+0.02}_{-0.05}$	$0.86^{+0.01}_{-0.01}$	$-5.15^{+0.10}_{-0.13}$	$-5.15^{+0.10}_{-0.13}$	$-4.37^{+0.07}_{-0.09}$	$7.69^{+0.08}_{-0.08}$	$7.69^{+0.08}_{-0.08}$	311^{+243}_{-285}
Keck24	$1.95^{+0.10}_{-0.09}$	$1.92^{+0.10}_{-0.09}$	$4.11^{+0.03}_{-0.04}$	$4.12^{+0.03}_{-0.04}$	$+0.34^{+0.00}_{-0.00}$	$+0.41^{+0.00}_{-0.00}$	$0.43^{+0.00}_{-0.00}$	$-4.13^{+0.16}_{-0.17}$	$-4.11^{+0.10}_{-0.18}$	$-4.52^{+0.11}_{-0.10}$	$8.03^{+0.11}_{-0.13}$	$8.03^{+0.15}_{-0.16}$	30^{+69}_{-24}
Keck26	$1.82^{+0.11}_{-0.13}$	$1.80^{+0.11}_{-0.17}$	$4.17^{+0.06}_{-0.06}$	$4.18^{+0.06}_{-0.07}$	$+0.47^{+0.03}_{-0.01}$	$+0.49^{+0.12}_{-0.01}$	$0.69^{+0.02}_{-0.02}$	$-4.17^{+0.25}_{-0.23}$	$-4.16^{+0.20}_{-0.28}$	$-4.40^{+0.13}_{-0.20}$	$8.04^{+0.19}_{-0.23}$	$8.04^{+0.21}_{-0.22}$	$\ldots$
Keck27	$1.94^{+0.05}_{-0.04}$	$1.71^{+0.04}_{-0.05}$	$4.11^{+0.02}_{-0.02}$	$4.23^{+0.02}_{-0.03}$	$-0.06^{+0.00}_{-0.01}$	$+0.40^{+0.02}_{-0.02}$	$0.63^{+0.00}_{-0.00}$	$-4.55^{+0.09}_{-0.07}$	$-4.44^{+0.08}_{-0.09}$	$-4.57^{+0.05}_{-0.06}$	$7.90^{+0.05}_{-0.06}$	$7.80^{+0.08}_{-0.07}$	<1
Keck28	$1.98^{+0.04}_{-0.05}$	$1.86^{+0.04}_{-0.04}$	$4.10^{+0.02}_{-0.02}$	$4.15^{+0.02}_{-0.02}$	$-0.07^{+0.01}_{-0.01}$	$+0.17^{+0.03}_{-0.03}$	$0.86^{+0.00}_{-0.00}$	$-4.49^{+0.08}_{-0.08}$	$-4.43^{+0.09}_{-0.08}$	$-4.15^{+0.06}_{-0.06}$	$8.12^{+0.06}_{-0.05}$	$8.03^{+0.05}_{-0.06}$	49^{+33}_{-44}
Keck29	$2.00^{+0.10}_{-0.12}$	$1.89^{+0.13}_{-0.13}$	$4.09^{+0.05}_{-0.05}$	$4.13^{+0.06}_{-0.06}$	$+0.11^{+0.09}_{-0.07}$[b]	$+0.33^{+0.10}_{-0.12}$[b]	$0.92^{+0.01}_{-0.01}$	$-4.28^{+0.19}_{-0.25}$[b]	$-4.23^{+0.21}_{-0.24}$[b]	$-4.06^{+0.15}_{-0.15}$	$8.23^{+0.14}_{-0.15}$[b]	$8.17^{+0.19}_{-0.23}$[b]	$\ldots$
Keck30	$2.08^{+0.11}_{-0.09}$	$2.06^{+0.09}_{-0.09}$	$4.06^{+0.03}_{-0.03}$	$4.07^{+0.03}_{-0.04}$	$+0.41^{+0.01}_{-0.01}$	$+0.44^{+0.01}_{-0.01}$	$0.75^{+0.01}_{-0.00}$	$-3.87^{+0.18}_{-0.16}$	$-3.86^{+0.16}_{-0.13}$	$-4.02^{+0.12}_{-0.11}$	$8.37^{+0.15}_{-0.11}$	$8.37^{+0.14}_{-0.12}$	1107^{+562}_{-773}

TABLE 13
Emission-line Ratios, Electron Densities and Temperatures, and Gas-Phase Metallicities for [O III] λ4363-detected Galaxies

(1)	(2)	(3)	(4)	(5)	(6)	(7)	(8)	(9)	(10)	(11)	(12)	(13)	(14)
Keck31	$1.75^{+0.03}_{-0.04}$	$1.75^{+0.04}_{-0.04}$	$4.20^{+0.02}_{-0.02}$	$4.20^{+0.02}_{-0.02}$	$+0.11^{+0.01}_{-0.01}$	$+0.11^{+0.02}_{-0.01}$	$0.80^{+0.01}_{-0.00}$	$-4.66^{+0.07}_{-0.08}$	$-4.66^{+0.07}_{-0.07}$	$-4.35^{+0.04}_{-0.07}$	$7.82^{+0.05}_{-0.05}$	$7.82^{+0.06}_{-0.05}$	78^{+37}_{-29}
Keck32	$1.48^{+0.09}_{-0.14}$	$1.47^{+0.08}_{-0.16}$	$4.37^{+0.09}_{-0.12}$	$4.38^{+0.12}_{-0.10}$	$+0.26^{+0.04}_{-0.02}$	$+0.29^{+0.03}_{-0.04}$	$0.82^{+0.02}_{-0.02}$	$-4.79^{+0.21}_{-0.32}$	$-4.78^{+0.23}_{-0.30}$	$-4.70^{+0.12}_{-0.20}$	$7.56^{+0.15}_{-0.27}$	$7.57^{+0.26}_{-0.28}$	$\cdots$
Keck33	$1.59^{+0.05}_{-0.05}$	$1.59^{+0.05}_{-0.05}$	$4.29^{+0.03}_{-0.04}$	$4.29^{+0.03}_{-0.04}$	$+0.19^{+0.02}_{-0.02}$	$+0.19^{+0.02}_{-0.02}$	$0.73^{+0.01}_{-0.01}$	$-4.85^{+0.09}_{-0.13}$	$-4.85^{+0.09}_{-0.13}$	$-4.63^{+0.06}_{-0.08}$	$7.58^{+0.08}_{-0.09}$	$7.58^{+0.08}_{-0.09}$	75^{+60}_{-66}

Note. — (1): Abbreviated name for MMT/Keck [O III] λ4363-detected galaxy. (2)–(3): Flux ratio of [O III]λλ4959,5007 to [O III] λ4363. (4)–(5): Electron temperature from [O III] λ4363 (i.e., O^{++}). (6)–(7): Flux ratio of [O II]/Hβ. (8): Flux ratio of [O III]λλ4959,5007/Hβ. (9)–(10): Gas-phase abundance of O$^+$/H$^+$. (11): Gas-phase abundance of O^{++}/H$^+$. (12)–(13): Gas-phase oxygen abundance. (14): Electron density in units of cm^{-3}. Columns 3, 5, 7, 10, and 13 include dust attenuation corrections (see Section 4.1). Uncertainties are reported at 68% confidence levels.

[a] This source is likely a LINER, so metallicity determinations are not trustworthy (see Section 2 of Paper II).

[b] [O II] fluxes were unavailable. We adopt a relation between [O II]/Hβ and [O III]/Hβ (see Figure 28).

TABLE 14
EMISSION-LINE RATIOS, ELECTRON DENSITIES AND TEMPERATURES, AND
GAS-PHASE METALLICITIES FOR [O III] λ4363-NON-DETECTED GALAXIES

ID	$\log\left(\frac{[\text{O III}]}{[\text{O III}]\ \lambda4363}\right)$		$\log\left(T_e/\text{K}\right)$		$\log\left(\frac{[\text{O II}]}{\text{H}\beta}\right)$		$\log\left(\frac{[\text{O III}]}{\text{H}\beta}\right)$	$\log\left(\frac{\text{O}^+}{\text{H}^+}\right)$		$\log\left(\frac{\text{O}^{++}}{\text{H}^+}\right)$	$12+\log\left(\frac{\text{O}}{\text{H}}\right)$		n_e
	(dex)	(dex)	(dex)	(dex)	(dex)	(dex)	(dex)	(dex)	(dex)	(dex)	(dex)	(dex)	(cm^{-3})
(1)	(2)	(3)	(4)	(5)	(6)	(7)	(8)	(9)	(10)	(11)	(12)	(13)	(14)
MK05	>1.98	>1.86	<4.10	<4.15	$+0.51^{+0.00}_{-0.01}$	$+0.73^{+0.06}_{-0.03}$	$0.64^{+0.01}_{-0.01}$	>-3.92	>-3.86	>-4.38	>8.25	>8.26	$\ldots$
MK06	>2.35	>2.30	<3.97	<3.98	$+0.43^{+0.00}_{-0.01}$	$+0.52^{+0.01}_{-0.01}$	$0.66^{+0.00}_{-0.00}$	>-3.50	>-3.47	>-3.84	>8.68	>8.68	2^{+123}_{-2}
MK07	>2.00	>1.95	<4.09	<4.11	$+0.44^{+0.02}_{-0.01}$	$+0.56^{+0.02}_{-0.04}$	$0.61^{+0.02}_{-0.01}$	>-3.95	>-3.92	>-4.29	>8.24	>8.24	$\ldots$
MK08	>1.90	>1.89	<4.13	<4.13	$+0.40^{+0.02}_{-0.01}$	$+0.42^{+0.02}_{-0.01}$	$0.70^{+0.01}_{-0.01}$	>-4.14	>-4.13	>-4.27	>8.10	>8.10	<1
MK09	>2.26	>2.26	<4.00	<4.00	$+0.36^{+0.01}_{-0.00}$	$+0.37^{+0.00}_{-0.01}$	$0.45^{+0.00}_{-0.00}$	>-3.69	>-3.69	>-4.11	>8.45	>8.45	791^{+148}_{-170}
MK10	>2.19	>2.15	<4.02	<4.03	$+0.41^{+0.01}_{-0.02}$	$+0.49^{+0.02}_{-0.02}$	$0.83^{+0.01}_{-0.01}$	>-3.72	>-3.70	>-3.84	>8.54	>8.54	$\ldots$
MK11	>2.38	>2.38	<3.96	<3.96	$+0.48^{+0.01}_{-0.00}$	$+0.49^{+0.00}_{-0.00}$	$0.60^{+0.00}_{-0.00}$	>-3.41	>-3.41	>-3.82	>8.73	>8.73	<1
MK12	>1.93	>1.88	<4.12	<4.14	$+0.55^{+0.01}_{-0.01}$	$+0.66^{+0.01}_{-0.01}$	$0.63^{+0.01}_{-0.01}$	>-3.94	>-3.91	>-4.36	>8.22	>8.22	<1
MMT40	>1.83	>1.76	<4.17	<4.20	$+0.53^{+0.02}_{-0.00}$	$+0.66^{+0.02}_{-0.02}$	$0.58^{+0.01}_{-0.01}$	>-4.12	>-4.09	>-4.56	>8.04	>8.04	<1
MMT41	>1.87	>1.82	<4.15	<4.17	$+0.44^{+0.01}_{-0.02}$	$+0.53^{+0.02}_{-0.01}$	$0.64^{+0.01}_{-0.01}$	>-4.16	>-4.13	>-4.43	>8.05	>8.05	$\ldots$
MMT42	>2.22	>2.17	<4.01	<4.03	$+0.26^{+0.02}_{-0.03}$	$+0.34^{+0.03}_{-0.03}$	$0.81^{+0.02}_{-0.02}$	>-3.86	>-3.83	>-3.86	>8.47	>8.46	$\ldots$
MMT43	>2.26	>2.19	<4.00	<4.02	$+0.14^{+0.01}_{-0.01}$	$+0.27^{+0.01}_{-0.02}$	$0.89^{+0.01}_{-0.01}$	>-3.92	>-3.87	>-3.74	>8.52	>8.50	313^{+126}_{-124}
MMT44	>2.12	>2.07	<4.04	<4.06	$+0.11^{+0.02}_{-0.03}$	$+0.20^{+0.03}_{-0.02}$	$0.88^{+0.01}_{-0.02}$	>-4.12	>-4.09	>-3.89	>8.35	>8.33	$\ldots$
MMT45	>2.22	>2.16	<4.01	<4.03	$+0.50^{+0.01}_{-0.01}$	$+0.62^{+0.02}_{-0.01}$	$0.65^{+0.01}_{-0.01}$	>-3.60	>-3.56	>-4.01	>8.56	>8.57	61^{+53}_{-57}
MMT46	>2.21	>2.15	<4.01	<4.04	$+0.38^{+0.01}_{-0.01}$	$+0.49^{+0.02}_{-0.02}$	$0.42^{+0.01}_{-0.01}$	>-3.74	>-3.70	>-4.27	>8.39	>8.40	$\ldots$
MMT47	>2.35	>2.29	<3.97	<3.99	$+0.52^{+0.01}_{-0.01}$	$+0.65^{+0.01}_{-0.02}$	$0.60^{+0.01}_{-0.01}$	>-3.41	>-3.36	>-3.93	>8.72	>8.74	$\ldots$
MMT48	>2.40	>2.35	<3.96	<3.97	$+0.41^{+0.01}_{-0.01}$	$+0.51^{+0.02}_{-0.01}$	$0.66^{+0.01}_{-0.01}$	>-3.46	>-3.42	>-3.80	>8.72	>8.73	$\ldots$
MMT49	>2.06	>2.01	<4.07	<4.09	$-0.13^{+0.04}_{-0.02}$	$-0.01^{+0.01}_{-0.03}$	$0.88^{+0.01}_{-0.01}$	>-4.44	>-4.41	>-3.96	>8.21	>8.17	$\ldots$
MMT50	>1.84	>1.76	<4.16	<4.20	$-0.11^{+0.01}_{-0.05}$	$+0.00^{+0.07}_{-0.02}$	$0.81^{+0.01}_{-0.02}$	>-4.76	>-4.72	>-4.33	>7.89	>7.82	$\ldots$
MMT51	>1.95	>1.92	<4.11	<4.12	$+0.47^{+0.03}_{-0.01}$	$+0.48^{+0.11}_{-0.01}$	$0.62^{+0.02}_{-0.02}$	>-3.99	>-3.97	>-4.32	>8.19	>8.19	<1
MMT52	>2.23	>2.14	<4.01	<4.04	$+0.34^{+0.02}_{-0.02}$	$+0.52^{+0.02}_{-0.06}$	$0.81^{+0.02}_{-0.02}$	>-3.75	>-3.69	>-3.88	>8.53	>8.53	$\ldots$
MMT55	>2.47	>2.47	<3.93	<3.93	$+0.39^{+0.01}_{-0.01}$	$+0.40^{+0.01}_{-0.02}$	$0.83^{+0.01}_{-0.01}$	>-3.40	>-3.40	>-3.49	>8.86	>8.86	$\ldots$
MMT56[a]	>1.77	>1.68	<4.19	<4.24	$-0.25^{+0.07}_{-0.09}$	$-0.10^{+0.13}_{-0.06}$	$0.94^{+0.03}_{-0.02}$	>-5.00	>-4.96	>-4.30	>7.87	>7.79	$\ldots$
MMT57[a]	>1.72	>1.64	<4.22	<4.27	$+0.13^{+0.03}_{-0.04}$	$+0.31^{+0.02}_{-0.08}$	$0.90^{+0.03}_{-0.03}$	>-4.69	>-4.66	>-4.40	>7.86	>7.79	$\ldots$
MMT58	>2.17	>2.12	<4.03	<4.04	$+0.26^{+0.03}_{-0.03}$	$+0.36^{+0.02}_{-0.03}$	$0.80^{+0.02}_{-0.02}$	>-3.90	>-3.87	>-3.91	>8.42	>8.41	823^{+1661}_{-823}
MMT59	>1.80	>1.74	<4.18	<4.21	$+0.22^{+0.04}_{-0.01}$	$+0.34^{+0.02}_{-0.03}$	$0.93^{+0.03}_{-0.02}$	>-4.47	>-4.45	>-4.22	>8.01	>7.98	$\ldots$
MMT60	>1.83	>1.78	<4.16	<4.19	$+0.27^{+0.01}_{-0.11}$	$+0.33^{+0.05}_{-0.07}$	$0.98^{+0.04}_{-0.05}$	>-4.42	>-4.40	>-4.13	>8.09	>8.06	$\ldots$
MMT61	>2.00	>2.00	<4.09	<4.09	$+0.28^{+0.06}_{-0.06}$	$+0.29^{+0.05}_{-0.10}$	$1.00^{+0.05}_{-0.04}$	>-4.13	>-4.13	>-3.85	>8.33	>8.33	$\ldots$
MMT62	>2.26	>2.21	<4.00	<4.01	$+0.26^{+0.03}_{-0.01}$	$+0.38^{+0.01}_{-0.03}$	$0.75^{+0.02}_{-0.02}$	>-3.78	>-3.74	>-3.86	>8.51	>8.50	<1
MMT63	>1.51	>1.46	<4.35	<4.39	$+0.24^{+0.06}_{-0.04}$	$+0.35^{+0.06}_{-0.03}$	$0.81^{+0.03}_{-0.05}$	>-4.80	>-4.69	>-4.72	>7.58	>7.59	$\ldots$

TABLE 14
EMISSION-LINE RATIOS, ELECTRON DENSITIES AND TEMPERATURES, AND
GAS-PHASE METALLICITIES FOR [O III] λ4363-NON-DETECTED GALAXIES

MMT64[a]	>1.91	>1.91	<4.13	<4.13	$-0.53^{+0.06}_{-0.08}$	$-0.50^{+0.03}_{-0.11}$	$0.98^{+0.02}_{-0.03}$	>-5.06	>-5.06	>-3.97	>8.07	>8.07	...
MMT65	>2.12	>1.96	<4.05	<4.10	$+0.10^{+0.03}_{-0.01}$	$+0.41^{+0.02}_{-0.02}$	$0.78^{+0.01}_{-0.01}$	>-4.13	>-4.04	>-4.11	>8.28	>8.23	...
MMT66	>2.49	>2.49	<3.93	<3.93	$+0.35^{+0.01}_{-0.01}$	$+0.35^{+0.01}_{-0.01}$	$0.70^{+0.01}_{-0.01}$	>-3.41	>-3.41	>-3.60	>8.80	>8.80	...
MMT67	>2.22	>2.22	<4.01	<4.01	$+0.46^{+0.02}_{-0.01}$	$+0.46^{+0.02}_{-0.01}$	$0.71^{+0.01}_{-0.01}$	>-3.64	>-3.64	>-3.89	>8.55	>8.55	...
MMT69	>2.00	>1.98	<4.09	<4.10	$+0.21^{+0.01}_{-0.01}$	$+0.24^{+0.01}_{-0.02}$	$0.99^{+0.01}_{-0.01}$	>-4.19	>-4.18	>-3.89	>8.30	>8.29	<1
MMT70[a]	>1.80	>1.73	<4.18	<4.21	$+0.16^{+0.05}_{-0.04}$	$+0.29^{+0.04}_{-0.06}$	$0.93^{+0.03}_{-0.02}$	>-4.53	>-4.51	>-4.24	>7.99	>7.95	...
MMT71	>1.94	>1.89	<4.12	<4.14	$+0.37^{+0.02}_{-0.02}$	$+0.48^{+0.02}_{-0.03}$	$0.69^{+0.01}_{-0.01}$	>-4.11	>-4.09	>-4.30	>8.13	>8.12	<1
MMT72	>1.66	>1.60	<4.25	<4.29	$+0.30^{+0.01}_{-0.02}$	$+0.42^{+0.01}_{-0.03}$	$0.67^{+0.01}_{-0.01}$	>-4.62	>-4.61	>-4.67	>7.70	>7.66	...
MMT73	>2.17	>2.17	<4.03	<4.03	$+0.45^{+0.02}_{-0.01}$	$+0.45^{+0.02}_{-0.01}$	$0.64^{+0.01}_{-0.01}$	>-3.71	>-3.71	>-4.02	>8.47	>8.47	...
MMT75	>2.18	>2.09	<4.03	<4.06	$+0.20^{+0.04}_{-0.02}$	$+0.36^{+0.06}_{-0.04}$	$0.85^{+0.02}_{-0.03}$	>-3.94	>-3.89	>-3.90	>8.44	>8.41	...
MMT76	>2.07	>2.05	<4.06	<4.07	$+0.50^{+0.02}_{-0.01}$	$+0.54^{+0.02}_{-0.01}$	$0.71^{+0.01}_{-0.01}$	>-3.80	>-3.79	>-4.08	>8.39	>8.39	...
MMT78	>2.45	>2.45	<3.94	<3.94	$+0.32^{+0.01}_{-0.01}$	$+0.32^{+0.01}_{-0.01}$	$0.74^{+0.01}_{-0.01}$	>-3.50	>-3.50	>-3.61	>8.75	>8.75	...
MMT79[a]	>1.81	>1.72	<4.17	<4.22	$+0.44^{+0.01}_{-0.01}$	$+0.59^{+0.05}_{-0.03}$	$0.65^{+0.01}_{-0.01}$	>-4.24	>-4.21	>-4.53	>7.98	>7.96	...
MMT80	>2.29	>2.28	<3.99	<3.99	$+0.34^{+0.00}_{-0.01}$	$+0.37^{+0.01}_{-0.01}$	$0.67^{+0.01}_{-0.01}$	>-3.67	>-3.66	>-3.86	>8.55	>8.55	...
MMT81	>2.17	>2.17	<4.03	<4.03	$+0.46^{+0.01}_{-0.01}$	$+0.47^{+0.01}_{-0.01}$	$0.55^{+0.01}_{-0.01}$	>-3.71	>-3.71	>-4.10	>8.44	>8.44	...
MMT82[a]	>1.86	>1.80	<4.15	<4.18	$+0.33^{+0.02}_{-0.03}$	$+0.46^{+0.02}_{-0.03}$	$0.87^{+0.02}_{-0.01}$	>-4.27	>-4.24	>-4.22	>8.10	>8.07	...
MMT85[a]	>2.07	>2.05	<4.06	<4.07	$+0.51^{+0.01}_{-0.01}$	$+0.53^{+0.01}_{-0.01}$	$0.49^{+0.01}_{-0.01}$	>-3.80	>-3.79	>-4.30	>8.33	>8.33	442^{+94}_{-120}
MMT86	>1.93	>1.87	<4.12	<4.15	$+0.31^{+0.01}_{-0.02}$	$+0.43^{+0.02}_{-0.02}$	$0.80^{+0.01}_{-0.01}$	>-4.19	>-4.16	>-4.20	>8.14	>8.12	<1
MMT87	>1.83	>1.78	<4.16	<4.19	$+0.37^{+0.07}_{-0.04}$	$+0.47^{+0.08}_{-0.04}$	$0.87^{+0.06}_{-0.05}$	>-4.28	>-4.25	>-4.24	>8.08	>8.05	...
MMT88[a]	>1.78	>1.78	<4.19	<4.19	$+0.48^{+0.05}_{-0.03}$	$+0.48^{+0.05}_{-0.04}$	$0.72^{+0.03}_{-0.05}$	>-4.23	>-4.23	>-4.39	>8.00	>8.00	...
MMT89	>1.83	>1.80	<4.16	<4.18	$+0.51^{+0.04}_{-0.04}$	$+0.54^{+0.09}_{-0.04}$	$0.89^{+0.03}_{-0.04}$	>-4.14	>-4.12	>-4.20	>8.15	>8.14	...
Keck034	>2.20	>2.15	<4.02	<4.03	$+0.45^{+0.01}_{-0.01}$	$+0.54^{+0.01}_{-0.02}$	$0.64^{+0.01}_{-0.01}$	>-3.68	>-3.65	>-4.03	>8.49	>8.50	...
Keck035	>1.99	>1.95	<4.09	<4.11	$+0.43^{+0.01}_{-0.03}$	$+0.52^{+0.01}_{-0.04}$	$0.72^{+0.01}_{-0.01}$	>-3.99	>-3.96	>-4.19	>8.24	>8.24	...
Keck036[a]	>1.77	>1.73	<4.19	<4.21	$+0.34^{+0.05}_{-0.03}$	$+0.44^{+0.03}_{-0.06}$	$0.59^{+0.01}_{-0.01}$	>-4.40	>-4.38	>-4.58	>7.84	>7.83	...
Keck037	>2.09	>2.09	<4.06	<4.06	$+0.62^{+0.01}_{-0.03}$	$+0.62^{+0.01}_{-0.03}$	$0.65^{+0.01}_{-0.01}$	>-3.66	>-3.66	>-4.11	>8.47	>8.47	...
Keck038	>2.16	>2.16	<4.03	<4.03	$+0.54^{+0.01}_{-0.02}$	$+0.54^{+0.01}_{-0.02}$	$0.55^{+0.01}_{-0.01}$	>-3.64	>-3.64	>-4.12	>8.49	>8.49	<1
Keck039	>2.02	>2.02	<4.08	<4.08	$+0.71^{+0.01}_{-0.01}$	$+0.71^{+0.01}_{-0.01}$	$0.53^{+0.01}_{-0.01}$	>-3.66	>-3.66	>-4.30	>8.43	>8.43	<1
Keck040[a]	>1.26	>1.26	<4.59	<4.59	$+0.03^{+0.15}_{-0.06}$	$+0.03^{+0.15}_{-0.06}$	$0.55^{+0.07}_{-0.08}$	>-4.98	>-4.98	>-5.31	>7.19	>7.19	<1
Keck041	>2.17	>2.14	<4.03	<4.04	$+0.37^{+0.01}_{-0.01}$	$+0.40^{+0.06}_{-0.03}$	$0.49^{+0.01}_{-0.01}$	>-3.79	>-3.77	>-4.20	>8.36	>8.37	<1
Keck042	>1.93	>1.91	<4.12	<4.13	$+0.33^{+0.01}_{-0.01}$	$+0.38^{+0.04}_{-0.05}$	$0.19^{+0.01}_{-0.01}$	>-4.16	>-4.15	>-4.77	>7.94	>7.94	...
Keck043	>2.42	>2.39	<3.95	<3.96	$+0.35^{+0.12}_{-0.03}$[b]	$+0.43^{+0.10}_{-0.08}$[b]	$0.50^{+0.01}_{-0.01}$	>-3.48[b]	>-3.45[b]	>-3.91	>8.67[b]	>8.68[b]	...
Keck044	>2.32	>2.29	<3.98	<3.99	$+0.28^{+0.01}_{-0.01}$	$+0.32^{+0.05}_{-0.04}$	$0.62^{+0.01}_{-0.01}$	>-3.70	>-3.68	>-3.91	>8.52	>8.52	131^{+27}_{-21}
Keck046	>1.84	>1.84	<4.16	<4.16	$+0.42^{+0.03}_{-0.03}$	$+0.42^{+0.03}_{-0.03}$	$0.87^{+0.03}_{-0.02}$	>-4.22	>-4.22	>-4.17	>8.10	>8.10	<1

Keck047[a]	>1.71	>1.67	<4.22	<4.24	$+0.40^{+0.08\,\text{b}}_{-0.09}$	$+0.48^{+0.08\,\text{b}}_{-0.01}$	$0.57^{+0.02}_{-0.01}$	>-4.45[b]	>-4.44[b]	>-4.68	>7.77[b]	>7.76[b]	<1
Keck048[a]	>1.85	>1.85	<4.15	<4.15	$+0.45^{+0.02}_{-0.04}$	$+0.45^{+0.02}_{-0.04}$	$0.62^{+0.03}_{-0.02}$	>-4.17	>-4.17	>-4.41	>8.03	>8.03	<1
Keck049	>1.91	>1.88	<4.13	<4.14	$+0.33^{+0.02}_{-0.02}$	$+0.34^{+0.08}_{-0.01}$	$0.75^{+0.01}_{-0.01}$	>-4.20	>-4.19	>-4.25	>8.09	>8.08	<1
Keck050[a]	>1.54	>1.54	<4.33	<4.33	$+0.38^{+0.03}_{-0.05}$	$+0.38^{+0.03}_{-0.05}$	$0.47^{+0.03}_{-0.04}$	>-4.68	>-4.68	>-4.95	>7.51	>7.51	...
Keck051	>1.53	>1.49	<4.33	<4.36	$+0.53^{+0.02}_{-0.02}$	$+0.62^{+0.02}_{-0.02}$	$0.48^{+0.02}_{-0.03}$	>-4.53	>-4.44	>-5.01	>7.61	>7.66	...
Keck052	>1.92	>1.89	<4.12	<4.14	$+0.50^{+0.02}_{-0.02}$	$+0.55^{+0.04}_{-0.04}$	$0.79^{+0.02}_{-0.02}$	>-4.02	>-4.01	>-4.19	>8.22	>8.21	878^{+115}_{-187}
Keck053	>2.30	>2.12	<3.99	<4.04	$+0.29^{+0.02\,\text{b}}_{-0.03}$	$+0.63^{+0.03\,\text{b}}_{-0.03}$	$0.78^{+0.01}_{-0.00}$	>-3.72[b]	>-3.60[b]	>-3.93	>8.57[b]	>8.57[b]	...
Keck054	>1.80	>1.80	<4.18	<4.18	$+0.06^{+0.10\,\text{b}}_{-0.06}$	$+0.06^{+0.10\,\text{b}}_{-0.06}$	$0.96^{+0.02}_{-0.03}$	>-4.61[b]	>-4.61[b]	>-4.13	>8.00[b]	>8.00[b]	...
Keck055	>1.56	>1.52	<4.31	<4.34	$+0.14^{+0.02}_{-0.06}$	$+0.21^{+0.04}_{-0.05}$	$0.63^{+0.02}_{-0.02}$	>-4.94	>-4.86	>-4.81	>7.46	>7.46	<1
Keck056	>1.91	>1.91	<4.13	<4.13	$+0.23^{+0.04}_{-0.01}$	$+0.23^{+0.04}_{-0.01}$	$0.56^{+0.02}_{-0.03}$	>-4.28	>-4.28	>-4.39	>7.97	>7.97	...
Keck057	>1.88	>1.88	<4.14	<4.14	$+0.42^{+0.02}_{-0.01}$	$+0.42^{+0.02}_{-0.01}$	$0.46^{+0.01}_{-0.02}$	>-4.15	>-4.15	>-4.54	>8.00	>8.00	...
Keck058	>1.93	>1.93	<4.12	<4.12	$+0.42^{+0.07\,\text{b}}_{-0.08}$	$+0.42^{+0.07\,\text{b}}_{-0.08}$	$0.59^{+0.02}_{-0.02}$	>-4.10[b]	>-4.10[b]	>-4.34	>8.10[b]	>8.10[b]	...
Keck059[a]	>1.79	>1.75	<4.18	<4.20	$+0.41^{+0.03\,\text{b}}_{-0.01}$	$+0.51^{+0.01\,\text{b}}_{-0.03}$	$0.63^{+0.02}_{-0.02}$	>-4.29[b]	>-4.27[b]	>-4.52	>7.93[b]	>7.92[b]	...
Keck060	>2.01	>2.01	<4.09	<4.09	$+0.22^{+0.02}_{-0.02}$	$+0.22^{+0.02}_{-0.02}$	$0.76^{+0.01}_{-0.01}$	>-4.17	>-4.17	>-4.08	>8.18	>8.18	...
Keck061	>0.93	>0.93	<4.82	<4.82	$+0.27^{+0.03}_{-0.03}$	$+0.27^{+0.03}_{-0.03}$	$1.08^{+0.03}_{-0.02}$	>-4.78	>-4.78	>-5.07	>7.40	>7.40	...
Keck063	>1.94	>1.79	<4.12	<4.18	$+0.48^{+0.03}_{-0.01}$	$+0.77^{+0.03}_{-0.01}$	$0.53^{+0.02}_{-0.02}$	>-4.00	>-3.93	>-4.57	>8.15	>8.16	<1
Keck065	>2.20	>2.17	<4.02	<4.03	$+0.35^{+0.01}_{-0.01}$	$+0.40^{+0.02}_{-0.05}$	$0.80^{+0.01}_{-0.01}$	>-3.77	>-3.75	>-3.85	>8.51	>8.50	440^{+39}_{-37}
Keck066[a]	>1.92	>1.92	<4.12	<4.12	$+0.04^{+0.02}_{-0.06}$	$+0.04^{+0.02}_{-0.06}$	$0.69^{+0.02}_{-0.02}$	>-4.49	>-4.49	>-4.25	>7.94	>7.94	<1
Keck067[a]	>2.22	>2.22	<4.01	<4.01	$+0.69^{+0.02}_{-0.01}$	$+0.69^{+0.02}_{-0.01}$	$0.68^{+0.02}_{-0.02}$	>-3.40	>-3.40	>-3.92	>8.71	>8.71	76^{+26}_{-21}
Keck068	>2.08	>1.93	<4.06	<4.12	$+0.42^{+0.01}_{-0.01}$	$+0.71^{+0.02}_{-0.01}$	$0.47^{+0.01}_{-0.01}$	>-3.87	>-3.79	>-4.46	>8.27	>8.29	65^{+72}_{-54}
Keck069	>1.79	>1.79	<4.18	<4.18	$+0.37^{+0.03}_{-0.01}$	$+0.37^{+0.03}_{-0.01}$	$0.74^{+0.01}_{-0.02}$	>-4.33	>-4.33	>-4.36	>7.96	>7.96	139^{+57}_{-55}
Keck070	>2.11	>2.11	<4.05	<4.05	$+0.29^{+0.01}_{-0.02}$	$+0.29^{+0.01}_{-0.02}$	$0.85^{+0.01}_{-0.01}$	>-3.96	>-3.96	>-3.87	>8.39	>8.39	<1
Keck071	>2.18	>2.18	<4.02	<4.02	$+0.38^{+0.02}_{-0.02}$	$+0.38^{+0.02}_{-0.02}$	$0.73^{+0.02}_{-0.02}$	>-3.77	>-3.77	>-3.91	>8.46	>8.46	11^{+34}_{-7}
Keck072	>2.27	>2.24	<4.00	<4.00	$+0.37^{+0.01}_{-0.04}$	$+0.41^{+0.04}_{-0.04}$	$0.54^{+0.01}_{-0.01}$	>-3.67	>-3.65	>-4.04	>8.49	>8.50	588^{+33}_{-48}
Keck073	>1.57	>1.54	<4.31	<4.33	$+0.51^{+0.00\,\text{b}}_{-0.01}$	$+0.51^{+0.10\,\text{b}}_{-0.00}$	$0.28^{+0.01}_{-0.01}$	>-4.55[b]	>-4.49[b]	>-5.15	>7.56[b]	>7.60[b]	...
Keck076	>1.68	>1.68	<4.24	<4.24	$+0.38^{+0.02}_{-0.03}$	$+0.38^{+0.02}_{-0.03}$	$0.76^{+0.02}_{-0.02}$	>-4.50	>-4.50	>-4.47	>7.81	>7.81	...
Keck077	>1.71	>1.71	<4.22	<4.22	$+0.49^{+0.01}_{-0.01}$	$+0.49^{+0.01}_{-0.01}$	$0.63^{+0.01}_{-0.01}$	>-4.35	>-4.35	>-4.57	>7.85	>7.85	<1
Keck078	>1.98	>1.98	<4.10	<4.10	$+0.51^{+0.02}_{-0.02}$	$+0.51^{+0.02}_{-0.02}$	$0.59^{+0.01}_{-0.01}$	>-3.92	>-3.92	>-4.28	>8.24	>8.24	...
Keck079[a]	>0.82	>0.82	<4.82	<4.82	$+0.34^{+0.12}_{-0.10}$	$+0.34^{+0.12}_{-0.10}$	$0.58^{+0.06}_{-0.06}$	>-4.71	>-4.71	>-5.58	>7.34	>7.34	...
Keck080	>1.83	>1.83	<4.16	<4.16	$+0.43^{+0.01\,\text{b}}_{-0.02}$	$+0.43^{+0.01\,\text{b}}_{-0.02}$	$0.70^{+0.01}_{-0.01}$	>-4.22[b]	>-4.22[b]	>-4.35	>8.02[b]	>8.02[b]	...
Keck081	>2.06	>2.06	<4.07	<4.07	$+0.00^{+0.06}_{-0.04}$	$+0.00^{+0.06}_{-0.04}$	$0.77^{+0.02}_{-0.02}$	>-4.30	>-4.30	>-4.00	>8.17	>8.17	<1
Keck082	>1.81	>1.78	<4.17	<4.19	$+0.50^{+0.02}_{-0.02}$	$+0.52^{+0.08}_{-0.02}$	$0.54^{+0.02}_{-0.02}$	>-4.18	>-4.17	>-4.57	>7.98	>7.98	<1
Keck083	>1.80	>1.80	<4.18	<4.18	$+0.56^{+0.02}_{-0.02}$	$+0.56^{+0.02}_{-0.02}$	$0.76^{+0.01}_{-0.01}$	>-4.14	>-4.14	>-4.33	>8.08	>8.08	<1

TABLE 14
Emission-line Ratios, Electron Densities and Temperatures, and
Gas-Phase Metallicities for [O III] λ4363-non-detected Galaxies

(1)	(2)	(3)	(4)	(5)	(6)	(7)	(8)	(9)	(10)	(11)	(12)	(13)	(14)
Keck085	>1.41	>1.37	<4.43	<4.47	$+0.42^{+0.02}_{-0.01}$	$+0.51^{+0.02}_{-0.02}$	$0.63^{+0.01}_{-0.02}$	>-4.63	>-4.55	>-5.04	>7.53	>7.57	1932^{+1217}_{-1302}
Keck086	>1.40	>1.40	<4.43	<4.43	$+0.53^{+0.02}_{-0.03}$	$+0.53^{+0.02}_{-0.03}$	$0.58^{+0.03}_{-0.03}$	>-4.53	>-4.53	>-5.04	>7.59	>7.59	<1
Keck087	>1.95	>1.95	<4.11	<4.11	$+0.35^{+0.05}_{-0.03}$	$+0.35^{+0.05}_{-0.03}$	$0.85^{+0.03}_{-0.04}$	>-4.09	>-4.09	>-4.05	>8.23	>8.23	337^{+173}_{-179}
Keck089[a]	>1.02	>0.98	<4.82	<4.82	$+0.37^{+0.04}_{-0.03}$	$+0.44^{+0.06}_{-0.03}$	$0.55^{+0.04}_{-0.03}$	>-4.68	>-4.60	>-5.60	>7.37	>7.44	1090^{+684}_{-735}
Keck090	>1.83	>1.79	<4.16	<4.18	$+0.63^{+0.02}_{-0.04}$	$+0.72^{+0.01}_{-0.05}$	$0.74^{+0.02}_{-0.02}$	>-4.04	>-4.02	>-4.36	>8.14	>8.14	...
Keck091	>2.00	>2.00	<4.09	<4.09	$+0.44^{+0.01}_{-0.01}$ [b]	$+0.44^{+0.01}_{-0.01}$ [b]	$0.72^{+0.01}_{-0.02}$	>-3.96 [b]	>-3.96 [b]	>-4.13	>8.27 [b]	>8.27 [b]	...
Keck092[a]	>1.61	>1.61	<4.28	<4.28	$+0.48^{+0.06}_{-0.06}$ [b]	$+0.48^{+0.06}_{-0.06}$ [b]	$0.31^{+0.03}_{-0.02}$	>-4.52 [b]	>-4.52 [b]	>-5.01	>7.60 [b]	>7.60 [b]	...
Keck093[a]	>1.73	>1.69	<4.21	<4.24	$+0.37^{+0.09}_{-0.09}$ [b]	$+0.45^{+0.11}_{-0.05}$ [b]	$0.54^{+0.02}_{-0.02}$	>-4.44 [b]	>-4.42 [b]	>-4.68	>7.78 [b]	>7.77 [b]	...
Keck094	>2.21	>2.18	<4.01	<4.02	$+0.28^{+0.01}_{-0.01}$	$+0.28^{+0.08}_{-0.01}$	$0.83^{+0.00}_{-0.00}$	>-3.84	>-3.82	>-3.82	>8.49	>8.49	219^{+24}_{-28}
Keck096[a]	>2.02	>2.00	<4.08	<4.09	$+0.16^{+0.02}_{-0.02}$	$+0.22^{+0.03}_{-0.06}$	$0.63^{+0.02}_{-0.02}$	>-4.21	>-4.19	>-4.23	>8.10	>8.09	126^{+50}_{-48}
Keck097	>1.83	>1.83	<4.16	<4.16	$+0.49^{+0.02}_{-0.01}$	$+0.49^{+0.02}_{-0.01}$	$0.49^{+0.01}_{-0.01}$	>-4.15	>-4.15	>-4.56	>7.99	>7.99	...
Keck098	>1.54	>1.54	<4.33	<4.33	$+0.44^{+0.01}_{-0.02}$	$+0.44^{+0.01}_{-0.02}$	$0.63^{+0.01}_{-0.01}$	>-4.62	>-4.62	>-4.80	>7.60	>7.60	...
Keck099	>2.19	>2.16	<4.02	<4.03	$+0.46^{+0.01}_{-0.01}$	$+0.49^{+0.05}_{-0.03}$	$0.32^{+0.01}_{-0.01}$	>-3.68	>-3.66	>-4.35	>8.41	>8.42	238^{+16}_{-15}
Keck100	>1.74	>1.74	<4.21	<4.21	$+0.49^{+0.01}_{-0.01}$	$+0.49^{+0.01}_{-0.01}$	$0.71^{+0.01}_{-0.01}$	>-4.30	>-4.30	>-4.45	>7.93	>7.93	314^{+56}_{-57}
Keck101	>2.51	>2.51	<3.93	<3.93	$+0.54^{+0.01}_{-0.01}$	$+0.54^{+0.01}_{-0.01}$	$0.63^{+0.01}_{-0.01}$	>-3.20	>-3.20	>-3.66	>8.93	>8.93	82^{+19}_{-11}
Keck102[a]	>1.00	>1.00	<4.82	<4.82	$+0.43^{+0.05}_{-0.01}$	$+0.43^{+0.05}_{-0.01}$	$0.35^{+0.05}_{-0.03}$	>-4.61	>-4.61	>-5.80	>7.42	>7.42	...
Keck103	>1.94	>1.94	<4.11	<4.11	$+0.53^{+0.02}_{-0.01}$	$+0.53^{+0.02}_{-0.01}$	$0.62^{+0.01}_{-0.01}$	>-3.96	>-3.96	>-4.30	>8.21	>8.21	<1
Keck104	>1.95	>1.95	<4.11	<4.11	$+0.48^{+0.01}_{-0.01}$	$+0.48^{+0.01}_{-0.02}$	$0.69^{+0.01}_{-0.01}$	>-3.99	>-3.99	>-4.22	>8.21	>8.21	131^{+44}_{-51}
Keck105	>2.32	>2.29	<3.98	<3.99	$+0.31^{+0.01}_{-0.01}$	$+0.36^{+0.04}_{-0.04}$	$0.55^{+0.01}_{-0.02}$	>-3.66	>-3.64	>-3.97	>8.52	>8.53	<1
Keck106	>1.73	>1.73	<4.22	<4.22	$-0.22^{+0.12}_{-0.12}$	$-0.22^{+0.12}_{-0.12}$	$0.89^{+0.04}_{-0.05}$	>-5.04	>-5.04	>-4.29	>7.78	>7.78	...
Keck107	>1.85	>1.82	<4.15	<4.17	$+0.34^{+0.02}_{-0.01}$	$+0.40^{+0.03}_{-0.05}$	$0.21^{+0.02}_{-0.02}$	>-4.28	>-4.27	>-4.85	>7.83	>7.83	130^{+57}_{-50}
Keck108[a]	>2.04	>2.04	<4.08	<4.08	$+0.32^{+0.03}_{-0.03}$	$+0.32^{+0.03}_{-0.03}$	$0.89^{+0.02}_{-0.03}$	>-4.02	>-4.02	>-3.92	>8.33	>8.33	98^{+43}_{-91}
Keck109	>1.82	>1.82	<4.17	<4.17	$+0.47^{+0.02}_{-0.02}$	$+0.47^{+0.02}_{-0.02}$	$0.67^{+0.02}_{-0.02}$	>-4.18	>-4.18	>-4.39	>8.03	>8.03	...
Keck110	>1.83	>1.68	<4.16	<4.24	$+0.41^{+0.05}_{-0.11}$ [b]	$+0.67^{+0.09}_{-0.07}$ [b]	$0.52^{+0.01}_{-0.01}$	>-4.28 [b]	>-4.22 [b]	>-4.72	>7.92 [b]	>7.90 [b]	...
Keck111	>2.32	>2.29	<3.98	<3.99	$+0.55^{+0.01}_{-0.01}$	$+0.56^{+0.07}_{-0.01}$	$0.63^{+0.01}_{-0.01}$	>-3.42	>-3.40	>-3.89	>8.72	>8.72	169^{+27}_{-23}

Note. — (1): Abbreviated name for MMT/Keck [O III] λ4363-non-detected galaxy. (2)–(3): Lower limit on flux ratio of [O III]λλ4959,5007 to [O III] λ4363. (4)–(5): Upper limit on electron temperature from [O III] λ4363 (i.e., O^{++}). (6)–(7): Flux ratio of [O II]/Hβ. (8): Flux ratio of [O III]λλ4959,5007/Hβ. (9)–(10): Lower limit on gas-phase abundance of O^+/H^+. (11): Lower limit on gas-phase abundance of O^{++}/H^+. (12)–(13): Lower limit on gas-phase oxygen abundance. (14): Electron density in units of cm^{-3}. Columns 3, 5, 7, 10, and 13 include dust attenuation corrections (see Section 4.1). Uncertainties are reported at 68% confidence levels.

[a] Excluded from [O III] λ4363-non-detected sample with stricter [O III]λ5007 flux limit for $M_\star-Z$ relation analyses.

[b] [O II] fluxes were unavailable. We adopt a relation between [O II]/Hβ and [O III]/Hβ (see Figure 28).

TABLE 15
Luminosities, Stellar Properties, and Star Formation Rates for the
[O III] λ4363-detected Sample

ID	M_B	$\log\left[\frac{\mathrm{SFR(H\alpha)}}{M_\odot/\mathrm{yr}}\right]$ Obs.	De-red.	$\log\left[\frac{\mathrm{SFR(H\beta)}}{M_\odot/\mathrm{yr}}\right]$ Obs.	De-red.	$\log\left(\mathrm{M_\star}/M_\odot\right)$	$Z_\star/Z_\odot$ [b]	$\log\left(t_{\mathrm{age}}/\mathrm{yr}\right)$	A_V
	(mag)	(dex)	(dex)	(dex)	(dex)	(dex)		(dex)	(mag)
(1)	(2)	(3)	(4)	(5)	(6)	(7)	(8)	(9)	(10)
MK01	-18.98	+0.04	$+0.11^{+0.00}_{-0.00}$	. . .	. . .	$8.50^{+0.11}_{-0.10}$	0.4	$7.90^{+0.42}_{-0.46}$	$0.7^{+0.2}_{-0.2}$
MK02	-20.23	+0.70	$+0.70^{+0.00}_{-0.00}$	. . .	. . .	$8.53^{+0.30}_{-0.00}$	1.0	$7.10^{+0.82}_{-0.07}$	$0.7^{+0.2}_{-0.2}$
MK03	-17.61	-0.62	$-0.62^{+0.02}_{-0.01}$	. . .	. . .	$7.88^{+0.07}_{-0.06}$	0.2	$8.70^{+0.16}_{-0.40}$	$0.0^{+0.1}_{-0.0}$
MK04	-18.70	+0.12	$+0.19^{+0.01}_{-0.00}$	. . .	. . .	$8.07^{+0.03}_{-0.00}$	0.4	$7.50^{+0.24}_{-0.06}$	$0.4^{+0.2}_{-0.0}$
MMT01	-18.67	. . .	. . .	+0.09	$+0.69^{+0.17}_{-0.19}$	$8.10^{+0.13}_{-0.00}$	0.2	$7.70^{+0.63}_{-0.15}$	$0.0^{+0.4}_{-0.0}$
MMT02	-19.39	. . .	. . .	-0.35	$+0.41^{+0.24}_{-0.23}$	$9.09^{+0.03}_{-0.11}$	0.4	$8.70^{+0.25}_{-0.40}$	$0.8^{+0.1}_{-0.2}$
MMT03	-20.15	. . .	. . .	-0.48	$-0.44^{+0.18}_{-0.24}$	$9.43^{+0.10}_{-0.11}$	0.2	$8.70^{+0.34}_{-0.42}$	$0.9^{+0.2}_{-0.2}$
MMT05	-16.43	-0.58	$-0.58^{+0.01}_{-0.01}$	. . .	. . .	$7.05^{+0.09}_{-0.14}$	0.2	$7.50^{+0.49}_{-0.37}$	$0.1^{+0.5}_{-0.1}$
MMT07	-17.59	-0.09	$+0.10^{+0.01}_{-0.00}$	. . .	. . .	$7.71^{+0.00}_{-0.01}$	0.2	$7.40^{+0.10}_{-0.00}$	$0.6^{+0.0}_{-0.2}$
MMT08	-20.02	. . .	. . .	+0.14	$+0.64^{+0.17}_{-0.19}$	$8.84^{+0.05}_{-0.01}$	0.2	$7.00^{+0.07}_{-0.00}$	$1.6^{+0.1}_{-0.1}$
MMT09	-19.52	-0.53	$-0.43^{+0.03}_{-0.03}$	. . .	. . .	$8.99^{+0.03}_{-0.12}$	0.2	$8.70^{+0.21}_{-0.42}$	$0.5^{+0.1}_{-0.2}$
MMT10	-14.51	-1.70	$-1.61^{+0.01}_{-0.01}$	. . .	. . .	$6.63^{+0.51}_{-0.00}$	0.2	$7.00^{+1.82}_{-0.00}$	$1.6^{+0.1}_{-0.9}$
MMT11	-17.33	-0.76	$-0.65^{+0.01}_{-0.01}$	. . .	. . .	$7.98^{+0.04}_{-0.19}$	0.2	$8.30^{+0.30}_{-0.63}$	$0.7^{+0.4}_{-0.3}$
MMT13	-17.52	-0.46	$-0.46^{+0.01}_{-0.02}$	. . .	. . .	$7.57^{+0.00}_{-0.05}$	0.2	$7.70^{+0.00}_{-0.10}$	$0.0^{+0.1}_{-0.0}$
MMT15	-15.49	-2.15	$-2.15^{+0.02}_{-0.02}$	. . .	. . .	$7.30^{+0.18}_{-0.17}$	0.2	$7.70^{+0.62}_{-0.61}$	$1.4^{+0.2}_{-0.5}$
MMT16	-14.79	-2.24	$-2.16^{+0.04}_{-0.04}$	. . .	. . .	$7.39^{+0.17}_{-0.13}$	0.2	$9.30^{+0.47}_{-0.52}$	$0.3^{+0.4}_{-0.3}$
MMT17	-18.62	-1.93	$-1.85^{+0.03}_{-0.03}$	. . .	. . .	$8.92^{+0.00}_{-0.07}$	0.2	$8.60^{+0.03}_{-0.50}$	$0.6^{+0.3}_{-0.0}$
MMT18	-16.26	-1.13	$-1.13^{+0.05}_{-0.04}$	. . .	. . .	$7.14^{+0.00}_{-0.05}$	0.2	$7.60^{+0.04}_{-0.08}$	$0.2^{+0.1}_{-0.1}$
MMT19	-17.78	-0.39	$-0.33^{+0.01}_{-0.01}$	. . .	. . .	$7.80^{+0.01}_{-0.00}$	0.2	$7.60^{+0.10}_{-0.02}$	$0.2^{+0.0}_{-0.2}$
MMT20	-19.60	-0.42	$-0.37^{+0.02}_{-0.03}$	. . .	. . .	$9.32^{+0.04}_{-0.15}$	0.4	$8.90^{+0.16}_{-0.40}$	$0.7^{+0.2}_{-0.2}$
MMT21	-17.17	-0.44	$-0.44^{+0.04}_{-0.05}$	. . .	. . .	$7.15^{+0.05}_{-0.05}$	0.2	$7.30^{+0.10}_{-0.17}$	$0.2^{+0.0}_{-0.1}$
MMT22	-18.38	-0.64	$-0.50^{+0.05}_{-0.05}$	. . .	. . .	$9.46^{+0.00}_{-0.68}$	0.2	$9.90^{+0.00}_{-2.30}$	$0.5^{+1.2}_{-0.2}$
MMT23	-17.97	-0.41	$-0.16^{+0.00}_{-0.00}$	. . .	. . .	$8.13^{+0.12}_{-0.04}$	0.2	$7.90^{+0.50}_{-0.04}$	$0.3^{+0.3}_{-0.2}$
MMT24	-18.02	. . .	. . .	-0.04	$-0.04^{+0.14}_{-0.10}$	$7.86^{+0.06}_{-0.00}$	0.4	$7.50^{+0.22}_{-0.04}$	$0.5^{+0.2}_{-0.0}$
MMT25	-17.51	-0.36	$-0.36^{+0.02}_{-0.01}$	. . .	. . .	$8.19^{+0.07}_{-0.07}$	0.4	$9.10^{+0.10}_{-0.20}$	$0.0^{+0.1}_{-0.0}$
MMT26	-18.73	-0.58	$-0.42^{+0.01}_{-0.01}$	. . .	. . .	$8.70^{+0.20}_{-0.14}$	0.4	$8.50^{+0.70}_{-0.53}$	$0.8^{+0.3}_{-0.5}$
MMT27	-14.39	-1.86	$-1.69^{+0.11}_{-0.10}$	. . .	. . .	$7.13^{+0.07}_{-0.10}$	0.2	$9.40^{+0.10}_{-0.30}$	$0.0^{+0.0}_{-0.0}$
MMT28	-16.32	-1.29	$-0.85^{+0.10}_{-0.12}$	. . .	. . .	$7.35^{+0.08}_{-0.03}$	0.4	$7.50^{+0.34}_{-0.17}$	$0.8^{+0.3}_{-0.1}$
MMT29	-18.21	-0.04	$+0.09^{+0.01}_{-0.01}$	. . .	. . .	$7.91^{+0.03}_{-0.04}$	0.4	$7.60^{+0.12}_{-0.20}$	$0.5^{+0.1}_{-0.2}$
MMT30	-19.17	-0.18	$-0.11^{+0.02}_{-0.03}$	. . .	. . .	$8.68^{+0.08}_{-0.14}$	0.4	$8.30^{+0.30}_{-0.74}$	$0.6^{+0.2}_{-0.2}$
MMT31	-19.36	+0.13	$+0.30^{+0.01}_{-0.01}$	. . .	. . .	$8.68^{+0.00}_{-0.00}$	0.4	$7.50^{+0.00}_{-0.00}$	$0.9^{+0.0}_{-0.0}$
MMT32	-15.68	-1.48	$-1.26^{+0.01}_{-0.01}$	. . .	. . .	$7.69^{+0.04}_{-0.34}$	1.0	$8.90^{+0.20}_{-1.11}$	$0.4^{+0.2}_{-0.3}$
MMT33	-17.42	-0.58	$-0.54^{+0.02}_{-0.02}$	. . .	. . .	$7.31^{+0.00}_{-0.06}$	0.2	$7.60^{+0.07}_{-0.12}$	$0.1^{+0.2}_{-0.0}$
MMT34	-17.89	-0.74	$-0.74^{+0.02}_{-0.02}$	. . .	. . .	$8.01^{+0.00}_{-0.05}$	0.2	$7.70^{+0.01}_{-0.10}$	$0.5^{+0.1}_{-0.1}$
MMT35	-18.20	. . .	. . .	-0.74	$+0.34^{+0.42}_{-0.35}$	$8.40^{+0.09}_{-0.07}$	0.2	$8.80^{+0.31}_{-0.20}$	$0.4^{+0.1}_{-0.1}$
MMT37	-19.32	. . .	. . .	+0.18	$+0.73^{+0.21}_{-0.18}$	$8.47^{+0.11}_{-0.00}$	0.4	$7.00^{+0.14}_{-0.00}$	$1.4^{+0.2}_{-0.0}$
MMT38	-16.95	. . .	. . .	-0.42	$-0.42^{+0.22}_{-0.26}$	$7.47^{+0.15}_{-0.10}$	0.2	$7.30^{+0.20}_{-0.26}$	$1.0^{+0.1}_{-0.2}$
Keck01	-17.99	. . .	. . .	+0.30	$+1.09^{+0.09}_{-0.10}$	$7.43^{+0.00}_{-0.00}$	0.2	$7.30^{+0.00}_{-0.00}$	$0.0^{+0.0}_{-0.0}$
Keck02	-18.32	. . .	. . .	-0.59	$-0.59^{+0.00}_{-0.00}$	$7.80^{+0.04}_{-0.06}$	0.2	$7.00^{+0.12}_{-0.00}$	$0.9^{+0.1}_{-0.1}$
Keck03	-21.14	. . .	. . .	+0.65	$+1.55^{+0.06}_{-0.06}$	$9.39^{+0.01}_{-0.00}$	1.0	$7.90^{+0.03}_{-0.10}$	$0.1^{+0.2}_{-0.1}$
Keck04	-19.47	. . .	. . .	+0.34	$+0.34^{+0.09}_{-0.10}$	$8.76^{+0.08}_{-0.14}$	0.4	$7.90^{+0.33}_{-0.60}$	$0.9^{+0.3}_{-0.3}$
Keck05	-17.97	. . .	. . .	-0.46	$-0.22^{+0.34}_{-0.34}$	$7.79^{+0.00}_{-0.06}$	0.2	$7.00^{+0.08}_{-0.00}$	$1.1^{+0.0}_{-0.1}$
Keck06	-17.25	. . .	. . .	-0.64	$-0.41^{+0.34}_{-0.34}$	$7.78^{+0.05}_{-0.14}$	0.2	$7.30^{+0.10}_{-0.30}$	$1.5^{+0.1}_{-0.1}$
Keck07	-17.84	. . .	. . .	+0.02	$+0.02^{+0.17}_{-0.14}$	$7.78^{+0.23}_{-0.10}$	0.4	$7.50^{+0.91}_{-0.28}$	$0.3^{+0.4}_{-0.3}$
Keck08	-18.95	. . .	. . .	+0.22	$+0.85^{+0.15}_{-0.14}$	$8.29^{+0.07}_{-0.04}$	0.2	$7.50^{+0.25}_{-0.06}$	$0.4^{+0.1}_{-0.2}$
Keck09	-18.25	. . .	. . .	-0.22	$-0.18^{+0.17}_{-0.20}$	$8.46^{+0.19}_{-0.21}$	1.0	$8.90^{+0.33}_{-0.62}$	$0.1^{+0.3}_{-0.1}$
Keck11	-17.86	. . .	. . .	-0.20	$-0.20^{+0.20}_{-0.17}$	$8.11^{+0.08}_{-0.00}$	0.2	$8.80^{+0.21}_{-0.01}$	$0.0^{+0.0}_{-0.0}$

Ly et al.

TABLE 15
Luminosities, Stellar Properties, and Star Formation Rates for the
[O III] λ4363-detected Sample

(1)	(2)	(3)	(4)	(5)	(6)	(7)	(8)	(9)	(10)
Keck12	-16.90	...	...	-0.94	$-0.94^{+0.37}_{-0.48}$	$7.29^{+0.37}_{-0.21}$	0.2	$7.20^{+1.20}_{-0.20}$	$0.8^{+0.2}_{-0.7}$
Keck13	-16.96	...	...	-0.80	$-0.56^{+0.35}_{-0.27}$	$7.47^{+0.21}_{-0.36}$	0.2	$7.40^{+0.87}_{-0.40}$	$0.7^{+0.4}_{-0.5}$
Keck14	-19.85	...	...	+0.54	$+0.84^{+0.05}_{-0.08}$	$8.85^{+0.07}_{-0.00}$	0.4	$8.70^{+0.10}_{-0.00}$	$0.0^{+0.0}_{-0.0}$
Keck15	-19.47	...	...	+0.19	$+0.66^{+0.14}_{-0.19}$	$8.57^{+0.07}_{-0.04}$	0.4	$8.50^{+0.13}_{-0.10}$	$0.0^{+0.1}_{-0.0}$
Keck16	-20.55	...	...	+0.33	$+1.33^{+0.17}_{-0.15}$	$9.59^{+0.11}_{-0.10}$	0.2	$8.70^{+0.40}_{-0.54}$	$0.9^{+0.2}_{-0.3}$
Keck18	-18.91	...	...	-0.14	$+0.24^{+0.16}_{-0.15}$	$9.14^{+0.11}_{-0.32}$	0.4	$9.30^{+0.28}_{-1.22}$	$0.4^{+0.9}_{-0.2}$
Keck19	-19.11	...	...	+0.38	$+0.38^{+0.06}_{-0.08}$	$8.37^{+0.00}_{-0.07}$	0.4	$8.40^{+0.05}_{-0.11}$	$0.0^{+0.0}_{-0.0}$
Keck20	-16.50	-1.25	$-1.25^{+0.05}_{-0.07}$	...	...	$7.82^{+0.03}_{-0.08}$	0.2	$9.10^{+0.09}_{-0.33}$	$0.0^{+0.2}_{-0.0}$
Keck21	-19.46	...	...	-0.17	$-0.15^{+0.21}_{-0.20}$	$9.05^{+0.05}_{-0.00}$	0.2	$7.60^{+0.10}_{-0.09}$	$1.3^{+0.2}_{-0.2}$
Keck23	-17.91	...	...	-0.41	$-0.41^{+0.19}_{-0.16}$	$7.92^{+0.06}_{-0.07}$	0.2	$8.40^{+0.11}_{-0.15}$	$0.0^{+0.1}_{-0.0}$
Keck24	-20.00	+0.23	$+0.41^{+0.01}_{-0.01}$	...	...	$8.77^{+0.30}_{-0.00}$	0.2	$7.10^{+0.97}_{-0.06}$	$1.4^{+0.1}_{-0.4}$
Keck26	-18.93	...	...	-0.19	$-0.00^{+0.28}_{-0.35}$	$8.65^{+0.05}_{-0.01}$	0.2	$7.60^{+0.29}_{-0.13}$	$1.0^{+0.4}_{-0.2}$
Keck27	-20.73	...	...	+1.28	$+3.00^{+0.06}_{-0.05}$	$8.66^{+0.00}_{-0.06}$	0.2	$7.30^{+0.02}_{-0.01}$	$0.5^{+0.0}_{-0.1}$
Keck28	-18.30	...	...	+0.17	$+1.07^{+0.09}_{-0.13}$	$7.79^{+0.00}_{-0.11}$	0.2	$7.30^{+0.08}_{-0.03}$	$0.4^{+0.0}_{-0.1}$
Keck29	-17.39	...	...	-0.60	$+0.15^{+0.30}_{-0.35}$	$7.92^{+0.06}_{-0.15}$	0.4	$8.40^{+0.03}_{-0.50}$	$0.0^{+0.1}_{-0.0}$
Keck30	-19.16	-0.07	$+0.02^{+0.02}_{-0.02}$	...	...	$8.85^{+0.02}_{-0.09}$	0.4	$8.60^{+0.19}_{-0.22}$	$0.6^{+0.2}_{-0.1}$
Keck31	-18.98	...	...	+0.04	$+0.04^{+0.14}_{-0.09}$	$8.56^{+0.06}_{-0.00}$	0.2	$7.70^{+0.09}_{-0.07}$	$0.7^{+0.1}_{-0.1}$
Keck32	-16.71	-1.07	$-1.03^{+0.06}_{-0.06}$	...	...	$7.83^{+0.17}_{-0.21}$	0.2	$8.70^{+0.59}_{-1.01}$	$0.5^{+0.4}_{-0.4}$
Keck33	-17.61	...	...	-0.28	$-0.28^{+0.16}_{-0.13}$	$7.64^{+0.02}_{-0.05}$	0.2	$8.00^{+0.20}_{-0.41}$	$0.0^{+0.1}_{-0.0}$

Note. — (1): Abbreviated name for MMT/Keck [O III] λ4363-detected galaxy. (2): Rest-frame absolute B-band magnitude. (3)–(4): Hα star formation rate. (5)–(6): Hβ star formation rate. (7): Stellar mass from SED fitting. (8): Assumed stellar metallicity in SED fitting model. (9): Light-weighted stellar age from SED fitting. (10): Extinction at rest-frame 5500Å from SED fitting. All values assume a Chabrier (2003) IMF, and where applicable, dust attenuation follows Calzetti et al. (2000) formalism. Uncertainties are reported for 68% confidence levels.

[a] This source is likely a LINER, so SFR estimates are not trustworthy.

[b] The stellar metallicity is assumed to be one of three values, 0.2, 0.4, or 1.0 $Z_\odot$, based on the dust-corrected gas-phase metallicity (see Equations 18–20).

TABLE 16
LUMINOSITIES, STELLAR PROPERTIES, AND STAR FORMATION RATES FOR THE
[O III] λ4363-NON-DETECTED SAMPLE

ID	M_B	$\log\left[\frac{\mathrm{SFR(H\alpha)}}{M_\odot/\mathrm{yr}}\right]$		$\log\left[\frac{\mathrm{SFR(H\beta)}}{M_\odot/\mathrm{yr}}\right]$		$\log(\mathrm{M_\star}/M_\odot)$	$Z_\star/Z_\odot{}^a$	$\log(t_\mathrm{age}/\mathrm{yr})$	A_V
		Obs.	De-red.	Obs.	De-red.				
(1)	(2)	(3)	(4)	(5)	(6)	(7)	(8)	(9)	(10)
MK05	-19.83	...	...	+0.08	$+0.97^{+0.20}_{-0.15}$	$8.86^{+0.08}_{-0.29}$	0.4	$7.90^{+0.37}_{-0.90}$	$0.9^{+0.3}_{-0.2}$
MK06	-19.42	+0.29	$+0.52^{+0.01}_{-0.02}$	...	...	$9.05^{+0.04}_{-0.10}$	1.0	$8.60^{+0.22}_{-0.44}$	$0.7^{+0.2}_{-0.1}$
MK07	-18.91	-0.26	$+0.02^{+0.04}_{-0.04}$	...	...	$8.91^{+0.02}_{-0.10}$	0.4	$9.10^{+0.10}_{-0.33}$	$0.3^{+0.2}_{-0.1}$
MK08	-18.27	-0.58	$-0.55^{+0.02}_{-0.03}$	...	...	$8.60^{+0.01}_{-0.17}$	0.2	$9.00^{+0.16}_{-0.53}$	$0.3^{+0.3}_{-0.1}$
MK09	-20.32	+0.13	$+0.13^{+0.01}_{-0.01}$	...	...	$9.61^{+0.00}_{-0.12}$	1.0	$8.80^{+0.09}_{-0.45}$	$0.8^{+0.1}_{-0.1}$
MK10	-18.22	-0.47	$-0.26^{+0.04}_{-0.03}$	...	...	$8.35^{+0.10}_{-0.01}$	1.0	$8.40^{+0.30}_{-0.13}$	$0.2^{+0.2}_{-0.0}$
MK11	-19.46	+0.07	$+0.09^{+0.01}_{-0.01}$	...	...	$9.13^{+0.03}_{-0.08}$	1.0	$8.90^{+0.13}_{-0.20}$	$0.5^{+0.1}_{-0.2}$
MK12	-18.82	-0.42	$-0.14^{+0.02}_{-0.02}$	...	...	$8.94^{+0.10}_{-0.01}$	0.4	$8.90^{+0.30}_{-0.10}$	$0.7^{+0.1}_{-0.2}$
MMT40	-18.50	-0.80	$-0.47^{+0.05}_{-0.03}$	...	...	$8.47^{+0.22}_{-0.05}$	0.2	$7.70^{+1.00}_{-0.03}$	$0.9^{+0.1}_{-0.1}$
MMT41	-17.50	-1.04	$-0.77^{+0.02}_{-0.02}$	...	...	$8.56^{+0.14}_{-0.13}$	0.2	$9.40^{+0.30}_{-0.45}$	$0.4^{+0.3}_{-0.2}$
MMT42	-16.97	-1.03	$-0.76^{+0.02}_{-0.02}$	...	...	$8.09^{+0.09}_{-0.06}$	1.0	$8.90^{+0.26}_{-0.22}$	$0.3^{+0.2}_{-0.2}$
MMT43	-16.02	-0.59	$-0.25^{+0.05}_{-0.03}$	...	...	$6.62^{+0.10}_{-0.00}$	1.0	$7.40^{+0.03}_{-0.02}$	$0.2^{+0.2}_{-0.1}$
MMT44	-16.18	-1.19	$-0.92^{+0.02}_{-0.02}$	...	...	$7.34^{+0.00}_{-0.04}$	0.4	$7.00^{+0.02}_{-0.00}$	$1.9^{+0.0}_{-0.1}$
MMT45	-18.00	-0.59	$-0.26^{+0.05}_{-0.03}$	...	...	$8.64^{+0.00}_{-0.04}$	1.0	$9.10^{+0.00}_{-0.10}$	$0.2^{+0.1}_{-0.0}$
MMT46	-17.67	-0.67	$-0.33^{+0.05}_{-0.03}$	...	...	$8.76^{+0.06}_{-0.04}$	1.0	$9.00^{+0.20}_{-0.19}$	$0.9^{+0.2}_{-0.3}$
MMT47	-18.62	-0.61	$-0.27^{+0.05}_{-0.03}$	...	...	$8.84^{+0.05}_{-0.17}$	1.0	$9.00^{+0.16}_{-0.62}$	$0.3^{+0.3}_{-0.1}$
MMT48	-17.57	-0.68	$-0.41^{+0.02}_{-0.02}$	...	...	$8.37^{+0.00}_{-0.15}$	1.0	$8.50^{+0.03}_{-0.60}$	$0.5^{+0.3}_{-0.1}$
MMT49	-15.77	-1.03	$-0.76^{+0.02}_{-0.02}$	...	...	$7.09^{+0.04}_{-0.05}$	0.4	$7.00^{+0.08}_{-0.00}$	$1.5^{+0.1}_{-0.1}$
MMT50	-16.45	-1.05	$-0.61^{+0.09}_{-0.09}$	...	...	$7.21^{+0.08}_{-0.04}$	0.2	$7.60^{+0.45}_{-0.09}$	$0.2^{+0.4}_{-0.2}$
MMT51	-17.47	-1.05	$-0.89^{+0.20}_{-0.20}$	...	...	$8.59^{+0.04}_{-0.11}$	0.4	$9.60^{+0.13}_{-0.23}$	$0.1^{+0.1}_{-0.1}$
MMT52	-17.57	-0.45	$-0.01^{+0.09}_{-0.09}$	...	...	$8.00^{+0.07}_{-0.00}$	1.0	$8.70^{+0.10}_{-0.10}$	$0.0^{+0.0}_{-0.0}$
MMT55	-18.48	+0.22	$+0.22^{+0.06}_{-0.05}$	...	...	$8.78^{+0.00}_{-0.08}$	1.0	$9.30^{+0.02}_{-0.10}$	$0.0^{+0.0}_{-0.0}$
MMT56[b]	-16.59	...	...	-0.78	$-0.17^{+0.12}_{-0.12}$	$7.46^{+0.11}_{-0.12}$	0.2	$8.50^{+0.33}_{-0.71}$	$0.1^{+0.3}_{-0.1}$
MMT57[b]	-17.25	-0.69	$-0.25^{+0.09}_{-0.09}$	...	...	$7.52^{+0.10}_{-0.22}$	0.2	$7.70^{+0.40}_{-0.60}$	$0.5^{+0.2}_{-0.4}$
MMT58	-17.10	-1.09	$-0.82^{+0.02}_{-0.02}$	...	...	$8.28^{+0.10}_{-0.20}$	1.0	$9.10^{+0.27}_{-0.63}$	$0.4^{+0.5}_{-0.2}$
MMT59	-16.74	-1.15	$-0.88^{+0.02}_{-0.02}$	...	...	$7.55^{+0.41}_{-0.05}$	0.2	$7.70^{+1.60}_{-0.08}$	$0.5^{+0.1}_{-0.5}$
MMT60	-15.43	-1.50	$-1.23^{+0.02}_{-0.02}$	...	...	$7.56^{+0.12}_{-0.04}$	0.2	$9.20^{+0.31}_{-0.22}$	$0.1^{+0.4}_{-0.1}$
MMT61	-15.91	-1.44	$-1.44^{+0.13}_{-0.10}$	...	...	$7.85^{+0.15}_{-0.04}$	0.4	$9.20^{+0.44}_{-0.14}$	$0.2^{+0.4}_{-0.2}$
MMT62	-16.55	-0.84	$-0.57^{+0.02}_{-0.02}$	...	...	$7.64^{+0.02}_{-0.10}$	1.0	$8.70^{+0.13}_{-0.47}$	$0.0^{+0.2}_{-0.0}$
MMT63	-15.16	-1.53	$-1.26^{+0.02}_{-0.02}$	...	...	$6.92^{+0.45}_{-0.00}$	0.2	$7.70^{+1.61}_{-0.10}$	$0.4^{+0.2}_{-0.4}$
MMT64[b]	-15.54	-1.05	$-1.05^{+0.13}_{-0.10}$	...	...	$7.43^{+0.11}_{-0.04}$	0.2	$9.00^{+0.34}_{-0.14}$	$0.0^{+0.2}_{-0.0}$
MMT65	-16.66	-0.77	$+0.03^{+0.03}_{-0.03}$	...	...	$7.34^{+0.30}_{-0.00}$	0.4	$7.00^{+0.92}_{-0.00}$	$1.2^{+0.1}_{-0.4}$
MMT66	-18.77	-0.06	$-0.06^{+0.04}_{-0.03}$	...	...	$8.87^{+0.07}_{-0.07}$	1.0	$8.80^{+0.25}_{-0.40}$	$0.5^{+0.2}_{-0.2}$
MMT67	-18.35	-0.47	$-0.47^{+0.06}_{-0.05}$	...	...	$8.73^{+0.10}_{-0.11}$	1.0	$9.10^{+0.20}_{-0.37}$	$0.2^{+0.3}_{-0.1}$
MMT69	-17.76	-0.51	$-0.43^{+0.01}_{-0.01}$	...	...	$8.42^{+0.06}_{-0.17}$	0.4	$8.90^{+0.29}_{-0.54}$	$0.3^{+0.3}_{-0.2}$
MMT70[b]	-17.10	-0.73	$-0.40^{+0.05}_{-0.03}$	...	...	$7.99^{+0.02}_{-0.03}$	0.2	$8.60^{+0.02}_{-0.20}$	$0.0^{+0.5}_{-0.0}$
MMT71	-13.79	-2.54	$-2.27^{+0.02}_{-0.02}$	...	...	$6.40^{+0.10}_{-0.14}$	0.2	$7.50^{+0.48}_{-0.41}$	$1.1^{+0.2}_{-0.2}$
MMT72	-18.31	-0.84	$-0.51^{+0.05}_{-0.03}$	...	...	$8.31^{+0.00}_{-0.05}$	0.2	$7.60^{+0.04}_{-0.01}$	$0.7^{+0.0}_{-0.1}$
MMT73	-18.62	-0.32	$-0.32^{+0.04}_{-0.03}$	...	...	$8.90^{+0.05}_{-0.04}$	1.0	$9.00^{+0.09}_{-0.10}$	$0.3^{+0.2}_{-0.1}$
MMT75	-17.41	-0.45	$-0.01^{+0.09}_{-0.09}$	...	...	$8.29^{+0.00}_{-0.07}$	1.0	$9.20^{+0.08}_{-0.20}$	$0.0^{+0.1}_{-0.0}$
MMT76	-18.64	-0.39	$-0.32^{+0.01}_{-0.01}$	...	...	$8.97^{+0.07}_{-0.00}$	1.0	$9.10^{+0.10}_{-0.01}$	$0.3^{+0.0}_{-0.1}$
MMT78	-17.92	-0.47	$-0.47^{+0.06}_{-0.05}$	...	...	$8.28^{+0.00}_{-0.11}$	1.0	$8.90^{+0.10}_{-0.34}$	$0.0^{+0.2}_{-0.0}$
MMT79[b]	-18.37	-0.42	$+0.02^{+0.09}_{-0.09}$	...	...	$8.58^{+0.13}_{-0.10}$	0.2	$8.30^{+0.54}_{-0.50}$	$0.8^{+0.3}_{-0.1}$
MMT80	-18.50	-0.52	$-0.44^{+0.01}_{-0.01}$	...	...	$8.83^{+0.00}_{-0.05}$	1.0	$9.10^{+0.10}_{-0.10}$	$0.1^{+0.1}_{-0.1}$
MMT81	-19.06	-0.56	$-0.56^{+0.06}_{-0.05}$	...	...	$9.11^{+0.00}_{-0.05}$	1.0	$9.00^{+0.10}_{-0.01}$	$0.4^{+0.0}_{-0.2}$
MMT82[b]	-17.88	-0.81	$-0.48^{+0.05}_{-0.03}$	...	...	$8.26^{+0.06}_{-0.03}$	0.2	$8.90^{+0.24}_{-0.10}$	$0.0^{+0.1}_{-0.0}$
MMT85[b]	-19.68	-0.21	$-0.13^{+0.01}_{-0.01}$	...	...	$9.23^{+0.00}_{-0.12}$	0.4	$8.90^{+0.09}_{-0.44}$	$0.7^{+0.3}_{-0.1}$

TABLE 16
Luminosities, Stellar Properties, and Star Formation Rates for the
[O III] λ4363-non-detected Sample

MMT86	-17.30	-0.72	$-0.38^{+0.05}_{-0.03}$	...	...	$7.72^{+0.00}_{-0.04}$	0.2	$7.60^{+0.03}_{-0.01}$	$0.5^{+0.0}_{-0.1}$
MMT87	-18.07	-0.57	$-0.30^{+0.02}_{-0.02}$	...	...	$8.46^{+0.07}_{-0.08}$	0.2	$8.30^{+0.33}_{-0.51}$	$1.1^{+0.1}_{-0.3}$
MMT88[b]	-16.69	-1.23	$-1.23^{+0.13}_{-0.10}$	...	...	$8.13^{+0.14}_{-0.09}$	0.2	$9.40^{+0.33}_{-0.20}$	$0.2^{+0.1}_{-0.2}$
MMT89	-17.60	-1.04	$-0.87^{+0.20}_{-0.20}$	...	...	$8.52^{+0.13}_{-0.02}$	0.2	$9.30^{+0.39}_{-0.13}$	$0.4^{+0.1}_{-0.3}$
Keck034	-18.55	-0.51	$-0.30^{+0.02}_{-0.02}$	...	...	$8.76^{+0.09}_{-0.06}$	1.0	$8.90^{+0.25}_{-0.18}$	$0.5^{+0.1}_{-0.2}$
Keck035	-17.67	-0.94	$-0.73^{+0.02}_{-0.02}$	...	...	$8.20^{+0.10}_{-0.11}$	0.4	$8.70^{+0.31}_{-0.43}$	$0.3^{+0.1}_{-0.2}$
Keck036[b]	-17.44	-0.79	$-0.57^{+0.02}_{-0.02}$	...	...	$8.62^{+0.19}_{-0.10}$	0.2	$9.40^{+0.44}_{-0.45}$	$0.6^{+0.4}_{-0.3}$
Keck037	-18.82	...	...	-0.43	$-0.43^{+0.18}_{-0.18}$	$8.90^{+0.23}_{-0.22}$	1.0	$9.10^{+0.40}_{-0.77}$	$0.2^{+0.6}_{-0.2}$
Keck038	-20.11	...	...	-0.17	$-0.17^{+0.11}_{-0.11}$	$10.24^{+0.00}_{-0.19}$	1.0	$9.80^{+0.40}_{-0.40}$	$0.7^{+0.1}_{-0.3}$
Keck039	-19.65	...	...	-0.33	$-0.33^{+0.18}_{-0.18}$	$9.30^{+0.02}_{-0.10}$	1.0	$9.20^{+0.18}_{-0.20}$	$0.2^{+0.1}_{-0.1}$
Keck040[b]	-17.66	...	...	-0.62	$-0.62^{+0.18}_{-0.18}$	$8.54^{+0.09}_{-0.00}$	0.2	$9.50^{+0.10}_{-0.03}$	$0.0^{+0.0}_{-0.0}$
Keck041	-20.20	...	...	+0.11	$+0.32^{+0.15}_{-0.18}$	$9.44^{+0.02}_{-0.21}$	0.4	$8.90^{+0.15}_{-0.64}$	$0.6^{+0.2}_{-0.2}$
Keck042	-20.91	...	...	+0.29	$+0.50^{+0.15}_{-0.18}$	$9.76^{+0.12}_{-0.02}$	0.2	$8.70^{+0.42}_{-0.12}$	$0.9^{+0.1}_{-0.2}$
Keck043	-20.50	...	...	+0.44	$+0.65^{+0.15}_{-0.18}$	$9.77^{+0.11}_{-0.02}$	1.0	$9.20^{+0.22}_{-0.15}$	$0.5^{+0.1}_{-0.1}$
Keck044	-19.85	...	...	+0.31	$+0.53^{+0.15}_{-0.18}$	$8.93^{+0.12}_{-0.06}$	1.0	$8.30^{+0.53}_{-0.10}$	$0.1^{+0.2}_{-0.1}$
Keck046	-18.66	...	...	-0.26	$-0.26^{+0.11}_{-0.11}$	$8.38^{+0.08}_{-0.10}$	0.2	$8.70^{+0.10}_{-0.51}$	$0.0^{+0.2}_{-0.0}$
Keck047[b]	-18.41	-0.89	$-0.68^{+0.02}_{-0.02}$	...	...	$8.86^{+0.10}_{-0.03}$	0.2	$9.40^{+0.23}_{-0.10}$	$0.2^{+0.1}_{-0.1}$
Keck048[b]	-19.18	...	...	-0.30	$-0.30^{+0.11}_{-0.11}$	$8.89^{+0.13}_{-0.15}$	0.2	$8.50^{+0.49}_{-0.74}$	$0.8^{+0.2}_{-0.4}$
Keck049	-18.71	...	...	-0.03	$+0.18^{+0.15}_{-0.18}$	$8.04^{+0.09}_{-0.07}$	0.2	$7.00^{+0.25}_{-0.00}$	$1.1^{+0.1}_{-0.2}$
Keck050[b]	-18.83	...	...	-0.60	$-0.60^{+0.18}_{-0.18}$	$8.52^{+0.05}_{-0.00}$	0.2	$7.00^{+0.13}_{-0.00}$	$1.9^{+0.1}_{-0.1}$
Keck051	-19.19	-0.48	$-0.27^{+0.02}_{-0.02}$	...	...	$8.84^{+0.10}_{-0.07}$	0.2	$8.70^{+0.32}_{-0.22}$	$0.6^{+0.1}_{-0.2}$
Keck052	-20.51	...	...	+0.32	$+0.53^{+0.15}_{-0.18}$	$9.31^{+0.14}_{-0.13}$	0.4	$8.30^{+0.50}_{-0.57}$	$0.5^{+0.3}_{-0.2}$
Keck053	-19.56	+0.17	$+1.09^{+0.02}_{-0.02}$	...	...	$8.80^{+0.10}_{-0.13}$	1.0	$8.10^{+0.49}_{-0.41}$	$0.5^{+0.1}_{-0.2}$
Keck054	-16.07	-0.64	$-0.64^{+0.14}_{-0.15}$	...	...	$7.01^{+0.09}_{-0.05}$	0.2	$7.00^{+0.26}_{-0.00}$	$1.0^{+0.1}_{-0.2}$
Keck055	-17.77	-0.92	$-0.70^{+0.02}_{-0.02}$	...	...	$8.12^{+0.08}_{-0.20}$	0.2	$8.60^{+0.21}_{-0.92}$	$0.3^{+0.3}_{-0.1}$
Keck056	-19.16	...	...	-0.07	$-0.07^{+0.11}_{-0.11}$	$8.71^{+0.04}_{-0.06}$	0.2	$7.50^{+0.21}_{-0.29}$	$1.6^{+0.2}_{-0.1}$
Keck057	-18.99	-0.27	$-0.27^{+0.13}_{-0.13}$	...	...	$9.13^{+0.02}_{-0.11}$	0.2	$9.10^{+0.18}_{-0.45}$	$0.8^{+0.3}_{-0.2}$
Keck058	-19.24	...	...	-0.41	$-0.41^{+0.18}_{-0.18}$	$8.34^{+0.42}_{-0.01}$	0.2	$7.10^{+1.40}_{-0.10}$	$1.1^{+0.1}_{-0.6}$
Keck059[b]	-18.17	-0.93	$-0.72^{+0.02}_{-0.02}$	...	...	$8.45^{+0.09}_{-0.08}$	0.2	$8.80^{+0.30}_{-0.30}$	$0.5^{+0.2}_{-0.2}$
Keck060	-18.41	...	...	-0.13	$-0.13^{+0.11}_{-0.11}$	$8.88^{+0.00}_{-0.11}$	0.4	$9.40^{+0.07}_{-0.25}$	$0.1^{+0.2}_{-0.1}$
Keck061	-18.48	...	...	-0.66	$-0.66^{+0.18}_{-0.18}$	$8.30^{+0.00}_{-0.05}$	0.2	$7.00^{+0.09}_{-0.00}$	$1.8^{+0.1}_{-0.1}$
Keck063	-19.13	-0.34	$+0.44^{+0.02}_{-0.02}$	...	...	$9.15^{+0.07}_{-0.13}$	0.2	$8.80^{+0.21}_{-0.50}$	$1.0^{+0.1}_{-0.2}$
Keck065	-19.64	...	...	+0.16	$+0.37^{+0.15}_{-0.18}$	$9.03^{+0.06}_{-0.06}$	1.0	$8.50^{+0.02}_{-0.06}$	$0.1^{+0.1}_{-0.1}$
Keck066[b]	-18.55	...	...	-0.12	$-0.12^{+0.11}_{-0.11}$	$8.22^{+0.14}_{-0.07}$	0.2	$7.60^{+0.84}_{-0.12}$	$0.4^{+0.3}_{-0.2}$
Keck067[b]	-20.62	...	...	+0.05	$+0.05^{+0.11}_{-0.11}$	$9.38^{+0.06}_{-0.00}$	1.0	$8.50^{+0.01}_{-0.11}$	$0.0^{+0.3}_{-0.0}$
Keck068	-18.37	-0.40	$+0.38^{+0.02}_{-0.02}$	...	...	$8.60^{+0.13}_{-0.14}$	0.4	$8.00^{+0.50}_{-0.53}$	$1.6^{+0.2}_{-0.4}$
Keck069	-18.44	...	...	-0.15	$-0.15^{+0.11}_{-0.11}$	$8.17^{+0.00}_{-0.07}$	0.2	$7.60^{+0.06}_{-0.11}$	$0.4^{+0.2}_{-0.1}$
Keck070	-17.65	...	...	-0.23	$-0.23^{+0.18}_{-0.18}$	$7.75^{+0.26}_{-0.09}$	0.4	$7.10^{+1.00}_{-0.10}$	$1.2^{+0.1}_{-0.6}$
Keck071	-19.02	...	...	-0.12	$-0.12^{+0.11}_{-0.11}$	$8.81^{+0.14}_{-0.18}$	1.0	$8.90^{+0.32}_{-0.50}$	$0.0^{+0.3}_{-0.0}$
Keck072	-19.88	...	...	+0.31	$+0.52^{+0.15}_{-0.18}$	$9.32^{+0.00}_{-0.06}$	1.0	$8.40^{+0.12}_{-0.04}$	$0.7^{+0.0}_{-0.3}$
Keck073	-20.06	...	...	-0.43	$-0.20^{+0.27}_{-0.27}$	$9.32^{+0.08}_{-0.12}$	0.2	$8.90^{+0.20}_{-0.43}$	$0.6^{+0.2}_{-0.1}$
Keck076	-18.57	-0.56	$-0.56^{+0.14}_{-0.15}$	...	...	$8.53^{+0.11}_{-0.07}$	0.2	$8.60^{+0.31}_{-0.40}$	$0.5^{+0.2}_{-0.2}$
Keck077	-19.66	...	...	-0.11	$-0.11^{+0.11}_{-0.11}$	$8.69^{+0.10}_{-0.09}$	0.2	$7.20^{+0.36}_{-0.20}$	$1.4^{+0.1}_{-0.2}$
Keck078	-18.76	-0.27	$-0.27^{+0.14}_{-0.15}$	...	...	$8.80^{+0.02}_{-0.11}$	0.4	$8.90^{+0.12}_{-0.34}$	$0.5^{+0.2}_{-0.1}$
Keck079[b]	-18.30	...	...	-0.70	$-0.70^{+0.20}_{-0.20}$	$8.37^{+0.10}_{-0.04}$	0.2	$7.10^{+0.22}_{-0.10}$	$1.9^{+0.1}_{-0.1}$
Keck080	-19.03	...	...	-0.28	$-0.28^{+0.11}_{-0.11}$	$8.61^{+0.06}_{-0.36}$	0.2	$8.10^{+0.39}_{-1.05}$	$0.8^{+0.4}_{-0.3}$
Keck081	-18.30	...	...	-0.12	$-0.12^{+0.11}_{-0.11}$	$8.20^{+0.10}_{-0.18}$	0.4	$7.50^{+0.27}_{-0.50}$	$1.1^{+0.3}_{-0.3}$
Keck082	-20.14	...	...	-0.04	$+0.17^{+0.15}_{-0.18}$	$9.07^{+0.09}_{-0.05}$	0.2	$7.70^{+0.52}_{-0.11}$	$0.7^{+0.4}_{-0.1}$
Keck083	-19.26	...	...	-0.24	$-0.24^{+0.11}_{-0.11}$	$8.59^{+0.21}_{-0.00}$	0.2	$7.70^{+0.94}_{-0.05}$	$0.5^{+0.3}_{-0.1}$
Keck085	-17.89	-0.93	$-0.72^{+0.02}_{-0.02}$	...	...	$8.19^{+0.00}_{-0.05}$	0.2	$7.70^{+0.05}_{-0.10}$	$0.7^{+0.2}_{-0.1}$

TABLE 16
Luminosities, Stellar Properties, and Star Formation Rates for the
[O III] λ4363-non-detected Sample

(1)	(2)	(3)	(4)	(5)	(6)	(7)	(8)	(9)	(10)
Keck086	-19.56	...	...	-0.39	$-0.39^{+0.18}_{-0.18}$	$8.99^{+0.07}_{-0.12}$	0.2	$8.50^{+0.20}_{-0.49}$	$0.7^{+0.2}_{-0.2}$
Keck087	-18.75	...	...	-0.11	$-0.11^{+0.11}_{-0.11}$	$8.36^{+0.20}_{-0.00}$	0.4	$7.90^{+0.40}_{-0.17}$	$0.1^{+0.4}_{-0.1}$
Keck089[b]	-17.67	-0.92	$-0.70^{+0.02}_{-0.02}$	...	...	$8.61^{+0.08}_{-0.06}$	0.2	$9.60^{+0.10}_{-0.22}$	$0.0^{+0.2}_{-0.0}$
Keck090	-18.55	-0.66	$-0.44^{+0.02}_{-0.02}$	...	...	$8.64^{+0.07}_{-0.07}$	0.2	$8.70^{+0.28}_{-0.40}$	$0.6^{+0.2}_{-0.2}$
Keck091	-17.95	...	...	-0.36	$-0.36^{+0.18}_{-0.18}$	$8.36^{+0.07}_{-0.08}$	0.4	$9.10^{+0.19}_{-0.11}$	$0.0^{+0.1}_{-0.0}$
Keck092[b]	-19.19	...	...	-0.44	$-0.44^{+0.18}_{-0.18}$	$8.81^{+0.07}_{-0.18}$	0.2	$7.60^{+0.32}_{-0.53}$	$1.6^{+0.2}_{-0.0}$
Keck093[b]	-19.24	-0.62	$-0.40^{+0.02}_{-0.02}$	...	...	$8.90^{+0.16}_{-0.01}$	0.2	$8.30^{+0.67}_{-0.07}$	$0.8^{+0.2}_{-0.2}$
Keck094	-19.82	...	...	+0.53	$+0.74^{+0.15}_{-0.18}$	$9.10^{+0.08}_{-0.02}$	1.0	$9.00^{+0.10}_{-0.10}$	$0.0^{+0.1}_{-0.0}$
Keck096[b]	-19.55	...	...	+0.28	$+0.49^{+0.15}_{-0.18}$	$8.69^{+0.09}_{-0.12}$	0.2	$8.00^{+0.45}_{-0.50}$	$0.5^{+0.3}_{-0.4}$
Keck097	-19.46	-0.20	$-0.20^{+0.13}_{-0.13}$	...	...	$9.47^{+0.08}_{-0.10}$	0.2	$9.50^{+0.16}_{-0.20}$	$0.5^{+0.2}_{-0.1}$
Keck098	-18.23	-0.67	$-0.67^{+0.14}_{-0.15}$	...	...	$8.56^{+0.08}_{-0.12}$	0.2	$8.90^{+0.23}_{-0.40}$	$0.5^{+0.3}_{-0.1}$
Keck099	-21.59	...	...	+0.99	$+1.20^{+0.15}_{-0.18}$	$10.35^{+0.03}_{-0.29}$	1.0	$9.30^{+0.10}_{-1.00}$	$0.1^{+0.9}_{-0.1}$
Keck100	-19.00	...	...	-0.32	$-0.32^{+0.11}_{-0.11}$	$8.69^{+0.14}_{-0.15}$	0.2	$8.30^{+0.65}_{-0.47}$	$0.5^{+0.3}_{-0.5}$
Keck101	-20.35	...	...	+0.23	$+0.23^{+0.11}_{-0.11}$	$9.51^{+0.10}_{-0.02}$	1.0	$9.10^{+0.21}_{-0.10}$	$0.4^{+0.1}_{-0.1}$
Keck102[b]	-19.55	...	...	-0.47	$-0.47^{+0.18}_{-0.18}$	$8.80^{+0.04}_{-0.06}$	0.2	$7.00^{+0.14}_{-0.00}$	$1.9^{+0.0}_{-0.1}$
Keck103	-19.21	...	...	-0.15	$-0.15^{+0.11}_{-0.11}$	$8.85^{+0.01}_{-0.20}$	0.4	$8.80^{+0.19}_{-0.62}$	$0.3^{+0.3}_{-0.2}$
Keck104	-18.80	...	...	-0.34	$-0.34^{+0.18}_{-0.18}$	$8.12^{+0.05}_{-0.06}$	0.4	$7.00^{+0.06}_{-0.00}$	$1.2^{+0.2}_{-0.1}$
Keck105	-19.93	...	...	+0.56	$+0.77^{+0.15}_{-0.18}$	$8.89^{+0.13}_{-0.07}$	1.0	$7.60^{+0.70}_{-0.15}$	$0.6^{+0.2}_{-0.1}$
Keck106	-16.09	...	...	-0.84	$-0.84^{+0.20}_{-0.20}$	$7.84^{+0.17}_{-0.22}$	0.2	$9.30^{+0.20}_{-0.48}$	$0.0^{+0.2}_{-0.0}$
Keck107	-19.47	...	...	+0.85	$+1.06^{+0.15}_{-0.18}$	$8.79^{+0.55}_{-0.06}$	0.2	$7.70^{+2.00}_{-0.11}$	$0.9^{+0.3}_{-0.9}$
Keck108[b]	-18.59	...	...	-0.15	$-0.15^{+0.11}_{-0.11}$	$8.53^{+0.23}_{-0.07}$	0.4	$7.70^{+0.92}_{-0.23}$	$0.8^{+0.6}_{-0.3}$
Keck109	-19.48	...	...	-0.23	$-0.23^{+0.11}_{-0.11}$	$8.98^{+0.09}_{-0.14}$	0.2	$8.80^{+0.35}_{-0.55}$	$0.3^{+0.3}_{-0.2}$
Keck110	-19.21	-0.40	$+0.38^{+0.02}_{-0.02}$	...	...	$9.15^{+0.08}_{-0.03}$	0.2	$9.50^{+0.10}_{-0.18}$	$0.0^{+0.2}_{-0.0}$
Keck111	-20.09	...	...	+0.25	$+0.46^{+0.15}_{-0.18}$	$9.20^{+0.05}_{-0.00}$	1.0	$8.50^{+0.03}_{-0.14}$	$0.1^{+0.4}_{-0.1}$

Note. — (1): Abbreviated name for MMT/Keck [O III] λ4363-non-detected galaxy. (2): Rest-frame absolute B-band magnitude. (3)–(4): Hα star formation rate. (5)–(6): Hβ star formation rate. (7): Stellar mass from SED fitting. (8): Assumed stellar metallicity in SED fitting model. (9): Light-weighted stellar age from SED fitting. (10): Extinction at rest-frame 5500Å from SED fitting. All values assume a Chabrier (2003) IMF, and where applicable, dust attenuation follows Calzetti et al. (2000) formalism. Uncertainties are reported for 68% confidence levels.

[a] The stellar metallicity is assumed to be one of three values, 0.2, 0.4, or 1.0 $Z_{\odot}$, based on the dust-corrected gas-phase metallicity (see Equations 18–20).
[b] Excluded from [O III] λ4363-non-detected sample with stricter [O III] λ5007 flux limit for $M_{\star}-Z$ relation analyses.

TABLE 17
SPECTRAL ENERGY DISTRIBUTIONS FOR THE [O III] λ4363-DETECTED SAMPLE

ID	FUV (μJy)	NUV (μJy)	U (μJy)	B (μJy)	V (μJy)	IA598 (μJy)	R_C (μJy)	IA679 (μJy)	i' (μJy)	z_b (μJy)	z' (μJy)	z_r (μJy)	J (μJy)	H (μJy)	K (μJy)
(1)	(2)	(3)	(4)	(5)	(6)	(7)	(8)	(9)	(10)	(11)	(12)	(13)	(14)	(15)	(16)
MK01	1.72	2.85	3.23	3.03	4.96	4.56	7.19	7.89	6.09	7.26	7.02	5.87	6.15	7.04	7.23
...	±0.06	±0.05	±0.04	±0.01	±0.01	±0.03	±0.01	±0.02	±0.01	±0.04	±0.03	±0.10	±0.14	±0.35	±0.22
...	−0.02	−0.12	−0.21	−0.34	−0.84	−0.58	−2.18	−3.66	−1.31	−2.14	−1.85	−0.26	−0.19	−0.19	−0.17
MK02	3.81	7.68	9.12	8.67	12.16	9.23	11.13	9.81	16.30	9.73	13.32	27.41	11.35	13.88	13.34
...	±0.11	±0.15	±0.04	±0.01	±0.01	±0.02	±0.01	±0.03	±0.01	±0.04	±0.03	±0.10	±0.18	±0.35	±0.29
...	−0.05	−0.40	−0.60	−0.89	−2.29	−0.99	−1.32	−0.40	−6.76	−0.82	−2.92	−10.01	−0.52	−0.41	−0.40
MK03	0.55	1.35	0.62	0.57	0.95	1.13	1.42	0.90	1.57	1.00	1.26	1.19	0.74	0.92	0.64
...	±0.05	±0.05	±0.04	±0.01	±0.01	±0.02	±0.01	±0.03	±0.01	±0.04	±0.03	±0.09	±0.35	±0.31	±0.27
...	...	−0.03	−0.05	−0.08	−0.12	−0.06	−0.36	−0.24	−0.61	−0.07	−0.24	−0.08	−0.04	−0.03	−0.03
MK04	1.47	2.48	2.21	1.97	3.11	3.05	3.95	2.31	5.10	2.72	4.03	3.74	3.06	3.55	3.35
...	±0.06	±0.07	±0.04	±0.01	±0.01	±0.02	±0.01	±0.03	±0.01	±0.04	±0.03	±0.10	±0.17	±0.35	±0.24
...	−0.01	−0.11	−0.18	−0.29	−0.71	−0.26	−1.12	−0.66	−2.28	−0.24	−1.08	−0.57	−0.17	−0.17	−0.16
MMT01	0.26	0.93	0.96	0.91	1.06	1.20	1.47	1.29	2.46	1.15	1.22	1.15	1.11	1.68	1.50
...	±0.04	±0.03	±0.03	±0.01	±0.01	±0.02	±0.01	±0.03	±0.01	±0.04	±0.03	±0.09	±0.17	±0.33	±0.27
...	...	...	−0.03	−0.05	−0.12	−0.56	−0.34	−0.13	−1.21	−0.09	−0.12	−0.10	−0.11	−0.14	−0.23
MMT02	0.62	1.46	1.87	2.12	4.00	5.18	5.51	4.51	6.28	6.28	7.22	7.99	6.05	9.14	9.07
...	±0.05	±0.04	±0.04	±0.01	±0.01	±0.02	±0.01	±0.03	±0.01	±0.04	±0.03	±0.10	±0.58	±0.36	±1.01
...	...	...	−0.02	−0.05	−0.30	−0.06	−0.26	−0.17	−0.51	−0.13	−0.43	−0.22	−0.07	−0.17	−0.19
MMT03	0.70	1.96	2.85	3.06	5.47	6.87	8.54	8.32	9.79	10.44	11.40	15.06	11.78	16.52	17.41
...	±0.05	±0.04	±0.04	±0.01	±0.01	±0.03	±0.01	±0.02	±0.01	±0.04	±0.03	±0.10	±0.59	±0.32	±1.04
...	...	−0.04	−0.06	−0.08	−0.31	−0.05	−0.08	−0.05	−0.27	−0.11	−0.32	−0.97	−0.05	−0.04	−0.04
MMT05	...	...	0.47	0.44	0.65	0.59	1.54	2.86	0.96	1.04	0.94	0.36	0.59	≤0.79	0.38
...	...	...	±0.04	±0.01	±0.01	±0.03	±0.01	±0.02	±0.01	±0.04	±0.03	±0.09	±0.16	...	±0.22
...	...	...	−0.08	−0.12	−0.18	−0.22	−0.96	−2.65	−0.42	−0.65	−0.48	−0.07	−0.06	...	−0.04
MMT07	0.63	1.11	1.26	1.20	1.81	1.58	3.76	5.43	2.56	3.22	2.88	1.79		2.54	1.99
...	±0.04	±0.04	±0.04	±0.01	±0.01	±0.03	±0.01	±0.02	±0.01	±0.04	±0.03	±0.09	...	±0.31	±0.26
...	...	−0.07	−0.14	−0.24	−0.52	−0.53	−2.15	−4.48	−1.16	−1.95	−1.52	−0.22	...	−0.20	−0.18
MMT08	0.17	1.11	1.69	1.88	2.60	4.45	4.50	3.53	5.79	5.26	5.51	6.09	6.14	7.74	6.04
...	±0.03	±0.04	±0.04	±0.01	±0.01	±0.02	±0.01	±0.03	±0.01	±0.04	±0.03	±0.10	±0.58	±0.32	±0.98
...	...	−0.01	−0.04	−0.06	−0.14	−1.15	−0.47	−0.17	−0.81	−0.08	−0.10	−0.10	−0.10	−0.12	−0.18
MMT09	0.85	2.12	2.17	2.05	3.48	4.09	4.87	4.66	5.70	5.32	5.85	7.66	5.00	6.85	3.07
...	±0.05	±0.06	±0.04	±0.01	±0.01	±0.03	±0.01	±0.02	±0.01	±0.04	±0.03	±0.10	±0.58	±0.32	±0.92
...	...	−0.02	−0.03	−0.05	−0.22	−0.03	−0.07	−0.03	−0.44	−0.06	−0.21	−0.84	−0.04	−0.04	−0.04
MMT10	0.82	1.15	1.85	2.69	5.24	4.02	4.91	3.31	5.01	4.45	4.73	5.32	5.22		3.31
...	±0.06	±0.03	±0.04	±0.01	±0.01	±0.02	±0.01	±0.03	±0.01	±0.04	±0.03	±0.10	±0.41	...	±0.31
...	−0.09	−0.14	−0.40	−0.43	−1.79	−0.16	−0.93	−0.43	−1.06	−0.18	−0.17	−0.15	−0.22	...	−0.20
MMT11	1.93	2.77	3.32	4.08	7.37	8.95	6.37	5.84	7.68	6.71	6.93	6.93	8.27	7.92	7.58
...	±0.09	±0.09	±0.04	±0.01	±0.01	±0.03	±0.01	±0.02	±0.01	±0.04	±0.03	±0.10	±0.19	±0.32	±0.27
...	−0.05	−0.13	−0.30	−0.67	−1.77	−3.51	−0.45	−0.27	−1.38	−0.32	−0.29	−0.17	−0.21	−0.21	−0.21
MMT13	0.51	0.84	0.63	0.67	0.92	0.74	0.92	0.85	1.32	0.63	0.99	2.17	0.63	0.85	1.21
...	±0.04	±0.06	±0.03	±0.01	±0.01	±0.02	±0.01	±0.03	±0.01	±0.04	±0.03	±0.09	±0.16	±0.31	±0.26
...	...	−0.04	−0.06	−0.09	−0.57	−0.12	−0.13	−0.04	−0.64	−0.16	−0.33	−0.99	−0.06	−0.04	−0.04
MMT15	2.00	2.90	3.98	5.34	8.77	9.65	10.34	8.34	11.55	11.87	12.52	14.09	13.24	16.11	13.73
...	±0.11	±0.06	±0.04	±0.01	±0.01	±0.02	±0.01	±0.03	±0.01	±0.04	±0.03	±0.10	±0.60	±0.32	±1.02
...	−0.05	−0.07	−0.19	−0.20	−0.44	−0.06	−0.35	−0.15	−0.42	−0.06	−0.06	−0.05	−0.08	−0.06	−0.06
MMT16	1.23	1.27	1.82	2.80	4.39	4.41	4.90	3.90	5.33	5.19	5.48	5.62	6.18	6.54	4.19
...	±0.06	±0.04	±0.04	±0.01	±0.01	±0.02	±0.01	±0.03	±0.01	±0.04	±0.03	±0.10	±0.41	±0.34	±0.31
...	−0.03	−0.05	−0.12	−0.38	−0.34	−0.05	−0.28	−0.11	−0.37	−0.06	−0.05	−0.04	−0.06	−0.06	−0.06
MMT17	14.68	21.82	44.15	85.81	133.74	157.12	161.76	136.27	183.69	196.16	210.99	236.24	187.72	298.17	194.15
...	±0.16	±0.14	±0.20	±0.06	±0.12	±0.18	±0.10	±0.31	±0.13	±0.40	±0.30	±1.00	±1.72	±2.80	±1.61
...	−0.05	−0.09	−0.25	−0.28	−0.51	−0.09	−0.56	−0.23	−0.90	−0.11	−0.10	−0.08	−0.12	−0.11	−0.12
MMT18	0.72	1.60	0.80	0.85	1.12	0.99	1.41	1.21	1.39	1.06	1.17	1.21	1.39	0.86	1.33
...	±0.05	±0.06	±0.03	±0.01	±0.01	±0.02	±0.01	±0.03	±0.01	±0.04	±0.03	±0.09	±0.17	±0.31	±0.27
...	−0.02	−0.05	−0.09	−0.17	−0.10	−0.42	−0.41	−0.04	−0.31	−0.10	−0.10	−0.06	−0.05	−0.05	−0.04
MMT19	5.89	4.27	3.73	3.72	4.76	4.13	7.55	7.61	6.30	4.79	5.14	5.58	6.25	7.08	5.82
...	±0.13	±0.07	±0.04	±0.01	±0.01	±0.02	±0.01	±0.03	±0.01	±0.04	±0.03	±0.10	±0.42	±0.34	±0.32
...	−0.07	−0.20	−0.39	−0.88	−0.52	...	−3.11	−0.22	−1.55	−0.40	−0.41	−0.32	−0.29	−0.26	−0.25
MMT20	0.94	2.12	2.68	3.17	6.69	7.15	9.15	8.85	9.83	11.51	12.16	12.61	13.07	13.24	14.12
...	±0.04	±0.05	±0.04	±0.01	±0.01	±0.03	±0.01	±0.02	±0.01	±0.04	±0.03	±0.10	±0.42	±0.83	±0.32
...	...	−0.04	−0.07	−0.11	−0.29	−0.16	−0.32	−0.60	−0.19	−0.89	−0.72	−0.08	−0.06	−0.06	−0.05
MMT21	0.58	0.75	0.71	0.65	0.75	0.63	0.67	0.54	1.19	0.51	0.69	1.71	≤0.61	≤0.30	≤1.06
...	±0.05	±0.03	±0.03	±0.01	±0.01	±0.03	±0.01	±0.02	±0.01	±0.04	±0.03	±0.09	...	...	...
...	...	−0.04	−0.06	−0.08	−0.17	−0.18	−0.13	−0.05	−0.70	−0.04	−0.20	−1.01	...	...	−0.04
MMT22	0.24	0.55	0.65	0.68	1.23	1.33	1.73	1.73	2.72	3.14	3.53	4.43	5.45	5.87	7.92
...	±0.04	±0.03	±0.04	±0.01	±0.01	±0.03	±0.01	±0.02	±0.01	±0.04	±0.03	±0.10	±0.19	±0.38	±0.27
...	...	−0.01	−0.03	−0.04	−0.15	−0.07	−0.07	−0.03	−0.21	−0.03	−0.19	−0.79	−0.03	−0.03	−0.03

TABLE 17
Spectral Energy Distributions for the [O III] λ4363-detected Sample

MMT23	0.20	0.40	0.44	0.55	0.90	1.02	1.19	1.08	1.69	1.22	1.42	2.14	1.54	1.42	1.07
...	±0.03	±0.03	±0.03	±0.01	±0.01	±0.03	±0.01	±0.02	±0.01	±0.04	±0.03	±0.09	±0.18	±0.37	±0.25
...	...	−0.01	−0.02	−0.04	−0.13	−0.08	−0.07	−0.04	−0.50	−0.26	−0.33	−0.78	−0.04	−0.05	−0.05
MMT24	0.66	1.54	1.17	1.12	1.74	1.74	2.32	1.36	3.15	1.76	2.56	2.55	1.46	3.50	5.39
...	±0.04	±0.05	±0.04	±0.01	±0.01	±0.02	±0.01	±0.03	±0.01	±0.04	±0.03	±0.09	±0.52	±0.31	±0.97
...	−0.02	−0.11	−0.17	−0.25	−0.57	−0.18	−0.84	−0.50	−1.76	−0.22	−0.78	−0.27	−0.14	−0.11	−0.10
MMT25	0.49	0.78	0.48	0.53	0.82	0.80	0.93	0.75	1.61	0.89	1.20	2.26	0.89	0.99	1.60
...	±0.05	±0.05	±0.03	±0.01	±0.01	±0.02	±0.01	±0.03	±0.01	±0.04	±0.03	±0.09	±0.17	±0.32	±0.27
...	...	−0.04	−0.06	−0.09	−0.21	−0.11	−0.14	−0.04	−0.80	−0.05	−0.27	−1.00	−0.05	−0.04	−0.04
MMT26	4.59	6.72	8.27	10.04	16.62	18.70	18.08	16.55	20.75	20.02	21.47	22.88	25.49	28.83	23.51
...	±0.10	±0.10	±0.04	±0.01	±0.01	±0.03	±0.01	±0.02	±0.01	±0.04	±0.03	±0.10	±0.42	±0.80	±0.33
...	−0.04	−0.12	−0.29	−0.89	−0.78	−3.25	−0.77	−0.19	−1.89	−0.30	−0.30	−0.24	−0.23	−0.26	−0.26
MMT27	0.10	0.42	0.10	0.22	0.37	0.67	0.41	0.31	0.44	0.34	0.43	0.48	0.26	≤0.34	0.72
...	±0.04	±0.03	±0.02	±0.01	±0.01	±0.03	±0.01	±0.02	±0.01	±0.04	±0.03	±0.09	±0.15	...	±0.24
...	...	...	−0.02	−0.05	−0.08	−0.40	−0.09	−0.01	−0.12	−0.04	−0.03	−0.02	−0.02	...	−0.02
MMT28	0.47	0.74	0.92	0.98	1.51	2.14	1.75	1.42	1.81	1.59	1.74	1.82	2.41	2.43	2.58
...	±0.04	±0.04	±0.04	±0.01	±0.01	±0.03	±0.01	±0.02	±0.01	±0.04	±0.03	±0.09	±0.17	±0.33	±0.28
...	...	−0.02	−0.08	−0.09	−1.02	−0.27	−0.03	−0.24	−0.10	−0.09	−0.05	−0.04	−0.06	−0.07	
MMT29	2.30	3.13	2.94	2.71	3.85	3.09	5.51	8.64	3.40	6.22	5.74	3.86	4.20		3.85
...	±0.06	±0.07	±0.04	±0.01	±0.01	±0.03	±0.01	±0.02	±0.01	±0.04	±0.03	±0.10	±0.18	...	±0.27
...	−0.02	−0.10	−0.20	−0.35	−0.68	−0.22	−2.25	−6.29	−0.22	−3.25	−2.33	−0.25	−0.19	...	−0.20
MMT30	2.97	4.12	4.78	4.46	7.71	7.15	9.21	10.65	8.06	10.76	10.41	8.97	9.99	10.85	11.10
...	±0.10	±0.08	±0.04	±0.01	±0.01	±0.03	±0.01	±0.02	±0.01	±0.04	±0.03	±0.10	±0.18	±0.79	±0.27
...	−0.02	−0.10	−0.17	−0.30	−0.52	−0.15	−1.37	−3.61	−0.15	−2.73	−1.94	−0.18	−0.14	−0.15	−0.13
MMT31	3.42	4.80	5.98	5.88	9.77	8.71	12.78	15.45	10.80	17.07	16.09	14.27	16.15	19.12	18.98
...	±0.12	±0.10	±0.04	±0.01	±0.01	±0.03	±0.01	±0.02	±0.01	±0.04	±0.03	±0.10	±0.42	±0.33	±0.32
...	−0.02	−0.14	−0.28	−0.52	−0.99	−0.32	−2.69	−7.12	−0.33	−5.45	−3.91	−0.39	−0.28	−0.36	−0.32
MMT32	5.22	6.73	10.24	13.93	21.55	18.19	23.38	26.94	23.60	22.97	24.02	26.73	23.52	29.03	20.39
...	±0.16	±0.08	±0.04	±0.01	±0.01	±0.03	±0.01	±0.02	±0.01	±0.04	±0.03	±0.10	±0.60	±0.33	±1.04
...	−0.11	−0.21	−0.93	−0.78	−3.02	−0.43	−2.56	−7.37	−1.57	−0.38	−0.38	−0.39	−0.47	−0.54	−0.61
MMT33	0.44	0.58	0.60	0.49	0.77	1.39	1.46	0.75	1.27	1.06	1.12	0.89	1.11		1.04
...	±0.04	±0.03	±0.04	±0.01	±0.01	±0.02	±0.01	±0.03	±0.01	±0.04	±0.03	±0.09	±0.37	...	±0.29
...	...	−0.04	−0.07	−0.11	−0.15	−0.21	−0.69	−0.73	−0.53	−0.50	−0.47	−0.07	−0.06	...	−0.05
MMT34	0.47	0.78	0.77	0.70	1.20	1.44	1.63	1.13	1.87	1.49	1.87	1.87	2.10	2.90	2.22
...	±0.04	±0.03	±0.04	±0.01	±0.01	±0.02	±0.01	±0.03	±0.01	±0.04	±0.03	±0.09	±0.17	±0.89	±0.26
...	...	−0.02	−0.04	−0.06	−0.15	−0.05	−0.26	−0.21	−0.41	−0.10	−0.23	−0.12	−0.03	−0.03	−0.02
MMT35	0.49	1.01	0.75	0.81	1.47	1.88	2.02	1.49	2.17	2.04	2.32	2.38	2.81	2.68	2.15
...	±0.04	±0.04	±0.03	±0.01	±0.01	±0.02	±0.01	±0.03	±0.01	±0.04	±0.03	±0.09	±0.40	±0.34	±0.30
...	...	...	...	−0.02	−0.16	−0.04	−0.19	−0.19	−0.29	−0.08	−0.22	−0.10	−0.05	−0.15	−0.17
MMT37	0.10	0.79	1.07	1.16	1.54	2.31	2.46	1.76	3.42	2.47	2.71	2.92	2.34	4.10	3.80
...	±0.03	±0.05	±0.03	±0.01	±0.01	±0.02	±0.01	±0.03	±0.01	±0.04	±0.03	±0.09	±0.39	±0.35	±0.31
...	...	−0.01	−0.03	−0.05	−0.12	−0.77	−0.42	−0.14	−0.94	−0.08	−0.12	−0.10	−0.10	−0.13	−0.20
MMT38	≤0.03	0.13	0.12	0.18	0.22	0.28	0.31	0.20	0.60	0.20	0.37	0.26	0.55	≤0.31	0.66
...	...	±0.03	±0.03	±0.01	±0.01	±0.02	±0.01	±0.03	±0.01	±0.04	±0.03	±0.08	±0.33	...	±0.27
...	...	...	−0.01	−0.02	−0.03	−0.05	−0.05	−0.09	−0.07	−0.34	−0.04	−0.11	−0.02	−0.03	...	−0.02
Keck01	≤0.03	0.93	0.54	0.52	0.58	0.76	0.68	0.52	0.70	1.83	1.69	0.38	0.90	0.50	≤1.06
...	...	±0.05	±0.03	±0.01	±0.01	±0.02	±0.01	±0.03	±0.01	±0.04	±0.03	±0.09	±0.49	±0.28	...
...	...	...	−0.01	−0.02	−0.04	−0.07	−0.14	−0.26	−0.18	−1.65	−1.44	−0.08	−0.29	−0.14	−0.20
Keck02	0.15	0.62	0.59	0.61	0.73	0.91	1.03	0.84	1.32	0.92	0.99	0.97	0.98	≤0.39	1.28
...	±0.03	±0.03	±0.04	±0.01	±0.01	±0.02	±0.01	±0.03	±0.01	±0.04	±0.03	±0.09	±0.18	...	±0.25
...	...	−0.01	−0.02	−0.03	−0.05	−0.14	−0.09	−0.04	−0.28	−0.02	−0.02	−0.02	−0.02	...	−0.02
Keck03	≤0.03	3.70	4.15	3.83	4.70	4.45	6.14	7.30	7.85	9.94	9.52	8.51	9.51	10.32	9.02
...	...	±0.13	±0.04	±0.01	±0.01	±0.03	±0.01	±0.02	±0.01	±0.04	±0.03	±0.10	±0.60	±0.32	±1.01
...	...	...	−0.02	−0.03	−0.07	−0.12	−0.52	−1.52	−0.21	−2.53	−1.77	−0.11	−0.43	−0.25	−0.39
Keck04	≤0.03	0.55	0.79	0.81	1.04	1.10	1.32	0.95	1.59	1.56	2.32	1.83	2.21	1.91	2.01
...	...	±0.03	±0.04	±0.01	±0.01	±0.02	±0.01	±0.03	±0.01	±0.04	±0.03	±0.09	±0.33	±0.32	±0.32
...	...	−0.02	−0.05	−0.06	−0.09	−0.11	−0.23	−0.14	−0.31	−0.23	−0.64	−0.25	−0.24	−0.05	−0.05
Keck05	≤0.03	0.27	0.20	0.22	0.26	0.19	0.31	0.34	0.41	0.68	0.64	0.24	0.68	≤0.32	0.42
...	...	±0.02	±0.04	±0.01	±0.01	±0.03	±0.01	±0.02	±0.01	±0.04	±0.03	±0.08	±0.17	...	±0.22
...	...	...	...	−0.01	−0.02	−0.02	0.03	0.18	−0.05	−0.31	−0.26	−0.01	−0.06	...	−0.02
Keck06	≤0.03	≤0.03	≤0.03	0.11	0.14	0.13	0.17	0.09	0.16	0.54	0.42	0.13	0.51	≤0.32	≤0.28
...	...	...	...	±0.01	±0.01	±0.01	±0.01	±0.02	±0.01	±0.04	±0.03	±0.08	±0.16	...	...
...	...	...	...	...	−0.01	−0.02	−0.02	...	−0.04	−0.22	−0.16	−0.01	−0.04	...	−0.01
Keck07	≤0.03	0.38	0.29	0.28	0.34	0.30	0.39	0.46	0.44	0.67	0.95	0.30	0.97	≤0.32	0.57
...	...	±0.03	±0.04	±0.01	±0.01	±0.03	±0.01	±0.02	±0.01	±0.04	±0.03	±0.08	±0.18	...	±0.23
...	...	...	−0.01	−0.03	−0.03	−0.05	−0.06	−0.10	−0.17	−0.10	−0.39	−0.60	−0.05	−0.13	−0.03
Keck08	0.09	0.62	0.72	0.61	0.71	0.70	0.78	0.61	1.03	0.83	1.43	2.78	1.69	0.74	1.23
...	±0.03	±0.03	±0.04	±0.01	±0.01	±0.02	±0.01	±0.03	±0.01	±0.04	±0.03	±0.09	±0.18	±0.29	±0.25
...	...	...	−0.01	−0.02	−0.03	−0.05	−0.11	−0.08	−0.39	−0.05	−0.52	−1.55	−0.23	−0.09	−0.11
Keck09	≤0.03	0.28	0.25	0.27	0.31	0.26	0.37	0.35	0.48	0.61	0.78	0.46	0.71	0.74	0.46

TABLE 17
Spectral Energy Distributions for the [O III] λ4363-detected Sample

(1)	(2)	(3)	(4)	(5)	(6)	(7)	(8)	(9)	(10)	(11)	(12)	(13)	(14)	(15)	(16)
...	...	±0.03	±0.03	±0.01	±0.01	±0.03	±0.01	±0.02	±0.01	±0.04	±0.03	±0.09	±0.16	±0.31	±0.23
...	...	...	−0.01	−0.01	−0.02	−0.03	−0.07	−0.10	−0.08	−0.13	−0.29	−0.03	−0.06	−0.01	−0.01
Keck11	0.10	0.57	0.27	0.34	0.48	0.53	0.66	0.61	1.16	0.52	0.63	0.55	≤0.61	0.60	≤1.06
...	±0.03	±0.03	±0.03	±0.01	±0.01	±0.02	±0.01	±0.03	±0.01	±0.04	±0.03	±0.09	...	±0.29	...
...	...	−0.03	−0.04	−0.06	−0.09	−0.33	−0.21	−0.08	−0.52	−0.03	−0.05	−0.06	...	−0.03	−0.04
Keck12	≤0.03	0.11	0.12	0.10	0.13	0.12	0.12	0.14	0.15	0.23	0.24	0.12	≤0.19	≤0.32	≤0.28
...	...	±0.02	±0.03	±0.01	±0.01	±0.02	±0.01	±0.01	±0.01	±0.04	±0.03	±0.07	...	...	...
...	...	...	...	...	−0.01	−0.01	−0.02	−0.02	−0.09	−0.07	...	...	...	...	...
Keck13	≤0.03	0.11	0.05	0.10	0.12	0.05	0.13	0.12	0.14	0.29	0.29	≤0.10	≤0.61	≤0.32	2.02
...	...	±0.03	±0.02	±0.01	±0.01	±0.02	±0.01	±0.01	±0.01	±0.04	±0.03	...	...	...	±0.88
...	...	...	...	...	−0.01	−0.01	−0.01	−0.02	−0.12	−0.11	...	...	...	...	...
Keck14	0.08	1.86	2.02	1.79	2.08	2.98	2.50	1.89	2.66	4.36	4.08	2.64	4.24	3.24	3.08
...	±0.03	±0.04	±0.04	±0.01	±0.01	±0.02	±0.01	±0.03	±0.01	±0.04	±0.03	±0.09	±0.19	±0.31	±0.22
...	...	−0.01	−0.05	−0.07	−0.12	−0.17	−0.51	−1.22	−0.33	−2.57	−1.97	−0.10	−0.42	−0.12	−0.14
Keck15	0.08	1.20	1.22	1.12	1.23	1.56	1.42	1.03	1.74	2.44	2.38	1.55	1.98	1.39	1.84
...	±0.02	±0.06	±0.03	±0.01	±0.01	±0.02	±0.01	±0.03	±0.01	±0.04	±0.03	±0.09	±0.18	±0.37	±0.26
...	...	...	−0.02	−0.02	−0.04	−0.07	−0.20	−0.51	−0.13	−1.15	−0.92	−0.05	−0.19	−0.07	−0.08
Keck16	0.08	0.90	1.44	1.38	1.94	1.90	2.66	3.09	4.01	5.01	5.15	4.88	7.30	8.03	8.77
...	±0.02	±0.03	±0.04	±0.01	±0.01	±0.03	±0.01	±0.02	±0.01	±0.04	±0.03	±0.10	±0.19	±0.36	±0.27
...	...	...	...	−0.02	−0.04	−0.07	−0.33	−0.97	−0.18	−0.87	−0.68	−0.08	−0.33	−0.20	−0.32
Keck18	0.12	0.51	0.86	0.72	1.01	1.46	1.59	1.39	2.32	2.15	2.30	2.77	2.88	3.79	3.53
...	±0.03	±0.03	±0.04	±0.01	±0.01	±0.02	±0.01	±0.03	±0.01	±0.04	±0.03	±0.09	±0.18	±0.35	±0.28
...	...	...	−0.02	−0.04	−0.08	−0.48	−0.22	−0.08	−0.50	−0.04	−0.06	−0.07	−0.05	−0.05	−0.08
Keck19	0.05	1.12	1.10	0.97	1.09	1.58	1.34	0.96	1.31	2.92	2.51	1.23	1.65	0.69	1.63
...	±0.02	±0.06	±0.03	±0.01	±0.01	±0.02	±0.01	±0.03	±0.01	±0.04	±0.03	±0.09	±0.17	±0.30	±0.27
...	...	−0.03	−0.07	−0.08	−0.12	−0.15	−0.34	−0.68	−0.25	−1.83	−1.33	−0.06	−0.29	−0.06	−0.06
Keck20	0.28	0.46	0.30	0.33	0.59	0.53	0.84	1.18	0.68	0.90	0.86	0.58	0.59	≤0.32	0.69
...	±0.04	±0.03	±0.03	±0.01	±0.01	±0.03	±0.01	±0.02	±0.01	±0.04	±0.03	±0.09	±0.16	...	±0.25
...	...	−0.01	−0.02	−0.03	−0.05	−0.05	−0.16	−0.55	−0.03	−0.21	−0.15	−0.02	−0.02	...	−0.01
Keck21	≤0.03	0.52	0.39	0.53	0.67	0.84	0.90	0.67	1.33	1.40	1.95	2.39	2.20	4.16	4.49
...	...	±0.04	±0.03	±0.01	±0.01	±0.02	±0.01	±0.03	±0.01	±0.04	±0.03	±0.09	±0.39	±0.34	±0.31
...	...	...	−0.02	−0.02	−0.03	−0.04	−0.08	−0.05	−0.09	−0.08	−0.25	−0.10	−0.08	−0.02	−0.02
Keck23	0.10	0.58	0.33	0.33	0.37	0.28	0.42	0.48	0.38	1.42	1.08	0.30	0.62	≤0.35	0.33
...	±0.03	±0.04	±0.03	±0.01	±0.01	±0.03	±0.01	±0.02	±0.01	±0.04	±0.03	±0.08	±0.16	...	±0.21
...	...	...	−0.02	−0.02	−0.03	−0.04	−0.07	−0.11	−0.05	−0.65	−0.45	−0.01	−0.03	...	−0.02
Keck24	1.08	2.77	4.02	4.37	7.21	8.04	8.75	7.19	10.26	9.89	12.23	18.51	12.94	13.81	14.21
...	±0.06	±0.06	±0.04	±0.01	±0.01	±0.02	±0.01	±0.03	±0.01	±0.04	±0.03	±0.10	±0.42	±0.80	±0.32
...	...	−0.09	−0.17	−0.29	−0.89	−0.39	−0.52	−0.17	−1.31	−0.38	−1.60	−4.83	−0.19	−0.25	−0.25
Keck26	0.11	0.55	0.77	0.76	1.02	1.61	1.69	1.40	2.22	1.92	2.11	2.28	1.81	3.64	5.09
...	±0.03	±0.04	±0.04	±0.01	±0.01	±0.02	±0.01	±0.03	±0.01	±0.04	±0.03	±0.09	±0.53	±0.36	±0.97
...	...	−0.01	−0.03	−0.04	−0.09	−0.60	−0.26	−0.08	−0.42	−0.04	−0.04	−0.04	−0.04	−0.04	−0.05
Keck27	≤0.03	2.10	3.72	3.62	4.77	7.90	6.48	4.61	8.22	11.75	11.58	8.45	13.58	12.77	10.89
...	...	±0.05	±0.04	±0.01	±0.01	±0.02	±0.01	±0.03	±0.01	±0.04	±0.03	±0.10	±0.60	±0.36	±1.01
...	...	...	−0.02	−0.04	−0.15	−0.35	−1.81	...	−1.24	−10.01	−9.00	−0.90	−3.38	−4.10	−8.79
Keck28	0.12	0.68	0.73	0.74	0.83	0.96	1.06	0.77	1.63	0.86	1.09	0.66	0.77	0.58	1.26
...	±0.03	±0.04	±0.04	±0.01	±0.01	±0.02	±0.01	±0.03	±0.01	±0.04	±0.03	±0.09	±0.17	±0.33	±0.25
...	...	...	−0.01	−0.03	−0.07	−0.10	−0.26	−0.21	−0.83	−0.23	−0.47	−0.10	−0.11	−0.19	−0.33
Keck29	0.10	0.21	0.22	0.20	0.26	0.38	0.45	0.36	0.73	0.30	0.45	0.39	0.38	0.68	≤0.28
...	±0.03	±0.03	±0.04	±0.01	±0.01	±0.02	±0.01	±0.03	±0.01	±0.04	±0.03	±0.09	±0.16	±0.27	...
...	...	...	...	−0.02	−0.01	−0.04	−0.02	−0.25	−0.02	−0.02	−0.02	−0.02	−0.03	−0.05	...
Keck30	0.58	1.42	1.72	1.70	2.82	3.05	3.63	3.45	4.60	3.94	4.45	6.22	4.13	5.38	2.92
...	±0.03	±0.04	±0.04	±0.01	±0.01	±0.03	±0.01	±0.02	±0.01	±0.04	±0.03	±0.10	±0.57	±0.36	±0.92
...	...	−0.04	−0.08	−0.12	−0.42	−0.14	−0.18	−0.08	−0.90	−0.13	−0.52	−1.99	−0.08	−0.08	−0.08
Keck31	≤0.03	0.23	0.43	0.46	0.58	0.91	0.77	0.53	0.95	2.15	1.84	0.87	1.45	0.99	1.61
...	...	±0.03	±0.04	±0.01	±0.01	±0.02	±0.01	±0.03	±0.01	±0.04	±0.03	±0.09	±0.17	±0.32	±0.25
...	...	−0.02	−0.04	−0.05	−0.07	−0.09	−0.17	−0.31	−0.14	−1.00	−0.75	−0.04	−0.17	−0.03	−0.04
Keck32	0.15	0.19	0.22	0.25	0.41	0.46	0.54	0.38	0.66	0.57	0.65	0.68	0.66	0.92	0.46
...	±0.02	±0.03	±0.03	±0.01	±0.01	±0.02	±0.01	±0.03	±0.01	±0.04	±0.03	±0.09	±0.16	±0.33	±0.22
...	...	−0.01	−0.02	−0.03	−0.06	−0.02	−0.09	−0.04	−0.18	−0.02	−0.09	−0.05	−0.02	−0.01	−0.01
Keck33	0.24	1.05	0.49	0.46	0.53	0.67	0.72	0.58	1.11	0.46	0.56	0.51	≤0.43	≤0.31	0.39
...	±0.03	±0.01	±0.04	±0.01	±0.01	±0.03	±0.01	±0.02	±0.01	±0.04	±0.03	±0.09	...	...	±0.25
...	...	−0.03	−0.05	−0.07	−0.13	−0.39	−0.24	−0.12	−0.52	−0.04	−0.05	−0.07	...	...	−0.04

Note. — (1): Abbreviated name for MMT/Keck [O III] λ4363-detected galaxy. (2)–(16): Photometric fluxes from shorter to longer wavelengths. For each source, the observed fluxes are provided on the first row, the uncertainties in fluxes are provided on the second row, and the corrections for nebular emission (continuum and line) are provided in the third row (see Section 4.4 for nebular emission determinations). All fluxes and uncertainties are provided in units of μJy. All uncertainties are reported at 68% confidence levels.